

ADA 084792

Report SAM-TR-79-30

LEVEL 2

# PROCEDURAL TESTS FOR ANTI-G PROTECTIVE DEVICES

## Volume I: Procedural Tests for Anti-G Valves

Roy W. Thompson, M.S.  
Carmen E. Galvan, B.A.  
Paul E. Love  
Arnold G. Krueger  
Technology Incorporated  
511 West Rhapsody Drive  
San Antonio, Texas 78216

December 1979

Final Report for Period 1 October 1976 - 30 June 1978

Approved for public release; distribution unlimited.

Prepared for  
USAF SCHOOL OF AEROSPACE MEDICINE  
Aerospace Medical Division (AFSC)  
Brooks Air Force Base, Texas 78235



DDC FILE COPY

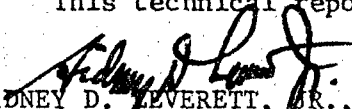
## NOTICES


This final report was submitted by the Life Sciences Division, Technology Incorporated, 511 West Rhapsody Drive, San Antonio, Texas 78216, under contract F33615-77-C-0610, job order 7930-12-13, with the USAF School of Aerospace Medicine, Aerospace Medical Division, AFSC, Brooks Air Force Base, Texas. Dr. Sidney D. Leverett, Jr. (USAFSAM/VNB) was the Laboratory Project Scientist-in-Charge.


When U.S. Government drawings, specifications, or other data are used for any purpose other than a definitely related Government procurement operation, the Government thereby incurs no responsibility nor any obligation whatsoever; and the fact that the Government may have formulated, furnished, or in any way supplied the said drawings, specifications, or other data is not to be regarded by implication or otherwise, as in any manner licensing the holder or any other person or corporation, or conveying any rights or permission to manufacture, use, or sell any patented invention that may in any way be related thereto.

This report has been reviewed by the Office of Public Affairs (PA) and is releasable to the National Technical Information Service (NTIS). At NTIS, it will be available to the general public, including foreign nations.

This technical report has been reviewed and is approved for publication.

  
SIDNEY D. LEVERETT, JR., Ph.D.  
Project Scientist

  
BRYCE O. HARTMAN, Ph.D.  
Supervisor

  
LAWRENCE J. ENDERS  
Colonel, USAF, MC  
Commander

UNCLASSIFIED

SECURITY CLASSIFICATION OF THIS PAGE (When Data Entered)

REPORT DOCUMENTATION PAGE		READ INSTRUCTIONS BEFORE COMPLETING FORM
1. REPORT NUMBER SAM-TR-79-30-V86-1	2. GOVT ACCESSION NO. AD-A084792	3. RECIPIENT'S CATALOG NUMBER 9
4. TITLE (and Subtitle) PROCEDURAL TESTS FOR ANTI-G PROTECTIVE DEVICES. Volume I. Procedural Tests for Anti-G Valves.		5. DATE OF REPORT & PERIOD COVERED Final RPT. 1 Oct 1976 - 30 June 1978
6. AUTHOR(s) Roy W. Thompson, Carmen E. Galvan, Paul E. Love, Arnold G. Krueger		7. PERFORMING ORG. REPORT NUMBER
8. CONTRACT OR GRANT NUMBER(s) F33615-77-C-0610		9. PERFORMING ORGANIZATION NAME AND ADDRESS Technology Incorporated 511 W. Rhapsody Dr. San Antonio, Texas 78216
10. PROGRAM ELEMENT, PROJECT, TASK AREA & WORK UNIT NUMBERS 62202F 793012-13		11. CONTROLLING OFFICE NAME AND ADDRESS USAF School of Aerospace Medicine (VNB) Aerospace Medical Division (AFSC) Brooks Air Force Base, Texas 78235
12. REPORT DATE December 1979		13. NUMBER OF PAGES 167
14. MONITORING AGENCY NAME & ADDRESS (if different from Controlling Office)		15. SECURITY CLASS. (of this report) UNCLASSIFIED
16. DISTRIBUTION STATEMENT (of this Report) Approved for public release; distribution unlimited.		17. DISTRIBUTION STATEMENT (of the abstract entered in Block 20, if different from Report)
18. SUPPLEMENTARY NOTES Appendix A applies to both volumes		
19. KEY WORDS (Continue on reverse side if necessary and identify by block number) Acceleration                      Equipment in jet aircraft Aircrew protection              Performance of anti-G valve Anti-G valve                      Test protocol for anti-G valve Data acquisition Data analysis		
20. ABSTRACT (Continue on reverse side if necessary and identify by block number) In the first volume of the two in this study report, the instrumentation, data recording, and computerized data analysis techniques for acceleration response and performance studies are described in detail. The results of performance testing of 5 anti-G valves are reported. The valves tested were the ALAR 8400A, Bendix FF139A2, USAFSAM Electronic, USAFSAM Ready Pressure, and the ALAR 8000A.		

401650

Jm

# CONTENTS

Section	Page
1. INTRODUCTION . . . . .	7
1.1 Preceding Investigations . . . . .	7
1.2 Contract Requirements . . . . .	8
2. STANDARDIZED ANTI-G VALVE TEST PROTOCOL . . . . .	9
2.1 Introduction . . . . .	9
2.2 Test Configuration . . . . .	9
2.3 Parameters Monitored . . . . .	12
2.3.1 Source Pressure ( $P_s$ ) . . . . .	12
2.3.2 Suit Pressure ( $P_v$ ) . . . . .	12
2.3.3 Air Flow ( $F_v$ ) . . . . .	13
2.3.4 Acceleration ( $G_z$ ) . . . . .	13
2.3.5 Valve Angle . . . . .	13
2.3.6 Suit Volume . . . . .	13
2.3.7 Signal Conditioning and Recording . . . . .	14
2.4 Test Description . . . . .	14
2.4.1 Phase I--Maximum Flow Capacity . . . . .	14
2.4.2 Phase II--Dynamic Response Testing . . . . .	15
2.4.3 Phase III--Complex Dynamic Response Testing . . . . .	15
2.5 Data Analysis . . . . .	15
2.6 Discussion . . . . .	17
3. DATA ACQUISITION AND HANDLING . . . . .	18
3.1 General Description . . . . .	18
3.2 Signal Transmission . . . . .	19
3.3 Pressure Transducers . . . . .	19
3.4 Flow Meters . . . . .	20
3.5 Force Transducers . . . . .	20
3.6 Control Console Signal Conditioners . . . . .	20
3.7 Data Collection Station Preamplifiers . . . . .	21
3.8 Strip-chart Recorders . . . . .	21
3.9 Electronic Filter . . . . .	21
3.10 Analog Magnetic Tape Recorder . . . . .	21
4. MATHEMATICS AND DATA ANALYSES . . . . .	22
4.1 Discussion . . . . .	22
4.2 GVALVPGM Output . . . . .	22
4.2.1 Performance Evaluation Table . . . . .	22
4.2.1.1 Definitions and Equations . . . . .	23
4.2.1.2 Discussion . . . . .	23
4.2.2 GVALVPGM Plot Descriptions . . . . .	28
5. ANTI-G VALVE TEST RESULTS . . . . .	32
5.1 ALAR 8400A Anti-G Valve Test Results . . . . .	32
5.1.1 Valve and Test Description . . . . .	32
5.1.2 Flow Tests . . . . .	33
5.1.3 Low G-Onset-Rate Tests . . . . .	35
5.1.4 High G-Onset-Rate Tests . . . . .	41
5.1.5 SACM Tests . . . . .	48
5.1.6 Conclusion on the ALAR 8400A's Performance . . . . .	49

Accession For	
NTIS. GR&I	<input checked="" type="checkbox"/>
DDC. TAB	<input type="checkbox"/>
Unannounced	<input type="checkbox"/>
Justification	
By	
Distribution	
Availability	
Dist	Availability
A	special

## CONTENTS (cont'd.)

Section	Page
5.2 Bendix FR139A2 Anti-G Valve Test Results . . . . .	49
5.2.1 Valve and Test Description . . . . .	49
5.2.2 Flow Tests . . . . .	60
5.2.3 Low G-Onset-Rate Tests . . . . .	64
5.2.4 High G-Onset-Rate Tests . . . . .	70
5.2.5 SACM Tests . . . . .	71
5.2.6 Conclusions on the FR139A2's Performance . . . . .	71
5.3 Electronic Anti-G Valve and Test Results . . . . .	86
5.3.1 Valve and Test Description . . . . .	86
5.3.2 Flow Tests . . . . .	87
5.3.3 Low G-Onset-Rate Tests . . . . .	89
5.3.4 High G-Onset-Rate Tests . . . . .	97
5.3.5 SACM Tests . . . . .	97
5.3.6 Conclusions on the E-Valve's Performance . . . . .	104
5.4 Ready Pressure Anti-G Valve (RPV) Test Results . . . . .	104
5.4.1 Valve and Test Description . . . . .	104
5.4.2 Flow Tests . . . . .	113
5.4.3 Low G-Onset-Rate Tests . . . . .	113
5.4.4 High G-Onset-Rate Tests . . . . .	114
5.4.5 SACM Tests . . . . .	123
5.4.6 Conclusions on the RPV's Performance . . . . .	136
5.5 ALAR 8000A Anti-G Valve Test Results . . . . .	136
5.5.1 Valve and Test Description . . . . .	136
5.5.2 Flow Tests . . . . .	136
5.5.3 Low G-Onset-Rate Tests . . . . .	140
5.5.4 High G-Onset-Rate Tests . . . . .	145
5.5.5 SACM Tests . . . . .	153
5.5.6 Conclusions on the ALAR 8000A's Performance . . . . .	164
ABBREVIATIONS, ACRONYMS, AND SYMBOLS . . . . .	167

## FIGURES

Figure No.		
1	SVTP open-flow configuration . . . . .	10
2	SVTP dynamic test configuration . . . . .	11
3	Simulated Air Combat Maneuver (SACM) . . . . .	16
4	Key to symbols in Figures 5 to 109 . . . . .	32
	<u>ALAR 8400A Anti-G Valve</u>	
5	flow as a function of source pressure . . . . .	36
6	variation (three sigma) in flow as a function of source pressure . . . . .	37
7	0.1 G/sec pressure profile as a function of source pressure . . . . .	38
8	0.1 G/sec pressure stability as a function of source pressure . . . . .	39
9	0.1 G/sec decreasing pressure profile as a function of source pressure . . . . .	40
10	0.1 G/sec pressure hysteresis as a function of source pressure . . . . .	42

CONTENTS ("ALAR 8400A AGV," cont'd.)

<u>Figure No.</u>		<u>Page</u>
11	pressure profile comparison as a function of onset rate . . . . .	43
12	pressure profile as a function of G-onset rate . . . . .	44
13	dP/dG as a function of G-onset rate . . . . .	45
14	1.5 G/sec pressure profile as a function of source pressure . . . . .	46
15	1.5 G/sec pressure variation as a function of source pressure . . . . .	47
16	1.5 G/sec decreasing pressure profile as a function of source pressure . . . . .	50
17	1.5 G/sec pressure hysteresis as a function of source pressure . . . . .	51
18	SACM pressure profile comparison with minimum source pressure and maximum suit volume . . . . .	52
19	pressure deviation and dG/dt for the minimum source pressure and maximum suit volume SACM . . . . .	53
20	SACM pressure profile comparison with maximum source pressure and minimum suit volume . . . . .	54
21	pressure deviation and dG/dt for the maximum source pressure and minimum suit volume SACM . . . . .	55
22	SACM pressure profile comparison with median source pressure and suit volume . . . . .	56
23	pressure deviation and dG/dt for the median source pressure and suit volume SACM . . . . .	57
24	SACM pressure profile comparison with G vector misalignment . . . . .	58
25	pressure deviation and dG/dt for the G vector misalignment SACM . . . . .	59
<u>Bendix FRI39A2 Anti-G Valve:</u>		
26	flow as a function of source pressure . . . . .	62
27	flow three sigma as a function of $G_z$ . . . . .	63
28	0.1 G/sec pressure profile as a function of source pressure . . . . .	65
29	0.1 G/sec pressure stability as a function of source pressure . . . . .	66
30	0.1 G/sec decreasing pressure profile as a function of source pressure . . . . .	67
31	0.1 G/sec pressure hysteresis as a function of source pressure . . . . .	68
32	pressure profile comparison as a function of onset rate . . . . .	69
33	pressure profile as a function of G-onset rate . . . . .	72
34	dP/dG as a function of G-onset rate . . . . .	73
35	1.5 G/sec pressure profile as a function of source pressure . . . . .	74
36	1.5 G/sec pressure variation as a function of source pressure . . . . .	75
37	1.5 G/sec decreasing pressure profile as a function of source pressure . . . . .	76
38	1.5 G/sec pressure hysteresis as a function of source pressure . . . . .	77

CONTENTS ("Bendix FRI39A2 AGV," cont'd.)

<u>Figure</u> <u>No.</u>		<u>Page</u>
39	SACM pressure profile comparison with minimum source pressure and maximum suit volume . . . . .	78
40	pressure deviation and $dG/dt$ for the minimum source pressure and maximum suit volume SACM . . . . .	79
41	SACM pressure profile comparison with maximum source pressure and minimum suit volume . . . . .	80
42	pressure deviation and $dG/dt$ for the maximum source pressure, minimum suit volume SACM . . . . .	81
43	SACM pressure profile comparison with median source pressure and suit volume .	82
44	pressure deviation and $dG/dt$ for the median source pressure and suit volume SACM . . . . .	83
45	SACM pressure profile comparison with G vector misalignment . . . . .	84
46	pressure deviation and $dG/dt$ for the G vector misalignment SACM . . . . .	85
<u>Electronic Anti-G Valve:</u>		
47	flow as a function of source pressure . . . . .	90
48	flow three sigma as a function of source pressure . . . . .	91
49	0.1 G/sec pressure profile as a function of source pressure . . . . .	92
50	0.1 G/sec pressure stability as a function of source pressure . . . . .	93
51	0.1 G/sec decreasing pressure profile as a function of source pressure . . . .	94
52	0.1 G/sec pressure hysteresis as a function of source pressure . . . . .	95
53	pressure-profile comparison as a function of onset rate . . . . .	96
54	pressure profile as a function of G-onset rate . . . . .	98
55	$dP/dG$ as a function of G-onset rate . . . . .	99
56	1.5 G/sec pressure profile as a function of source pressure . . . . .	100
57	1.5 G/sec pressure variation as a function of source pressure . . . . .	101
58	1.5 G/sec decreasing pressure profile as a function of source pressure . . . .	102
59	1.5 G/sec pressure hysteresis as a function of source pressure . . . . .	103
60	SACM pressure-profile comparison with minimum source pressure and maximum suit volume . . . . .	105
61	pressure deviation and $dG/dt$ for the minimum source pressure and maximum suit volume SACM . . . . .	106
62	SACM pressure-profile comparison with maximum source pressure and minimum suit volume . . . . .	107
63	pressure deviation and $dG/dt$ for the maximum source pressure and minimum suit volume SACM . . . . .	108
64	SACM pressure-profile comparison with median source pressure and suit volume .	109

# CONTENTS ("Electronic ACV," cont'd.)

Figure No.		Page
65	pressure deviation and $dG/dt$ for the median source pressure and suit volume SACM . . . . .	110
66	SACM pressure-profile comparison with the G vector misaligned . . . . .	111
67	pressure deviation and $dG/dt$ for the G vector misaligned SACM . . . . .	112
<u>Ready Pressure Anti-G Valve:</u>		
68	flow as a function of source pressure . . . . .	116
69	flow three sigma as a function of source pressure . . . . .	117
70	pressure profile as a function of source pressure . . . . .	118
71	0.1 G/sec pressure stability as a function of source pressure . . . . .	119
72	0.1 G/sec decreasing pressure profile as a function of source pressure . . . . .	120
73	0.1 G/sec pressure hysteresis as a function of source pressure . . . . .	121
74	pressure-profile comparison as a function of onset rate . . . . .	122
75	pressure profile as a function of G-onset rate . . . . .	124
76	$dP/dG$ as a function of G-onset rate . . . . .	125
77	1.5 G/sec pressure profile as a function of source pressure . . . . .	126
78	1.5 G/sec pressure variation as a function of source pressure . . . . .	127
79	1.5 G/sec decreasing pressure profile as a function of source pressure . . . . .	128
80	1.5 G/sec pressure hysteresis as a function of source pressure . . . . .	129
81	SACM pressure-profile comparison with minimum source pressure and maximum suit volume . . . . .	130
82	pressure deviation and $dG/dt$ for the minimum source pressure and maximum volume SACM . . . . .	131
83	SACM pressure-profile comparison with maximum source pressure and minimum suit volume . . . . .	132
84	pressure deviation and $dG/dt$ for the maximum source pressure and minimum suit volume SACM . . . . .	133
85	SACM pressure-profile comparison with median source pressure and suit volume . . . . .	134
86	pressure deviation and $dG/dt$ for the median source pressure and suit volume SACM . . . . .	135
87	SACM pressure-profile comparison with the G vector misaligned . . . . .	138
88	pressure deviation and $dG/dt$ for the G vector misalignment SACM . . . . .	139
<u>ALAR 8000A Anti-G Valve:</u>		
89	flow as a function of source pressure . . . . .	141
90	flow three sigma as a function of source pressure . . . . .	142
91	0.1 G/sec pressure profile as a function of source pressure . . . . .	143



CONTENTS ("ALAR 8000A ACV," cont'd.)

Figure No.		Page
92	0.1 G/sec pressure stability as a function of source pressure . . . . .	144
93	0.1 G/sec decreasing pressure profile as a function of source pressure . . . . .	146
94	0.1 G/sec pressure hysteresis as a function of source pressure . . . . .	147
95	pressure-profile comparison as a function of onset rate . . . . .	148
96	pressure-profile as a function of G-onset rate . . . . .	149
97	dP/dG as a function of G-onset rate . . . . .	150
98	1.5 G/sec pressure profile as a function of source pressure . . . . .	151
99	1.5 G/sec pressure variation as a function of source pressure . . . . .	152
100	1.5 G/sec decreasing pressure profile as a function of source pressure . . . . .	154
101	1.5 G/sec pressure hysteresis as a function of source pressure . . . . .	155
102	SACM pressure-profile comparison with minimum source pressure and maximum suit volume . . . . .	156
103	pressure deviation and dG/dt for the minimum source pressure and maximum suit volume SACM . . . . .	157
104	SACM pressure-profile comparison with maximum source pressure and minimum suit volume . . . . .	158
105	pressure deviation and dG/dt for the maximum source pressure and minimum suit volume SACM . . . . .	159
106	SACM pressure-profile comparison with median source pressure and suit volume . . . . .	160
107	pressure deviation and dG/dt for the median source pressure and suit volume SACM . . . . .	161
108	SACM pressure-profile comparison with G vector misalignment . . . . .	162
109	pressure deviation and dG/dt for the G vector misalignment SACM . . . . .	163

TABLES

Table No.		
1	Anti-G valve performance evaluation table definitions and equations . . . . .	24
2	ALAR 8400A anti-G valve performance evaluation table . . . . .	34
3	Bendix FRI39A2 anti-G valve performance evaluation table . . . . .	61
4	Electronic anti-G valve performance evaluation table . . . . .	88
5	Ready pressure anti-G valve performance evaluation table . . . . .	115
6	ALAR 8000A anti-G valve performance evaluation table . . . . .	137

## PROCEDURAL TESTS FOR ANTI-G PROTECTIVE DEVICES

### VOLUME I:

#### PROCEDURAL TESTS FOR ANTI-G VALVES

#### 1. INTRODUCTION

The Procedural Tests for Anti-G Protective Devices (PTAP) projects were conducted over an 18-month period by the Life Sciences Division of Technology Incorporated, under Air Force Contract F33615-77-C-0610. These tests were sponsored by the AFSC Aeronautical Systems Division and monitored by the USAF School of Aerospace Medicine (USAFSAM), Crew Technology Division, Biodynamics Branch (VNB), Brooks AFB, Texas. Most of the work was performed at Brooks AFB, where the facilities of VNB and the Data Sciences Division (BR) were used. This publication documents the PTAP investigations and fulfills the final report requirements of the contract.

The PTAP report consists of two volumes and an appendix: Volume I, Procedural Tests for Anti-G Valves, concerns the main thrust of the project--namely, the standardization of anti-G valve (AGV) performance testing. Volume II, G Sensitivity Tests, reports investigations into failure modes of two AGV's, and performance evaluations on various equipment related to the USAFSAM/VNB-PTAP missions. Appendix A, Anti-G Valve Performance Analysis (GVALVPGM), completely documents the FORTRAN programs used to evaluate the data from the standardized AGV tests.

#### 1.1 Preceding Investigations

The mission of USAFSAM/VNB is: first, "to investigate the physiologic and performance changes in experimental subjects exposed to sustained and simulated aerial combat maneuver (SACM) stress, and to determine the end points, using noninvasive instrumentation devices"; second, "to investigate methods--including anti-G suits, valves, and physiologic methods--to improve G tolerance." For these requirements to be met, an objective technique for evaluating the performance quality of acceleration protection equipment was needed as a means of conserving time and effort. The ultimate test of any system is in the operational environment for which it was designed; and, prior to testing in tactical aircraft, acceleration protection equipment must certainly be tested on human subjects in carefully controlled acceleration environments. However, evaluations by human subjects are, by definition, subjective; and even the resulting measured physiologic responses are prone to considerable variation. Thus, objective equipment tests, which were predictive (to some reasonable degree) of the ultimate performance quality of

---

EDITOR'S NOTE: Appendix A applies to, and supplements, Volumes I and II. (Information on how to order this Appendix appears at the close of each volume.)

anti-G suits and anti-G valves, would effect the desired time-and-effort economics.

In the initial program, Engineering Test and Evaluation During High G (TEHG), exhaustive studies were conducted on various anti-G valves, anti-G suits, and other devices used in studies of G effects on humans, animals, and equipment (consult USAFSAM-TRs 78-10, 78-11, and 78-12). From these studies, an economical, effective, and predictive set of tests for anti-G valves evolved. This set of tests was documented as the Standard Anti-G Valve Test Protocol (SVTP). At the same time, the background theory and preliminary framework were developed for a set of FORTRAN programs to evaluate the SVTP data. The PTAP program has refined these results, and empirically tested them.

## 1.2 Contract Requirements

The PTAP contract was modified on several occasions as the availability of test items and the specific needs of the Air Force and USAFSAM/VNB missions were better defined. The summary presented here is the result of that evolutionary process.

The PTAP program may be divided into three interdependent areas of effort:

- (1) refinement and evaluation of SVTP;
- (2) investigations of failure modes in anti-G valves; and
- (3) equipment performance evaluations.

The refinement and evaluation of SVTP includes, as a major objective, the generation of a computer software package and associated data handling procedures (GVALVPGM) for uniform evaluation of the results. Four anti-G valves were to be tested, using SVTP and GVALVPGM. In the process of testing the multi-valve mode of operation of GVALVPGM, testing a fifth valve became necessary, and the data are included in this report.

A thorough search for information on AGV failure modes and frequency in the U.S. Air Force resulted in inconclusive data. These data are reported and supplemented with engineering evaluations of possible failure modes and empirical testing of induced failures. Those failures which seemed conducive to testing were subject to SVTP and GVALVPGM.

The previous contractual effort (TEHG) had assembled a considerable inventory of talent, technology, and facilities in the field of evaluation of hardware performance in a high-acceleration environment. This inventory was used to considerable advantage during the course of the PTAP contract in support of the mission of both USAFSAM/VNB and PTAP. The results of these evaluations are in Volume II, section 2.

---

EDITOR'S NOTE: Available, on p. 167, is a selective list (plus definitions) of the "Abbreviations, Acronyms, and Symbols" used throughout this volume.

## 2. STANDARDIZED ANTI-G VALVE TEST PROTOCOL

The SVTP was developed under the TEHG contract and formally presented in that final report (SAM-TR-78-11). A complete copy of that protocol (with editorial alterations to reflect PTAP refinements) is included here for the convenience of the reader. The work reported in the remainder of this volume is predicated on this protocol.

### 2.1 Introduction

The purpose of the SVTP is to describe a uniform test procedure for evaluating the relative performance characteristics of anti-G valves. The data resulting from this protocol should provide a standard of performance.

The SVTP--designed to augment, not replace, MIL-V-93/OD [available through the Aeronautical Standards Groups (ASG), 8719 Colesville Rd., Silver Spring, Md. 20910]--deals only with the active or dynamic elements of anti-G valve testing. (It does not deal with physical dimensional specifications, material specifications, environmental specifications, or static performance specifications.) The dynamic tests described are intended to be performed on the USAFSAM/VNB human centrifuge at Brooks AFB, Texas.

One of the projected uses of the SVTP is to develop a data base for design selection of anti-G protective subsystem components for existing and proposed weapon system-mission combinations at the earliest feasible time. Because of the almost infinite variety of conditions and requirements of such subsystems, this protocol does not propose to simulate all possible combinations. Rather, the intention is that limits of conditions be set, allowing an indication of acceptability of a particular valve for a particular mission. This procedure will allow selection of existing anti-G valves for more explicit testing before their application to a specific weapon system-mission combination.

### 2.2 Test Configuration

Two basic test configurations will be used for evaluating anti-G valves. The first (Fig. 1) will be used only for the flow tests (refer to section 3.4.1). The second test configuration (Fig. 2) is identical to the first except for the addition of the sink volume. (All transducers and data-handling equipment are discussed in section 2.3.)

The pressure-source configuration will involve the installation, in the gondola, of standard "K bottles" containing 220 SCF air at 2200 psig. A remotely controlled solenoid valve will be installed in the system. The valve will be used to conserve air. This unit will be capable of switching up to 300 psig. The valve will be controlled by a relay--mounted in the gondola--which will, in turn, be controlled by low-current lines through the slip rings to control console-mounted switches.

---

**EDITOR'S NOTE:** As indicated by the authors, the information in section 2 parallels (of necessity) that in corresponding passages in SAM-TR-78-11.

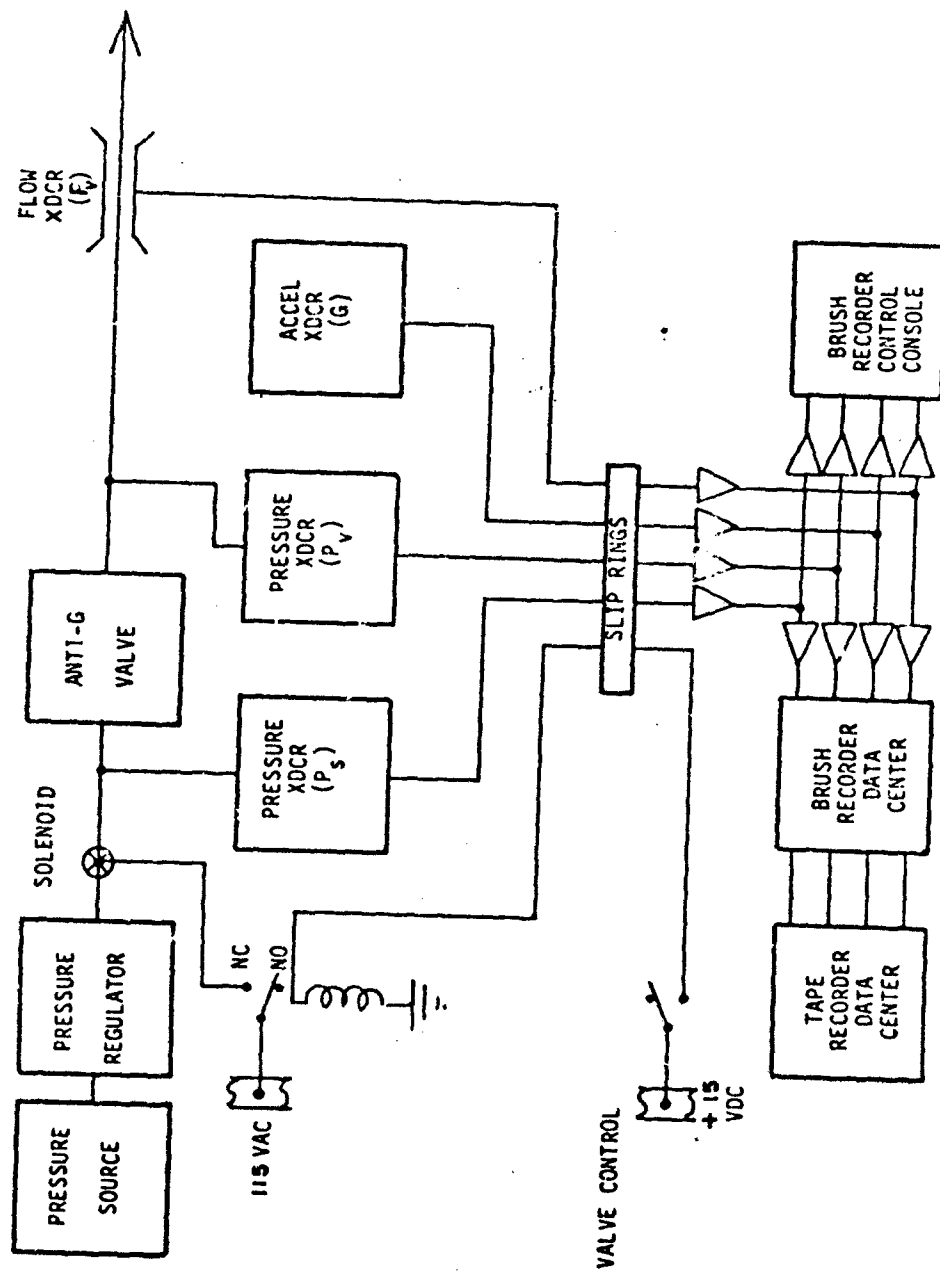


Figure 1. Open-flow test configuration established by the Standardized Anti-G Valve Test Protocol.  
 [F<sub>V</sub> = air flow; NC = normally closed; NO = normally open; P<sub>S</sub> = source pressure;  
 P<sub>V</sub> = suit pressure; XDCR = transducer; and VAC = volts alternating current]

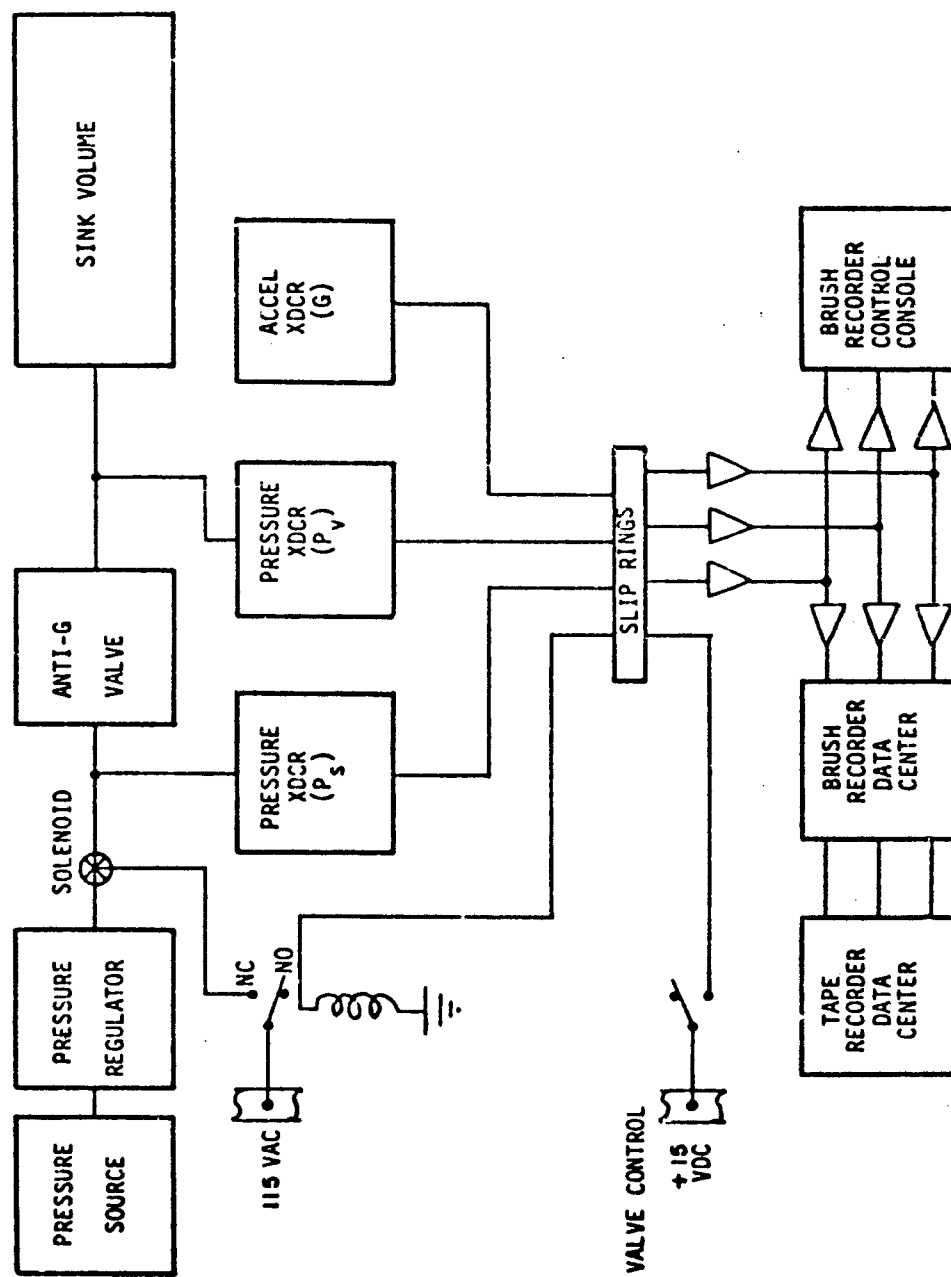


Figure 2. Dynamic test configuration established by the Standardized Anti-G Valve Test Protocol.  
[For abbreviations, see legend for Fig. 1]

Regulation of the source pressure to the anti-G valve under test is an especially critical system requirement. The regulation system must be capable of maintaining the source pressure, plus or minus 10% (preferably  $\pm 5\%$ ), through a wide range of flow rates (i.e., 0 - 30 SCFM). It may prove most practical to use two regulation systems. Because the open-flow tests (i.e., open-flow test configuration) will contain all of the higher flow rates, a wide dynamic range regulation system may be used exclusively for these tests. A less bulky standard regulator mounted directly on the K bottle pressure source will probably be sufficient for dynamic test configurations.

The anti-G valve will be mounted on a plate which is indexed and scaled in degrees. This plate may be locked in any angular position, and will be used to facilitate testing the sensitivity of the anti-G valves to mounting angle. This plate will be mounted on a test stand and will be aligned as nearly as possible with the gondola accelerometer to reduce acceleration error. This test stand will also be used to mount such equipment as flow meters, relays, and solenoid valves.

The sink volume used to terminate the valve under test should be a "flexible volume" at the volume specified to simulate an anti-G suit properly. "Rigid volumes" will not be acceptable. If an actual anti-G suit is used, a minimum flow impedance model should be selected (e.g., the CSU-15/P). The specified volume is intended to represent the incompressible volume, or the volume of water required to fill the suit, at 5 psig. Stretch in the flexible volume should be limited to an increase of 10% at 10 psig over the 5 psig volume.

The terminal plumbing in both test systems configurations should be very carefully designed to minimize the flow impedance downstream from the anti-G valve. It is suggested that essentially the same plumbing fixtures be used in both test configurations. An adequate test for downstream impedance may be determined during the open-flow tests by limiting the pressure at the output of the anti-G valve to 1 psig at the maximum flow rate (approximately 30 SCFM).

## 2.3 Parameters Monitored

### 2.3.1 Source Pressure ( $P_s$ )

A source-pressure transducer will be located downstream from the solenoid valve, and will monitor the pressure supplied to the inlet port of the anti-G valve. The transducer port will be located to minimize errors due to pressure drop caused by supply-line restrictions and due to venturi effects.

### 2.3.2 Suit Pressure ( $P_v$ )

A suit-pressure transducer will be located immediately downstream from the anti-G valve and will monitor the pressure supplied by the valve to the remainder of the pneumatic system. The transducer port will be located to minimize errors due to pressure drop through the interconnecting tubing and due to venturi effects.

### 2.3.3 Air Flow (F<sub>y</sub>)

The flow measurement transducer should have a dynamic range of at least 1.0 - 30 SCFM, with additional high-range capability being desirable. It is suggested that a hot-wire type of sensor would be most advantageous to improve the response of the monitoring system and to detect high-frequency fluctuations in the valve's operation. (NOTE: Not all hot-wire sensors have good high-frequency response.) The flow sensor should be installed immediately downstream from the suit-pressure transducer and must be selected to avoid excess flow impedance.

### 2.3.4 Acceleration (G<sub>z</sub>)

Acceleration will be measured only in the +Z axis (i.e., in this case, parallel to the sensitive axis marked on the anti-G valve). The sensor should have a dynamic range of from 1 to 11 G, with additional high range capability being desirable. While the need for testing along other axes will be necessary in the foreseeable future, none of the valves or weapon systems in immediate prospect have this capability; and testing for this variation would significantly increase the complexity of this protocol.

### 2.3.5 Valve Angle

The valve under test will be attached to a circular plate, indexed in degrees, and mounted in a position such that the centerline is parallel to a line through the center of the mounting plate and the zero degree index mark. The plate will be attached to a frame through a single point at its center such that it may be firmly fixed at any desired angle. The mounting plate will be referenced to the frame to assure alinement of the valve's acceleration sensor with the resultant G vector in the gondola.

### 2.3.6 Suit Volume

The sink volume (simulating anti-G suit volume) will be measured by evacuating the volume with a mild vacuum, then pressurizing to 5 psig from a known volume at known initial and final pressures. The sink volume will then be calculated from the pressure drop in the source bottle according to the following relationship:

$$\frac{(P_0 - P_R)(V_0)}{P_I - P_S} = V_S$$

in which P<sub>0</sub> = initial known volume pressure in psig;

P<sub>R</sub> = final known volume pressure in psig;

P<sub>S</sub> = final suit pressure in psig;

P<sub>I</sub> = initial suit pressure in psig;

V<sub>0</sub> = known volume in in.<sup>3</sup> (or liters); and

V<sub>S</sub> = unknown suit volume in in.<sup>3</sup> (or liters).



This relationship assumes the temperature of the air does not change.  $V_S$  and  $V_0$  are the "incompressible volumes" or volumes of water required to fill the space as opposed to the "standard air volume" or the volume of air at standard temperature and pressure to fill the volume at the subject pressure.

#### 2.3.7 Signal Conditioning and Recording

The majority of the data recorded for these tests should utilize standard techniques similar to those presently being used for the majority of tests run on the USAFSAM human centrifuge. These techniques involve passing the electrical signals through slip rings to the control console where they are amplified or attenuated as necessary, recording the most important of the processed signals on the control console Brush recorder, filtering and rescaling the signals in the data center, recording the reprocessed signals on magnetic tape, and recording the output of the tape recorder playback electronics in one or two Brush recorders in the data center.

#### 2.4 Test Description

The performance evaluation tests for anti-G valves will be conducted in three phases. It is essential that the test setup and instrumentation (described in sections 2.2 and 2.3) be carefully prepared. However, each phase need not be conducted independently or continuously, as long as sufficient documentation is maintained to assure that the proper data are used for each element of the data analysis.

The term "trapezoid run" should be defined for the purposes of this test description. The actual G profile of a trapezoidal run on a strip-chart recorder, with time recorded as one axis, will approximate a geometric trapezoid. The data of interest are contained in the increasing and decreasing slopes, and none are extracted from the flat top. The quality of the data will be significantly enhanced if trapezoids are run from 1 to 11 G, and from 11 to 1 G (instead of 1 to 10 G). Termination of the data in the computer at 10 G results in significant program economies. It is important that the operator allow enough time between the increasing and decreasing slopes of a trapezoidal to permit the data analyst to separate the data in the computer. The time required is approximately 2 min of analog tape time.

##### 2.4.1 Phase I--Maximum Flow Capacity

The purpose of this test is to determine the maximum flow capability of the anti-G valve under test. (The test setup already shown in Fig. 1 is used.) Three source pressures are selected for one major variable and include the design maximum, minimum, and optimum median value for the valve under test.

Three trapezoidal runs are made at each source pressure, using 0.1 G/sec onset and offset rates. During these runs, the operator must monitor the data very carefully to assure that the source pressure remains within  $\pm 10\%$  of the desired value (preferably  $\pm 5\%$ ), and that the pressure at the valve output never exceeds 1 psig. The total recorded data for this phase are 9 trapezoidal runs.

#### 2.4.2 Phase II--Dynamic Response Testing

The purpose of this test is to determine the dynamic response capability of the anti-G valve under test. (The test setup shown in Fig. 2 is used.) All tests are run with the valve terminated in a flexible sink volume of 10 liters (refer to section 2.2).

Three 0.1 G/sec trapezoids are run at each source pressure (i.e., minimum, median, and maximum source pressure). A fourth set of three 0.1-G/sec trapezoids are run at a selected valve angle (i.e., 20°, or the maximum design capability of the valve) with a median source pressure. An identical set of data runs are recorded using 1.5 G/sec onset and offset rates. Additional sets of three trapezoids are run at the median source pressure using 0.5 G/sec and 1.0 G/sec onset and offset rates. The total recorded data for this phase consist of 30 trapezoidal runs.

#### 2.4.3 Phase III--Complex Dynamic Response Testing

This phase of testing provides a measure of the relative capability of an anti-G valve to function under SACM conditions. The G profile used is the SACM shown in Figure 3. In order to compare the relative performance under varying conditions, four sets of 3 iterations of the SACM are run. If the G profile is manually controlled, the best example of the set is used for data analysis. Where the G profile is automatically controlled, data from all three iterations may be combined if the magnitude of sigma for the G profile approaches the 6 sigma magnitude resulting from instrument uncertainty.

The first set of SACM's utilizes a median flexible volume (10 liters) at the median source pressure. The second set is made under identical conditions, except that the anti-G valve is misaligned to the vertical by the angle selected for Phase II. The third set of SACM's is run with a maximum suit volume (14 liters) and the minimum source pressure; the fourth set, with the minimum suit volume (6 liters) and the maximum source pressure.

#### 2.5 Data Analysis

To achieve true test uniformity, the analysis of the resulting data must be as carefully duplicated as the tests themselves. In an effort to assure this duplication, data recording, processing, and manipulation procedures were developed and documented. The initial stages of this data handling process, described briefly in sections 2.2 and 2.3, are reviewed in greater detail in section 3. The remainder is included in the GVALVPGM description.

The essential elements of the GVALVPGM, necessary to the understanding of the data in this volume, are in section 4. A detailed description and analysis of GVALVPGM is presented in "Appendix A: Anti-G Valve Performance Analysis (GVALVPGM)."

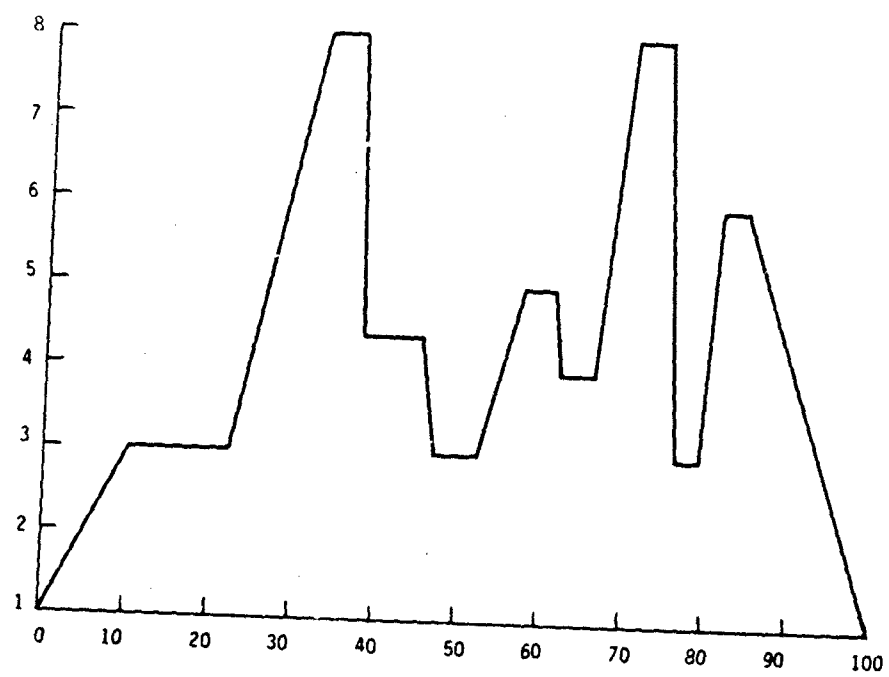


Figure 3. The G profile of a simulated aerial combat maneuver (SACM).

## 2.6 Discussion

The Standard Anti-G Valve Test Protocol provides a common denominator which an investigator may use to study anti-G valves. By subjecting all valves to the same test conditions and processing the results through identical (or at least similar) algorithms, the investigator may make valid direct performance comparisons. This technique is the most direct available to circumvent the "spec-man-ship" practiced by most manufacturers in describing their products.

For direct comparison, the Performance Evaluation Table (PET) is the most valuable tool; but it should not be expected to stand alone as evidence for designating the best valve for a particular aircraft-mission requirement. The conditions under which the valve is to be used will have a definite bearing on the suitability of a particular end item in a particular situation. In order to evaluate properly the effects of various conditions on a valve's performance, the graphic performance results are essential; for they permit the investigator to evaluate which input parameters (i.e., factors influencing the valve's performance) are most critical to the degradation of the output.

This protocol may also be used for specific performance evaluations when the designer wishes to choose among several candidates for a specific aircraft-mission situation. The input parameters (e.g., source pressures, suit volumes, valve angles, and onset rates) may thus be tailored to the specific requirements of the problem, so that a precise performance evaluation may be made. After all, the aim of this protocol is to provide the investigator with background data to determine not only the most likely set of candidates for these specific tests but also the guidelines for those tests.

The PET does not distinguish between these two sources of performance variation. Consequently, the comparison of single and multiple item tests would probably be biased in favor of the former. The significance of this bias tends to decrease as the number of test valves increases (i.e., the comparison of 8- and 10-item tests is probably valid, while the comparison of 1- and 3-item tests certainly is not valid).

It is not practical to display graphically the mean pressure profile or pressure errors of multiple SACM runs. Because the  $G_z$  profile will be (in most cases) manually controlled, too much run-to-run inconsistency will occur to make a mean presentation meaningful. The purpose of multiple iterations of SACM's is to allow the investigator the opportunity of choosing the "most typical" for analysis.

One of the variables used in this protocol deserves special attention. Using the function,  $\int_0^t G(t)dt$ , in the graphs and PET serves to weight suit-pressure errors proportionally to the  $G_z$  level at which they occur. In other words, in the graphic presentation, the abscissa increases in value (with respect to elapsed time) at a rate proportional to the  $G_z$  magnitude. As a result, the area under the error curve is proportional to the importance of the error.

### 3. DATA ACQUISITION AND HANDLING

The following discussion, of the data acquisition systems used during the course of the PTAP contract, is intended to provide general information only, and does not attempt to describe the specific arrangement of instrumentation peculiar to any one test. A standard test setup (Figs. 1 and 2) was used for all anti-G valves (SVTP) in protocol testing. To facilitate data handling, the analog tape and Brush chart channel assignments, as well as the calibration sequences, were standardized for SVTP tests.

The production of magnetic analog tapes, compatible with the data-processing systems presently in use in the USAFSAM Data Sciences Division, was one of the major governing factors during the planning stages of all tests.

The choice of signal conditioners used was dictated by the output of the associated transducer and was limited to the preamplifiers on inventory at the USAFSAM Human Centrifuge Facility. Signal conditioners were selected and matched to transfer outputs so that they were utilized as near as possible to the middle of their measurement range.

The sequencing of the following descriptions of the tasks involved in setting up for data acquisition is the same as was used during the actual performance of the tasks. This careful description of the system and procedures is presented to document the validity of the measurements made and assure their repeatability by following investigators.

#### 3.1 General Description

When the equipment, test stand, and control devices were secured in place in the gondola, all required signal outputs were connected through slip rings to the control console patch panel. The signal pairs coming from the gondola were input into the appropriate preamplifier or signal conditioner. The outputs of these preamplifiers and/or signal conditioners branch (parallel) to the Brush strip-chart recorder at the control console and to the data collection station patch panel.

At the data collection station, the signals were patched through 60 Hz rejection filters into preamplifier inputs. The preamplifiers at the data collection station were used to condition all signals to be recorded by the analog magnetic tape recorder. After all patching was completed, the instrumentation was turned on and left in the standby positions to warm up for at least 5 min. After the instrumentation stabilized, all channels were calibrated, using either the control console strip-chart recorder or a digital voltmeter as the readout. All pressure transducers were calibrated by applying pressure derived from the Datametrics digital pressure calibration system installed in the gondola. Force gages mounted on a mannequin to measure anti-G suit forces during some tests were calibrated by placing a 10-lb weight upon the load sensing surfaces.

---

**EDITOR'S NOTE:** As indicated by the authors, the information in section 3 parallels (of necessity) that in corresponding passages in SAM-TR-78-10.

The flow meter and the gondola accelerometer were calibrated by a signal generated when the appropriate switch was placed in the "CAL" position to generate the calibration signal.

After all signal conditioners and preamplifiers were calibrated, electrical signals corresponding to zero and full scale were sent to the data collection station to be used for spanning the preamplifiers that are input into the magnetic tape recorder. The outputs from the tape recorder were monitored by the strip-chart recorder.

The first signals to be recorded on the analog tape were the voice-annotated headers which were followed by the calibration runs. At least a two-point calibration on each data channel was used. The usual calibration points were "minimum" (which was almost always zero) and "maximum" (which was generally full scale).

The minimum length of the calibration was 30 sec. The time code from the magnetic tape (read out by the time code translator) was recorded at the beginning and end of each data run and served to locate the data on the tape. The time code also was used by data processing personnel to insert "start" and "stop" flags to control the digitizer during the digitization of the analog magnetic tapes.

During the process of digitizing the analog magnetic tapes, some additional conditioning equipment such as high and low cutoff filters were used to condition the data by removing unwanted high-frequency noise and "glitches."

The end products of the digitization of the analog magnetic tapes were digital magnetic tapes which were used to input data into the digital computer. The analyzed data from the computer were recorded in final form either as X-Y plots or in tabular form.

### 3.2 Signal Transmission

At several locations in the gondola, access to the signal lines from the gondola to the control console is available. The signal lines are AWG #20 single conductor shielded wire. These are not continuous runs, but are broken into sections terminating or beginning at the slip rings while having terminal boards between the slip rings and the control console. The average dc resistance of these signal lines is 4 ohms. The 60 Hz noise riding on the signal lines averages 10  $\mu$ V P-P.

### 3.3 Pressure Transducers

Two types of pressure transducers were utilized during the PTAP program for the measurement of air pressure (i.e., the strain-gage type and the potentiometric diaphragm type).

A Taber Teledyne type 176 transducer, which has a range of 0 - 500 psig, was used for higher pressures. For the lower pressures, where high-frequency response was not required, a Giannini (potentiometric diaphragm type) model 451212-4, 0 - 30 psia transducer was used.

### 3.4 Flow Meters

A Datametrics linear flow meter model 800-LM matched with a Datametrics flow sensor model 1000-2B were utilized for measuring air flow. The range of this flow meter is 0 - 60 SCFM, and the maximum error of the system is 2% of reading or 0.5% full scale, whichever is greater. Repeatability is within 1% of reading or 0.1% full scale. The response time for the sensor is 1 msec. This system has a linear output of 0 - 10 V (for 0 to full scale) available for recording.

### 3.5 Force Transducers

The force exerted upon the mannequin by an anti-G suit was measured by placing load washers on the surface of the mannequin at selected points. The load washers (Houston Scientific model 1200-15C) were especially calibrated for this purpose. The range of these transducers is 0 - 15 lb, linearity is  $\pm 1\%$  of full-scale output, and hysteresis is  $\pm 2\%$  of full-scale output. The load washers are of the full-bridge strain-gage type.

### 3.6 Control Console Signal Conditioners

A preamplifier (Brush model RD4215-10) is used to amplify the signal level of the higher output transducers to the  $\pm 2.5$  V required by the strip-chart recorder. The sensitivity of the preamplifier is 100  $\mu$ V/chart line, and the measurement range is 100  $\mu$ V - 500 V. The linearity is 0.2% full scale, the step response is 90% in 2 msec, and the frequency response is down 10% at 200 Hz. The accuracy of the preamplifier is  $\pm 1\%$  of full scale.

Low-level signals (requiring high gain), such as the signals from dc excited strain-gage transducers, require a Brush model RD4251-70 preamplifier. The sensitivity of this preamplifier is 1  $\mu$ V/chart line, and the measurement range is 1  $\mu$ V - 50 V. The linearity is 0.2% full scale, 10% - 90% step response is 2 msec, and the frequency response is 1.0 dB down at 200 Hz.

A carrier preamplifier (Brush model RD4212-00) is used for both half-bridge and full-bridge strain-gage transducers. This carrier preamplifier provides ac transducer excitation at a constant 5 V rms at 2 kHz. The sensitivity of this model is such that, with essentially all strain gages, a sensitivity of at least 1  $\mu$ in. per chart line is attainable. The linearity is 0.2% full scale, the step response is 90% in 2 msec, and the frequency response is 10% down at 200 Hz.

A universal coupler-preamplifier (Brush model 13-4218-00) is used when high or low cutoff filters are required to condition the input signals. This model will handle either ac or dc signals. The dc maximum sensitivity is 1 mV/chart division, and the ac maximum sensitivity is 20  $\mu$ V/chart division. The measurement range for direct current is 1 mV - 25 V, and the range for alternating current is 20  $\mu$ V - 25 mV. The signal output linearity is  $\pm 0.1\%$  full scale. The frequency response, for the ac ranges, is 0.05 Hz - 10 kHz ( $-3$  dB); and, for the dc ranges, is dc - 10 kHz ( $-3$  dB). The accuracy of this model is 1% of full scale.

### 3.7 Data Collection Station Preamplifiers

At the data collection station, Brush model 13-4185-02 preamplifiers are used, thus providing 8 channels of medium gain amplification. The input impedance is 50 kilohms, single ended, with polarity reversing switches for each channel. The maximum sensitivity is 50 mV per chart division, and the measurement range is  $\pm 125V$  full scale. The linearity of this model is  $\pm 0.05\%$  full scale.

### 3.8 Strip-chart Recorders

Two models of Brush recorders are used--a model 200 at the control console, and a model 2607-70 at the data collection station. Electrically, the characteristics of these models are essentially identical; but they differ mechanically in their paper takeup systems and in the arrangements for mounting. The input sensitivity is  $\pm 2.5 V$  (fixed 100 mV per chart division), and the non-linearity is less than 0.5% full scale. The frequency response is reported flat within  $\pm 2\%$  full scale from dc to 55 Hz, although informal tests indicate that this specification is suspect.

Twelve chart speeds, available in the range of 0.05 - 200 mm/sec, are electrically selectable by pushbuttons.

### 3.9 Electronic Filter

A 14-channel frequency rejection filter is available to be patched in between the data collection patch panel and the Brush preamplifiers. These are passive (L-C type) filters with a center frequency of 60 Hz. The 3 dB bandwidth of these filters is  $\pm 6$  Hz, the source impedance is 10 kilohms, and the load impedance is 100 kilohms.

### 3.10 Analog Magnetic Tape Recorder

A Sangamo model 3562 tape recorder/reproducer provided 14 channels of recording and/or playback. All tapes used during the PTAP program had time codes previously dubbed on channels 13 and 14, so no record modules were present in these channels. Channel 12 was used for voice recording and had direct record and playback modules. The remaining 11 channels were available for data collection. The tape speeds available are 60, 30, 15, 7-1/2, 3-3/4, and 1-7/8 in./sec; but all data were recorded during this project at 3-3/4 in./sec. For FM recording, the input sensitivity is 0.1 V to 25 V rms, adjustable with the input attenuator to achieve  $\pm 40\%$  deviation. The recorder was set up for a nominal  $\pm 1.4 V$  peak for  $\pm 40\%$  deviation, which is considered the optimum condition. The input impedance is 100 kilohms resistive. The center frequency of the carrier is 6.750 kHz at a tape speed of 3-3/4 in./sec as IRIG (Interrange Instrumentation Group, DOD) intermediate frequency is being used. The frequency response at 3-3/4 in./sec is flat from dc to 1250 Hz, and the output level is  $\pm 1.40 V$  peak into 1000 ohms.



#### 4. MATHEMATICS AND DATA ANALYSES

Specifics of the program used to analyze the anti-G valve data (including data requirements, required deck structure, mathematics, flow charts, listing, output, etc.) are available in the "Anti-G Valve Performance Analysis" (GVALVPCM) in "Appendix A" of this report. The following discussion is a brief synopsis of the information in that Appendix.

##### 4.1 Discussion

Using various concepts, techniques, and algorithms, GVALVPCM models, analyzes, and plots valve data. The analog test data were recorded at USAFSAM/VNB Human Centrifuge Facility, using the "Standard Anti-G Valve Test Protocol" (section 2.0). The data then were converted to digital data, using the USAFSAM/BRP analog-to-digital support facility. This procedure is documented by Stevens in General Purpose Data Conversion Programs for the PDP-12 Computer, USAF School of Aerospace Medicine, Brooks AFB, Texas 78235, SAM-TR-77-25, November 1977.

The digital data then were calibrated, scaled, and stored in appropriate arrays by run number and type of test (run-type). Once all data for up to five valves were processed in the foregoing manner, modeling of each run-type data set was accomplished. A combination of least squares fitting procedure and cubic splines was used to model each run-type data set.

##### 4.2 GVALVPCM Output

GVALVPCM produces two types of output--a performance evaluation table, and a series of plots.

###### 4.2.1 Performance Evaluation Table

The first output of GVALVPCM is an anti-G valve performance evaluation table containing valve performance numbers. Samples of this table are in section 5, titled "Anti-G Valve Performance Evaluation Table" (PET). The anti-G valve table is intended to provide the investigator with a quantitative measure of the relative performance of anti-G valves. The primary advantage of these evaluation numbers is in their direct comparison of different valves performing identical tasks.

The performance evaluation numbers are defined in section 4.2.1.1, "Performance Table Definitions." These performance numbers are weighted with appropriate weighting functions  $W_i$  (section 4.2.1.1.D). These functions were chosen: to weight the particular performance number with respect to other table entries; to weight the performance number with respect to high or low G force; to average the performance number over G; or for combinations of these reasons.

The various performance numbers vary widely with valve performance and the valve's pressure profile. These numbers are sensitive to a valve's design, linearity, hysteresis, high-onset performance, and angular performance. Thus, the performance numbers and the performance total will reflect the valve's performance, both in part and as a whole.

#### 4.2.1.1 Performance Table Definitions and Equations

Listed in Table 1 are the definitions and equations used to compile the performance evaluation tables presented in section 5.

#### 4.2.1.2 Performance Table Discussion

The "Anti-G Valve Performance Evaluation Table" is divided into six separate groups of entries. These are: test standards, design numbers, flow numbers, low-onset numbers, high-onset numbers, and SACM numbers. In addition, a total is calculated for the valve and entered at the end of the table.

The purpose of these characteristic numbers and test standards is to aid the investigator in evaluating a valve's performance and applicability to various aircraft.

A. Test Standards: The test standards include appropriate entries for source pressure, mounting angle, and suit size (volume). With the exception of the suit sizes, which are constant, the entries are the medium and/or extreme valve design limits.

B. Design Numbers: The design numbers compare, with pre-defined standards, the valve's design minimum and maximum source pressures, and design maximum mounting angle. The calculated ratios will increase as the design limits become more restrictive. The design numbers are: XSPMX, XSPMN, and XTHTA.

C. Flow Numbers: The flow characteristic numbers are defined to index the average flow, the difference in flow with respect to source pressure, and the variation (three sigma) in the flow profiles. The numbers increase as the average flow drops, the differences increase, or the standard deviation increases. The flow numbers are: XFLBR, XDELF, XDDLFL, and XSIGF.

D. Low-Onset Numbers: The low-onset numbers are defined to index valve performance while operating under  $\pm 0.1$  G/sec onset rates. The characteristic numbers index linearity between 3 G and 8 G, profile variation with respect to source pressure, standard deviation in the profile, and valve hysteresis. The characteristic numbers will increase in value with increasing nonlinearity, increasingly large variations, increasingly large standard deviation, and increasing hysteresis. The low-onset numbers are: XCCP1, XDDP1, XSGP1, and XDPP1.

TABLE 1. ANTI-G VALVE PERFORMANCE EVALUATION TABLE DEFINITIONS AND EQUATIONS

1. SPMIN = design minimum source pressure
2. SPMID = design medium source pressure
3. SPMAX = design maximum source pressure
4. THETA = design maximum angle with respect to G-vector
5. SVMIN = minimum test suit volume
6. SVMID = medium test suit volume
7. SVMAX = maximum test suit volume
8. XSPMX =  $W_8 \cdot (300/SPMAX)$
9. XSPMN =  $W_9 \cdot (SPMIN/30)$
10. XTHTA =  $W_{10} \cdot (20/THETA)$
11. Design Total = sum of 8, 9, and 10
12.  $XFLBR = W_{12} \sum_{k=1}^{10} \left[ \sum_{i=1}^{N_k} (F_{MN_{i,k}} - F_{MD_{i,k}} + F_{MX_{i,k}} - F_{MD_{i,k}})^{-0.75} \right]$
13.  $XDELF = W_{13} \sum_{k=1}^{10} \left[ \sum_{i=1}^{N_k} |F_{MX_{i,k}} - F_{MN_{i,k}}| \right]$
14.  $XDDL F = W_{14} \sum_{k=1}^{10} \left[ \sum_{i=1}^{N_k} (|F_{MN_{i,k}} - F_{MD_{i,k}}| + |F_{MX_{i,k}} - F_{MD_{i,k}}|) \right]$
15.  $XSIGF = W_{15}(G) \int_1^{10} \left[ \frac{\rho_{F_{MN}}}{(1+F_{MN})} + \frac{\rho_{F_{MD}}}{(1+F_{MD})} + \frac{\rho_{F_{MX}}}{(1+F_{MX})} \right] dG$
16. Flow Total = Sum of 12, 13, 14, and 15
17.  $XCCP1 = W_{17} \left( \left[ \frac{1}{R_{MN}^L} + \frac{1}{R_{MD}^L} + \frac{1}{R_{MX}^L} + \frac{1}{R_y^L} + \frac{1}{R_\theta^L} \right] - 5.0 \right); \frac{dG}{dt} = 0.1 \text{ G/sec}$
18.  $XDDP1 = W_{18}(G) \sum_{k=1}^{10} \left[ \sum_{i=1}^{N_k} (|P_{MN_{i,k}}^L - P_{MD_{i,k}}^L| + |P_{MX_{i,k}}^L - P_{MD_{i,k}}^L|) \right]; \frac{dG}{dt} = 0.1 \text{ G/sec}$
19.  $XSGP1 = G \cdot W_{19}(G) \int_1^{10} \left[ \rho_{P_{MN}}^L + \rho_{P_{MD}}^L + \rho_{P_{MX}}^L + \rho_{P_x}^L + \rho_{P_\theta}^L \right] dG; \frac{dG}{dt} = 0.1 \text{ G/sec}$
20.  $XDPP1 = W_{20} \int_1^{10} \left[ |H_{MN}^L| + |H_{MD}^L| + |H_{MX}^L| + |H_\theta^L| \right] dG; \frac{dG}{dt} = 0.1 \text{ G/sec}$
21. Low-onset Total = Sum of 17, 18, 19, and 20
22.  $XCCP2 = W_{22} \left( \left[ \frac{1}{R_{MX}^H} + \frac{1}{R_{MD}^H} + \frac{1}{R_{MN}^H} + \frac{1}{R_x^H} + \frac{1}{R_\theta^H} \right] - 5.0 \right); \frac{dG}{dt} = 1.5 \text{ G/sec}$

(CONT'D. ON NEXT PAGE)

TABLE 1. (Cont'd.)

$$23. \quad XDDP2 = W_{23}(G) \sum_{k=1}^{10} \sum_{i=1}^{N_k} (|P_{MN,i,k}^N - P_{MD,i,k}^H| + |P_{MX,i,k}^H - P_{MD,i,k}^H|); \frac{dG}{dt} = 1.5 \text{ G/sec}$$

$$24. \quad XSGP2 = G \cdot W_{24}(G) \int_1^{10} [P_{MN}^H + P_{MD}^H + P_{MX}^H + P_X^H + P_\emptyset^H] dG; \frac{dG}{dt} = 1.5 \text{ G/sec}$$

$$25. \quad XDPP2 = W_{25} \int_1^{10} [|H_{MN}^H| + |H_{MD}^H| + |H_{MX}^H| + |H_\emptyset^H|] dG; \frac{dG}{dt} = 1.5 \text{ G/sec}$$

$$26. \quad XTDP2 = W_{26} \sum_{k=1}^{10} \sum_{i=1}^{N_k} (|P_{MN,i,k}^L - P_{MN,i,k}^H| + |P_{MD,i,k}^L - P_{MD,i,k}^H| + |P_{MX,i,k}^L - P_{MX,i,k}^H| + |P_{X,i,k}^L - P_{X,i,k}^H| + |P_{\emptyset,i,k}^L - P_{\emptyset,i,k}^H|)$$

$$27. \quad \text{High-onset Total} = \text{Sum of 22, 23, 24, 25, and 26}$$

$$28. \quad XIDPA = \frac{1}{50} \cdot \int_0^{MX} |\Delta P_1(\tau)| d\tau$$

$$29. \quad XIDPB = \frac{1}{50} \cdot \int_0^{MX} |\Delta P_2(\tau)| d\tau$$

$$30. \quad XIDPC = \frac{1}{50} \cdot \int_0^{MX} |\Delta P_3(\tau)| d\tau$$

$$31. \quad XIDPD = \frac{1}{50} \cdot \int_0^{MX} |\Delta P_4(\tau)| d\tau$$

$$32. \quad \text{SACM Total} = \text{Sum of 28, 29, 30, and 31}$$

$$33. \quad \text{Valve Total} = \text{Sum of 11, 16, 21, 27, and 32}$$

(A) VARIABLE NOTATION:

W = weighting function

F = flow in SCFM, as derived from the fitted data

G = G-force in the Z-direction

$\sigma$  = standard deviation

R = a coefficient of linear correlation between 3G and 8G for a given G-P profile

P = suit pressure delivered by the valve, as derived from the fitted data

(CONT'D. ON NEXT PAGE)

TABLE 1. (Cont'd.)

H = the difference between the increasing pressure and decreasing pressure for a given suit size, onset rate, source pressure, and angle (NOTE: H is also a function of G)

$$\tau = \int_0^t G(t)dt \quad (\text{NOTE: } \tau_{MX} = \text{maximum value of } \tau)$$

t = time in seconds

$\Delta P$  = the difference between P-real and P-ideal during an SACM. P-ideal is defined by the Mid/Mid slow onset trapezoidal runs.

$\Delta P_1$  = refers to the Min Vol/Max source pressure, no angle, SACM

$\Delta P_2$  = refers to the Max Vol/Min source pressure, no angle, SACM

$\Delta P_3$  = refers to the Mid/Mid, no angle, SACM

$\Delta P_4$  = refers to the Mid/Mid, maximum angle, SACM

(B) SUBSCRIPTS:

MN = minimum source pressure

MD = medium source pressure

MX = maximum source pressure

F = flow

X = exhaust

$\theta$  = maximum angle WRT the Z-axis

$N_k$  = number of fitted data points in the  $k^{\text{th}}$  (G-force) interval

(C) SUPERSSCRIPTS:

L = low-onset rate ( $dG/dt = 0.1 \text{ G/sec}$ )

H = high-onset rate ( $dG/dt = 1.5 \text{ G/sec}$ )

(D) WEIGHTING FUNCTIONS:

$$W_8 = 1$$

$$W_{18}(G) = 0.013333 \cdot G / (1 + P_{MD}^L)$$

$$W_9 = 1$$

$$W_{19}(G) = 0.3 / (11 - G)$$

(CONT'D. ON NEXT PAGE)

TABLE 1. (Cont'd.)

$w_{10} = 1$	$w_{20} = 0.01$
$w_{12} = 0.0255$	$w_{22} = 25$
$w_{13} = 0.001333$	$w_{23}(G) = 0.013333 \cdot G / (1 + P_{MD}^H)$
$w_{14} = 0.001333$	$w_{24}(G) = 0.3 / (11 - G)$
$w_{15}(G) = 60 / (11 - G)$	$w_{25} = 0.01$
$w_{17} = 25$	$w_{26} = 0.0026666$

E. High-Onset Numbers: The high-onset numbers are defined to index valve performance while operating under  $\pm 1.5$  G/sec onset rates. The first four high-onset numbers are the same as their low-onset counterparts, and serve the same purpose. Moreover, one additional high-onset number is defined to index variations with respect to G-onset rate. The last high-onset number increases as the valve's performance increasingly differs from its low-onset performance. The high-onset numbers are: XCCP2, XDDP2, XSGP2, XDPP2, and XTDP2.

F. SACM Numbers: The SACM characteristic numbers are defined to index each SACM required by the test protocol. The SACM numbers increase as the valve's performance during a combat maneuver increasingly differs from its average performance under ideal conditions. The SACM numbers are: XIDPA, XIDPB, XIDPC, and XIDPD.

G. Totals: In addition to the individual characteristic numbers, the performance table contains entries representing category totals and a valve total. These totals are designed to provide the investigator with a summarized index of valve-to-valve performance.

#### 4.2.2 GVALVPGM Plot Descriptions

GVALVPGM currently generates 21 or more plots. Of these, 15 plots are unique, with the remaining being additional SACM plots. The 15 plots are described as follows.

A. Flow as a Function of Source Pressure: Flow, measured in SCFM, is plotted as a function of acceleration over the intervals 1 to 10 G. The graph contains three curves, one for each of the three design source pressures (minimum, medium, and maximum). The graph is entitled: " 'Valve' flow as a function of source pressure" [e.g., Vol. I: Figs. 5, 26, 47, 68, and 89; Vol. II: Figs. 24, 45, and 66].

B. Variation in Flow as a Function of Source Pressure: Variation in the flow (three sigma), measured in SCFM, is plotted as a function of acceleration over the intervals 1 to 10 G. The graph contains three curves, one for the variation in the flow using each of the design source pressures--minimum, medium, and maximum. The graph is entitled: " 'Valve' variation (three sigma) in flow as a function of source pressure" [e.g., Vol. I: Figs. 6, 27, 48, 69, and 90; Vol. II: Figs. 25, 46, and 67].

C. Suit Pressure as a Function of G-Onset: Using the medium source pressure and the medium suit size, with no angle in the valve mounting, the suit pressure is plotted as a function of acceleration between 1 G and 10 G. The four curves plotted represent the four G-onset rates: 0.1 G/sec, 0.5 G/sec, 1 G/sec, and 1.5 G/sec. Optional to the graph is the inclusion of MIL-V-9370D valve-pressure design limits. The graph is entitled: " 'Valve' pressure profile as a function of G-onset rate" [e.g., Vol. I: Figs. 12, 33, 54, 75, and 96; Vol. II: Figs. 31, 52, and 73].

D. Suit Pressure Rate-of-Change as a Function of G-onset: Using the medium source pressure and the medium suit size, with no angle in the valve mounting, the slope of the suit pressure profile with respect to acceleration ( $dP/dG$ ) is plotted as a function of acceleration between 1 and 10 G. The four curves plotted represent  $dP/dG$  as a function of four G-onset rates: 0.1 G/sec, 0.5 G/sec, 1 G/sec, and 1.5 G/sec. The graph is entitled: " 'Valve'  $dP/dG$  as a function of G-onset rate" [e.g., Vol. I: Figs. 13, 34, 55, 76, and 97; Vol. II: Figs. 32, 53, and 74].

E. Suit Pressure as a Function of Source Pressure (Low G-Onset): Using the medium suit size, and holding the G-onset rate at 0.1 G/sec, the suit pressure is plotted as a function of acceleration over the interval 1 to 10 G, for several source pressures and valve mounting angles. The four curves plotted represent: (1) minimum design source pressure with no angle in the valve's mounting; (2) median design source pressure with no angle in the valve's mounting; (3) maximum design source pressure with no angle in the valve's mounting; and (4) median design source pressure with the maximum design angle in the valve's mounting. Optional to the graph is the inclusion of MIL-V-9370D valve pressure design limits. The graph is entitled: " 'Valve' 0.1 G/sec pressure profile as a function of source pressure" [e.g., Vol. I: Figs. 7, 28, 49, 70, and 91; Vol. II: Figs. 26, 47, and 68].

F. Variation in Suit Pressure as a Function of Source Pressure (Low G-Onset): Using the medium suit size, and holding the G-onset rate at 0.1 G/sec, the variation in the suit pressure (three sigma) is plotted as a function of acceleration over the intervals 1 to 10 G for several source pressures and valve mounting angles. The four curves plotted represent the conditions specified in subsection 4.2.2.E. The graph is entitled: " 'Valve' 0.1 G/sec pressure stability as a function of source pressure" [e.g., Vol. I: Figs. 8, 29, 50, 71, and 92; Vol. II: Figs. 27, 48, and 69].

G. Pressure Hysteresis as a Function of Source Pressure (Low G-Onset): Using the medium suit size, and holding the G-onset rate at 0.1 G/sec (-0.1 G/sec decreasing), the hysteresis in the suit pressure is plotted as a function of acceleration over the G interval of 1 to 10 G for several source pressures and valve mounting angles. The four curves plotted represent the conditions specified in subsection 4.2.2.E. The graph is entitled: " 'Valve' 0.1 G/sec pressure hysteresis as a function of source pressure" [e.g., Vol. I: Figs. 10, 31, 52, 73, and 94; Vol. II: Figs. 29, 50, and 71].

H. Pressure as a Function of Source Pressure (High G-Onset): This is the same graph as subsection 4.2.2.E, with the G-onset rate held at 1.5 G/sec. The four curves represent the four conditions for source pressure and angle specified in that subsection. The graph is entitled: " 'Valve' 1.5 G/sec pressure profile as a function of source pressure" [e.g., Vol. I: Figs. 14, 35, 56, 77, and 98; Vol. II: Figs. 33, 54, and 75].



I. Variation in the Pressure as a Function of Source Pressure (High G-Onset): This is the same graph as subsection 4.2.2.F, with the G-onset rate held at 1.5 G/sec. The four curves represent the four conditions for source pressure and angle specified in subsection 4.2.2.E. The graph is entitled: " 'Valve' 1.5 G/sec pressure variation as a function of source pressure" [e.g., Vol. I: Figs. 15, 36, 57, 78, and 99; Vol. II: Figs. 34, 55, and 76].

J. Pressure Hysteresis as a Function of Source Pressure (High G-Onset): This is the same graph as subsection 4.2.2.G, with the G-onset rate held at 1.5 G/sec. The four curves represent the four conditions for source pressure and angle specified in subsection 4.2.2.E. The graph is entitled: " 'Valve' 1.5 G/sec pressure hysteresis as a function of source pressure" [e.g., Vol. I: Figs. 17, 38, 59, 80, and 101; Vol. II: Figs. 36, 57, and 78].

K. Hysteresis vs. Onset Compare: Using a medium size suit, median source pressure, and a zero degree valve attitude, increasing and decreasing pressure profiles are plotted as a function of acceleration over the G-interval 1 to 10 G. The four curves represent increasing and decreasing pressure profiles under low G-onset ( $\pm 0.1$  G/sec) and under high G-onset ( $\pm 1.5$  G/sec). The graph is entitled: " 'Valve' pressure profile comparison as a function of onset rate" [e.g., Vol. I: Figs. 11, 32, 53, 74, and 95; Vol. II: Figs. 30, 51, and 72].

L. Decreasing Pressure (Low G-Onset): This is the same graph as subsection 4.2.2.E, with the G-onset rate held at  $-0.1$  G/sec. The four curves represent the four conditions for source pressure and angle specified in that subsection. The graph is entitled: " 'Valve' 0.1 G/sec decreasing pressure profile as a function of source pressure" [e.g., Vol. I: Figs. 9, 30, 51, 72, and 93; Vol. II: Figs. 28, 49, and 70].

M. Decreasing Pressure (High G-Onset): This is the same graph as subsection 4.2.2.E, with the G-onset rate held at  $-1.5$  G/sec. The four curves represent the four conditions for source pressure and angle specified in that subsection. The graph is entitled: " 'Valve' 1.5 G/sec decreasing pressure profile as a function of source pressure" [e.g., Vol. I: Figs. 16, 37, 58, 79, and 100; Vol. II: Figs. 35, 56, and 77].

N. Ideal vs. Real Pressure Compare: Ideal and real suit pressure profiles are plotted as a function of time during standard SACM G-profile. Each SACM is approximately 100 sec in duration. The suit size, source pressure, and valve mounting angle are specified for each SACM, and are incorporated into the title. The four standard SACM parameter combinations are:

1) Maximum source pressure, minimum suit size, and no angle in the valve's mounting [e.g., Vol. I: Figs. 20, 41, 62, 83, and 104; Vol. II: Figs. 39, 60, and 81];

2) minimum source pressure, maximum suit size, and no angle in the valve's mounting [e.g., Vol. I: Figs. 18, 39, 60, 81, and 102; Vol. II: Figs. 37, 58, and 79];

3) median source pressure, medium suit size, and no angle in the valve's mounting [e.g., Vol. I: Figs. 22, 43, 64, 85, and 106; Vol. II: Figs. 41, 62, and 83]; and

4) median source pressure, medium suit size, and the maximum design angle in the valve's mounting [e.g., Vol. I: Figs. 24, 45, 66, 87, and 108; Vol. II: Figs. 43, 64, and 85].

Each graph is entitled: " 'Valve' SACM pressure profile comparison with 'specified source pressure, suit size, valve mounting angle.' "

0. Pressure Difference vs. G-Onset Compare: This graph consists of two curves graphed on two stacked axes. First, the difference between P-real and P-ideal (from subsection 4.2.2.N) is plotted as a function of the  $\tau$ , where  $\tau \equiv \int_0^t G \cdot dt$ .

Second,  $dG/dt$  (G-onset) is plotted as a function of  $\tau$ . This graph is produced for each SACM, with the parameter combinations specified in subsection 4.2.2.N:

1) Maximum source pressure, minimum suit size, and no angle in the valve's mounting [e.g., Vol. I: Figs. 21, 42, 63, 84, and 105; Vol. II: Figs. 40, 61, and 82];

2) minimum source pressure, maximum suit size, and no angle in the valve's mounting [e.g., Vol. I: Figs. 19, 40, 61, 82, and 103; Vol. II: Figs. 38, 59, and 80];

3) median source pressure, medium suit size, and no angle in the valve's mounting [e.g., Vol. I: Figs. 23, 44, 65, 86, and 107; Vol. II: Figs. 42, 63, and 84]; and

4) median source pressure, medium suit size, and the maximum design angle in the valve's mounting [e.g., Vol. I: Figs. 25, 46, 67, 88, and 109; Vol. II: Figs. 44, 65, and 86].

Each graph is entitled: " 'Valve' pressure deviation and  $dG/dt$  for 'specified source pressure, suit size, valve mounting angle.' "

## 5. ANTI-G VALVE TEST RESULTS

The performance of five anti-G valves was tested, using the SVTP described in section 3. The data from each set of tests were processed through GVALVPGM, which is described in section 4, and in Appendix A. The following sections are devoted to the results, implications, and conclusions from these tests and analyses. The symbols on the graphs are explained in Figure 4.

1	=	0.1 G/SEC G-ONSET RATE
2	=	0.5 G/SEC G-ONSET RATE
3	=	1.0 G/SEC G-ONSET RATE
4	=	1.5 G/SEC G-ONSET RATE
A	=	MAXIMUM DESIGN ANGLE
D	=	MEDIUM SOURCE PRESSURE, OR DECREASING (WITH RESPECT TO G)
I	=	INCREASING (WITH RESPECT TO G) OR P-IDEAL (ACMS)
N	=	MINIMUM SOURCE PRESSURE
R	=	P-REAL (ACMS ONLY)
X	=	MAXIMUM SOURCE PRESSURE
*	=	P-REAL LESS P-IDEAL OR G-ONSET

Figure 4. Key to symbols in Figures 5 to 109.  
[Symbols are shown as data points  
on the curves. See footnote.]

### 5.1 ALAR 8400A Anti-G Valve Test Results

#### 5.1.1 ALAR 8400A Valve and Test Description

The ALAR 8400A Anti-G Valve (designed and produced by ALAR Products, Inc., Macedonia, Ohio) uses a mass spring system for sensing acceleration and regulating anti-G suit pressure. Source pressure, ranging from 30 to 300 psig, is connected to the inlet fitting on the left side of

---

EDITOR'S NOTE: Due to the limitations of the technique initially used, these symbols are not always discernible on the respective curves. In such cases, however, the symbols are insignificant as compared with the close relationship obvious between the curves in each figure.

the valve. As acceleration force ( $G_z$ ) is encountered, the mass at the top of the valve is forced down against the spring and bears against a diaphragm regulator assembly and a valve stem, thus opening a flow path to the suit outlet at the right of the valve. As suit pressure builds up in the suit, back pressure against the diaphragm reduces flow until the  $G_z$  force and the suit pressure are balanced, at which time the valve is closed. As  $G_z$  force is reduced, the spring moves the mass assembly and diaphragm upward, thus opening the exhaust valve and relieving the suit pressure until  $G_z$  force and pressure are again matched. When the valve is returned to a 1  $G_z$  condition, the valve vents the suit back to ambient pressure.

The ALAR 8400A is designed to actuate (i.e., to begin to apply suit pressure) between 1.5  $G_z$  and 2.0  $G_z$ . The design requires that the suit be linearly pressurized, and contain between 0.1 psig and 1.2 psig at 2  $G_z$  and between 8.7 - 11.0 psig at 10  $G_z$ .

This anti-G valve is fitted with a spring-loaded relief valve with sufficient flow capacity to limit the suit pressure to 11 psig with 300-psig source pressure. The relief valve is designed to open between 8.7 psig and 11.0 psig.

The ALAR 8400A has an exposed button at the top of the valve assembly which allows the G-sensing mass to be depressed manually and provides a functional test feature (i.e., "press-to-test").

For purposes of SVTP testing and GVALVPGM analysis, standard values were assigned for the 8400A and are shown on lines 1 through 7 of Table 2, the Performance Evaluation Table (PET). In addition to being the design values for the valve, the values shown on lines 1 through 4 of Table 2 were selected as standards for the GVALVPGM analysis because they permitted direct application of the unit to a wide variety of weapons systems in the present USAF inventory. Since these values are the GVALVPGM standard, the 8400A scored a perfect minimum of 3.0 on the PET design total.

#### 5.1.2 ALAR 8400A Flow Tests

The flow-test performance score of the ALAR 8400A AGV (line 16 of Table 2) was the median score of the five valves tested under this contract. The total open-flow test showed a median performance (line 12 of Table 2), with the Electronic AGV (E valve) and the Ready Pressure AGV (RPV) having significantly higher flows, the ALAR 8400A having slightly lower flows, and the Bendix AGV having significantly lower flow capability. The source pressure influence on the open-flow performance was moderately high (lines 13 and 14, Table 2), the median (Bendix) doing a slightly better job of responding to source pressure fluctuations, while the E valve did considerably worse (refer to discussion in section 5.3.2). A measure of the variations in the open flow of the 8400A (line 15, Table 2) indicates it is the most stable and repeatable of all valves tested, although the fluctuations in flow were essentially equal for all valves tested.

---

**EDITOR'S NOTE:** The information in section 5.1.1 parallels (of necessity) that in corresponding material in SAM-TR-78-11.

TABLE 2. ALAR 8400A ANTI-G VALVE PERFORMANCE EVALUATION TABLE

TEST STANDARDS:

1. SPMIN = 30. PSIG
2. SPMID = 125. PSIG
3. SPMAX = 300. PSIG
4. THETA = 20. DEGREES
5. SVMIN = 6. LITERS
6. SVMID = 10. LITERS
7. SVMAX = 14. LITERS

CHARACTERISTIC NUMBERS:

8. XSPMX = 1.000
9. XSPMN = 1.000
10. XTHIA = 1.000
11. DESIGN TOTAL: 3.000
12. XFLBR = 2.808
13. XDELF = 2.025
14. XDDLFF = 2.027
15. XSIGF = 0.173
16. FLOW TOTAL: 7.033
17. XCCP1 = 0.064
18. XDDP1 = 0.064
19. XSGP1 = 1.188
20. XDPP1 = 0.645
21. LOW-ONSET TOTAL: 2.857
22. XCCP2 = 4.384
23. XDDP2 = 6.642
24. XSGP2 = 3.809
25. XDPP2 = 3.272
26. XTDP2 = 10.051
27. HIGH-ONSET TOTAL: 28.158
28. XIDPA = 1.708
29. XIDPB = 2.642
30. XIDPC = 2.223
31. XIDPD = 2.954
32. SACM TOTAL: 9.527
33. VALVE: ALAR 8400A TOTAL: 50.575

The 8400A flow curves (Fig. 5) are very representative of a standard anti-G valve. The increase in flow, at a decreasing rate, with respect to applied G, reaching peak flow values at 6 G, are reasonably typical characteristics of an anti-G valve with adequate performance characteristics. The distribution of peak flow rates with respect to source pressure is also typical. In this valve, this distribution primarily reflects the flow impedance into the first stage regulator. The fluctuations in the open-flow data are shown in Figure 6, as the  $3\sigma$  values, and appear to increase with source pressure in a relatively linear manner.

The principal importance of this test is to estimate the time required by this valve to fill an anti-G suit under very high onset conditions. This consideration is especially important to estimating performance at G-onset rates beyond the capability of the test facility. In the case of the 8400A flow curves, the high slope (i.e., increase in flow rate) between 2 G and 3 G, and the moderately high total-flow values represent good prospects for good performance under high G-onset rates. On the other hand, it would be desirable to reach maximum flow values at a lower G level.

#### 5.1.3 ALAR 8400A Low G-Onset-Rate Tests

The low-onset-rate test-performance score (Table 2, line 21) for the 8400A was also the median score of the five AGV's tested. The Bendix and Electronic AGV's produced considerably higher (less desirable) scores, while the 8000A and RPV valves produced slightly better scores. Line 17 of the PET (Table 2) shows the 8400A scores moderately well in linearity (only the E valve exhibited a better performance), while line 18 shows a median score on source pressure influence. The 8400A exhibits a moderately high stability-repeatability score on line 19, while line 20 indicates a low median hysteresis score.

The low-onset-rate pressure profile for the 8400A is shown in Figure 7. Although only one test item was subjected to this protocol, previous experience indicates this profile is typical of 8400A performance. The dotted lines in Figure 7 indicate the band of acceptable pressure values according to MIL-V-9370D (source cited in section 2.1). The 8400A started applying pressure to the anti-G suit (AGS) at approximately 2.6 G (i.e., approximately 0.6 G late), reached acceptable pressure levels at approximately 3.1 G, and remained near the lower limit of acceptable pressure levels for all higher G levels. The variation in pressure profile with respect to source pressure is extremely small, as may be seen in Figure 7, while the variation due to angular displacement of the valve (shown by the "A" trace) is larger than expected. When the valve is rotated with respect to the G vector,  $20^\circ$  in this case, the response is expected to respond proportionally to the cosine of the angle of rotation. The 8400A response more closely represented  $30^\circ$  rotation, probably indicating the near dominance of frictional forces on the mass spring system. The increased variation in pressure (Fig. 8) over the normal runs supports this conclusion.

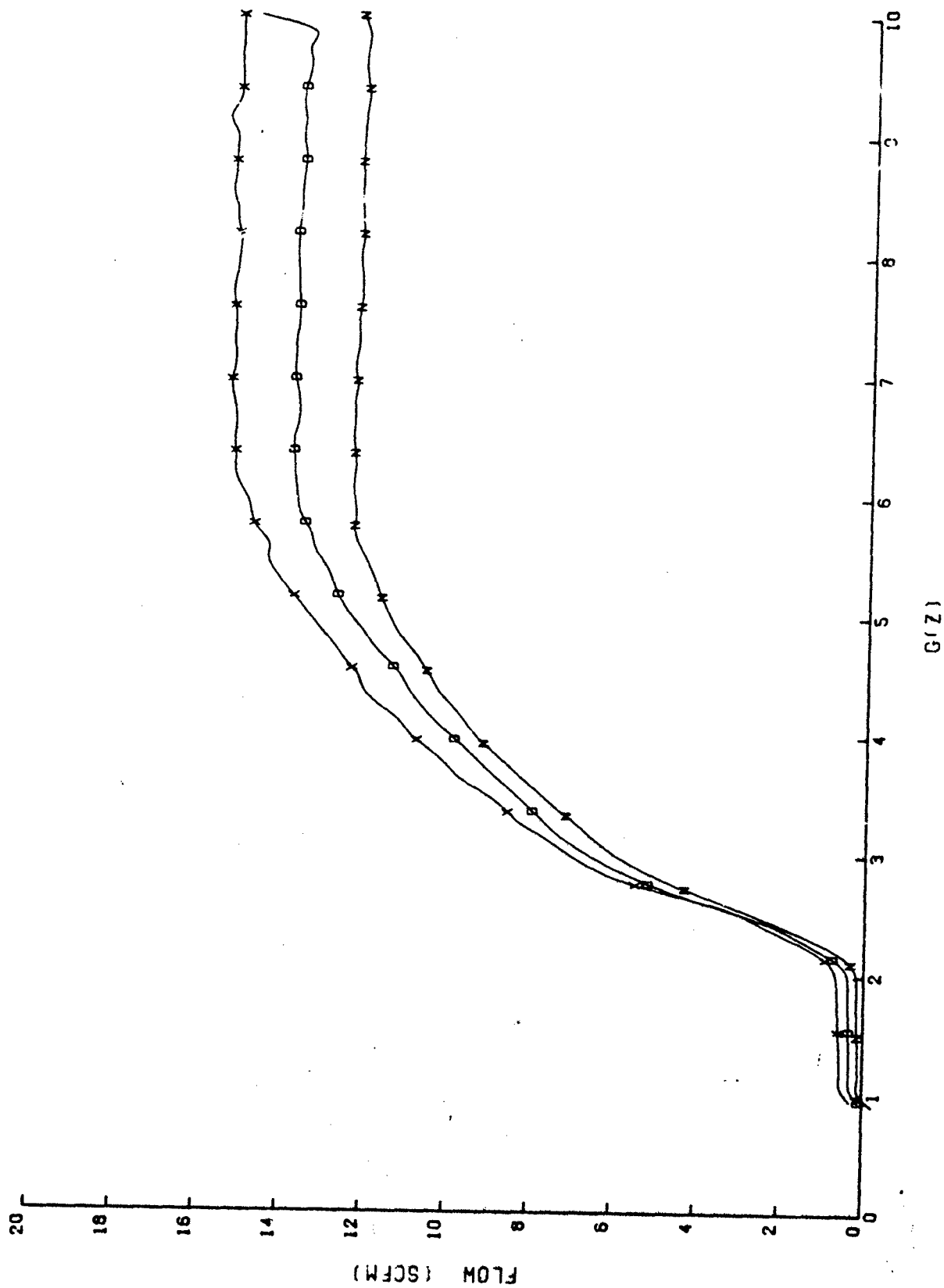


Figure 5. ALAR 8400A flow as a function of pressure.  
[Curves are: D, N, and X.]

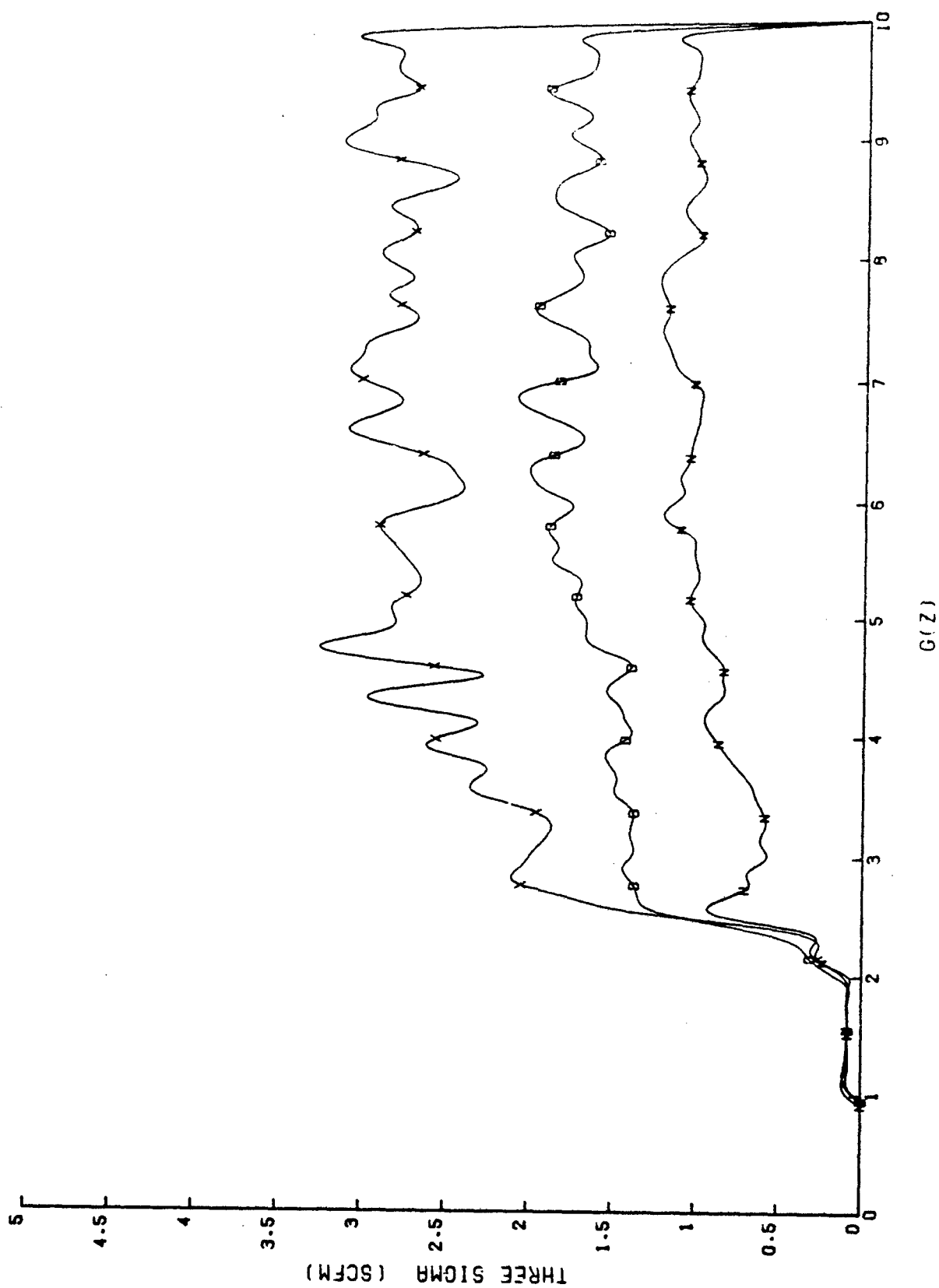


Figure 6. ALAR 34,00A variation (three sigma) in flow as a function of source pressure.  
[Curves are: D, N, and X.]



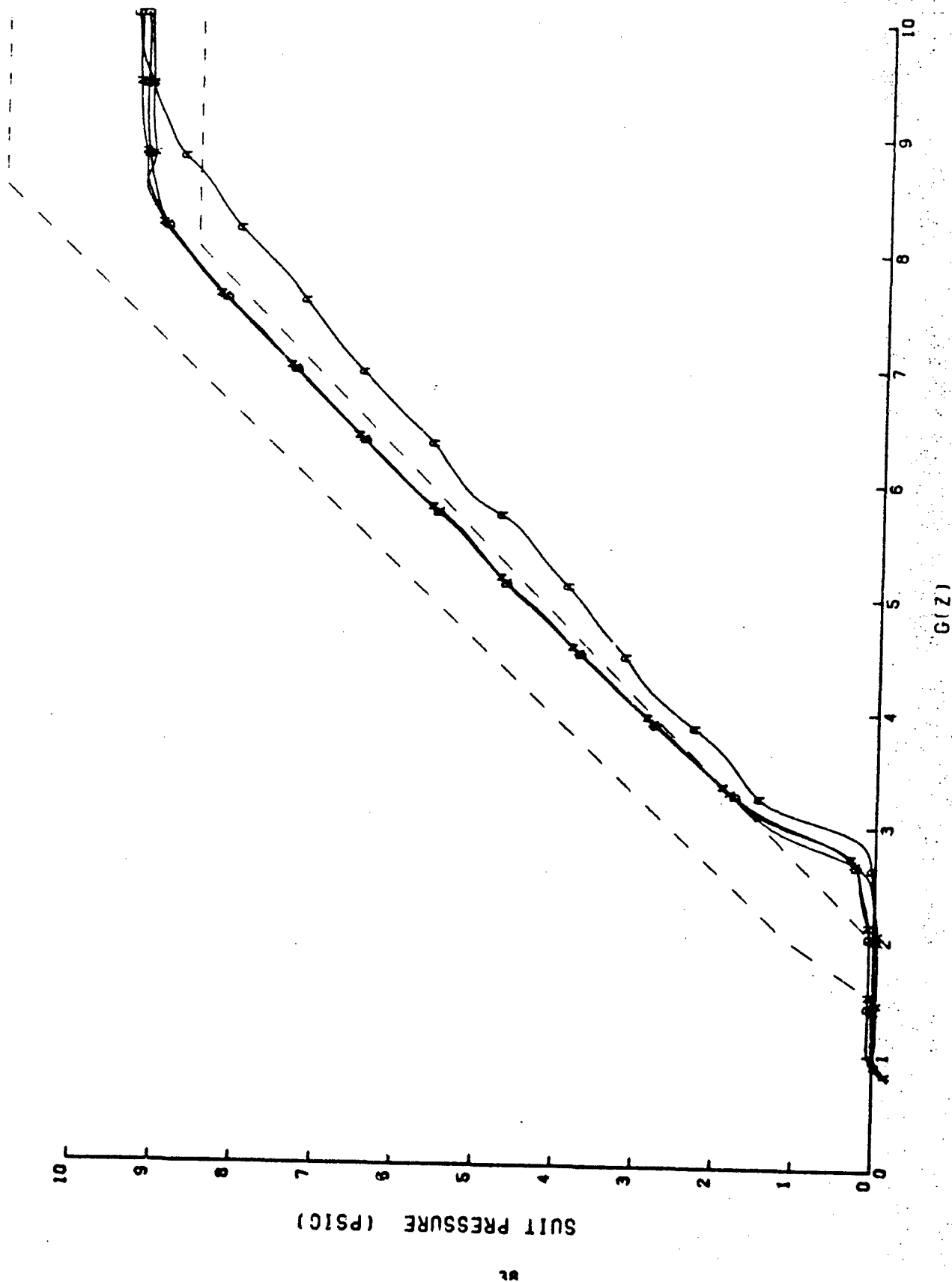


Figure 7. ALAR 8400A 0.1 G/sec pressure profile as a function of source pressure.  
[Curves are: A, D, N, and X.]

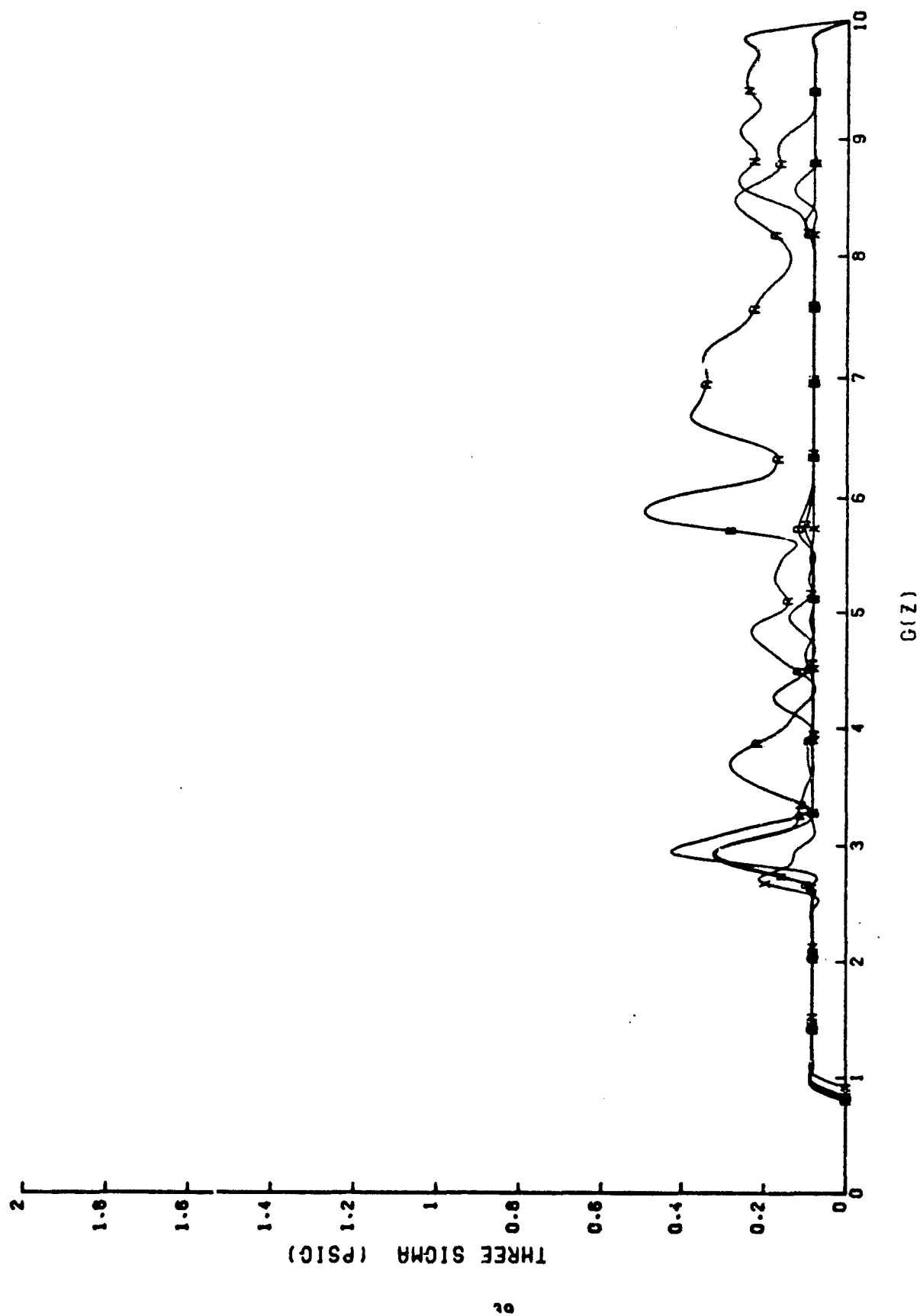


Figure 8. ALAR 8400A 0.1 G/sec pressure stability as a function of source pressure.  
 [Curves are: A, D, N, and X. For "Key," refer to Fig. 4.]

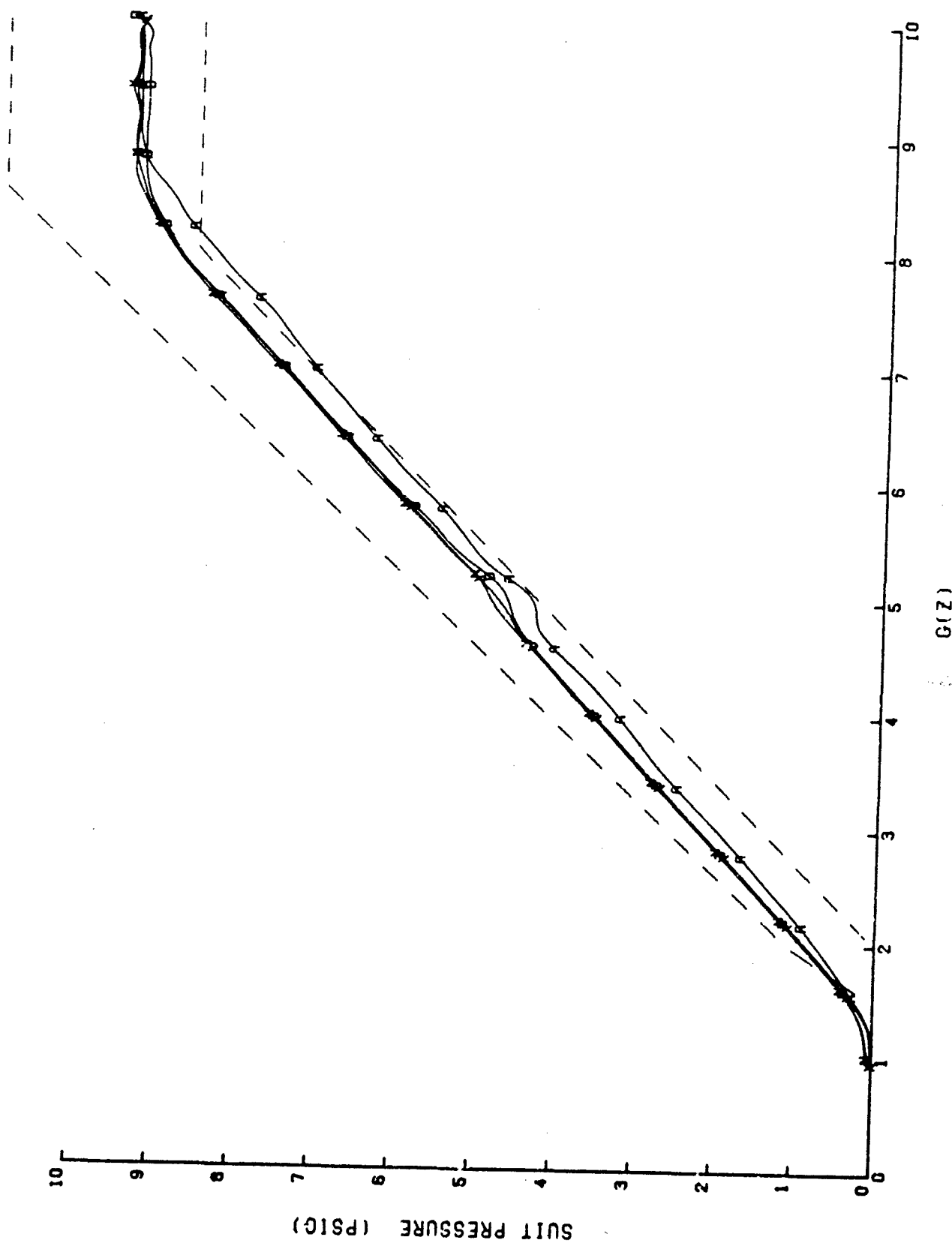


Figure 9. ALAR 8400A 0.1 G/sec decreasing pressure profile as a function of source pressure.  
[Curves are: A, D, N, and X.]

The low-onset decreasing G pressure profiles are shown in Figure 9. The variation with respect to source pressure is very small and essentially random, as expected. The decreasing G pressure profiles of the angularity displacement tests more closely represent theoretical values than the increasing G profile, especially at higher G levels. The perturbation in all decreasing G profiles at 5 G was never explained satisfactorily, and may be an idiosyncrasy of the test specimen.

The differences between the increasing and decreasing G pressure profiles (hysteresis) are shown in Figure 10. In most cases, these values are acceptably low. The large peak at 2.7 G is primarily the result of the characteristic late start exhibited by the 8400A. A comparison of the low-onset and high-onset pressure profiles (and hysteresis) is shown in Figure 11.

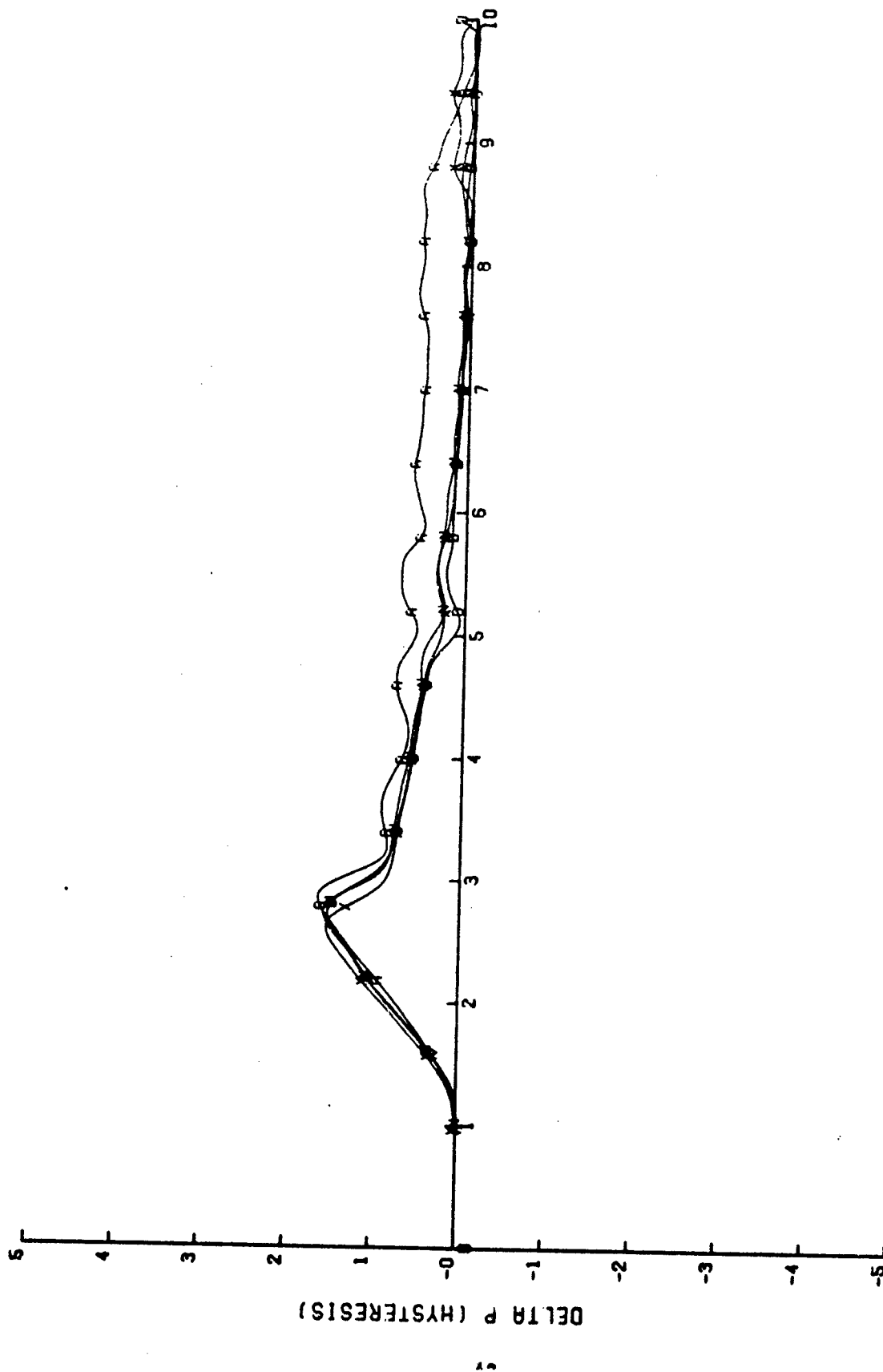
Although the pressure profile starts late and tends to remain near the lower limits of acceptable pressure, the ALAR 8400A performs in a reasonably acceptable manner at low G-onset rates.

#### 5.1.4 ALAR 8400A High G-Onset-Rate Tests

The ALAR 8400A scores 28.158 (refer to line 27 of the PET, Table 2) on the high onset-rate tests. This score is moderately higher than the mean of the five valves tested and well above the median (i.e., 8000A at 21.061) valve performance. The 8400A's linearity competed with the Bendix for worst linearity with the 4.384 shown on line 22 of the PET (Table 2). The source pressure influence on high G-onset response was acceptably low, the 6.642 shown on line 23 of the PET being the median of five valves tested and only slightly worse than the mean score of 6.597. The stability and repeatability score, shown on line 24, is a low median of 3.809, the mean of 4.591 resulting from a relatively poor performance by the Bendix AGV. Line 25 of Table 2 shows a hysteresis score of 3.272, matching a five-valve mean of 3.258 and a median of 3.030. The score shown on line 26 is related to the pressure profile lag resulting from increasing G-onset rates and, because of its importance, is weighted more heavily than the other high G-onset rate scores. The 8400A's 10.051 is relatively poor compared to the RPV's 2.768 and a five-valve mean of 8.134.

The influence of G-onset rate on the 8400A's pressure profile is shown in Figure 12. The increasing lag in pressurization of the AGS is caused by a "dead volume," characteristic of deflated bladders, which must be filled before pressure starts increasing. The increasing peak rate of pressure increase for increasing G-onset rates (through 1 G/sec), shown in Figure 13, indicates increased open-flow rates had been achieved by the valve (Fig. 5) before pressurization began. The unstable nature and decreased amplitude of the 1.5 G/sec profile in Figure 13 indicates the valve capacity was outrun by the G-onset rate.

The influence of source pressure on the high-onset performance of the 8400A is shown in Figure 14. These profiles, along with those of Figure 15, lend further credence to the observation that the 8400A was outrun by the 1.5 G/sec onset rate. The curves indicate the minimum source pressure resulted in the least pressure lag, while the maximum source pressure resulted in the greatest pressure lag. The extremely high run-to-run variation, indicated by Figure 15, suggests the relative position of these curves is nearly random and has no particular significance.



G(Z)

Figure 10. ALAR 8400A 0.1 G/sec pressure hysteresis as a function of source pressure.  
[Curves are: A, D, N, and X.]

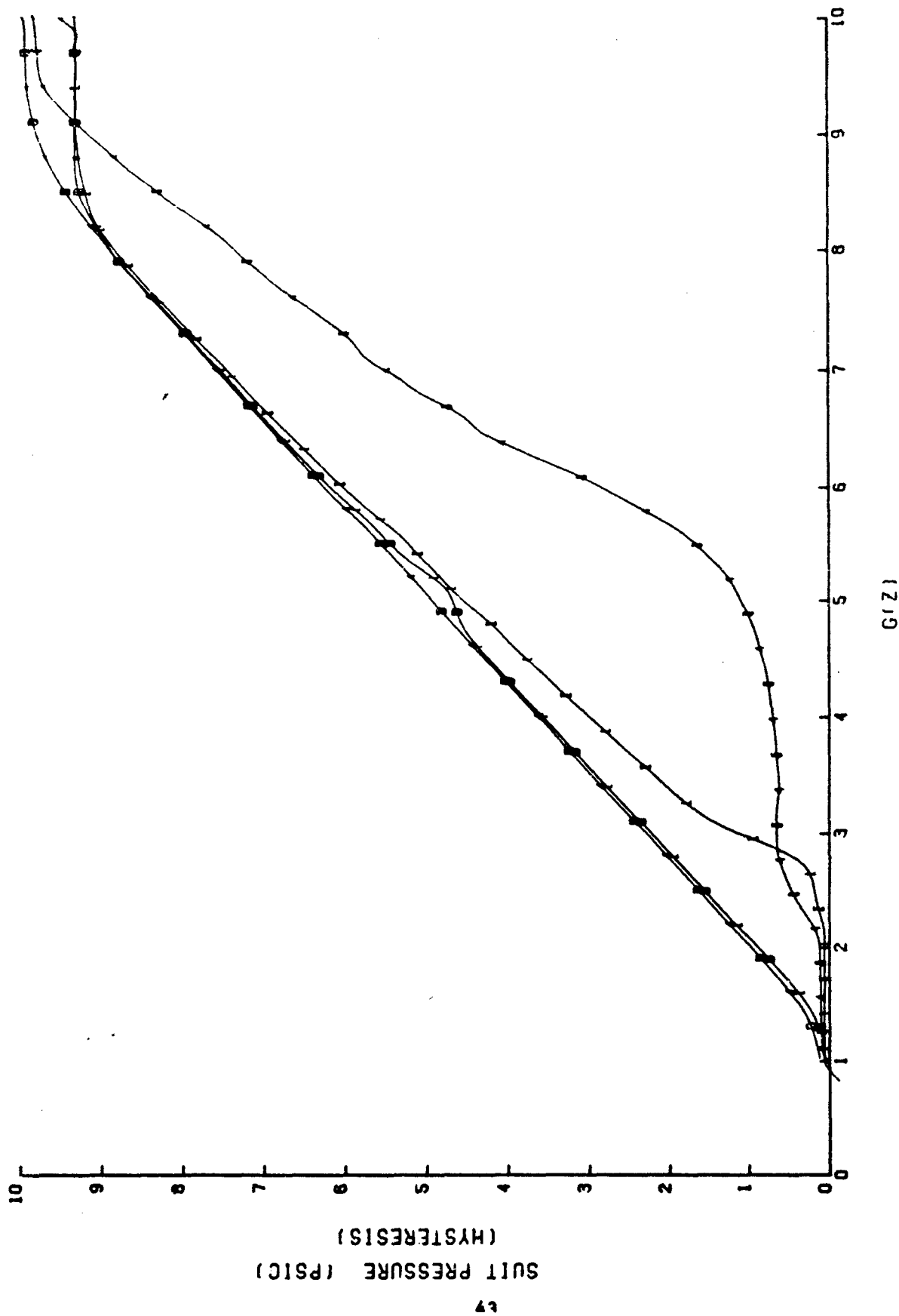


Figure 11. ALAR 8400A pressure profile comparison as a function of onset rate.  
[Curves are: 1I, 4I, 1D, and 4D.]

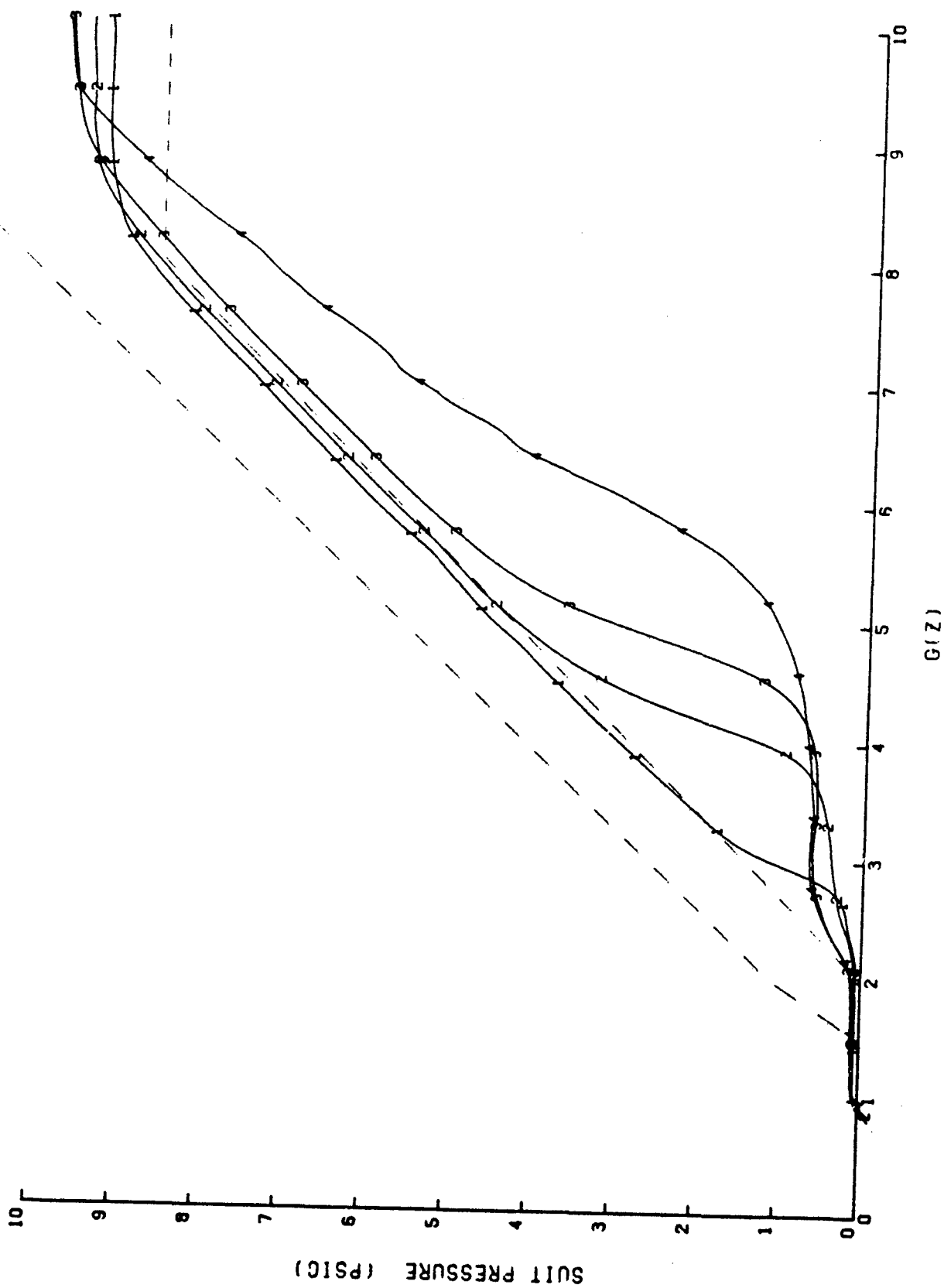


Figure 12. ALAR 8400A pressure profile as a function of G-onset rate.  
[Curves are: 1, 2, 3, and 4.]

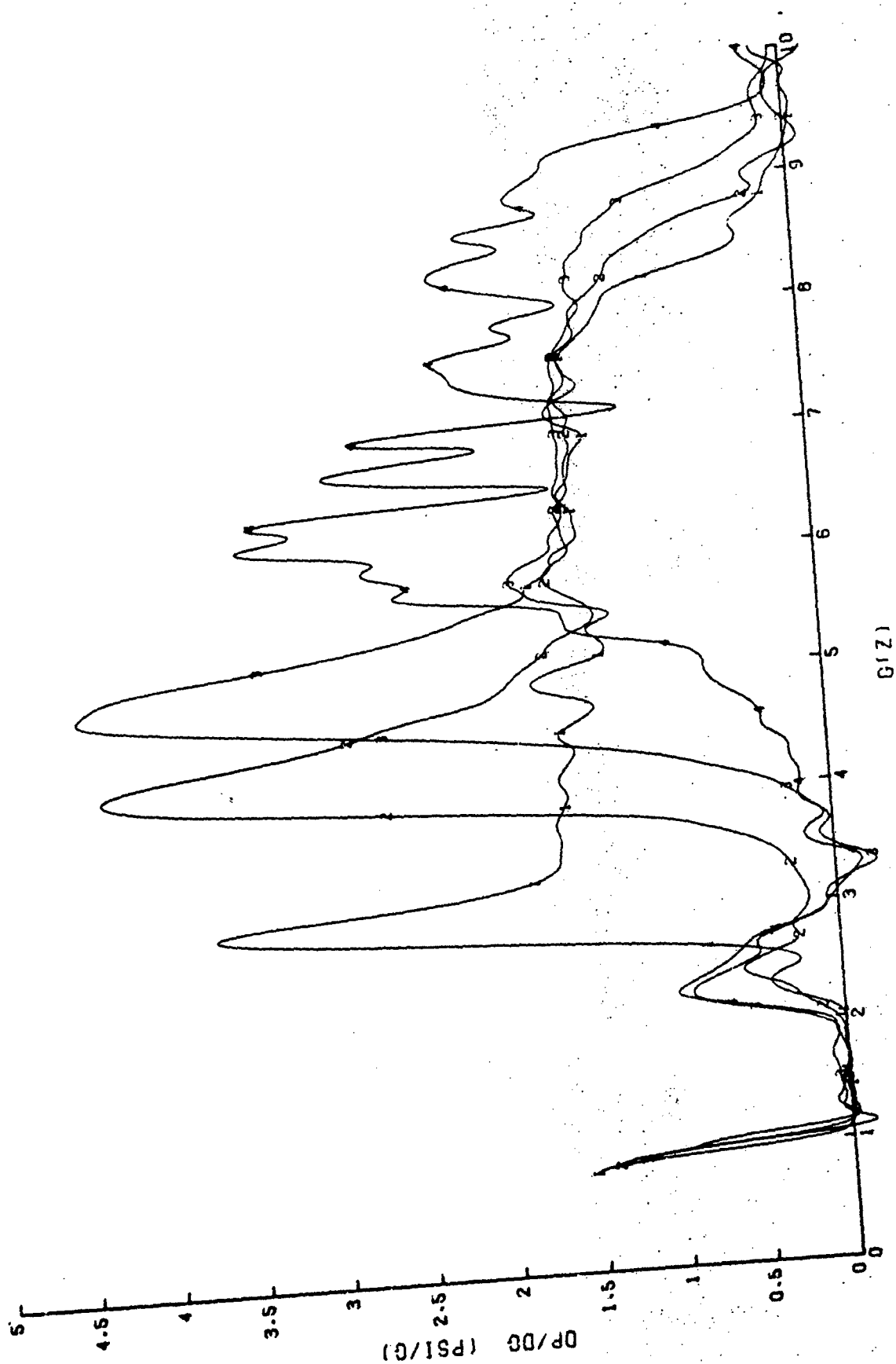


Figure 13. ALAR 8400A  $dP/dG$  as a function of G-onset rate.  
 [Curves are: 1, 2, 3, and 4. For "Key," refer to Fig. 4.]



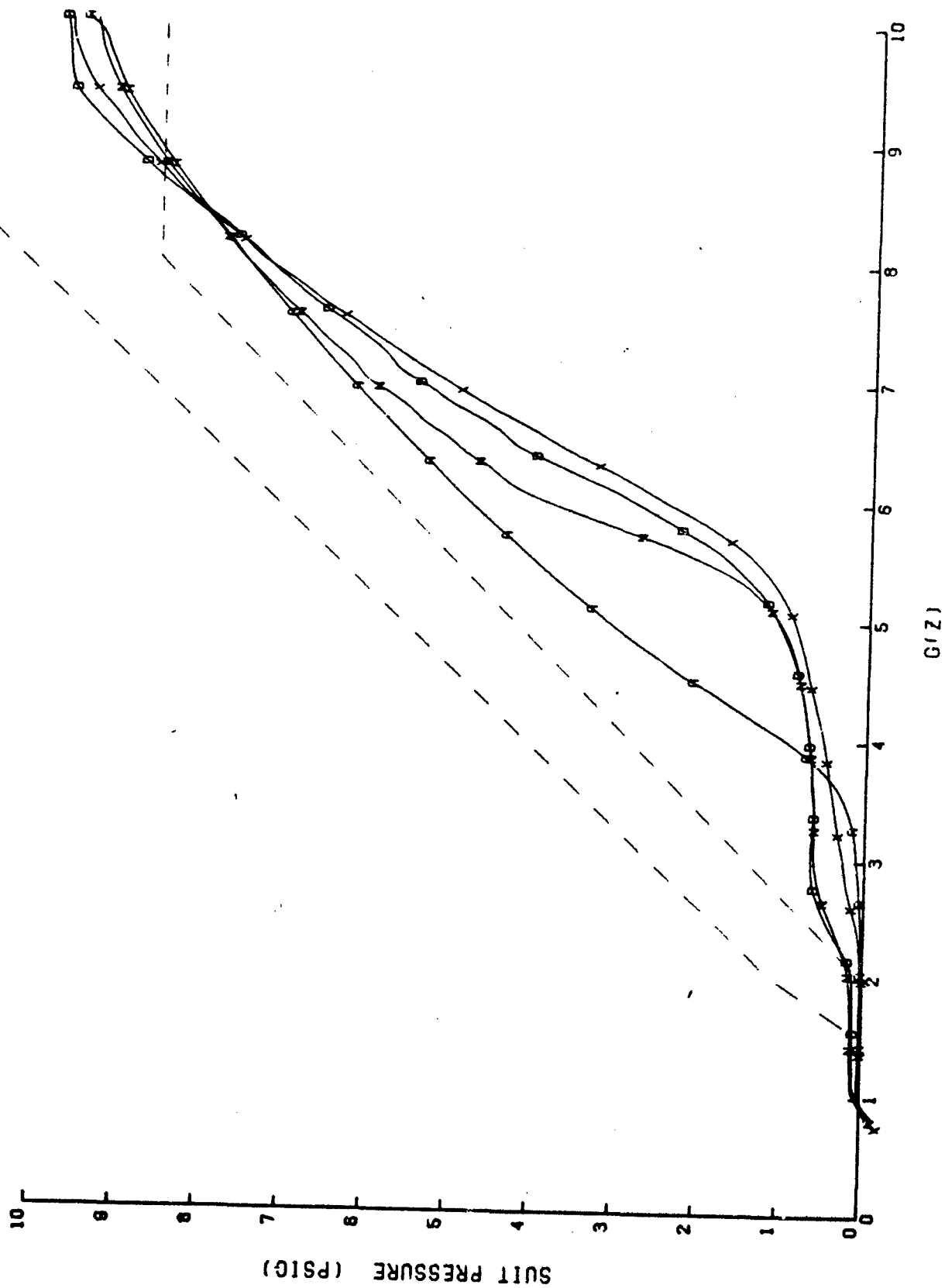


Figure 14. ALAR 8400A 1.5 G/sec pressure profile as a function of source pressure.  
[Curves are: A, D, N, and X.]

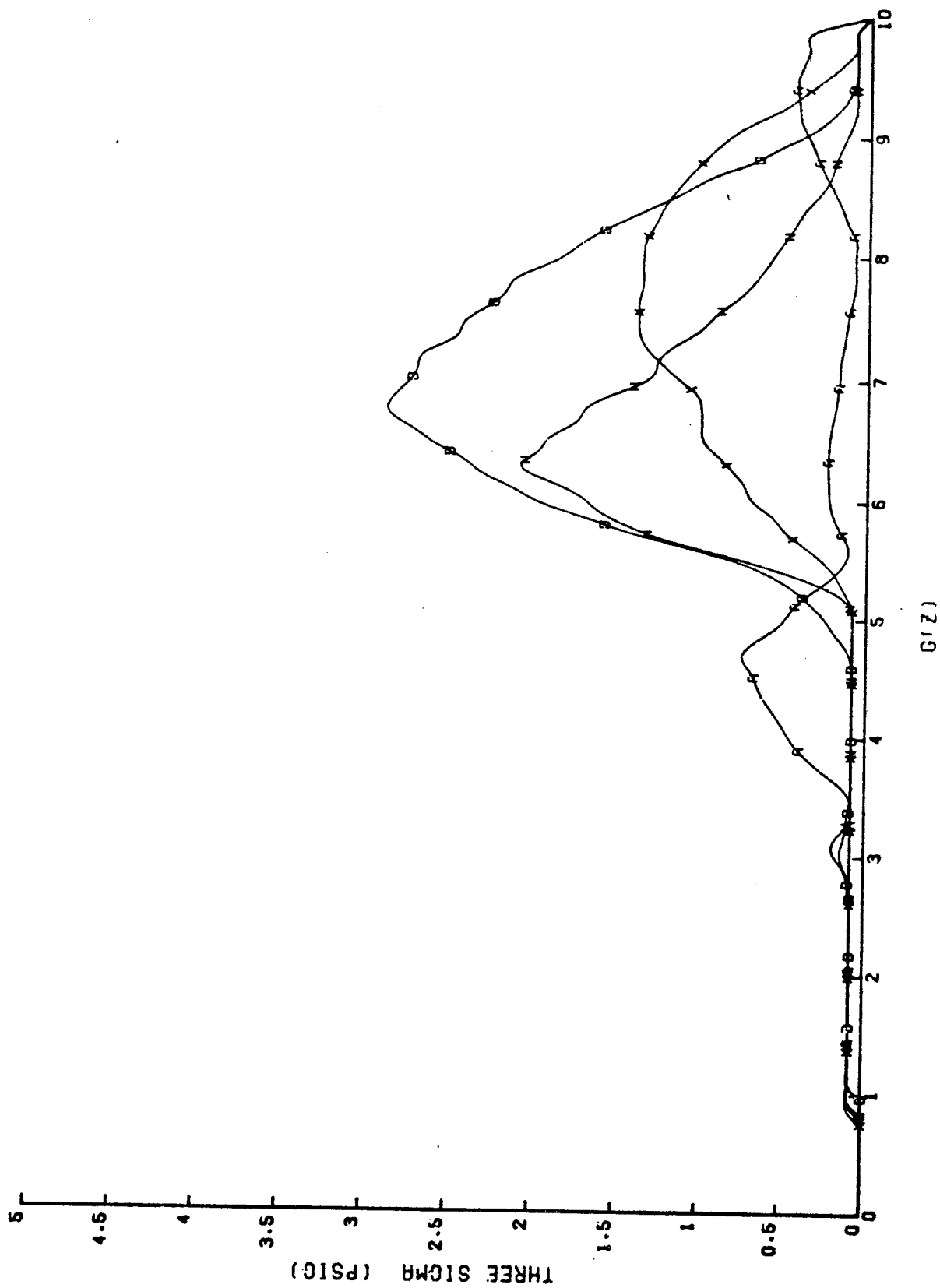


Figure 15. ALAR 8400A 1.5 G/sec pressure variation as a function of source pressure.  
[Curves are: A, D, N, and X.]

The 1.5 G/sec decreasing G profiles in Figure 16 indicate that the 8400A performs nearly as well at high "offset" rates as at low "offset" rates. The large hysteresis peaks shown in Figure 17 result entirely from the pressurization lag.

The ALAR 8400A performs acceptably at low G-onset rates. The performance may be rated marginal at 0.5 G/sec, probably unacceptable at 1.0 G/sec, and certainly unacceptable at 1.5 G/sec and higher.

#### 5.1.5 SACM Tests

The ALAR 8400A AGV scored a very respectable median, 9.527, on the SACM tests, as shown on line 32 of the PET (Table 2). The RPV scored only slightly better, while the Electronic AGV scored considerably better. A review of the individual line scores (lines 18 - 31 of the PET) indicates the 8400A and the RPV made essentially the same score, and together formed the median performance of the five valves tested. The 8400A scored better on lines 28 and 29, while the RPV did better on 30 and 31. The 28 → 31 progression of scores has no known significance. In all cases, the E valve did considerably better, while the 8000A did significantly worse, and the Bendix performed very poorly.

The pressure profiles in Figure 18 represent the actual and ideal pressures that should result from the G stimuli resulting from an SACM test, when a minimum source pressure is applied to the AGV and a maximum "suit" volume is attached. The ideal pressure for all SACM tests was derived from the mid-source pressure profile shown in Figure 7, and the actual instantaneous G value applied. The differences between the real and ideal pressures, along with corresponding onset rates, are shown in Figure 19. The abscissa of this graph represents the integral of G with respect to time. This device allows a real (unweighted) indication of magnitude, while the size of the excursion (actually the area under the curve) is weighted by the G level. In this manner, a 0.5-psig excursion at 6 G will appear twice as large as a 0.5-psig excursion at 3 G, even though the amplitudes are the same. The area under these curves is used as an evaluation factor in the PET (Table 2). The 8400A's "min-max" curves (Fig. 19) indicate frequent pressure excursions in excess of 1 psig (positive and negative), while the maximum onset rates achieved during the tests were +1.0 G/sec and -1.4 G/sec.

The SACM pressure profiles for the maximum source pressure and minimum suit volume are shown in Figure 20, while the associated difference curves are in Figure 21. In this case (Fig. 21), the pressure excursions never exceeded 0.8 psig, while the onset rates reached 1.1 G/sec and -1.5 G/sec. The median-source-pressure median-suit-volume case is shown in Figures 22 and 23. As might be expected, the pressure excursions reach 1 psig, larger than those in the min-max case. The onset rates attained in this SACM are comparable to those in the previous two tests ("mid-mid," and "max-min").

The last two figures (Figs. 24 and 25) are unique only in that the valve was run with its centerline at an angle of 20° to the G vector. Since the ideal pressure here was derived in the same manner as in the previous three sets, the actual pressure is expected to be low (section 5.1.3); and Figure 25

confirms this expectation. Otherwise, the curves are comparable with those in Figures 22 and 23 except that, perhaps, a little more tendency to overshoot is exhibited.

Comparing the results of the 8400A's high G-onset rate tests and the SACM tests suggests that they represent a dichotomy. The results of the SACM tests suggest very acceptable performance under simulated combat conditions, while the high G-onset tests suggest marginal to poor performance. Two comments pertain. First, the positive onset rates in the SACM's never exceeded 1.1 G/sec and were generally well below 1.0 G/sec; the high negative onset rates were never a problem, as indicated in Figure 16. Second, the SACM profile starts with a gentle 0.1 G/sec onset, allowing the valve to fill the dead space in the AGS, and eliminating the lag in onset pressurization, thus suggesting that a revised SACM profile should be considered.

#### 5.1.6 Conclusion on the ALAR 8400A's Performance

The ALAR 8400A performs very well under a wide variety of conditions. Failure tests (refer to Volume II, section 1.4.3, of this report) suggest that it is, in addition, an extremely reliable piece of equipment. The valve probably should be limited to weapon-system and mission combinations which do not require response to G-onset rates greater than 1 G/sec.

### 5.2 Bendix FRI39A2 Anti-G Valve Test Results

#### 5.2.1 Bendix FRI39A2 Valve and Test Description

The FRI39A2 anti-G valve (designed and produced by the Bendix Corporation, Instrument and Life Support Division, Davenport, Iowa) is one of four valves (FRI39A1, and -A2; FRI40A1, and -A2) which are identical except that: the FRI39 type has a straight outlet fitting, and the FRI40 has a curved outlet fitting; the A1 versions have a metal orifice, and the A2 versions have a jeweled orifice.

The FRI39A2 uses a mass spring system for sensing acceleration (G) force and regulation suit pressure. As G forces aligned with the vertical axis of the valve ( $G_z$ ) are encountered, the mass is forced down, compressing a spring and closing a valve on the top side of a diaphragm. Pressure is constantly being bled to both sides of this diaphragm through a small orifice so that, when the valve on top of the diaphragm is closed, pressure builds up on top of the diaphragm, forcing it down, closing the dump valve, and tipping the pilot valve open. When the pilot valve opens, pressure above the main valve diaphragm drops and the main valve opens, porting pressure to the suit outlet. When acceleration ( $G_z$ ) is reduced, the spring acting on the mass opens the valve above the diaphragm and opens the dump valve which vents suit pressure.

---

**EDITOR'S NOTE:** As indicated by the authors, the information in section 5.2.1 parallels (of necessity) corresponding passages in SAM-TR-78-11.

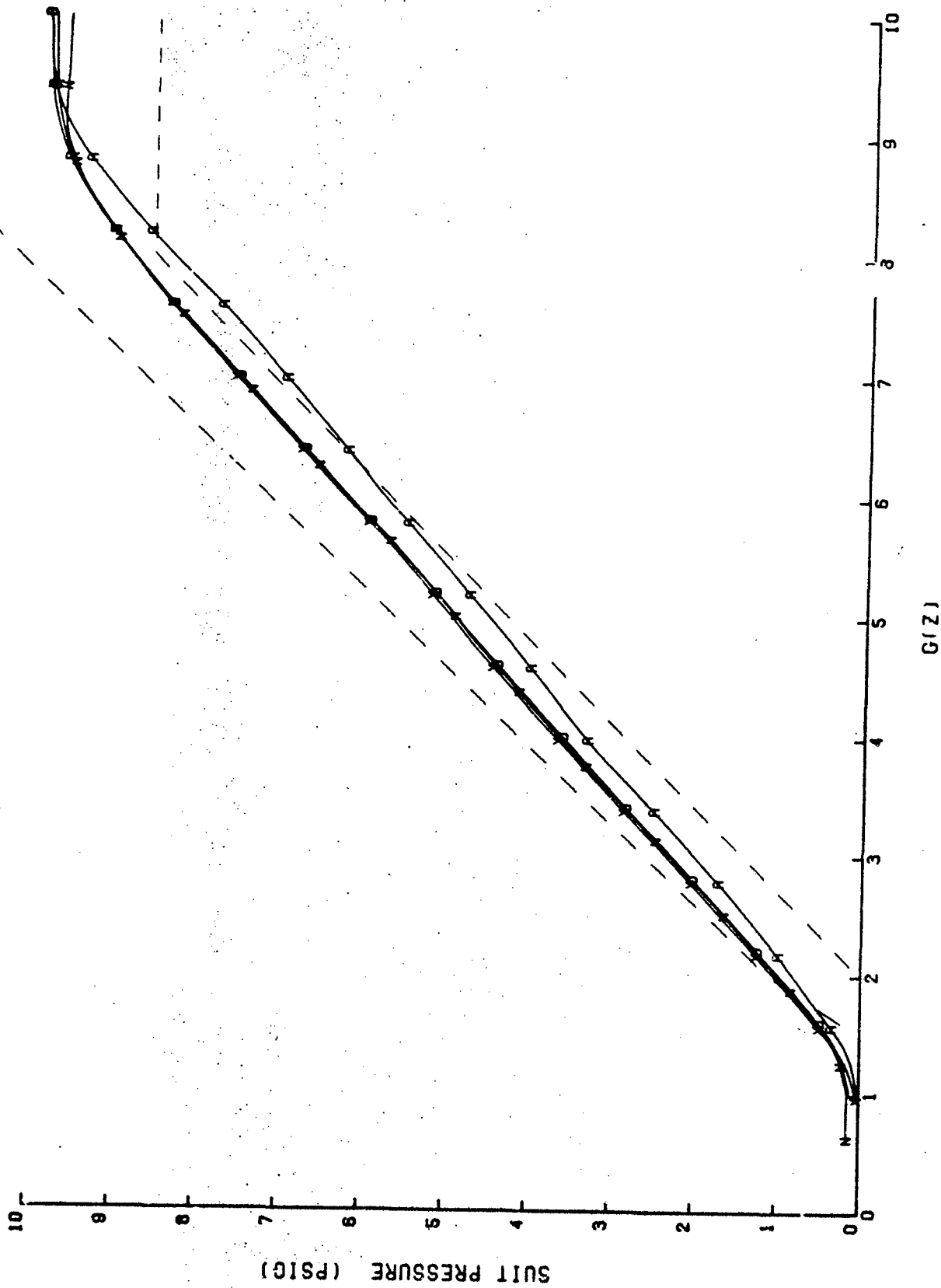
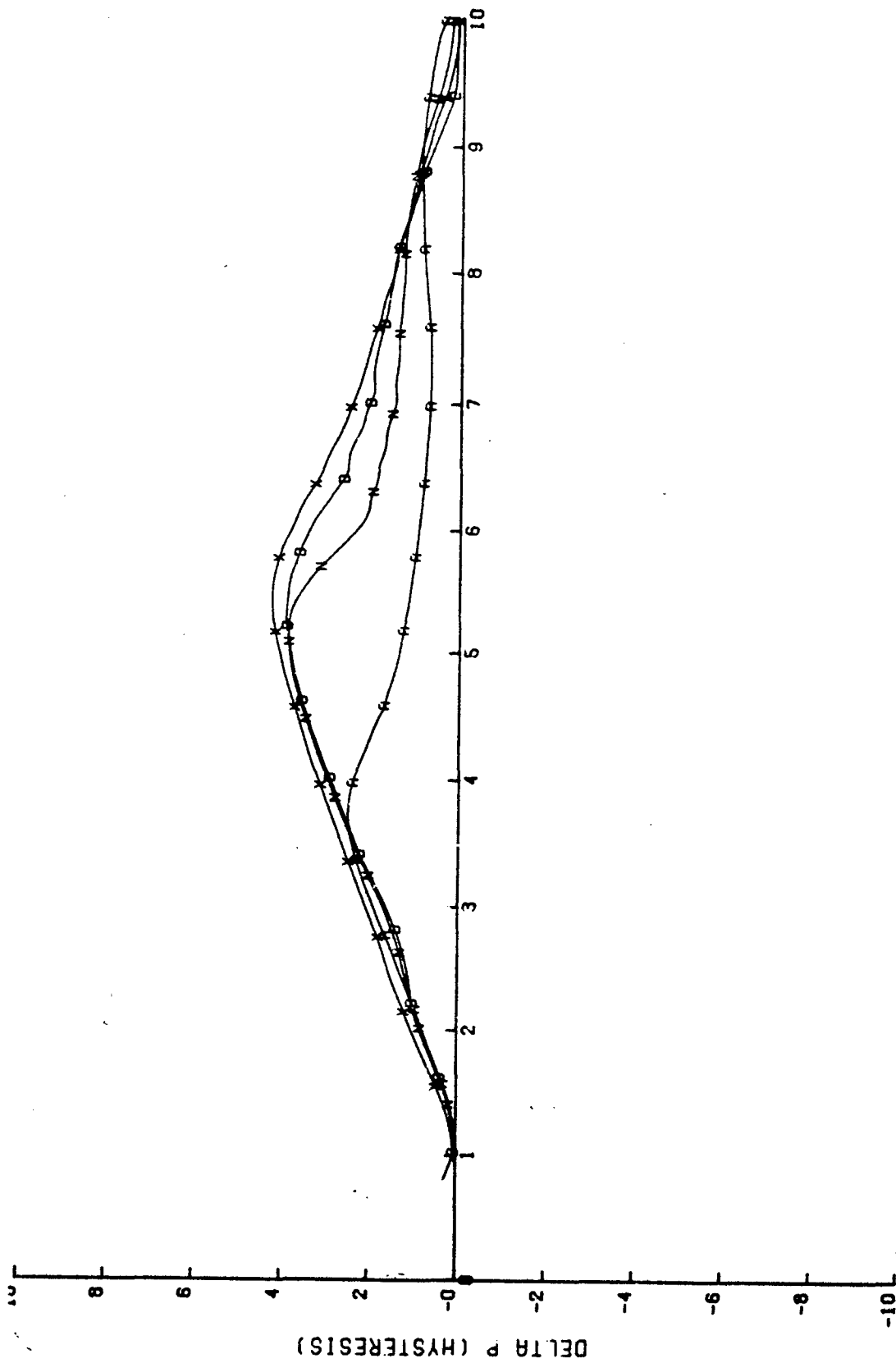


Figure 16. ALAR 8400A 1.5 G/sec decreasing pressure profile as a function of source pressure.  
[Curves are: A, D, N, and X.]



G(Z)

Figure 17. ALAR 8400A 1.5 G/sec pressure hysteresis as a function of source pressure.  
[Curves are: A, D, N, and X.]

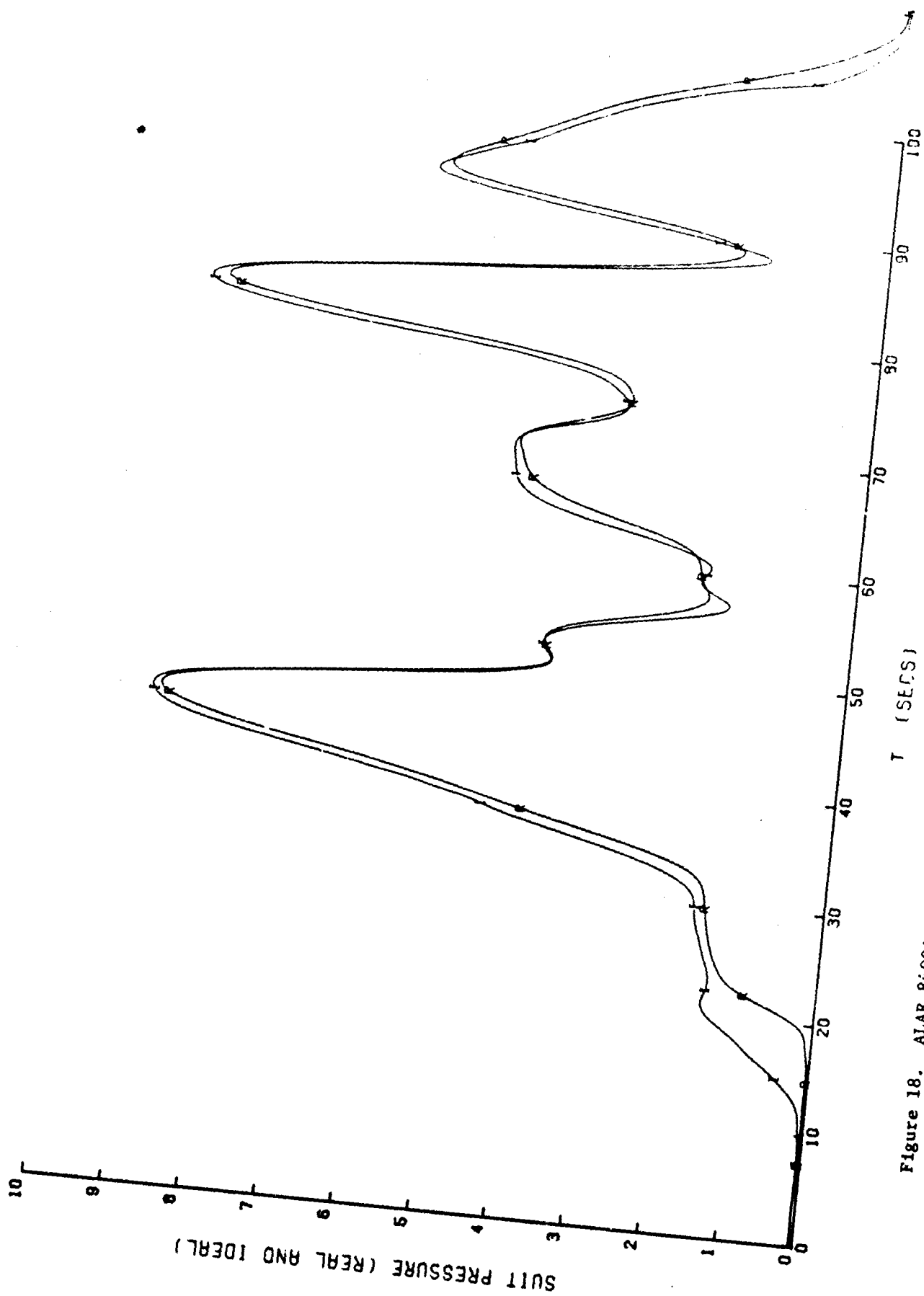


Figure 18. ALAR 8400A SACM pressure profile comparison with minimum source pressure and maximum suit volume. [Curves are: I and R.]

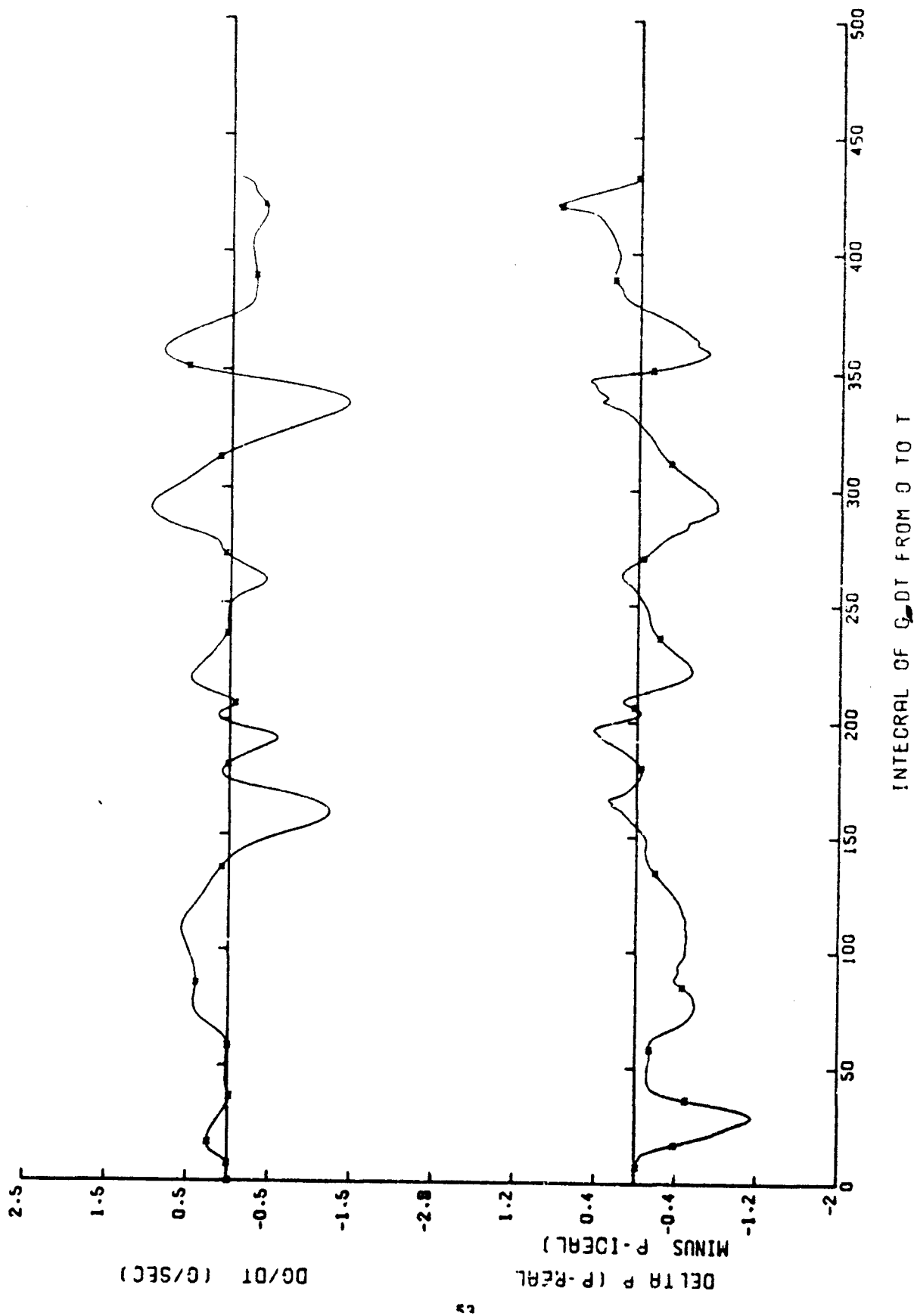


Figure 19. ALAR 8400A pressure deviation and  $dG/dt$  for the minimum source pressure and maximum suit volume SACM. [Curves are: \*.]



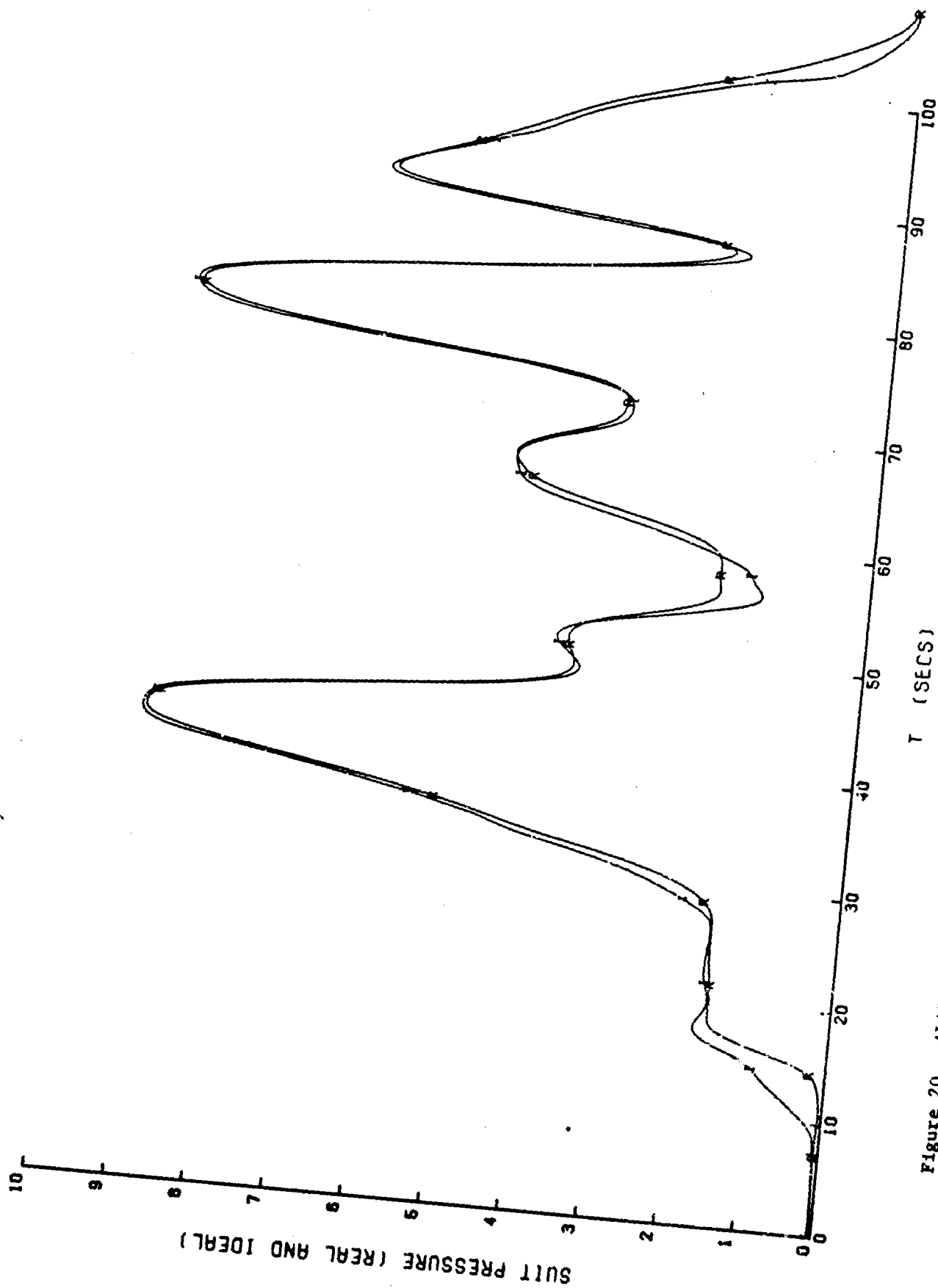


Figure 20. ALAR 8400A SACH pressure profile comparison with maximum source pressure and minimum suit volume. (Curves are: I and R.)

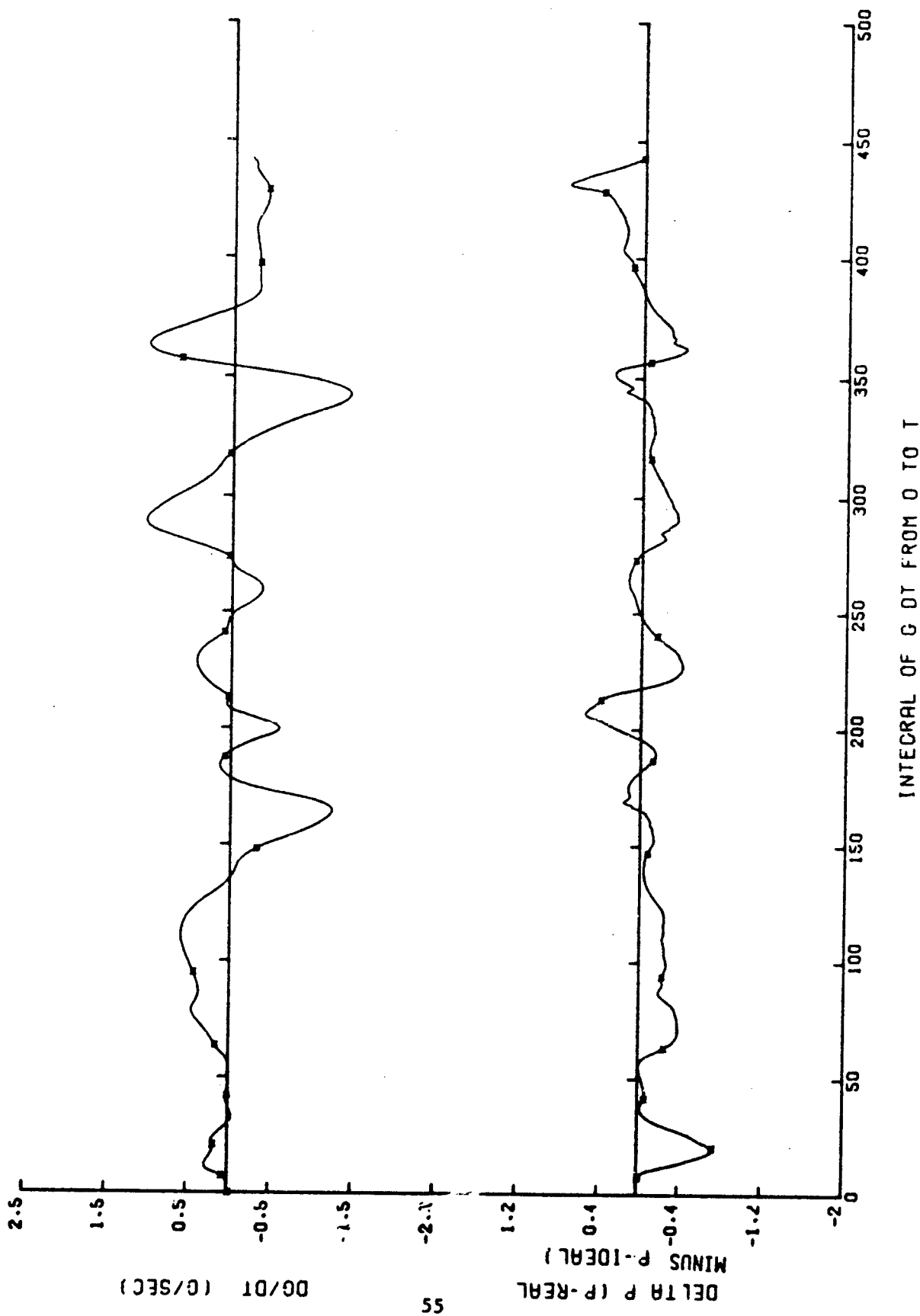


Figure 21. ALAR 8400A pressure deviation and  $dG/dt$  for the maximum source pressure and minimum suit volume SACM. [Curves are: +, ]

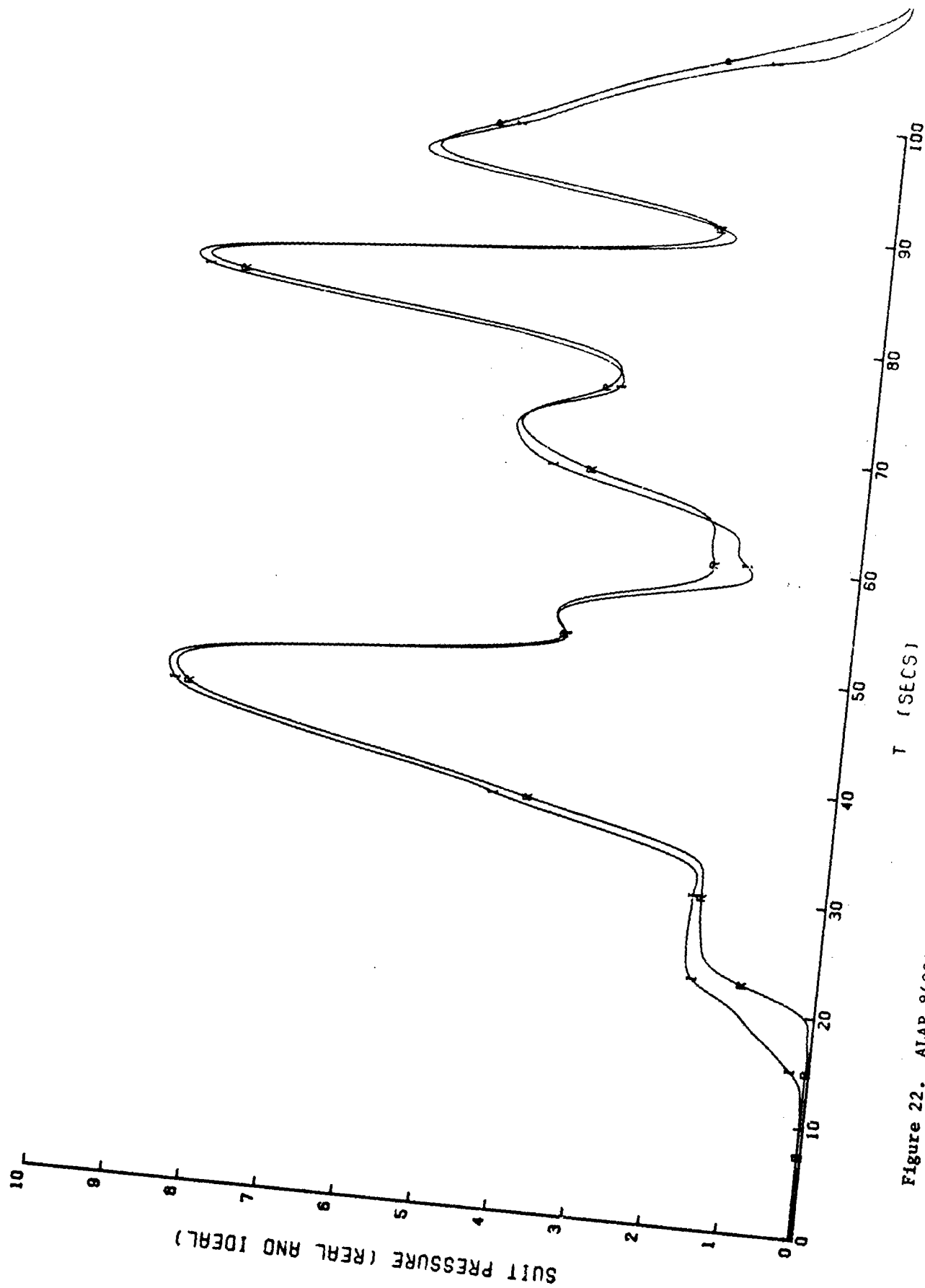
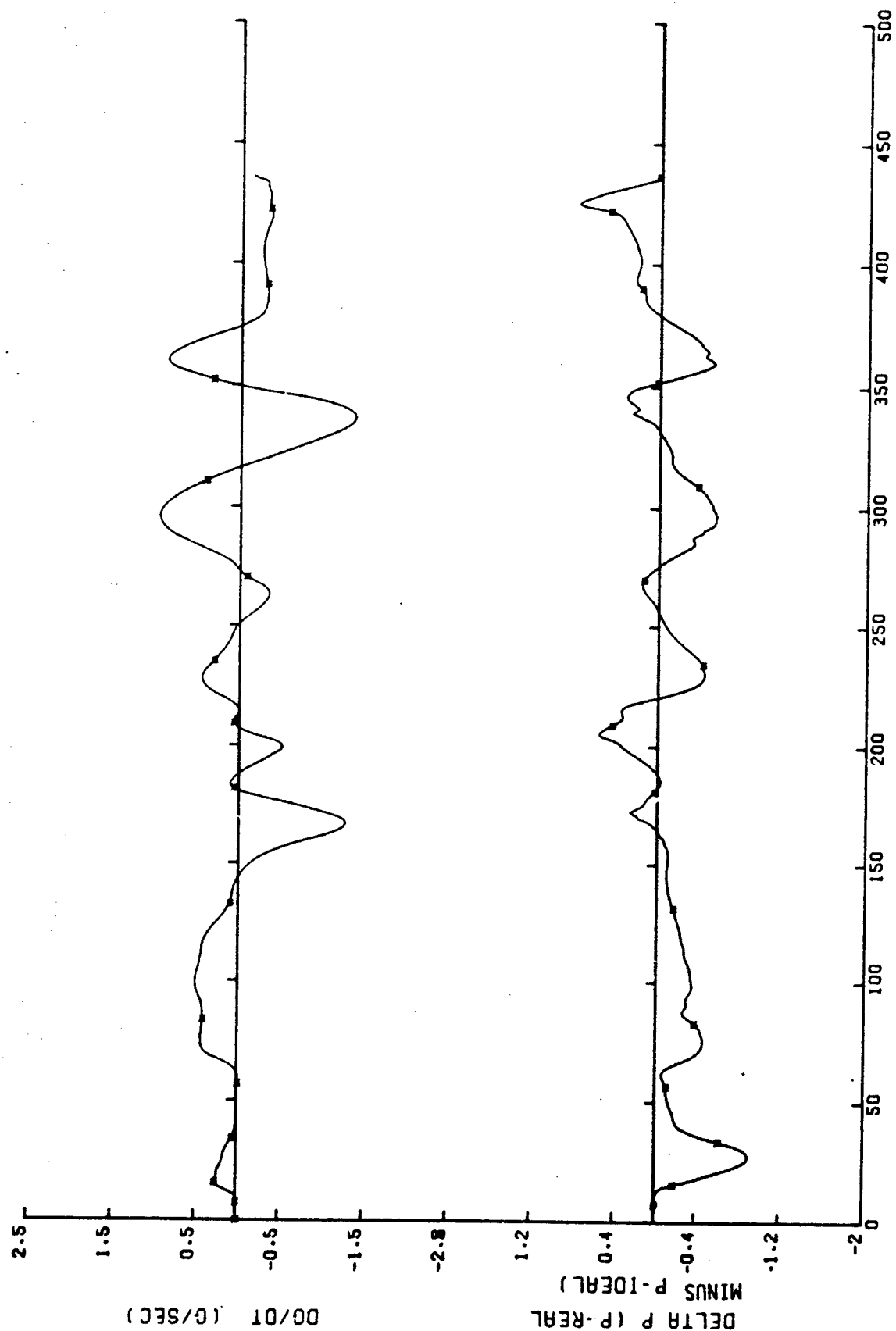


Figure 22. ALAR 8400A SACM pressure profile comparison with median source pressure and suit volume. [Curves are: I and R.]



INTEGRAL OF  $G/dt$  FROM 0 TO  $T$

Figure 23. ALAR 8400A pressure deviation and  $dG/dt$  for the median source pressure and suit volume SACM. [Curves are: \*.]

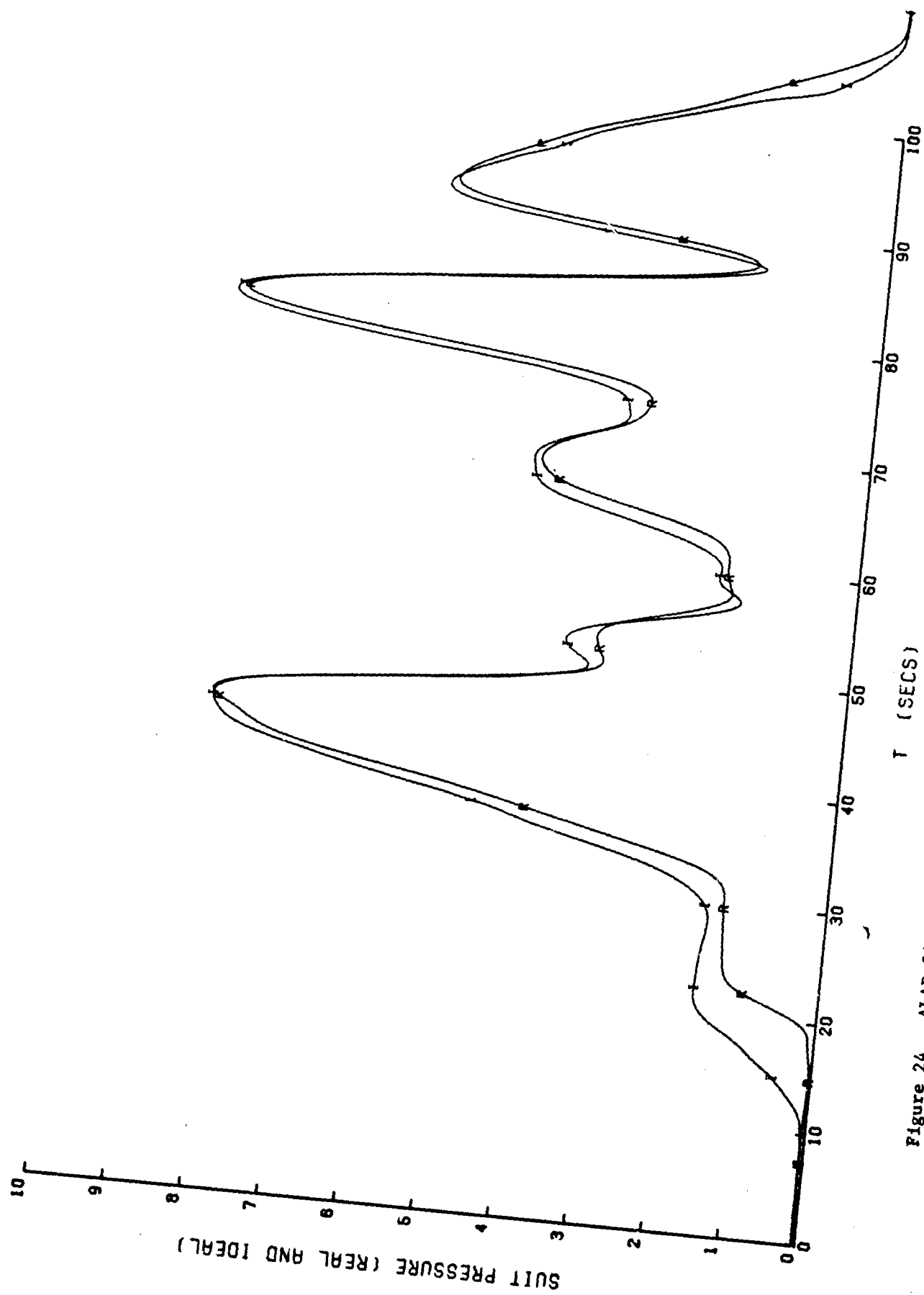


Figure 24. ALAR 8400A pressure profile comparison with G vector misalignment.  
 [Curves are: I and R.]

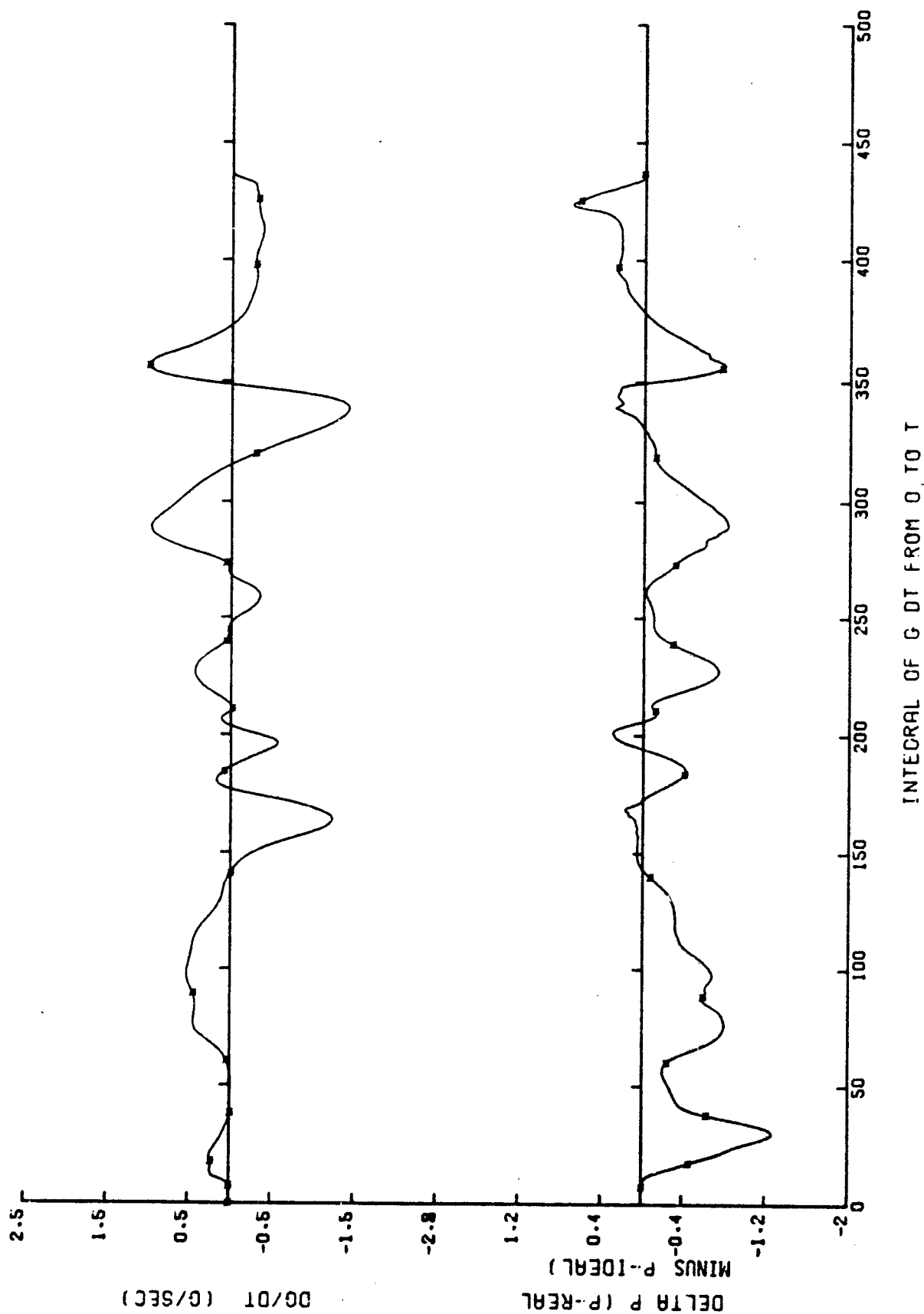


Figure 25. ALAR 8400A pressure deviation and  $dG/dt$  for the G vector misalignment SACM.  
[Curves are: \*.]

The FR139A2 is designed to actuate (i.e., to begin to apply suit pressure) at a nominal stimulus of 2.0 G<sub>z</sub>. The suit is pressurized at a nominal rate of 1.5 psig/G. Because the FR139A2 uses differential pressure across a diaphragm for pressure regulation, there is a constant pressure bleed through the valve when the G<sub>z</sub> and suit pressure inputs are balanced or when less than 2.0 G<sub>z</sub> is applied. This bleed rate varies with source pressure. At a source pressure of 70 psig, the bleed rate would be between 0.008 SCFM and 0.0095 SCFM.

The FR139A2 is fitted with a spring-loaded relief valve designed to open between 9 psig and 11 psig. This relief valve has sufficient flow to limit suit pressure to 11 psig with a source pressure of 55 psig.

The FR139A2 is designed to operate with a maximum supply pressure of 120 psig, and has been shown to operate properly with supply pressures as low as 40 psig. It is fitted with a button at the top of the valve which allows the mass to be depressed manually and provides a test feature.

The physical dimensions of the valve are 2.2 in. x 1.88 in. (5.59 cm x 4.78 cm). The FR139A2 weighs approximately 0.5 lb (1.1 kg).

For purposes of SVTP testing and GVALVPGM analysis, standard values were assigned for the FR139A2 and are shown in the PET (Table 3, lines 1 - 7). This valve was designed to accommodate a relatively narrow range of source pressures compared to the selected SVTP standard, the ALAR 8400A. This design limits, to some extent, the variety of aircraft to which this valve is applicable. As a result of this limitation, the PET design total for the FR139A2 is 4.8333.

#### 5.2.2 Bendix FR139A2 Flow Tests

The flow test performance score of the Bendix FR139A2 AGV, represented by line 16 of Table 2, was slightly higher (less desirable) than the median score of the five valves tested under this contract. The total open-flow test, shown on line 12 of Table 3, indicates the lowest air handling capacity of all valves tested. Tests for source pressure influence on the open-flow performance yielded a surprisingly low median score for the five valves tested, as shown on lines 13 and 14 of Table 3. The ALAR 8400A shows slightly more source pressure influence in the PET, while the E valve showed an even less desirable score (refer to section 5.3.2). In this case, the PET score does not properly represent the relative performance quality of the valve. Lines 13 and 14 of Table 3 are calculated from the cumulative differences between flows for the various source pressures. When total flows are low, differences are proportionally low and, in this case, yield favorable test values for the Bendix. The open-flow variation of the FR139A2 (Table 3, line 15) indicates it is the least stable and repeatable of all the valves tested.

The FR139A2 flow curves (Fig. 26) clearly indicate two modes of operation. The median and maximum source pressure cases indicate reasonably normal increases in flow with applied G (ignoring the low values, for the time being). The minimum source pressure case, on the other hand, indicates a "starved" pressure regulator and significantly reduced capability. The fluctuations in the open-flow data are shown (Fig. 27) as the three sigma values, and appear to increase with source pressure in a relatively linear manner.

TABLE 3. BENDIX FR139A2 ANTI-G VALVE PERFORMANCE EVALUATION TABLE

TEST STANDARDS:

1. SPMIN = 40. PSIG
2. SPMID = 70. PSIG
3. SPMAX = 120. PSIG
4. THETA = 20. DEGREES
5. SVMIN = 6. LITERS
6. SVMID = 10. LITERS
7. SVMAX = 14. LITERS

CHARACTERISTIC NUMBERS:

8. XSPMX = 2.5000
9. XSPMN = 1.3333
10. XTHTA = 1.0000
11. DESIGN TOTAL: 4.833
12. XFLBR = 3.542
13. XDOLF = 1.705
14. XDDLFF = 1.709
15. XSIGF = 0.191
16. FLOW TOTAL: 7.47
17. XCCP1 = 3.116
18. XDDP1 = 3.699
19. XSCP1 = 2.350
20. XDPP1 = 2.363
21. LOW-ONSET TOTAL: 11.527
22. XCCP2 = 4.929
23. XDDP2 = 13.810
24. XSGP2 = 11.772
25. XDPP2 = 7.457
26. XTDP2 = 16.616
27. HIGH-ONSET TOTAL: 54.585
28. XIDPA = 5.193
29. XIDPB = 11.766
30. XIDPC = 6.725
31. XIDPD = 9.392
32. SACM TOTAL: 33.076
33. VALVE: BENDIX FR139A2 TOTAL: 111.168



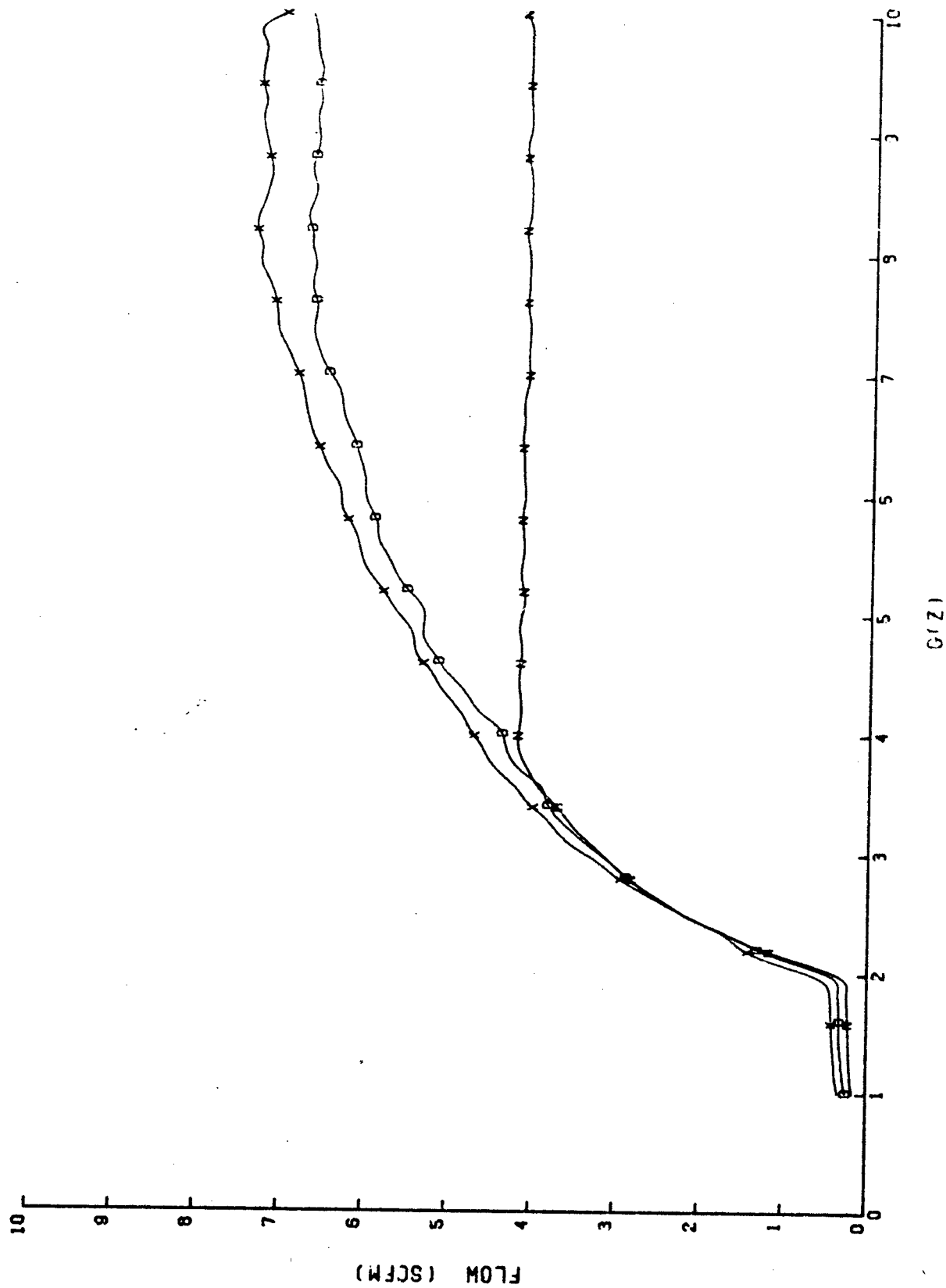


Figure 26. Bendix FR139A2 flow as a function of source pressure.  
[Curves are: N, D, and X.]

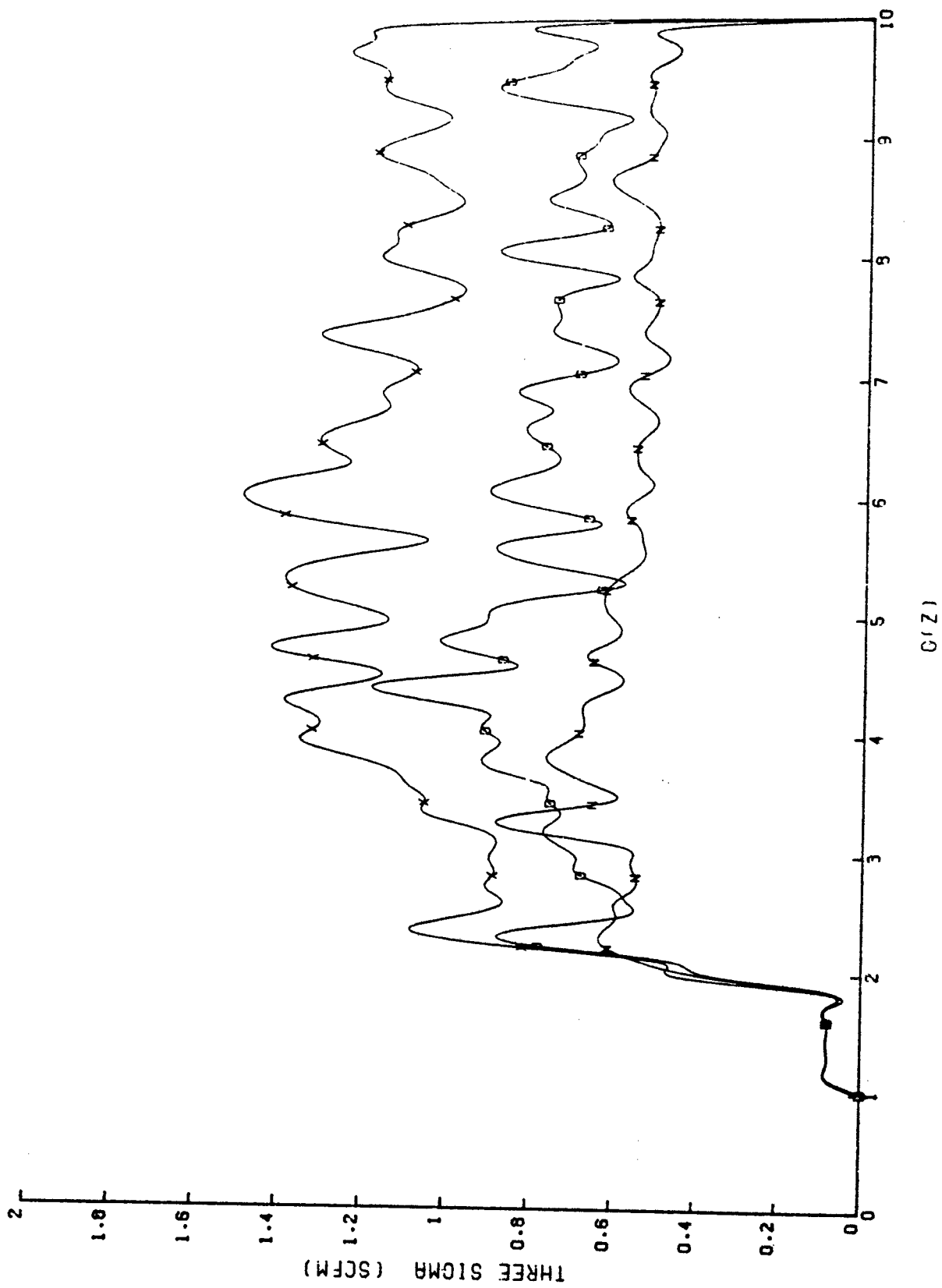


Figure 27. Bendix FRI39A2 flow three sigma as a function of  $C(Z)$ .  
[Curves are: D, N, and X.]

The principal importance of this test is to estimate the time required by this valve to fill an anti-G suit under very high onset conditions. This consideration is especially important in estimating performance at C-onset rates beyond the capability of the test facility. In the case of the FR139A2 flow curves, the low slope (increase in flow rate) between 2 G and 6 G, and the low total-flow values represent poor prospects for good performance under high G-onset rates.

### 5.2.3 Bendix FR139A2 Low G-Onset-Rate Tests

The low-onset-rate test-performance score (line 21, Table 3) for the Bendix AGV was highest (least desirable) of the five AGV's tested at 11.527. The Electronic AGV produced a considerably lower score, while the 8400A, 8000A, and RPV valves produced low G-onset (Tables 2, 4, 5, and 6) scores at one-fourth to one-fifth of the score of the Bendix tested. The relative line 21 scores are proportionally reflected in all low G-onset tests, ranking the Bendix the least desirable of all valves tested in linearity, source pressure influence, stability, and hysteresis.

In the low-onset-rate pressure profile for the FR139A2 (Fig. 28), the dotted lines indicate the band of acceptable pressure values according to MIL-V-9370D. The FR139A2 started applying pressure to the AGS at approximately 2.3 G (approximately 0.3 G late), reached acceptable pressure levels at approximately 2.6 G, and remained near the center of the band of acceptable pressure levels for almost all higher G levels. The failure of the FR139A2 to maintain sufficient suit pressure at high G with minimum source pressure is further evidence of valve "starving" under these conditions. The variation in pressure profile with respect to source pressure is acceptably small, as may be seen in Figure 28, while the variation due to angular displacement of the valve (shown by the "A" trace) is much larger than expected. When the valve is rotated, in respect to the G vector--20° in this case--the response is expected to respond proportionally to the cosine of the angle of rotation. The Bendix response more closely represented 35° to 50° rotation, perhaps indicating the near dominance of frictional forces on the mass spring system. The absence of significant increase in pressure variation (Fig. 29), over the normal runs, does not support this conclusion. Another proposed source of increased angular effects is the lack of alignment of the mass and the G-sensing control valve.

The low-onset decreasing G pressure profiles are shown in Figure 30. The variation with respect to source pressure is acceptably small and essentially random, as expected. The decreasing G pressure profile of the angular displacement tests more closely represents theoretical values than the increasing G profile, especially at higher G levels. The outstanding characteristic of these profiles, the stepwise release in suit pressure, was first mistakenly identified as a failure mode, but was later confirmed with manufacturers' representatives to be a design idiosyncrasy of the exhaust valve.

The differences between the increasing and decreasing G pressure profiles (hysteresis) are shown in Figure 31. The stepwise exhaust characteristic, and the "drooping" of the suit pressure at high G, are both very apparent in these profiles. A comparison of the low-onset and high-onset pressure profiles (and hysteresis) is shown in Figure 32.

The Bendix FR139A2 is probably an acceptable performer at low G-onset rates and in low peak-G environments. The low flow rates, valve "starving," and stepwise exhaust do not have significant effects under these conditions.

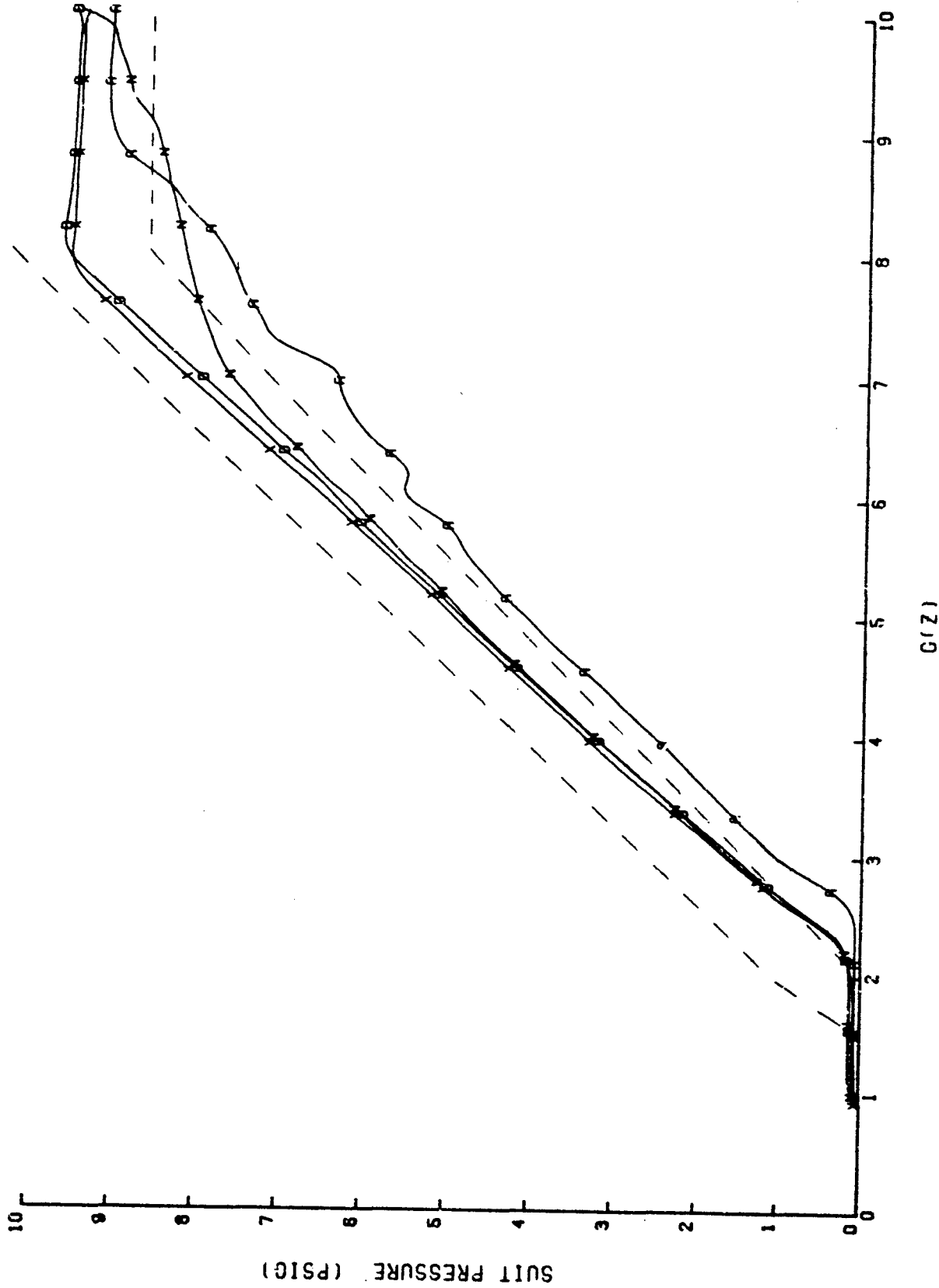


Figure 28. Bendix FRI39A2 0.1 G/sec pressure profile as a function of source pressure.  
[Curves are: A, D, N, and X.]

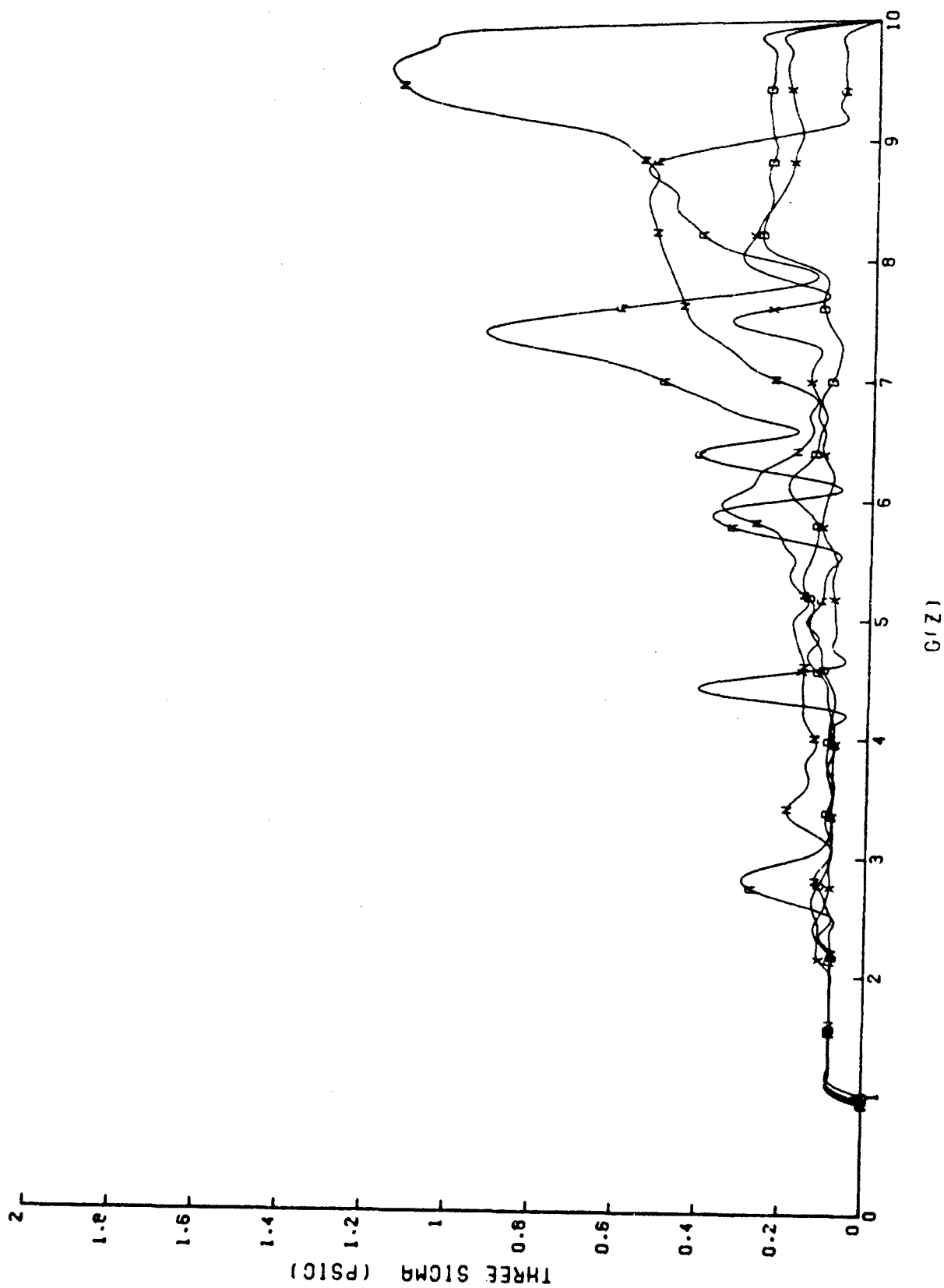


Figure 29. Bendix FR139A2 0.1 G/sec pressure stability as a function of source pressure.  
[Curves are: A, D, N, and X.]

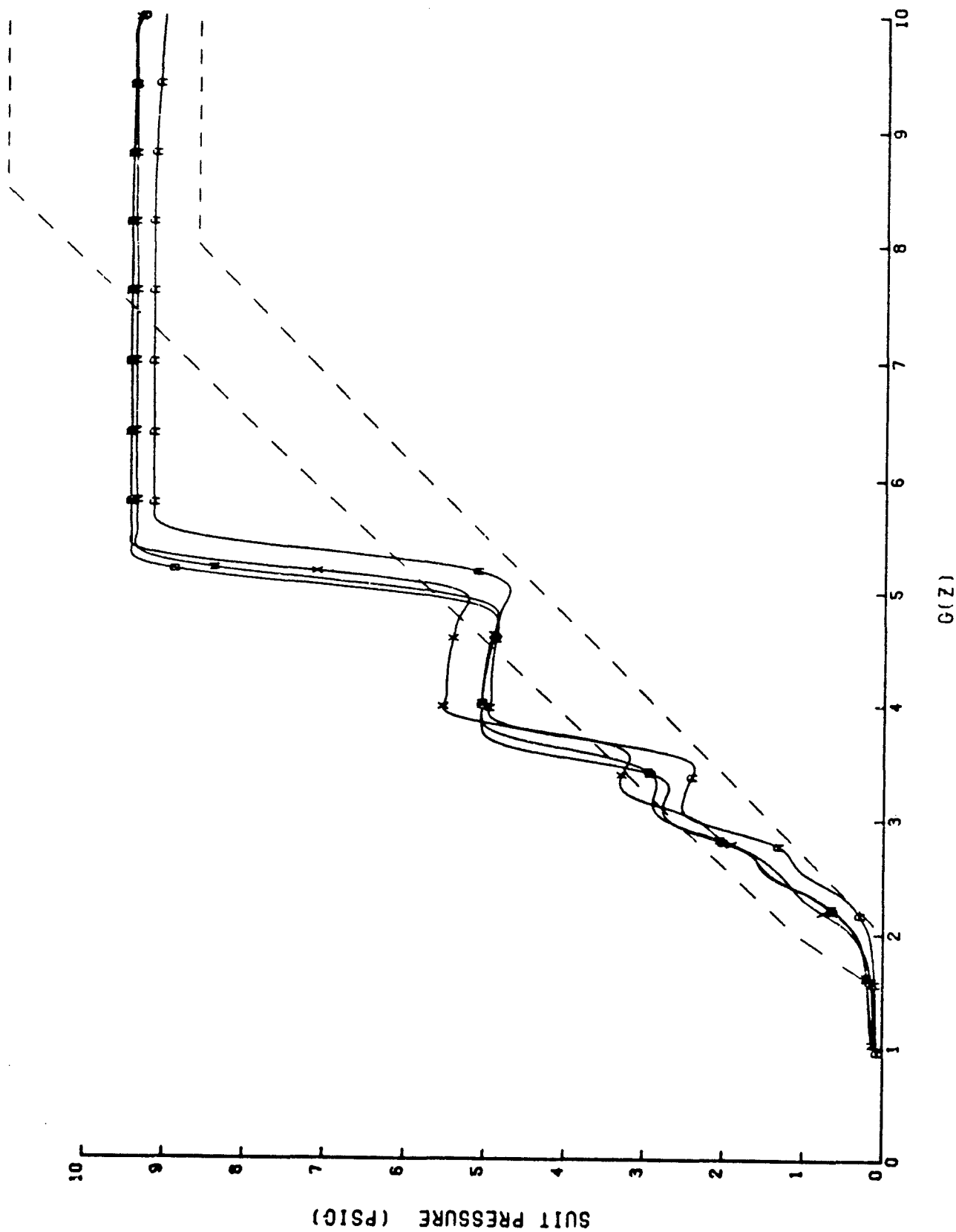
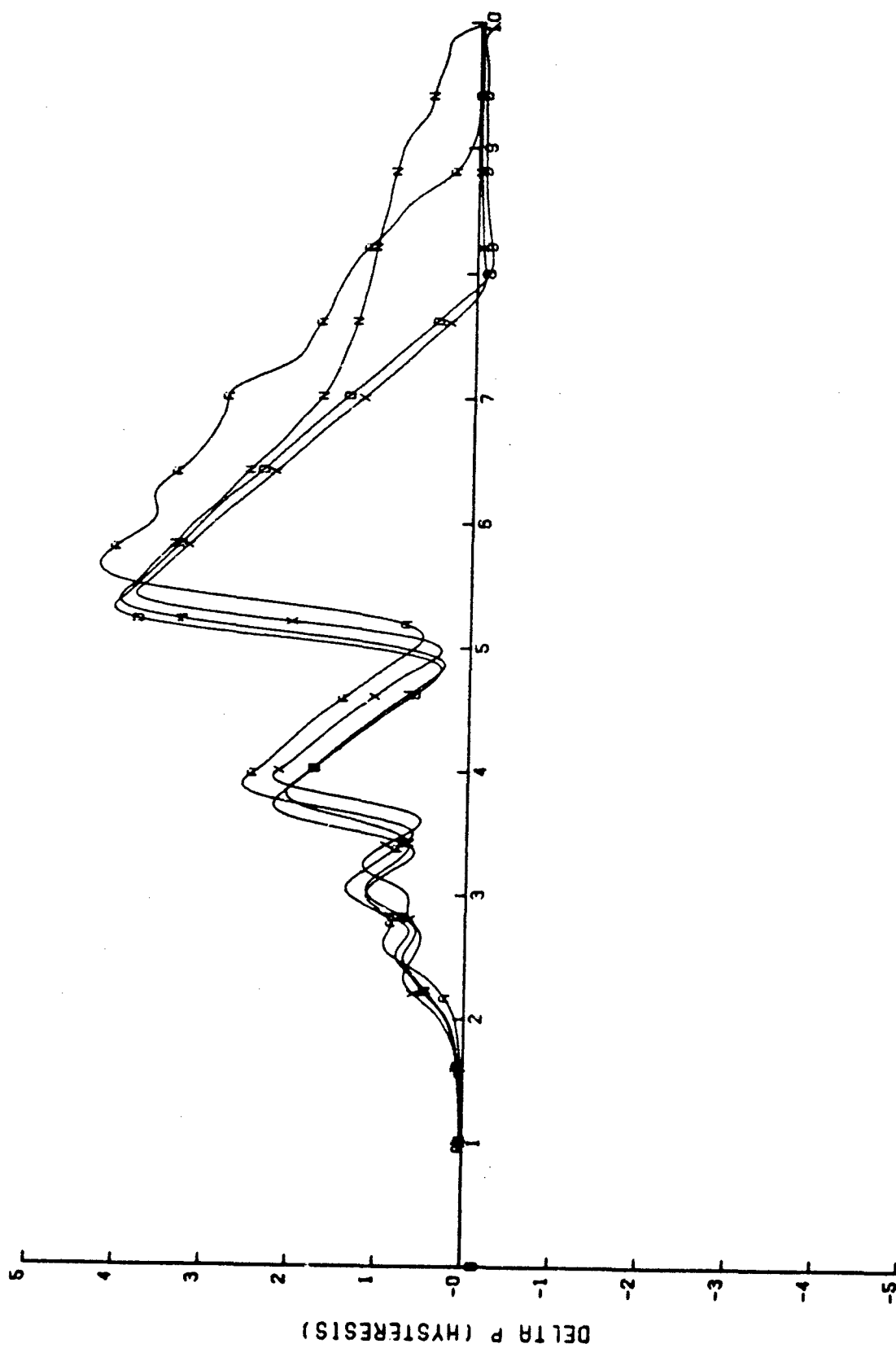


Figure 30. Bendix FRI39A2 0.1 G/sec decreasing pressure profile as a function of source pressure.  
[Curves are: A, D, N, and X.]



$G(Z)$

Figure 31. Bendix FRI39A2 0.1 G/sec pressure hysteresis as a function of source pressure.  
[Curves are: A, D, N, and X.]

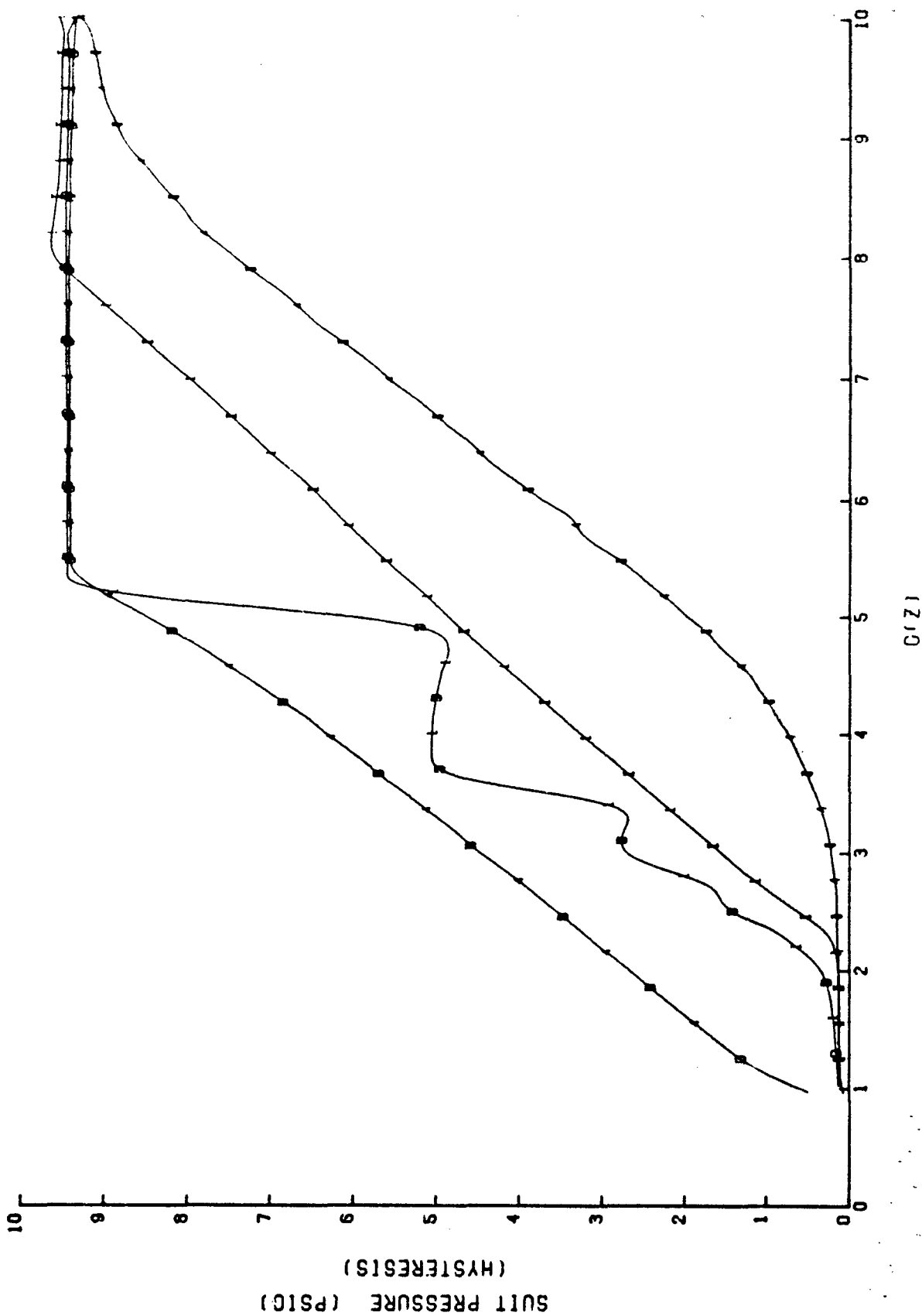


Figure 32. Bendix FRL39A2 pressure profile comparison as a function of onset rate.  
[Curves are: 1I, 4I, 1D, and 4D.]



#### 5.2.4 FR139A2 High G-Onset Rate Tests

The Bendix FR139A2 scores 54.585 (Table 3, line 27) on the high-onset-rate tests. This score is almost twice as high (undesirable) as that of the respective five valves tested, and well above the median (8000A at 21.061) valve performance. The Bendix competed with the 8400A for worst linearity, with the 4.929 shown on line 22 of the PET. The source pressure influence on high G-onset response was, again, almost twice as high as that of any other valve tested. The stability and repeatability score (Table 3, line 24) is a contract high of 11.772, almost three times the next highest score. Line 25 of the PET shows a hysteresis score of 7.457--doubling a five-valve mean of 3.258, and a median of 3.030. The score shown on line 26 of Table 3 is related to the pressure profile lag resulting from increasing G-onset rates and, because of its importance, is weighted more heavily than the other high G-onset-rate scores. The FR139A2's 16.616 is relatively undesirable compared to the RPV's 2.768 and a five-valve mean of 8.134.

Shown in Figure 33 is the influence of G-onset rate on the FR139A2's pressure profile. The increasing lag in pressurization of the AGS is caused by a "dead volume," characteristic of deflated bladders, which must be filled before pressure starts increasing. The decreasing peak rate of pressure increase for increasing G-onset rates (through 1 G/sec), shown in Figure 34, indicates an inability to adequately increase open-flow rates (Fig. 26) before pressurization begins.

The influence of source pressure on the high-onset performance of the 8400A is shown in Figure 35. These profiles, along with those of Figure 36, lend further credence to the observation that the Bendix was outrun by the 1.5 G/sec onset rate. The curves indicate the minimum source pressure resulted in significantly more pressure lag than median or maximum source pressure, supporting the "starved" valve conclusion. The extremely high run-to-run variation, indicated by Figure 36, suggests the valve was "outrun" by the high-onset rate.

The 1.5 G/sec decreasing G profiles (Fig. 37) indicate the Bendix AGV is outrun by high "offset" rates as well as high onset rates. The absence of the characteristic "step" response of the exhaust valve indicates the valve is not controlling the pressure during these tests. The large hysteresis peaks shown in Figure 38 result from both pressurization and exhaust lag.

The Bendix FR139A2 performs acceptably at low G-onset rates. The performance may be rated marginal at 0.5 G/sec, probably unacceptable at 1.0 G/sec, and certainly unacceptable at 1.5 G/sec and higher.

#### 5.2.5 SACM Tests

The Bendix FR139A2 AGV scored 33.076 on the SACM tests as shown in the PET (Table 3, line 32). This score is over three times as high (undesirable) as the 8400A's median of 9.527. A review of the individual line scores (lines 28 - 31 of the PET) indicates the FR139A2 was, by far (at least double, in all cases), the least effective performer of the five valves tested under this contract.

The pressure profiles shown in Figure 39 represent the actual and ideal pressures that should result from the G stimuli applied during SACM test when a minimum source pressure is applied to the AGV and a maximum suit volume is attached. The ideal pressure for all SACM tests was derived from the mid-source pressure profile (shown in Fig. 28), and from the actual instantaneous G value applied. The difference between the real and ideal pressures, along with corresponding onset rates, are shown in Figure 40. The abscissa of this graph represents the integral of G with respect to time. This device allows a real (unweighted) indication of magnitude, while the size of the excursion (actually the area under the curve) is weighted by the G level. In this manner, a 0.5-psig excursion at 6 G will appear twice as large as a 0.5-psig excursion at 3 G, even though the amplitudes are the same. The area under these curves is used as an evaluation factor in the PET. The FR139A2's "min-max" curves (Fig. 40) indicate frequent pressure excursions in excess of 1.5 psig positive and 3.5 psig negative, while the maximum onset rates achieved during the tests were +1.2 G/sec and -1.5 G/sec.

The SACM pressure profiles for the maximum source pressure and minimum suit volume are shown in Figure 41 and the associated difference curves are in Figure 42. In this case (Fig. 42), the pressure excursions frequently exceeded 1.5 psig positive, but only reached 2.2 psig negative, while the onset rates reached 1.2 G/sec and -1.5 G/sec. In the median-source-pressure median-suit-volume (mid-mid) case (Figs. 43 and 44), the pressure excursions reach 2.5 psig positive and negative, larger than in the min-max case. The onset rates attained in this SACM are comparable to those in the previous two tests.

The last two figures (Figs. 45 and 46) are unique only in that the valve was run with its centerline at an angle of 20° to the G vector. Since the ideal pressure here was derived in the same manner as in the previous three sets, the actual pressure is expected to be low (refer to section 5.2.3) and Figure 46 confirms this expectation. Otherwise the curves are comparable to those in Figures 43 and 44, except that perhaps a little more tendency to over-shoot is exhibited.

#### 5.2.6 Conclusions on the FR139A2's Performance

The Bendix FR139A2 may perform acceptably at low G-onset rates if: (a) the source pressure is maintained in the neighborhood of 70 psig or higher; and (b) the stepwise exhaust characteristic is judged physiologically acceptable.

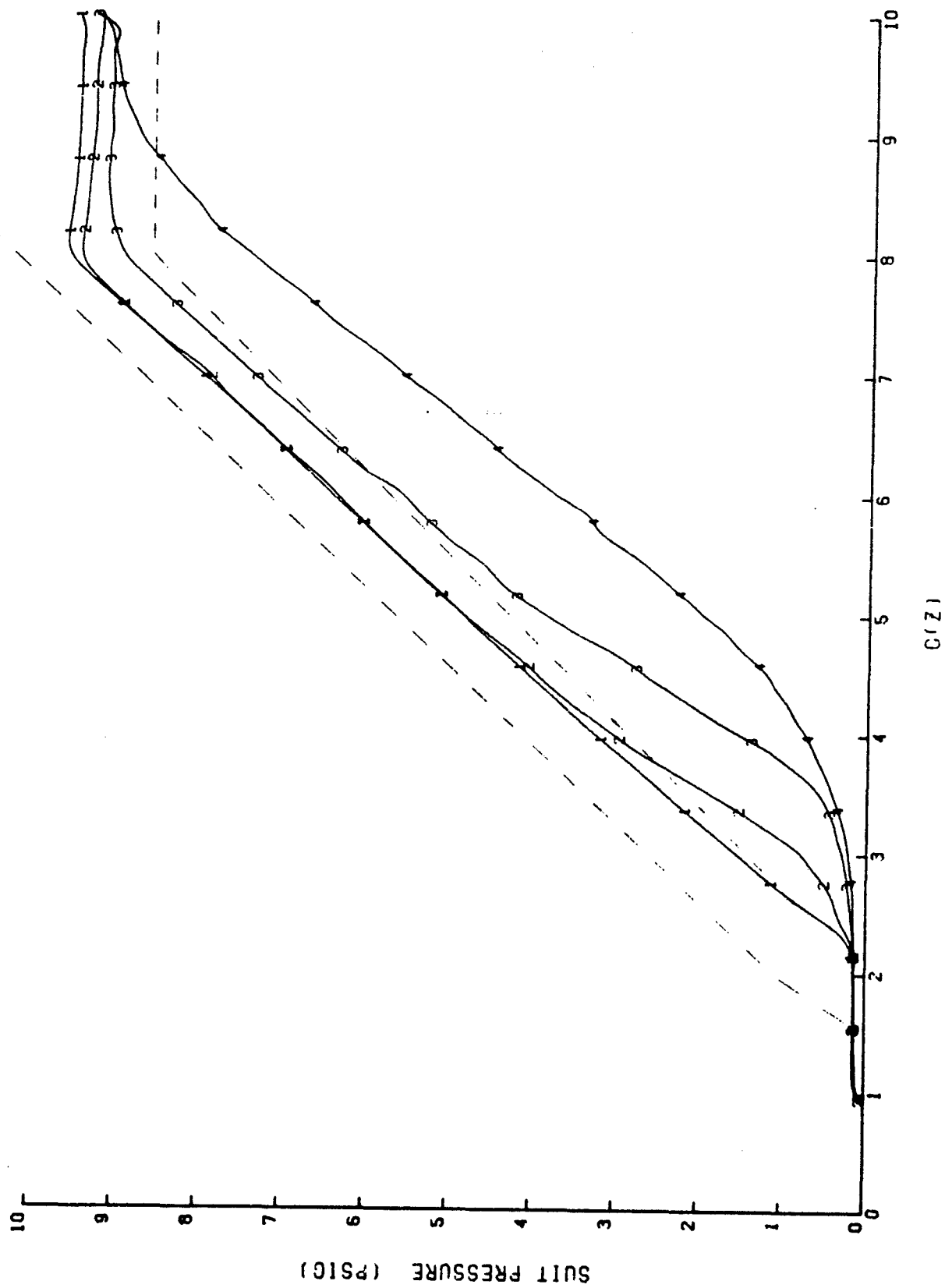


Figure 33. Bendix FR139A2 pressure profile as a function of C-onset rate.  
[Curves are: 1, 2, 3, and 4.]

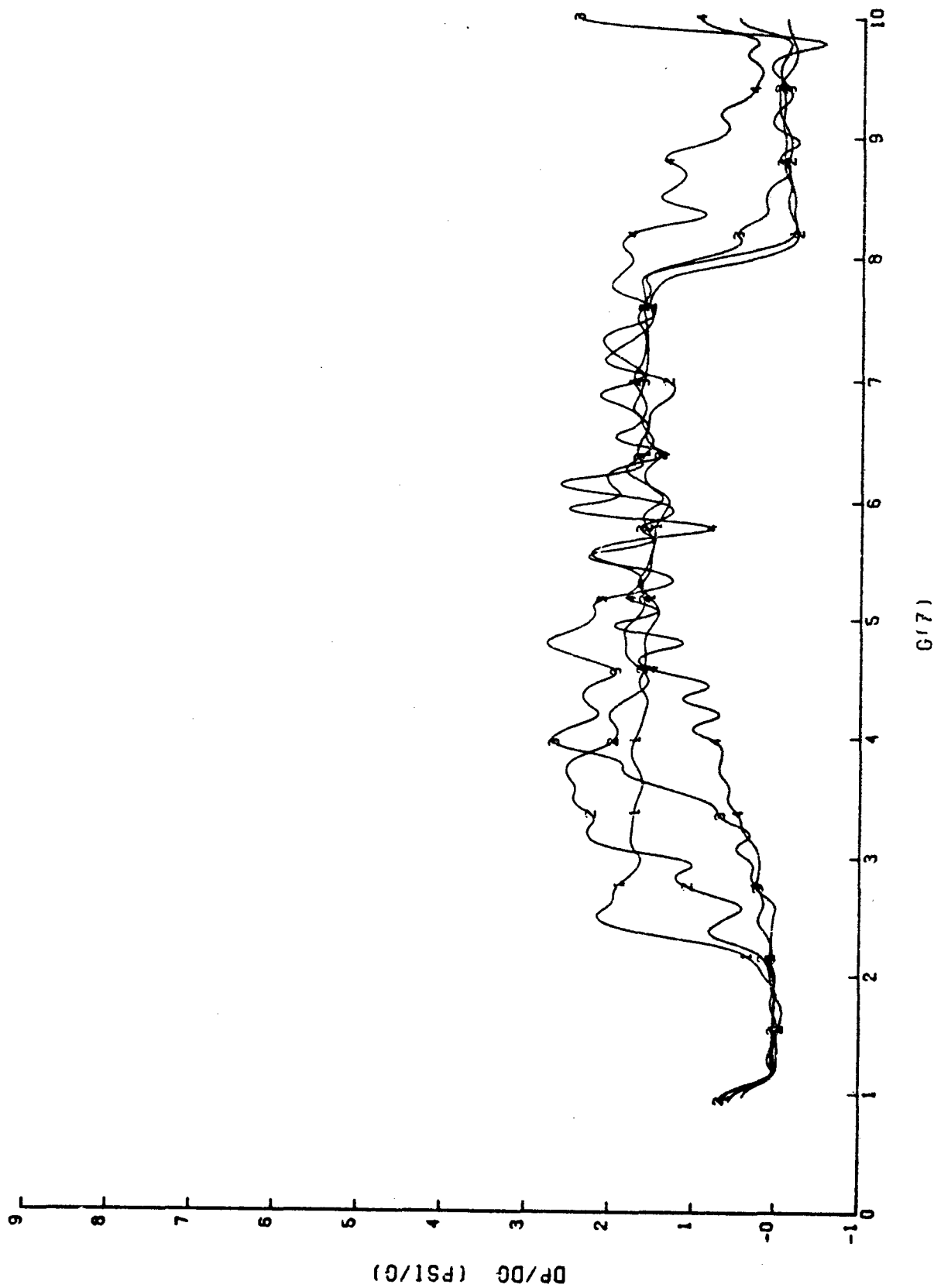


Figure 34. Bendix FR139A2  $dp/dG$  as a function of  $G$ -onset rate.  
[Curves are: 1, 2, 3, and 4.]

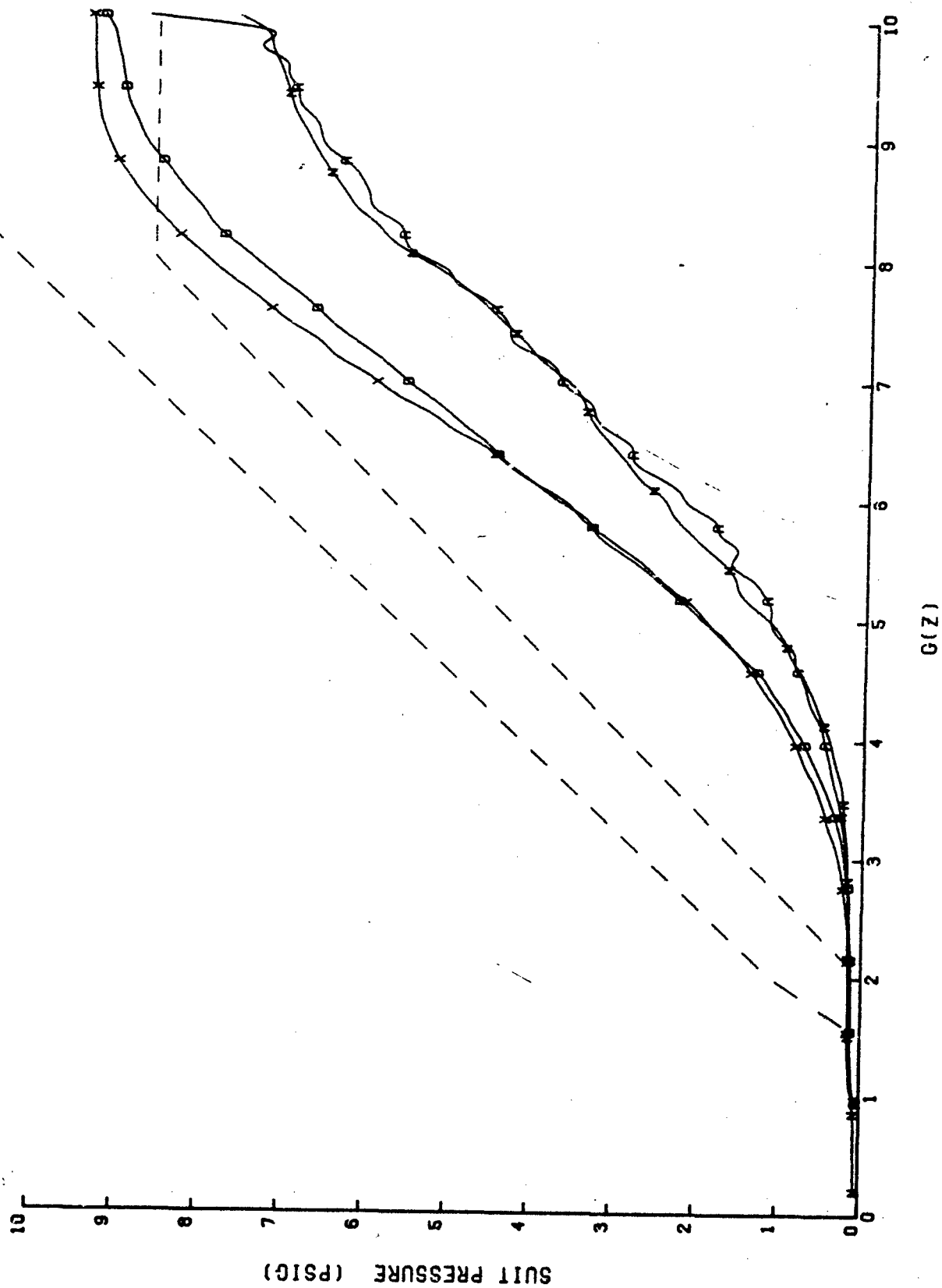


Figure 35. Bendix FR139A2 1.5 G/sec pressure profile as a function of source pressure.  
[Curves are: A, D, N, and X.]

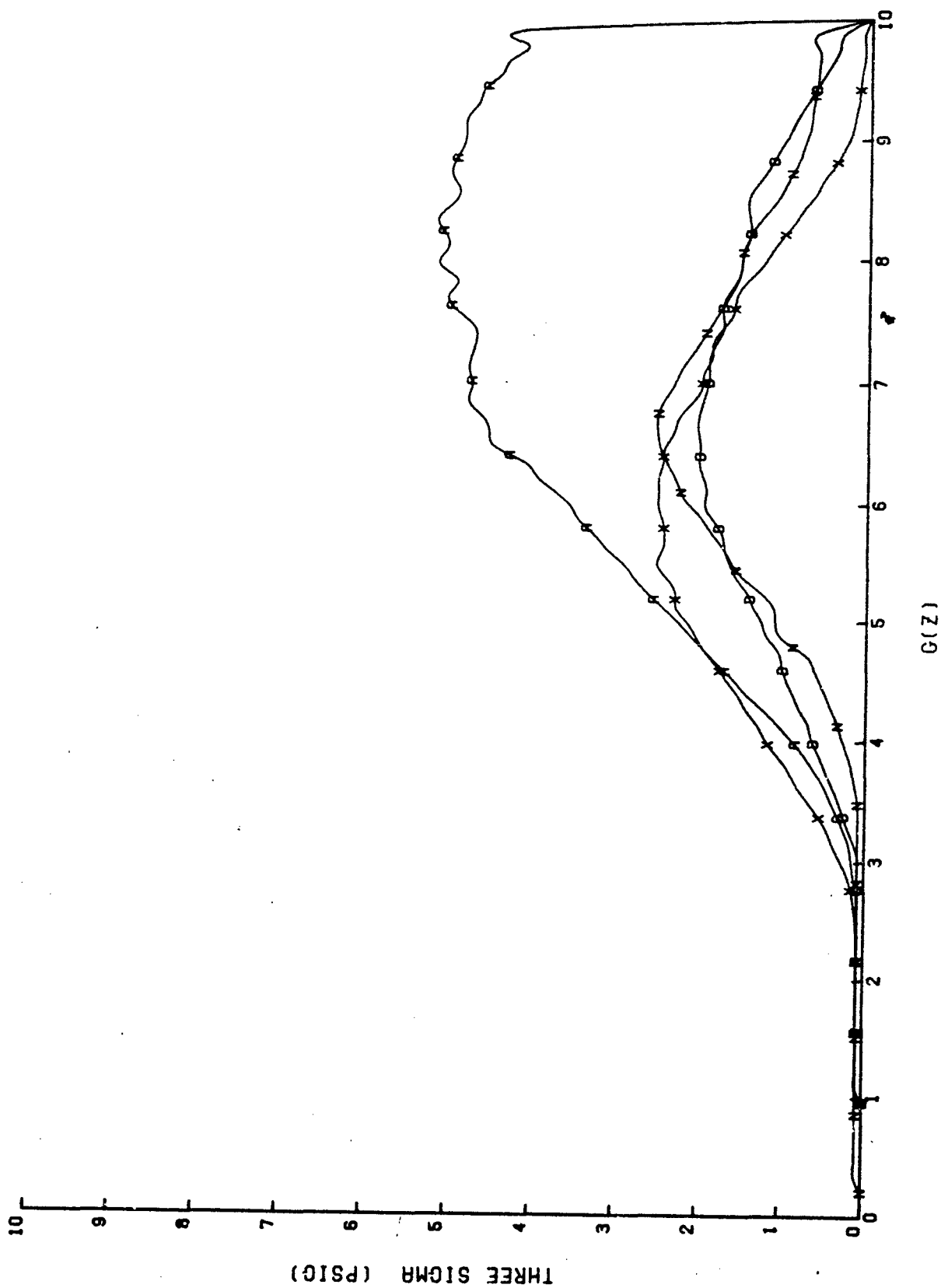


Figure 36. Bendix FR139A2 1.5 G/sec pressure variation as a function of source pressure.  
[Curves are: A, D, N, and X.]

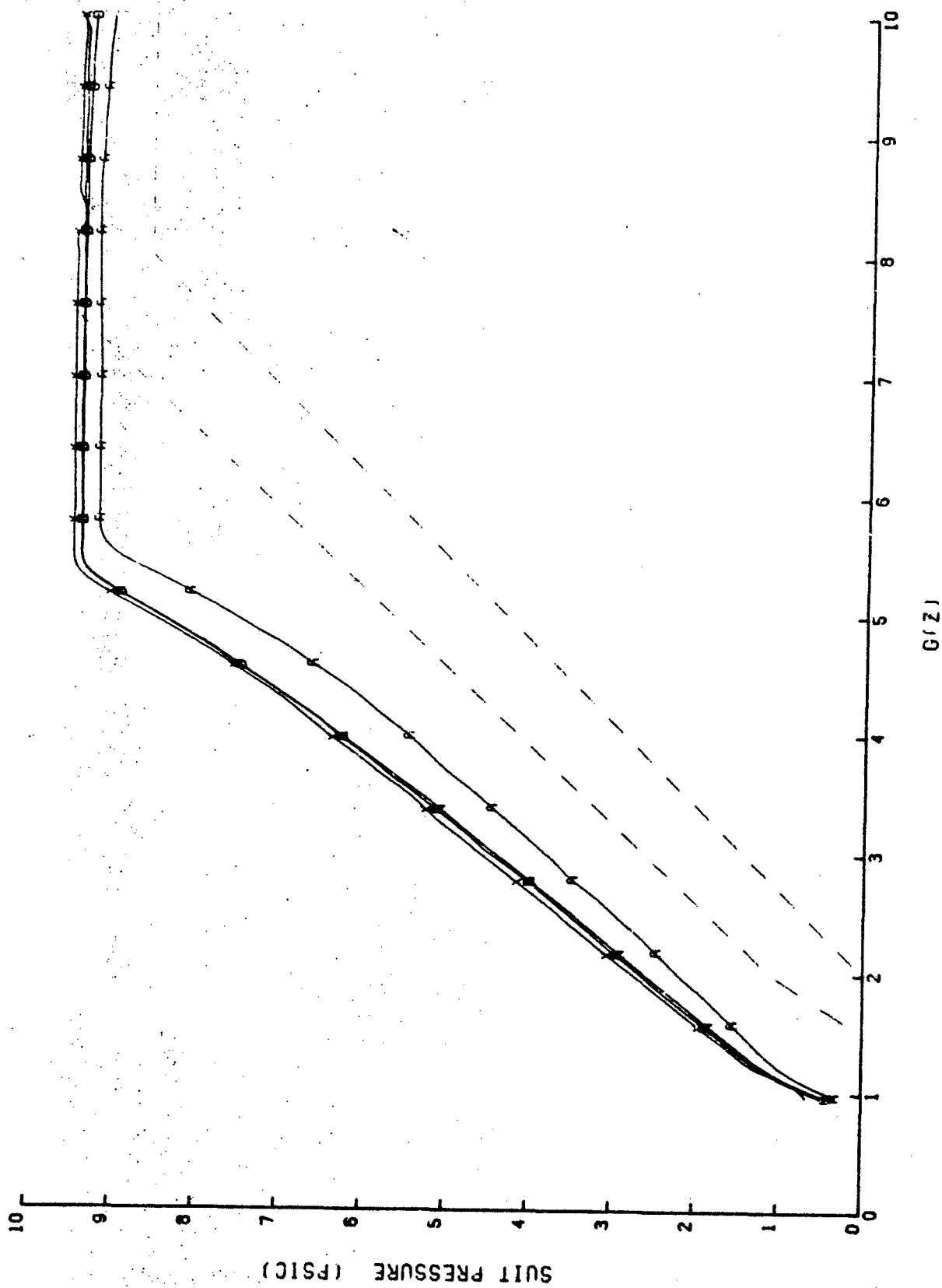
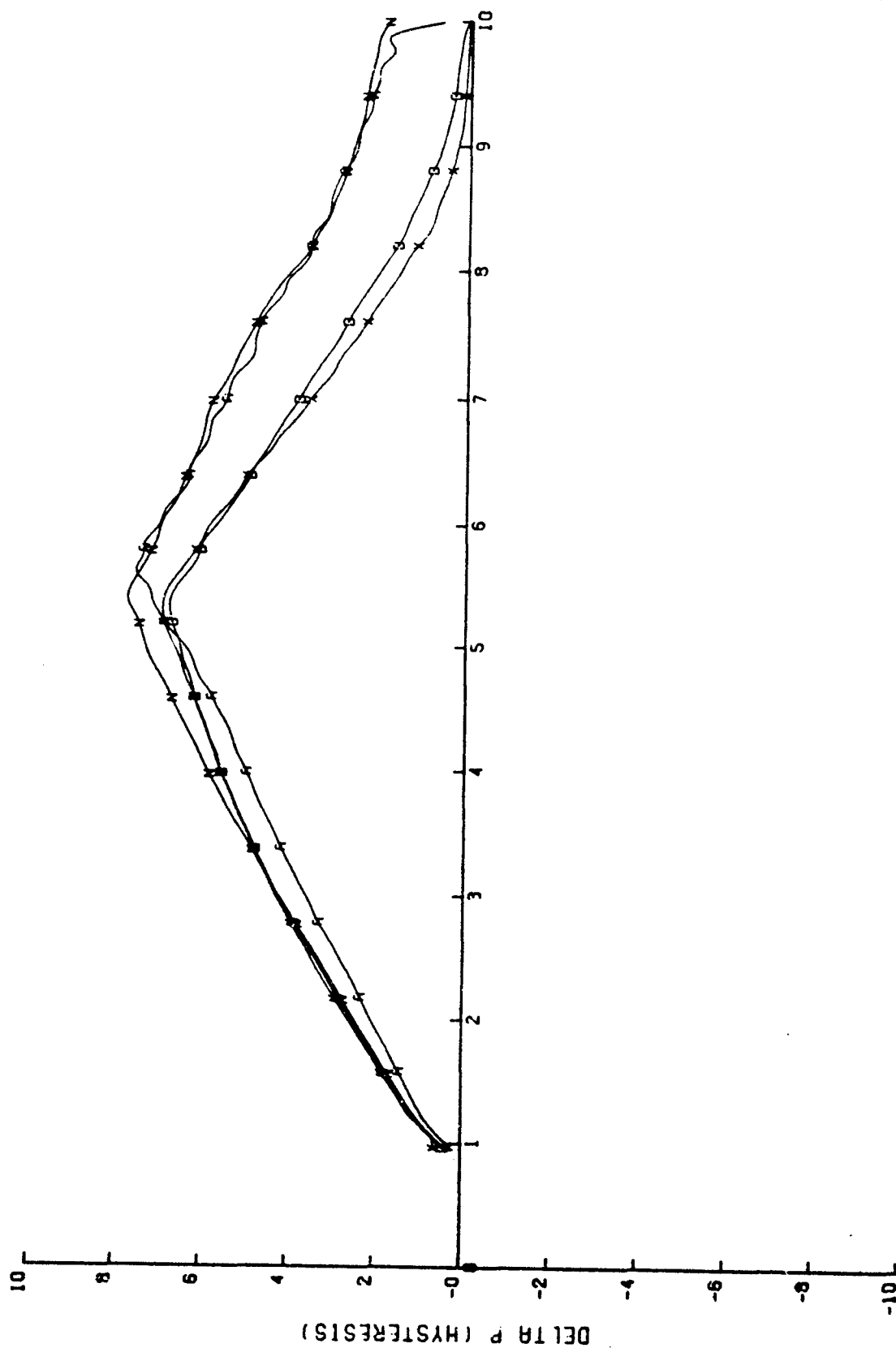


Figure 37. Bendix FR139A2 1.5 G/sec decreasing pressure profile as a function of source pressure.  
[Curves are: A, D, N, and X.]



C(Z)

Figure 38. Bendix FRI39A2 1.5 G/sec pressure hysteresis a function of source pressure.  
[Curves are: A, D, N, and X.]



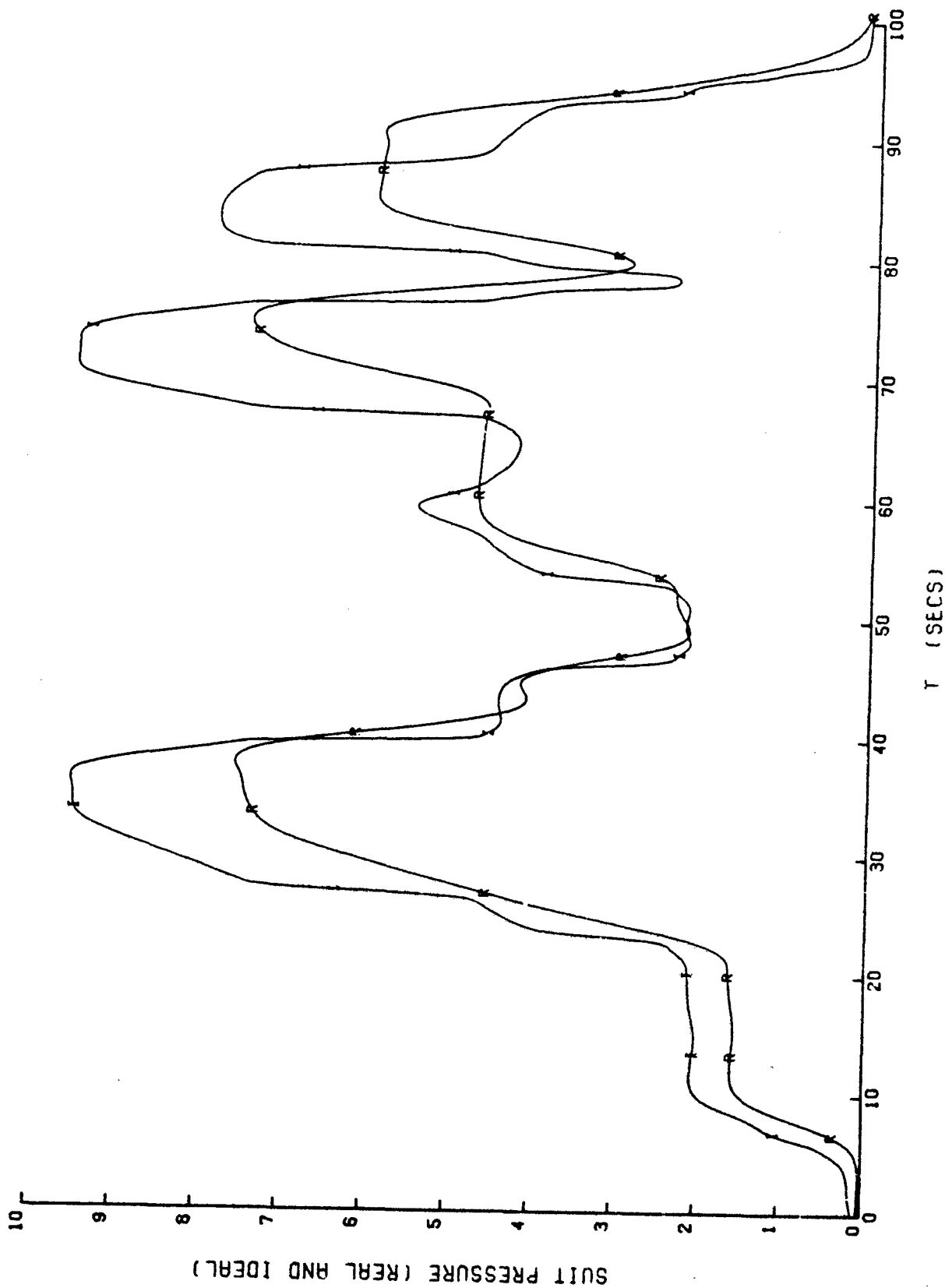
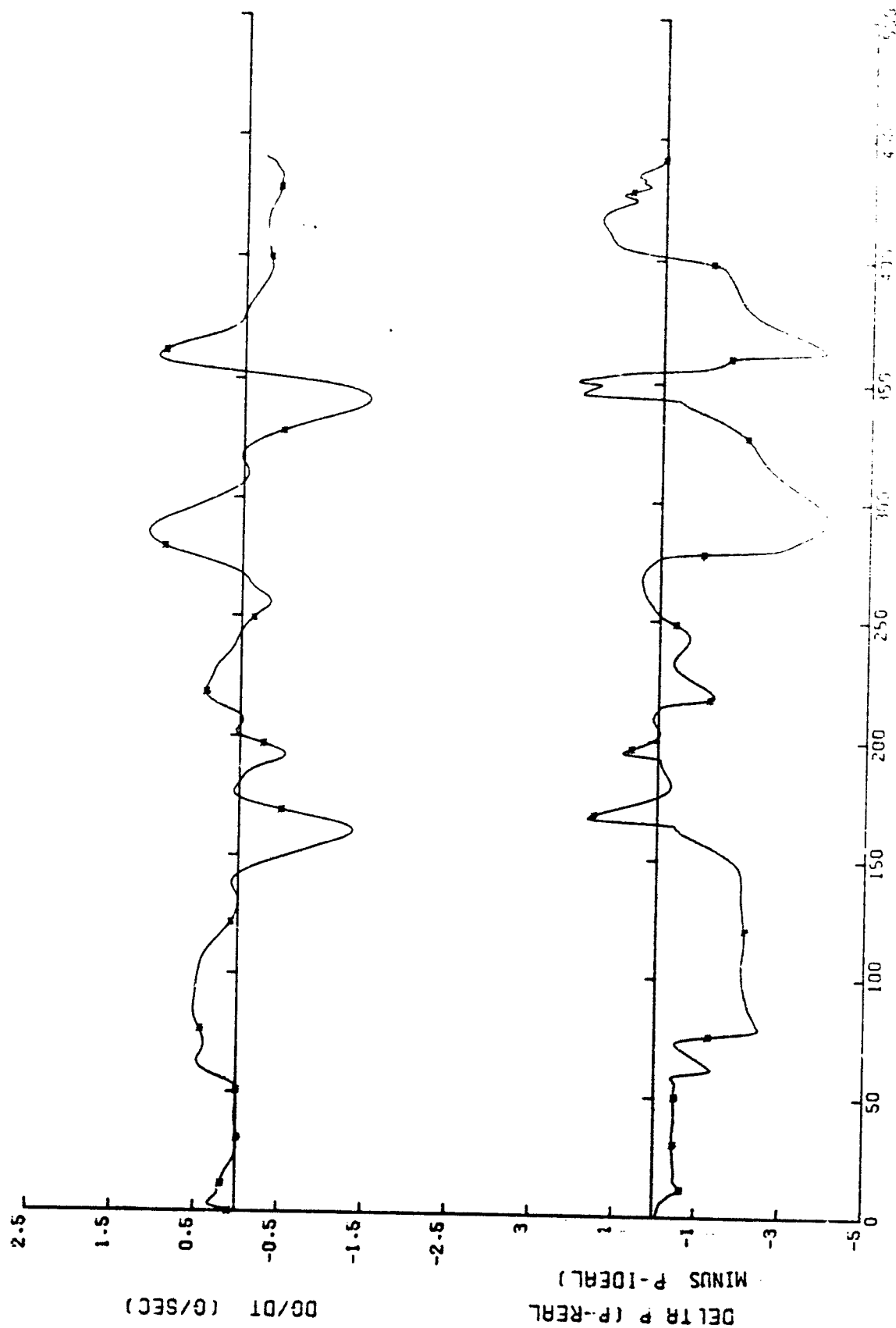


Figure 39. Bendix FRL39A2 SACM pressure profile comparison with minimum source pressure and maximum suit volume. [Curves are: I and R.]



INTEGRAL OF  $dG/dt$  FROM 0 TO 1

Figure 40. Bendix FRI 39A2 pressure deviation and  $dG/dt$  for the minimum pressure ( $p_{min}$ ) and maximum suit volume (SACM). [Curves are: 3.]

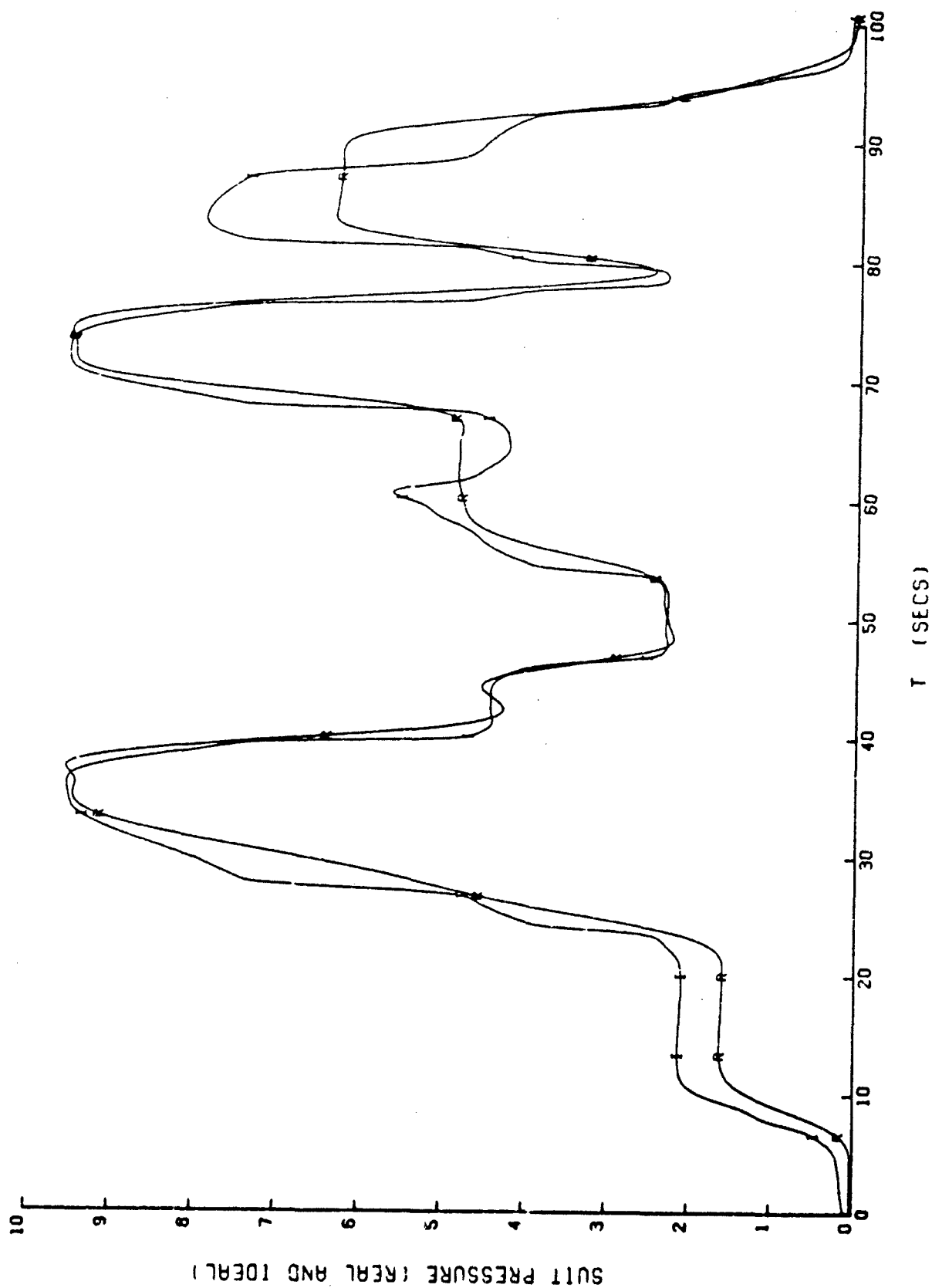


Figure 41. Bendix FR139A2 SACM pressure profile comparator with maximum source pressure and minimum suit volume. [Curves are: I and R.]

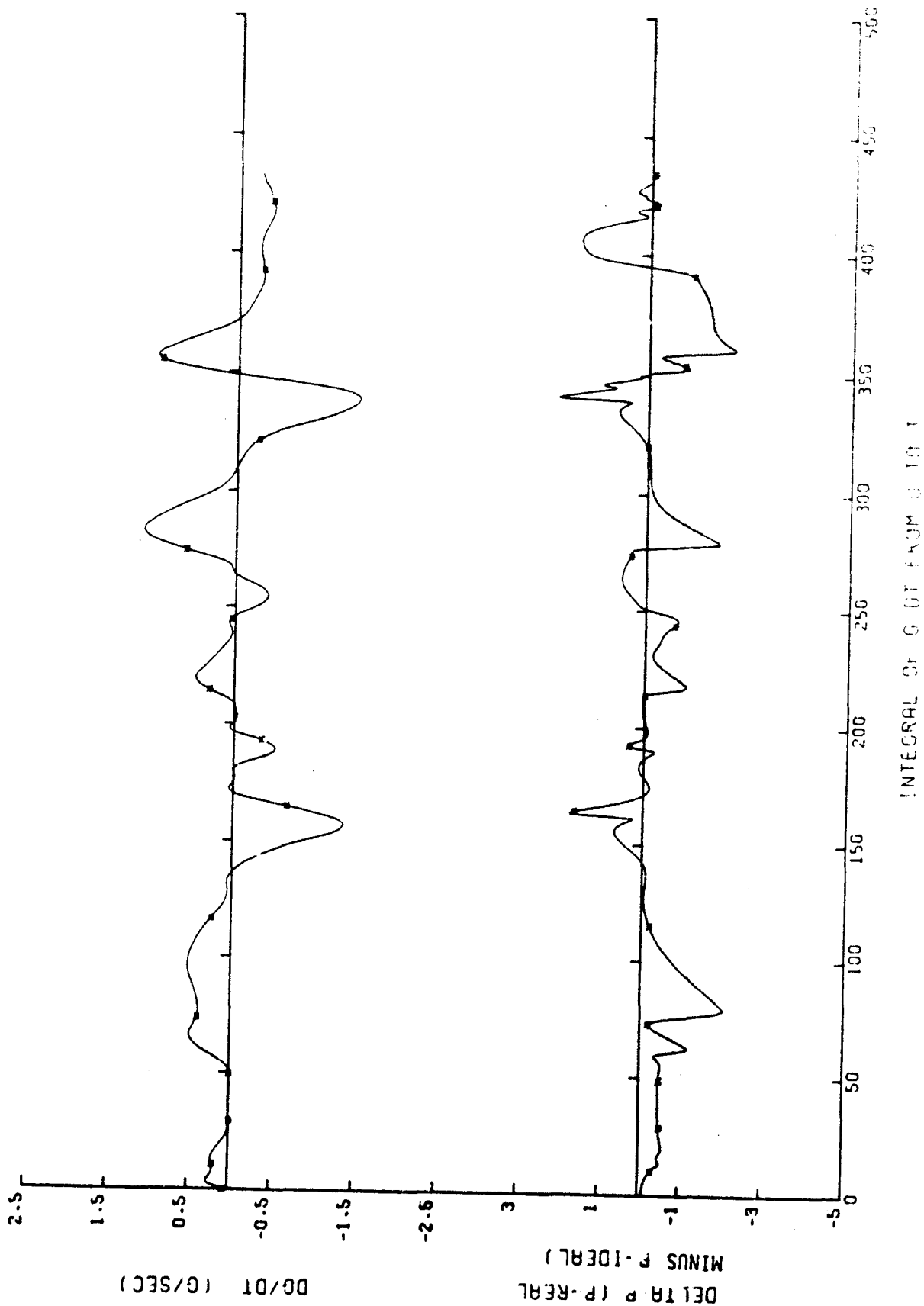


Figure 42. Bendix FR139A2 pressure deviation and  $dc/dt$  for the maximum source pressure and minimum suit volume SACM. [Curves are: #.]

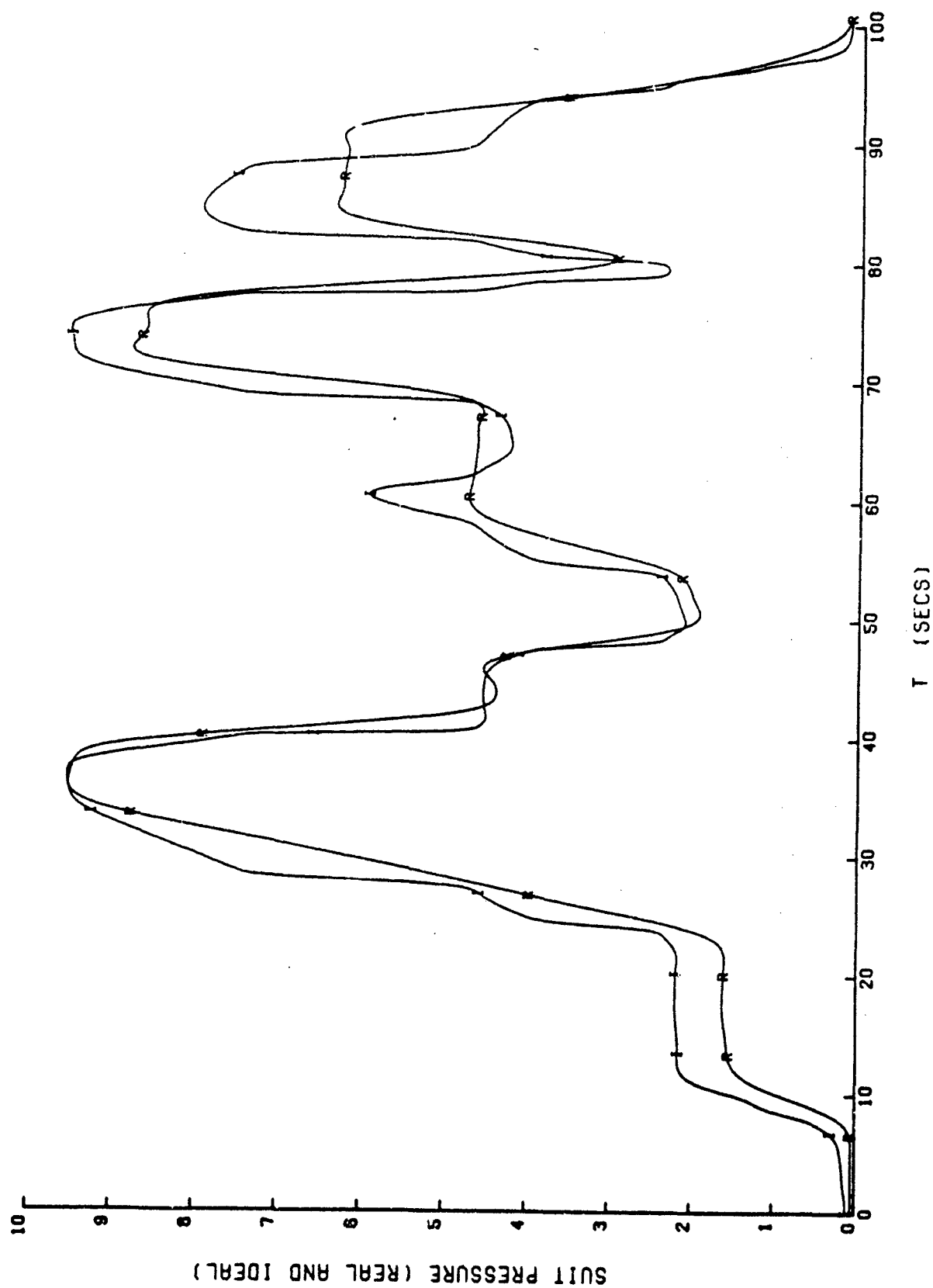


Figure 43. Bendix FRI39A2 SACM pressure profile comparison with median source pressure and suit volume. [Curves are: I and R.]

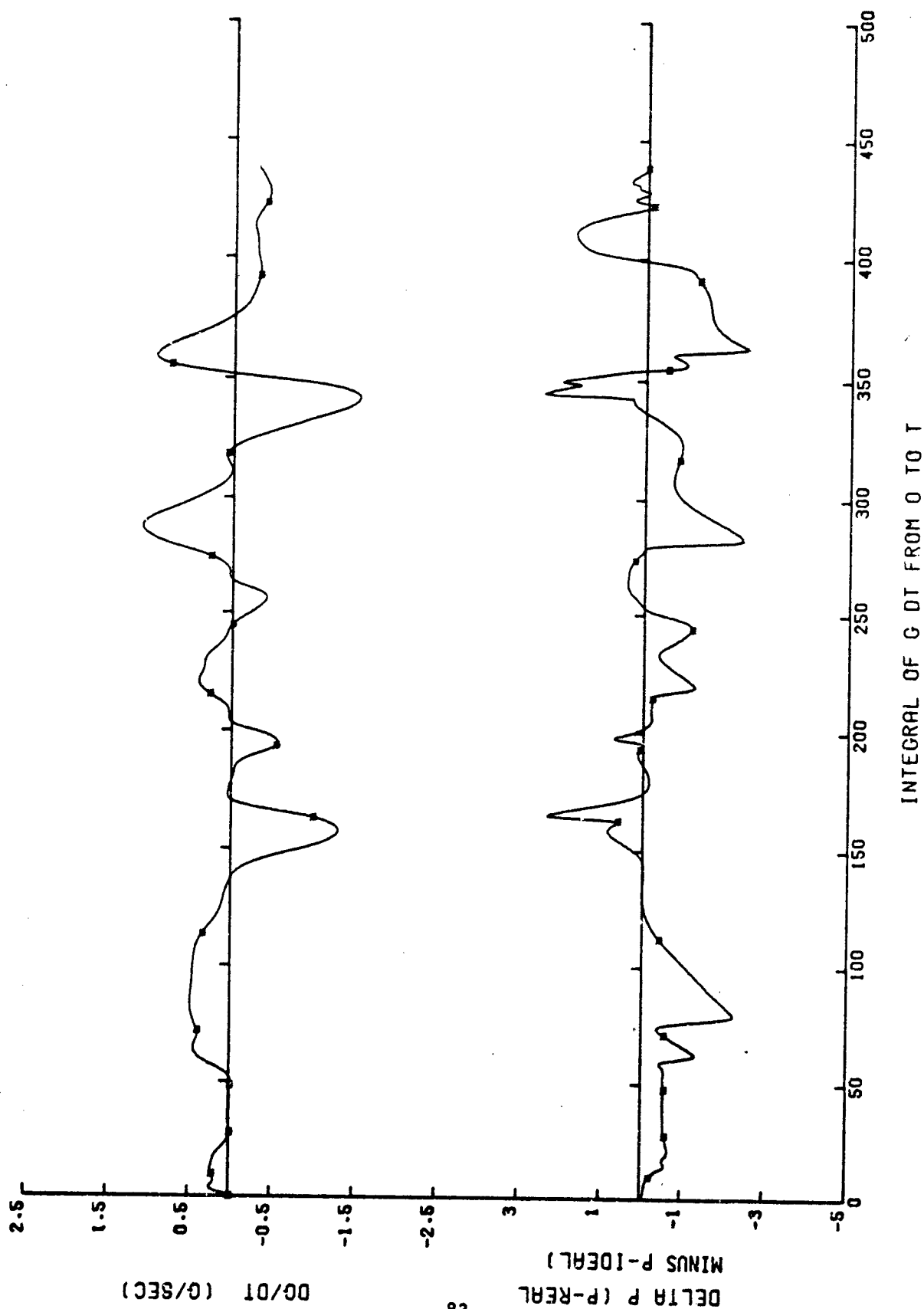


Figure 44. Bendix FR139A2 pressure deviation and  $dG/dt$  for the median source pressure and suit volume SACM. [Curves are: \*.]

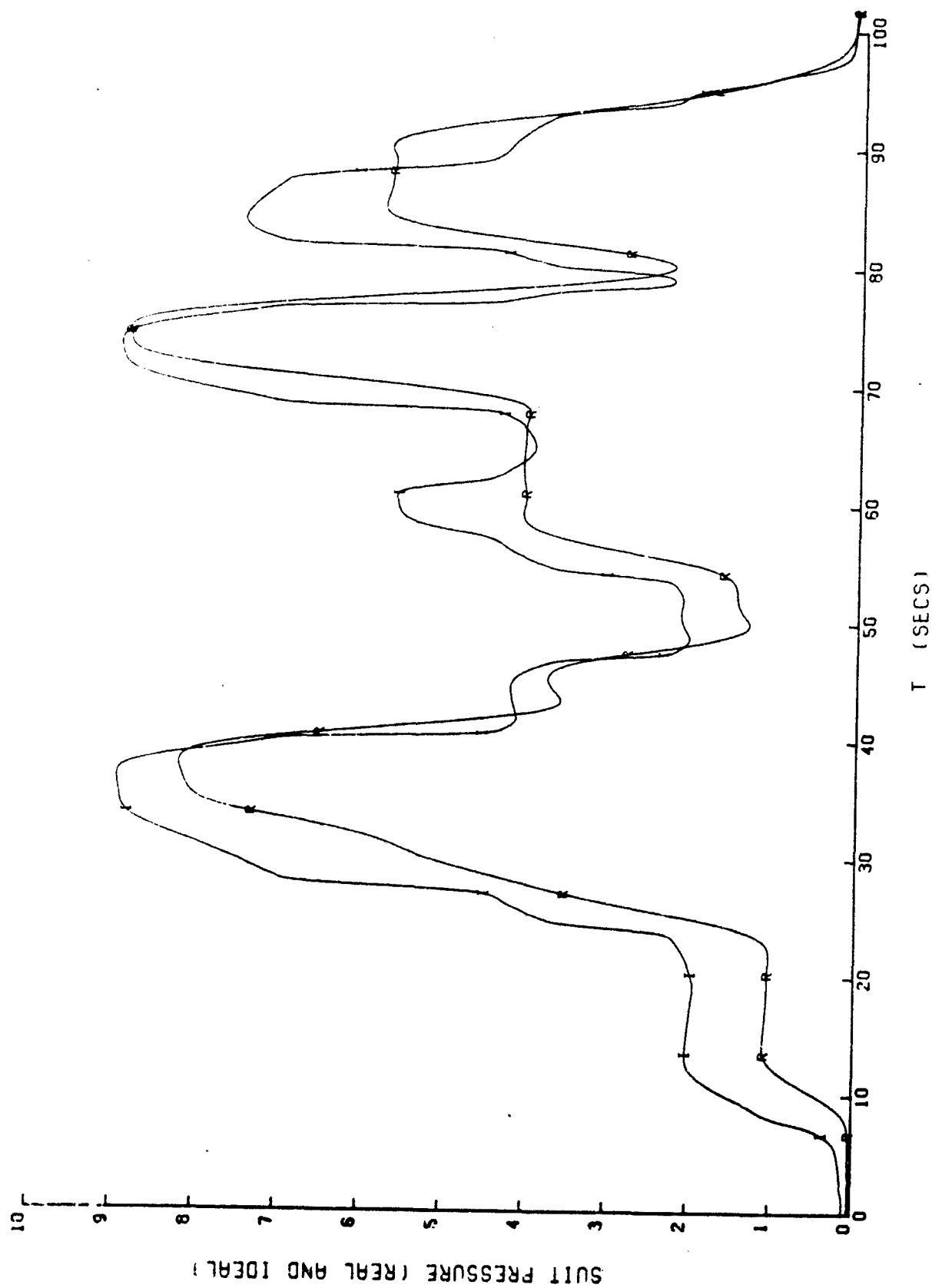


Figure 45. Bendix FR139A2 SACM pressure profile comparison with C vector misalignment.  
[Curves are: I and R.]

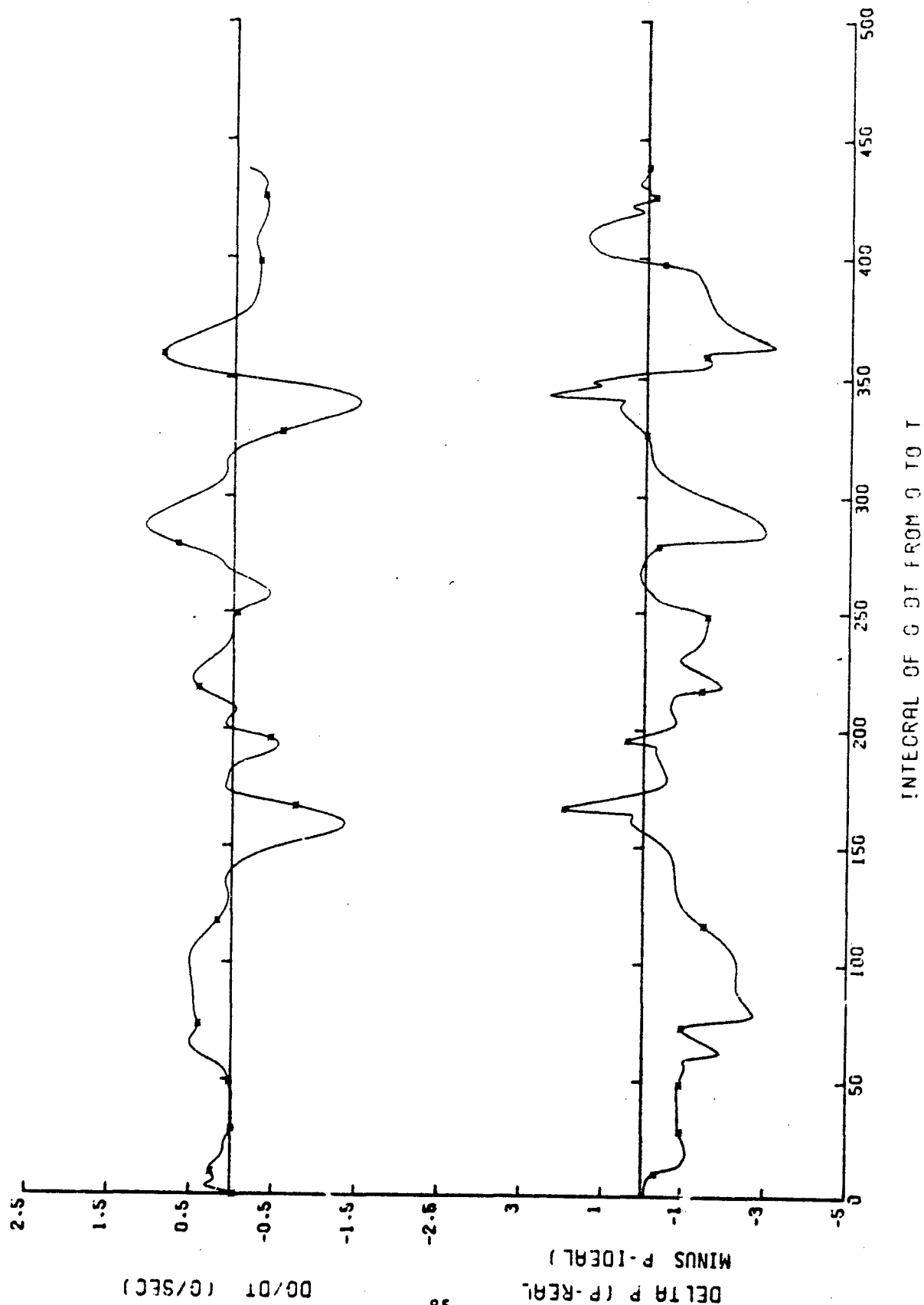


Figure 46. Bendix FR139A2 pressure deviation and  $dG/dt$  for the G vector misalignment SACM.  
[Curves are: \*.]



### 5.3 Electronic Anti-G Valve and Test Results

#### 5.3.1 Electronic Anti-G Valve and Test Description

The USAFSAM Electronic Anti-G Valve (E valve), the result of inhouse investigation, was designed and built by personnel assigned to the USAFSAM Human Centrifuge Facility. The E valve represents an "electronics controls" approach to the design and construction of a programmable anti-G valve suitable for research use on the human centrifuge at Brooks AFB.

The E valve offers considerable flexibility in programmable suit inflation schedules. Suit pressure per  $G_z$  is variable over the range 0 to 2 psi/G; and the "START LEVEL" control may be set to initiate suit inflation at any level between 1 G and 5 G. Two step functions are available. One is the "STEP PSI" which will, when a selected start level is reached, immediately inflate the suit to a preselected pressure within the range of 0 - 5 psig. The remaining step function--the "STFP DELAY"--is used to allow the valve to initiate suit inflation smoothly at the chosen start level, and to continue inflating at the rate determined by the setting of the "PSI/G" control until reaching the preselected G level chosen by the STEP DELAY control. At this level, the suit immediately inflates to the pressure that has been preselected by the STEP PSI setting.

The five main systems comprising the E valve are the G-sensing transducer, the pressure-sensing transducer, the control electronics, the power supply, and the direct current motor-driven modified ALAR anti-G valve. The G-sensing transducer is the accelerometer (an Endevco model 2262.25) permanently installed in the unit housing, while the suit-pressure-sensing transducer is a strain-gage type Statham PM131TC350. The two packages (electronics and power supply) were constructed within USAFSAM/VNB, and function to provide the driving signal which controls a modified ALAR anti-G valve.

In brief, the valve functions as follows: An increase in  $G_z$  (corresponding to acceleration in the gondola) will cause an increased output signal, from the accelerometer, which is input into the signal conditioning stage of the electronics package. When the  $G_z$  is such that the accelerometer signal exceeds a threshold set by the "START LEVEL" control, a motor-driving signal proportional to the setting of the PSI/G control is produced. The driving of the valve motor actuates the modified ALAR anti-G valve and allows air to flow into the suit. As the suit pressure increases, it is sensed by the PM131TC350 transducer, thus producing a signal which is opposite in polarity to the accelerometer signal and proportional to the suit pressure. The conditioned signals of the accelerometer and the pressure transducer are summed in a circuit that produces a motor-driving signal.

When the suit pressure reaches a level such that the summation of the pressure transducer signal and the accelerometer signal equals zero, the motor-driving signal is zero. Should the G level remain steady, the steady suit

---

**EDITOR'S NOTE:** The information in section 5.3.1 parallels (of necessity) that in corresponding passages in SAM-TR-78-11.

pressure at that G level will be proportional to the setting of the "PSI/G" control. Other stages of electronic circuitry (such as zero crossover detectors and comparators) are used to effect the programming of the step functions; however, their complexity precludes their inclusion in this brief discussion. Electric power is afforded by power supplies mounted in the power supply package.

The modified ALAR anti-G valve has had the mass spring mechanism removed and replaced by a spring-loaded plunger which is driven by a geared-down dc motor. The spring loading serves to return the plunger and remove suit pressure should the motor or drive fail. In addition, the first stage regulator was modified to provide a higher second-stage source pressure, and the second-stage control ports were enlarged to permit higher flow. The original relief valve is retained intact.

The electronics package is 6-1/4 in. wide x 5-1/4 in. deep x 8-3/4 in. high (15.9 cm x 13.3 cm x 22.2 cm), and weighs 7-1/2 lb (3.4 kg). The controls extend 1 in. (2.5 cm) in front of the package, while the hose inlets extend 1-1/4 in. (3.2 cm) to each side. The power supply package is 4 in. wide x 5 in. deep x 6 in. high (10.2 cm x 12.7 cm x 15.2 cm), weighs 1.05 lb (2.3 kg), and has a 5 in. x 7 in. (12.7 cm x 17.8 cm) mounting flange mounted on the bottom.

For purposes of SVTP testing and GVALVPGM analysis, standard values were assigned for the E valve and are shown in Table 4 (PET), lines 1 - 7. Since the design concept of the E valve is to replace the mass-spring assembly in an ALAR 8400 with an electronically controlled actuator, the design valves are identical to those in an 8400A which, in turn, were selected as standards for the GVALVPGM analysis because they permitted direct application of the unit to a wide variety of weapons systems in the present USAF inventory. Since they are the GVALVPGM standard, the E valve scored a perfect minimum of 3.0 on the PET design total.

#### 5.3.2 E Valve Flow Tests

The flow-test performance score of the E valve, represented by 13.128 on line 16 of Table 4, was the highest score of the five valves tested under this contract. The total open-flow test showed a below-median and below-mean performance of 1.972 (line 12, Table 4), with only the Ready Pressure AGV (RPV) having higher flows. The source pressure influence on the open flow severely degraded the E valve's flow scores (lines 13 and 14, Table 4). In both cases, the E valve generated the highest (least desirable) scores of the five valves tested under this contract. The cause of these low scores is discussed in the next paragraph. The stability of the open flow of the E valve (line 15, Table 4), was below mean and median at 0.181, although the fluctuations in flow were essentially equal for all valves tested.

The E valve flow curves (Fig. 47) show excellent potential, good for high G-onset response. The initiation of flow at or just below 2 G<sub>z</sub> and the very rapid increase to 13 SCFM at 3 G<sub>z</sub> are excellent characteristics. The very tight distribution of flow levels, up to 4 G, with respect to source pressure, is also very desirable. The PET discriminates against this valve, perhaps unfairly, because of the flattening of the minimum source pressure

TABLE 4. ELECTRONIC ANTI-G VALVE PERFORMANCE EVALUATION TABLE

TEST STANDARDS:

1. SPMIN = 30. PSIG
2. SPMID = 125. PSIG
3. SPMAX = 300. PSIG
4. THETA = 20. DEGREES
5. SVMIN = 6. LITERS
6. SVMID = 10. LITERS
7. SV MAX = 14. LITERS

CHARACTERISTIC NUMBERS:

8. XSPMX = 1.0000
9. XSPMN = 1.0000
10. XTHTA = 1.0000
11. DESIGN TOTAL: 3.000
12. XFLBR = 1.972
13. XDELF = 4.988
14. XDDL F = 5.986
15. XSIGF = 0.181
16. FLOW TOTAL: 13.128
17. XCCP1 = 0.002
18. XDDP1 = 3.138
19. XSGP1 = 1.847
20. XDPP1 = 0.120
21. LOW-ONSET TOTAL: 5.107
22. XCCP2 = 0.959
23. XDDP2 = 7.931
24. XSGP2 = 1.944
25. XDPP2 = 1.121
26. XTDP2 = 3.093
27. HIGH-ONSET TOTAL: 15.048
28. XIDPA = 1.063
29. XIDPB = 0.957
30. XIDPC = 0.831
31. XIDPD = 2.172
32. SACM TOTAL: 5.023
33. VALVE: ELECTRONIC TOTAL 41.305

flow curve. This flattening indicates a limitation in the flow capacity of the basic ALAR's first stage regulator and the subsequent "starving" of the now electronically controlled regulator in the second stage. It must be said that "starving" at 20 to 21 SCFM is not that shabby in terms of today's AGV technology. The span of 5 SCFM from  $F_{min}$  (open flow at minimum source pressure) to  $F_{med}$  (open flow at median source pressure) and 6 SCFM from  $F_{min}$  to  $F_{max}$  severely hurt the E valve's PET scores. The fluctuations in the open-flow data are shown in Figure 48 as the 3 $\sigma$  values, and appear to increase with source pressure in a relatively linear manner.

The principal importance of this test is to estimate the time required by this valve to fill an anti-G suit under very high-onset conditions. This consideration is especially important to estimating performance at G-onset rates beyond the capability of the test facility. In the case of the E-valve flow curves, the high slope (increase in flow rate), between 2 G and 3 G, and the high total flow values represent good prospects for good performance under G-onset rates.

#### 5.3.3 E Valve Low G-Onset-Rate Tests

The low-onset-rate test performance score of 5.107 (line 21, Table 4) for the E valve was slightly above the median and mean scores of the five AGV's tested. The Bendix AGV produced a considerably higher (less desirable) score, while the 8400A, 8000A, and RPV valves produced better scores. Line 17 of the PET (Table 4) shows the E-valve score of 0.002 which was the best score of the five valves tested, while line 18 shows a relatively high score of 3.138 on source-pressure influence. The E valve exhibits a high stability-repeatability score of 1.847 on line 19 (Table 4), while line 20 indicates a low hysteresis score of 0.120.

The low-onset-rate pressure profile for the E valve (Fig. 49), is very nearly ideal. The dotted lines in Figure 49 indicate the band of acceptable pressure values according to MIL-V-9370D. The E valve started applying pressure to the anti-G suit at approximately 1.9 G, and remained near the center of acceptable pressure level band for all higher G levels. The variation in pressure profile with respect to source pressure is extremely small (Fig. 49), while the variation due to angular displacement of the valve (shown by the "A" trace) is somewhat larger than expected. When the valve is rotated, in respect to the G vector--20° in this case--the response is expected to respond proportionally to the cosine of the angle of rotation. The E valve response more closely represented 28° rotation. The variation in pressure (Fig. 50) is extremely small compared to that of the other valves tested.

The low-onset, decreasing G pressure profiles are shown in Figure 51. The variation with respect to source pressure is very small. The decreasing G pressure profiles of the angular displacement tests are almost identical to the increasing G profiles.

The differences between the increasing and decreasing G pressure profiles (hysteresis) are shown in Figure 52. These plots make obvious the reason for the low score on line 20 of the PET. The low-onset and high-onset pressure profiles (and hysteresis) are compared in Figure 53.

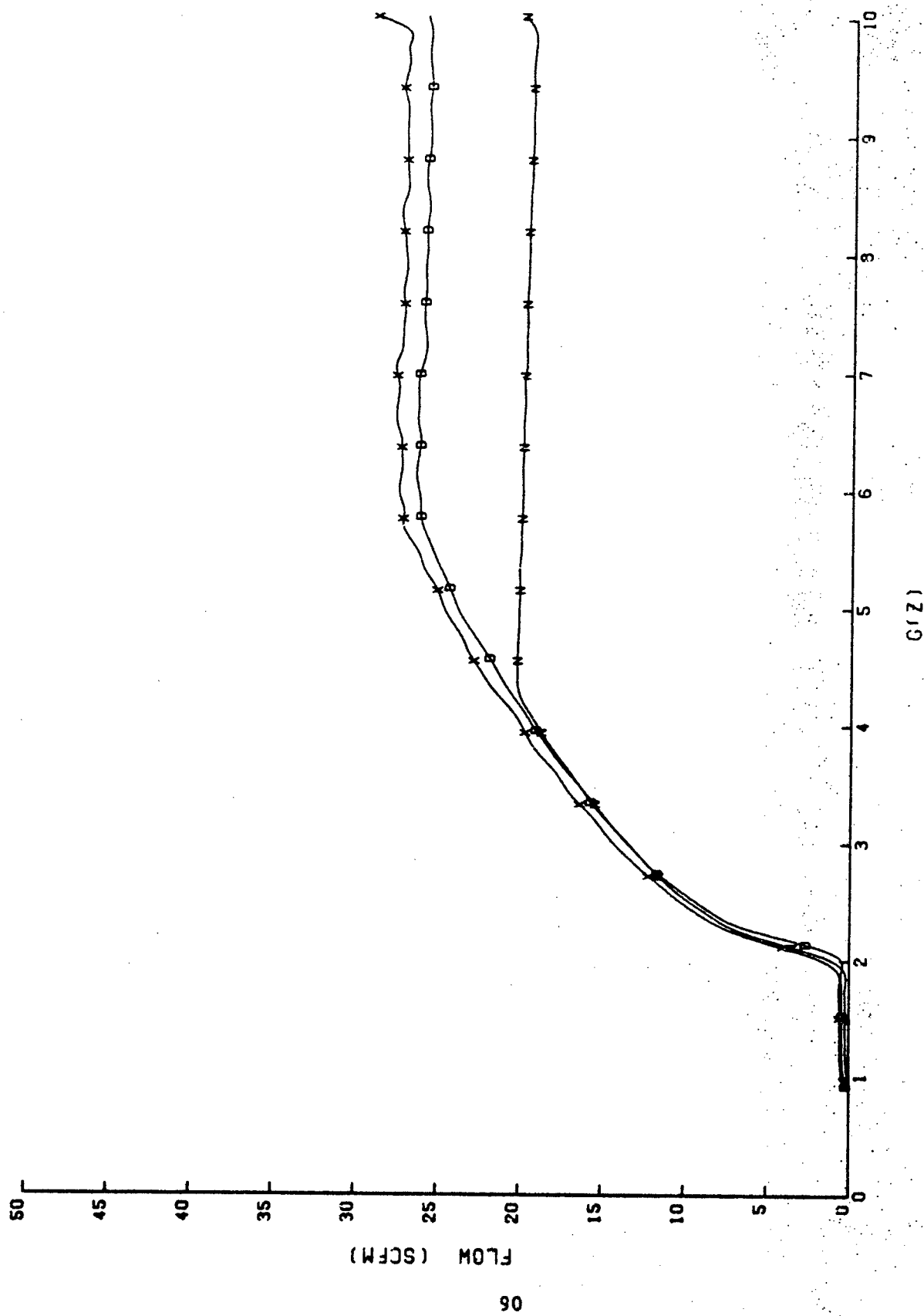


Figure 47. Electronic AGV flow as a function of source pressure.  
[Curves are: D, N, and X.]

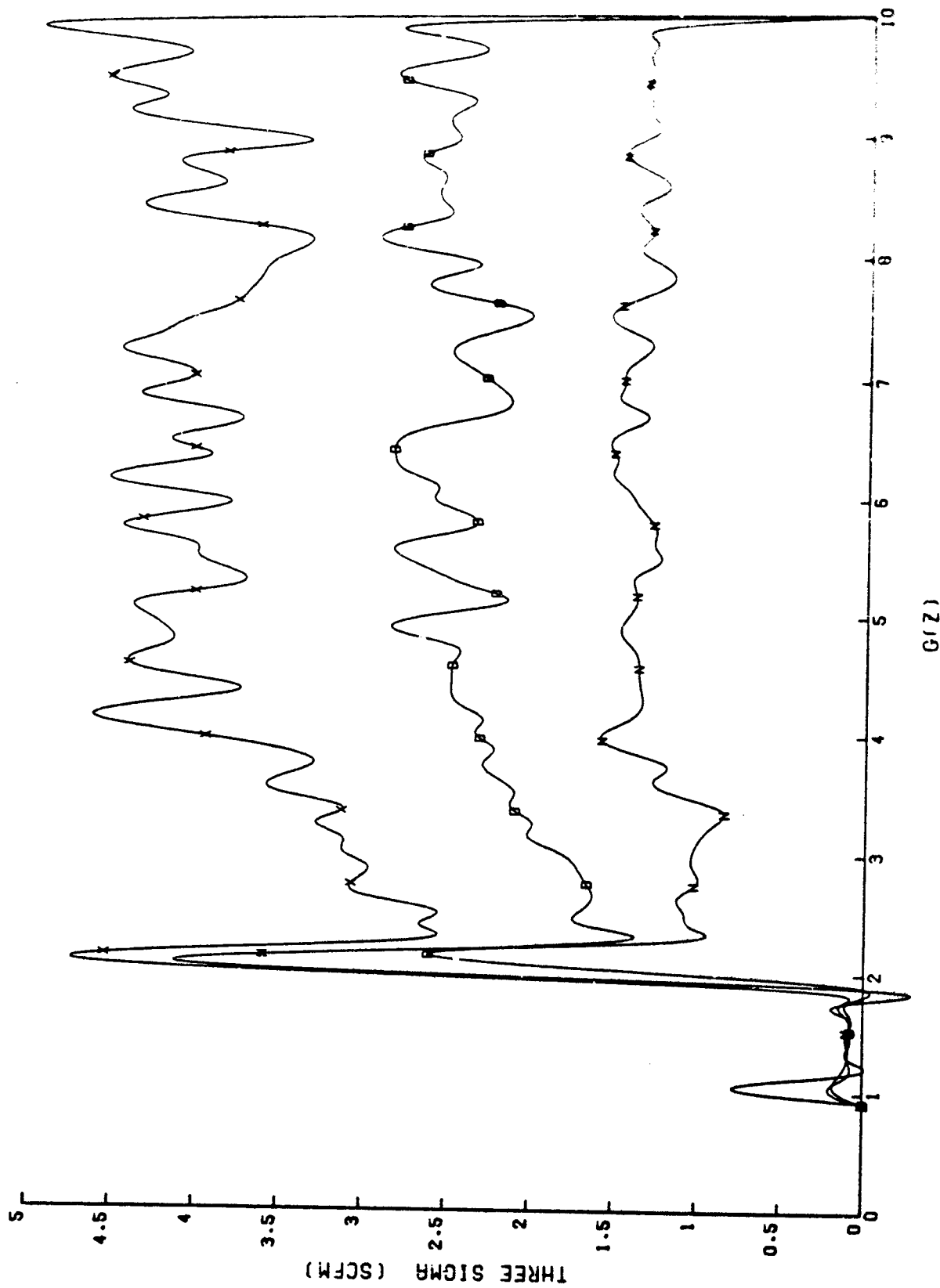


Figure 48. Electronic AGV flow three sigma as a function of source pressure.  
[Curves are: D, N, and X.]

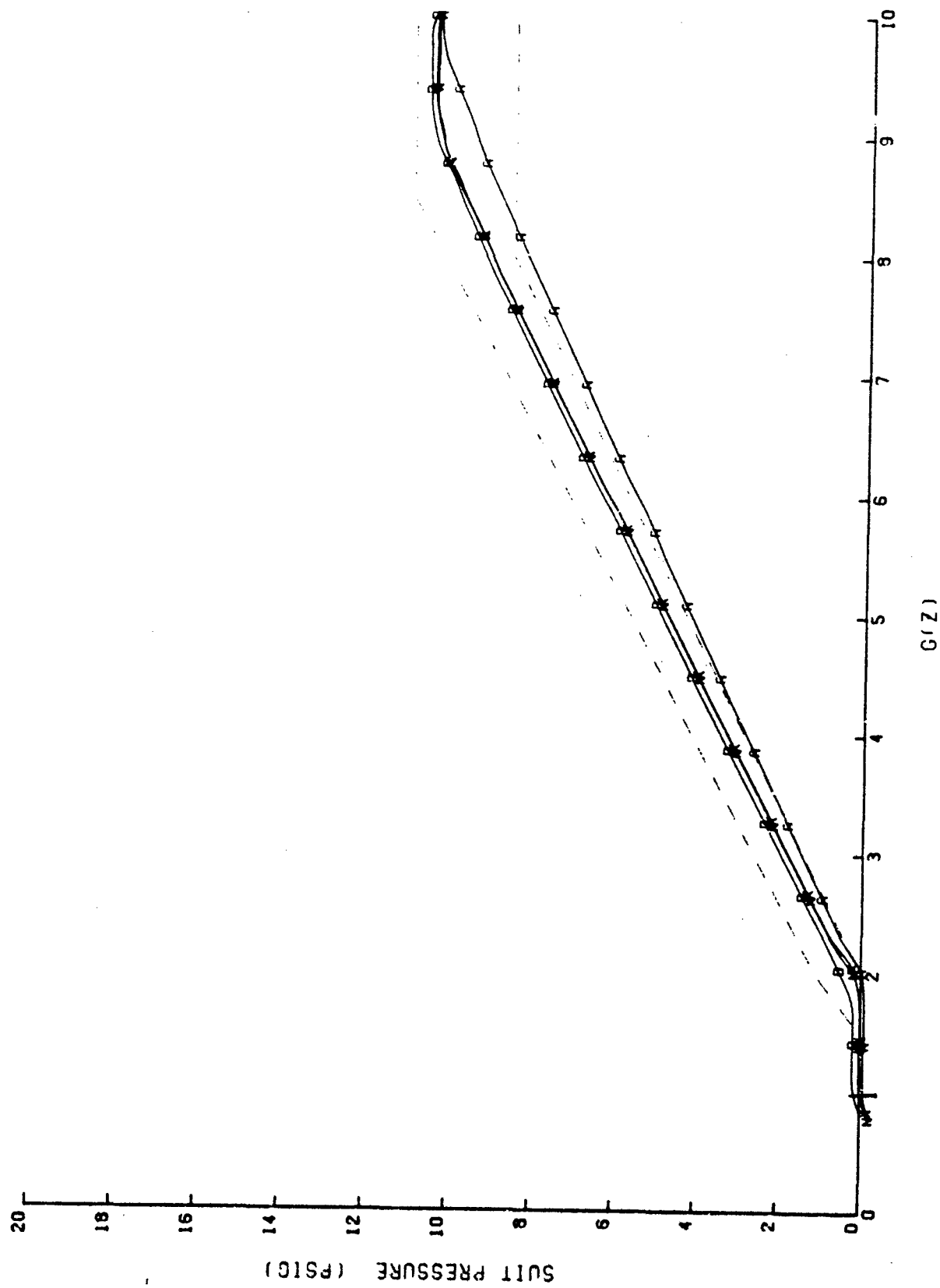


Figure 49. Electronic AGV 0.1 G/sec pressure profile as a function of source pressure.  
[Curves are: A, D, N, and X.]

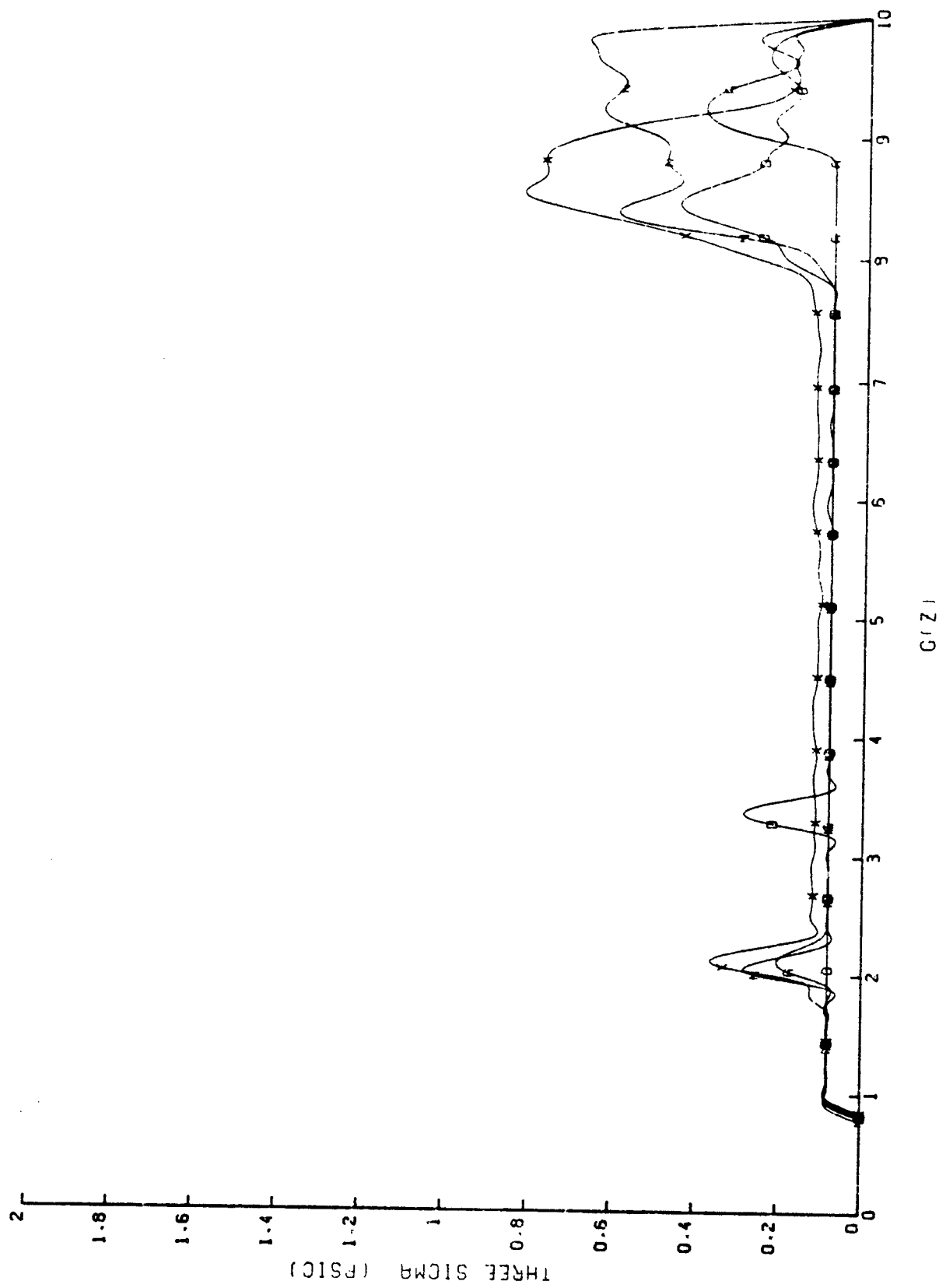


Figure 50. Electronic AGV 0.1 G/sec pressure stability as a function of source pressure.  
 [Curves are: A, D, N, and X.]



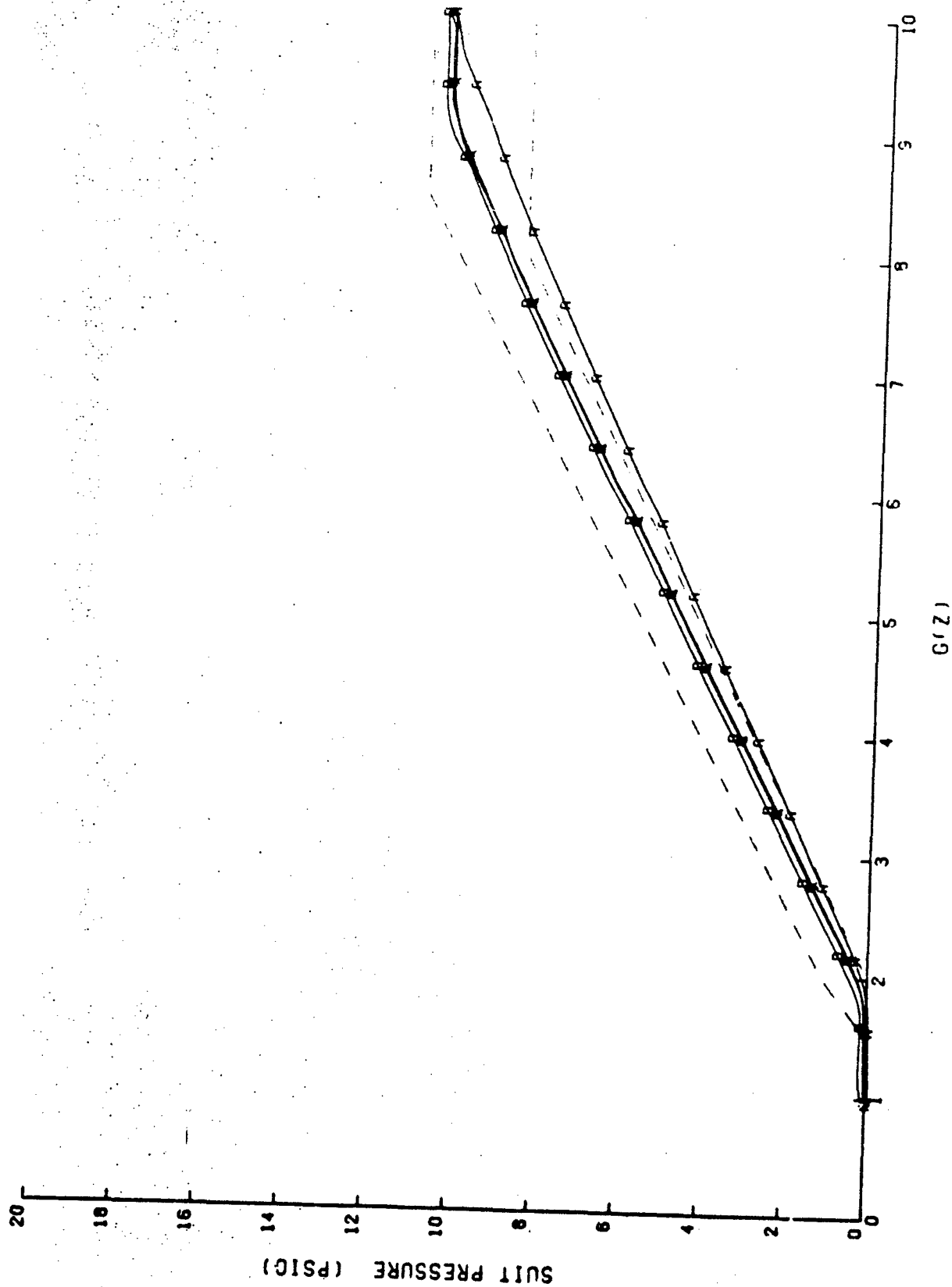
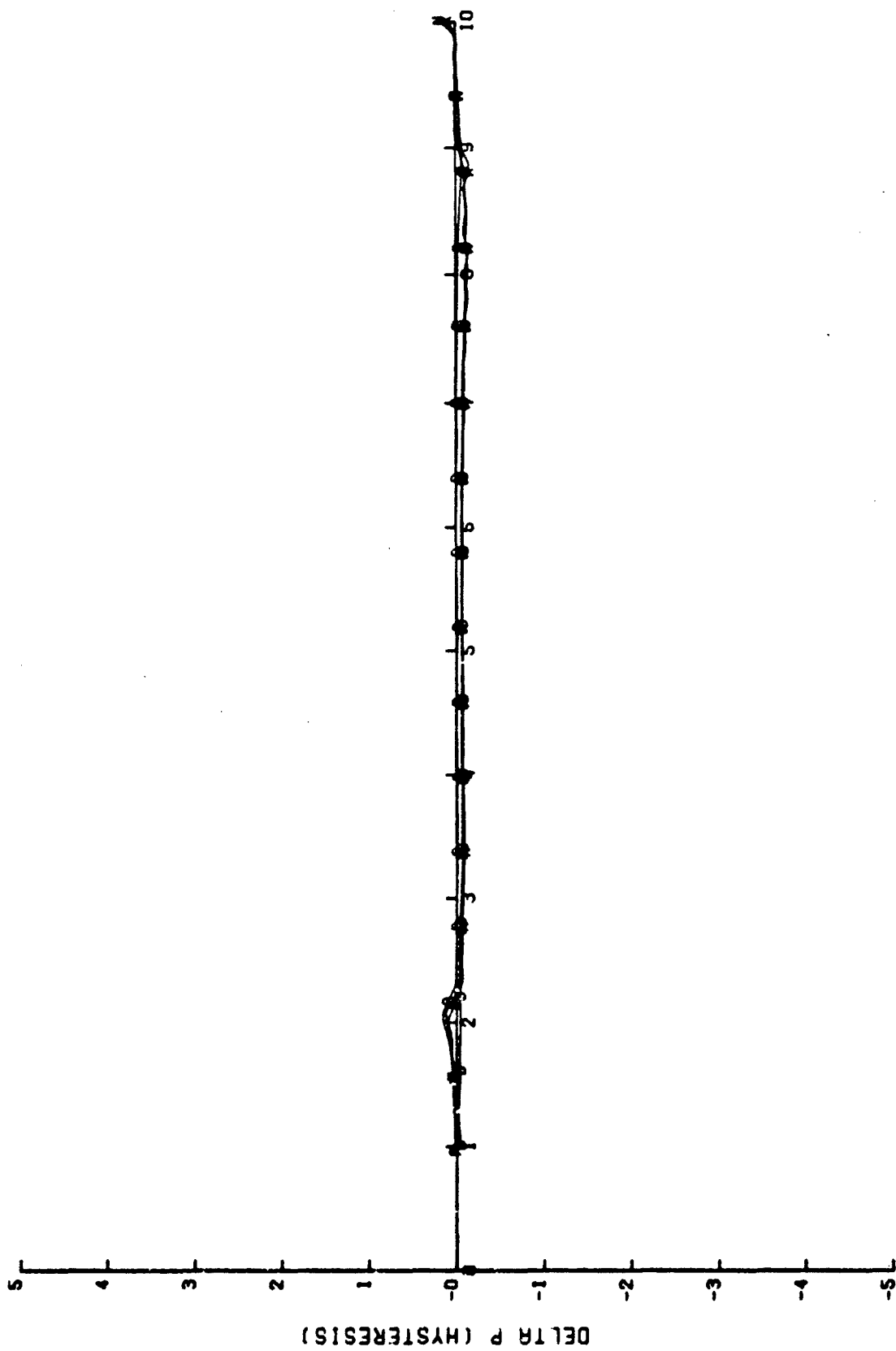


Figure 51. Electronic AGV 0.1 G/sec decreasing pressure profile as a function of source pressure.  
[Curves are: A, D, N, and X.]



G(Z)

Figure 52. Electronic AGV 0.1 G/sec pressure hysteresis as a function of source pressure.  
[Curves are: A, D, N, and X.]

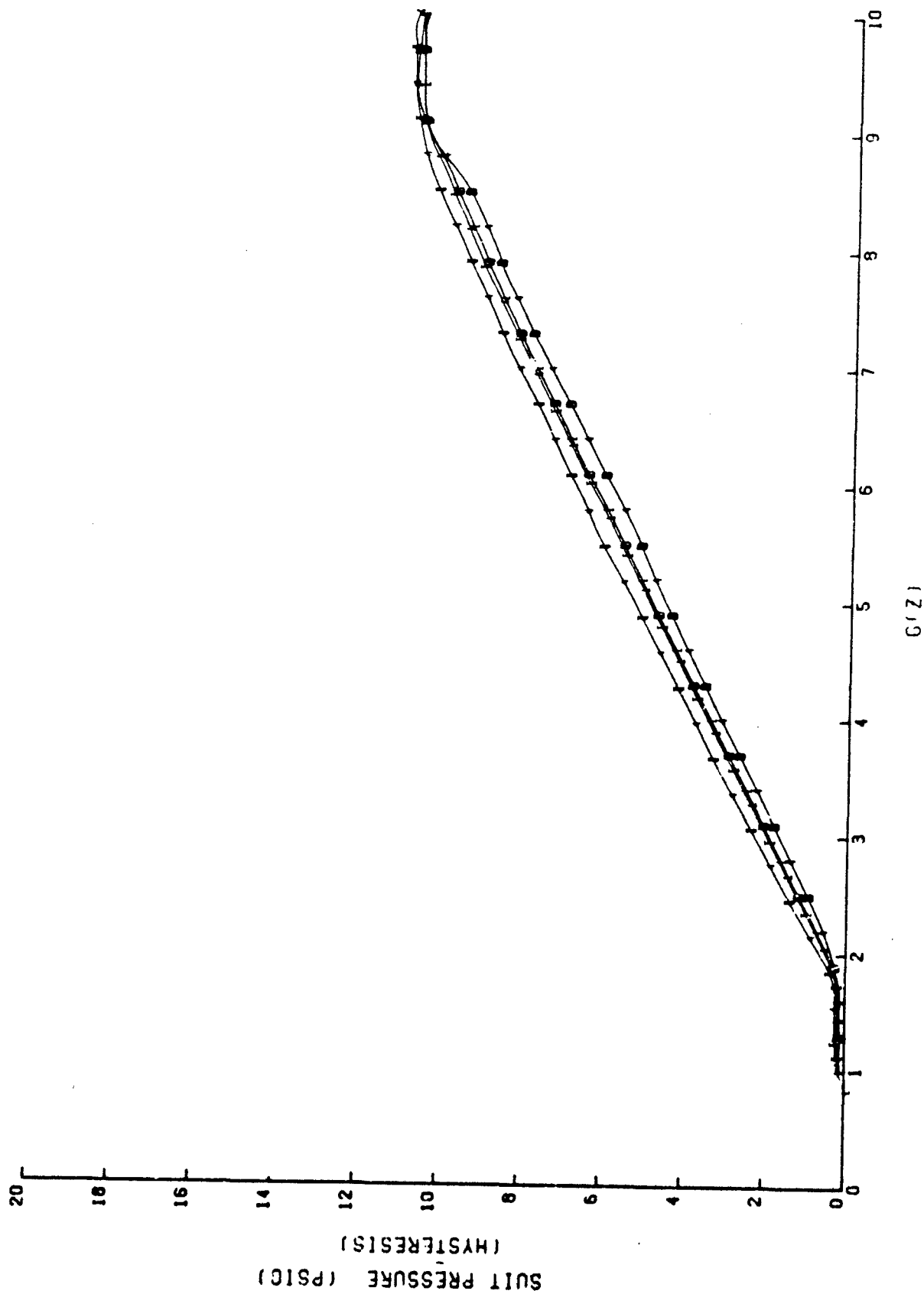


Figure 53. Electronic AGV pressure-profile comparison as a function of onset rate.

The low G-onset pressure profile of the E valve is nearly ideal under all tested conditions. This valve can be recommended for the precise control necessary for experimental studies.

#### 5.3.4 E-Valve High G-Onset-Rate Tests

The E-valve scores 15.048 in the PET (line 27, Table 4) on the high-onset-rate tests. Of the five valves tested, only the RPV performed better (and that, significantly). The E valve's linearity (line 22, PET), was surpassed (again) only by the RPV. The source pressure influence on high G-onset response at 7.931 (line 23, PET), competed favorably with the 8400A's median score of 6.642. The stability and repeatability score (line 24, PET) is 1.944, compared with a median of 3.809 and a mean of 4.591. Shown on line 25 (PET) is a hysteresis score of 1.121, matching the best score of the five valves tested. The score shown on line 26 is related to the pressure profile lag resulting from increasing G-onset rates and, because of its importance, is weighted more heavily than the other high G-onset-rate scores. The E valve's 3.093 is surpassed only by the RPV's 2.768, and compares favorably to a five-valve mean of 8.134.

The influence of G-onset rate on the 8400A's pressure profile may be observed in Figure 54. The almost random distribution of profiles within the MIL-V-9370D limits, along with the consistent values for rate of pressure increase for increasing G-onset rates (Fig. 55), indicates that the capacity of the E valve was never put to the test by the 1.5 G/sec capability of the USAFSAM centrifuge.

The influence of source pressure on the high-onset performance of the E valve is shown in Figure 56. The lags in the minimum and maximum source pressure runs and the associated high-profile variance for these curves (Fig. 57) were never satisfactorily explained.

The 1.5 G/sec decreasing G profiles (Fig. 58) indicate that the E valve performs equally well at high "offset" and "onset" rates. The negative hysteresis peaks (Fig. 59) are probably an electronic idiosyncrasy.

The E valve performs admirably under all of the conditions tested. Estimates derived from these data by the investigators imply that the E valve will perform, to specifications, at onset rates of over 3 G/sec.

#### 5.3.5 SACM Tests

The E valve consistently produced the best SACM scores of all valves tested, including the 5.023 total shown in the PET (Table 4, line 32). The RPV scored 9.292 (Table 5, line 32), while the Bendix AGV scored 33.076 (Table 3, line 32). The best E-valve score occurred in the median-source-pressure median-suit-volume test (Table 4, line 30), while the least desirable score occurred as expected (line 31) when the G vector was misaligned.

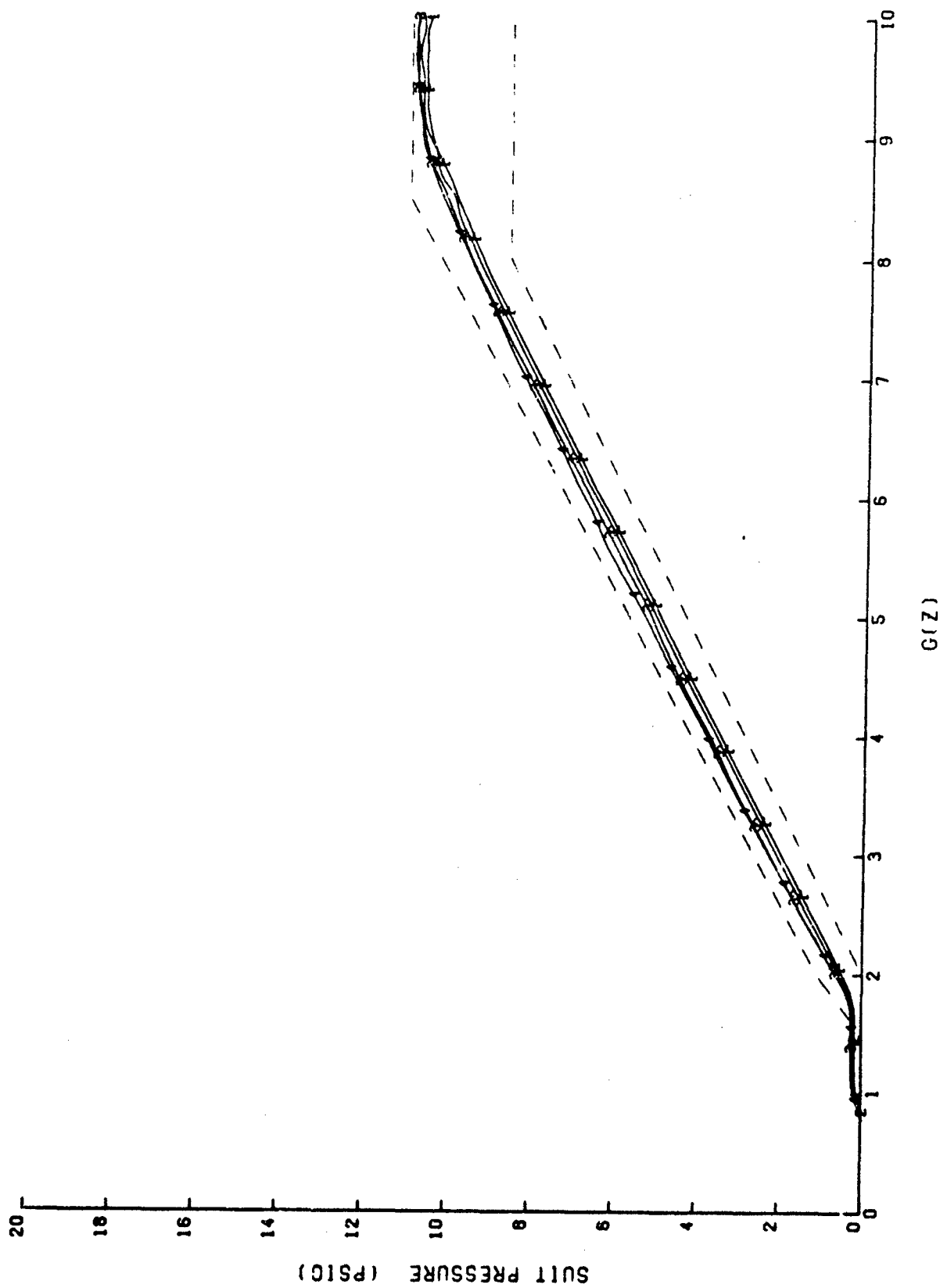


Figure 54. Electronic AGV pressure profile as a function of G-onset rate.  
[Curves are: 1, 2, 3, and 4.]

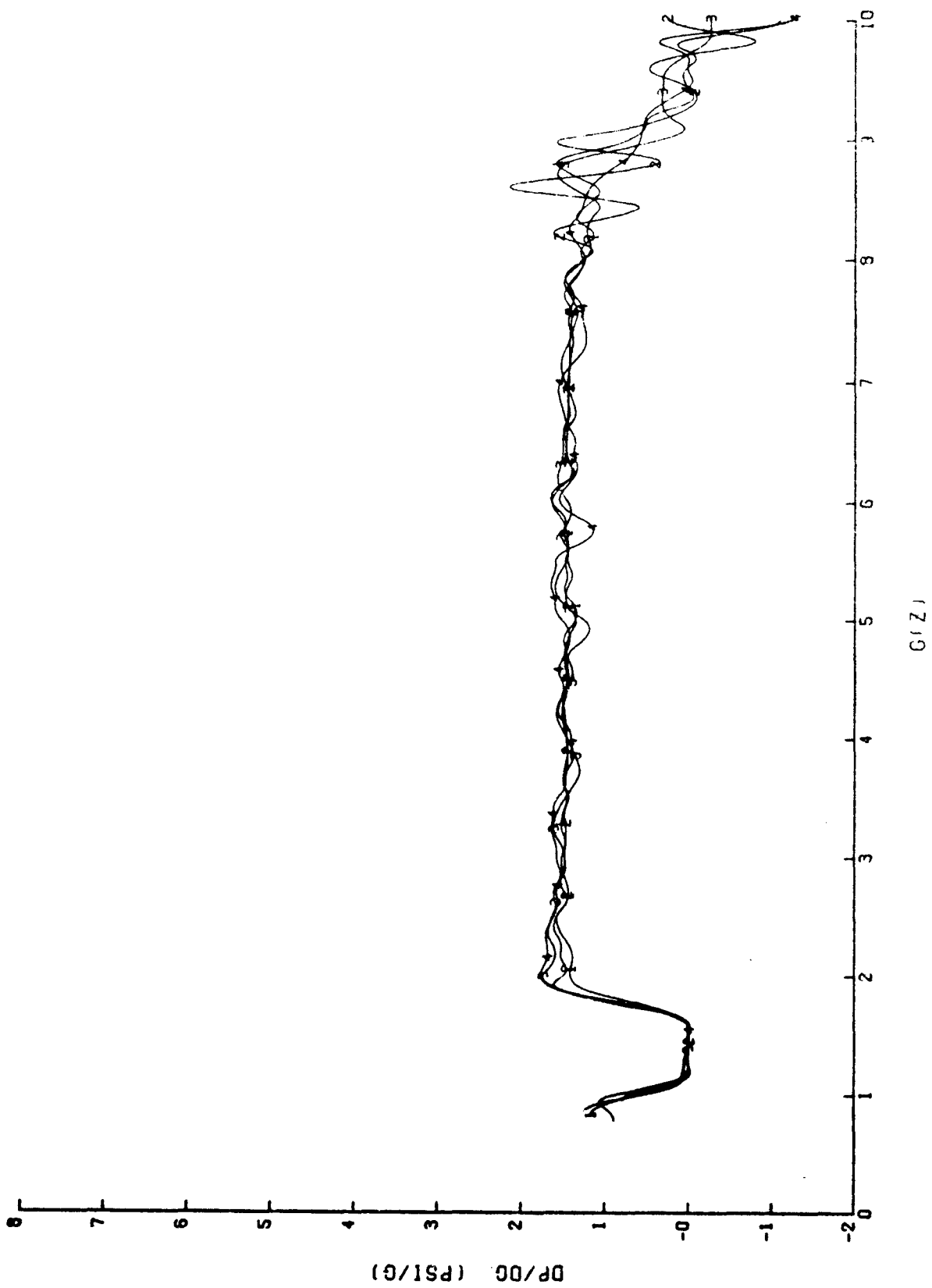


Figure 55. Electronic AGV  $dp/dG$  as a function of  $G$ -onset rate.  
[Curves are: 1, 2, 3, and 4.]

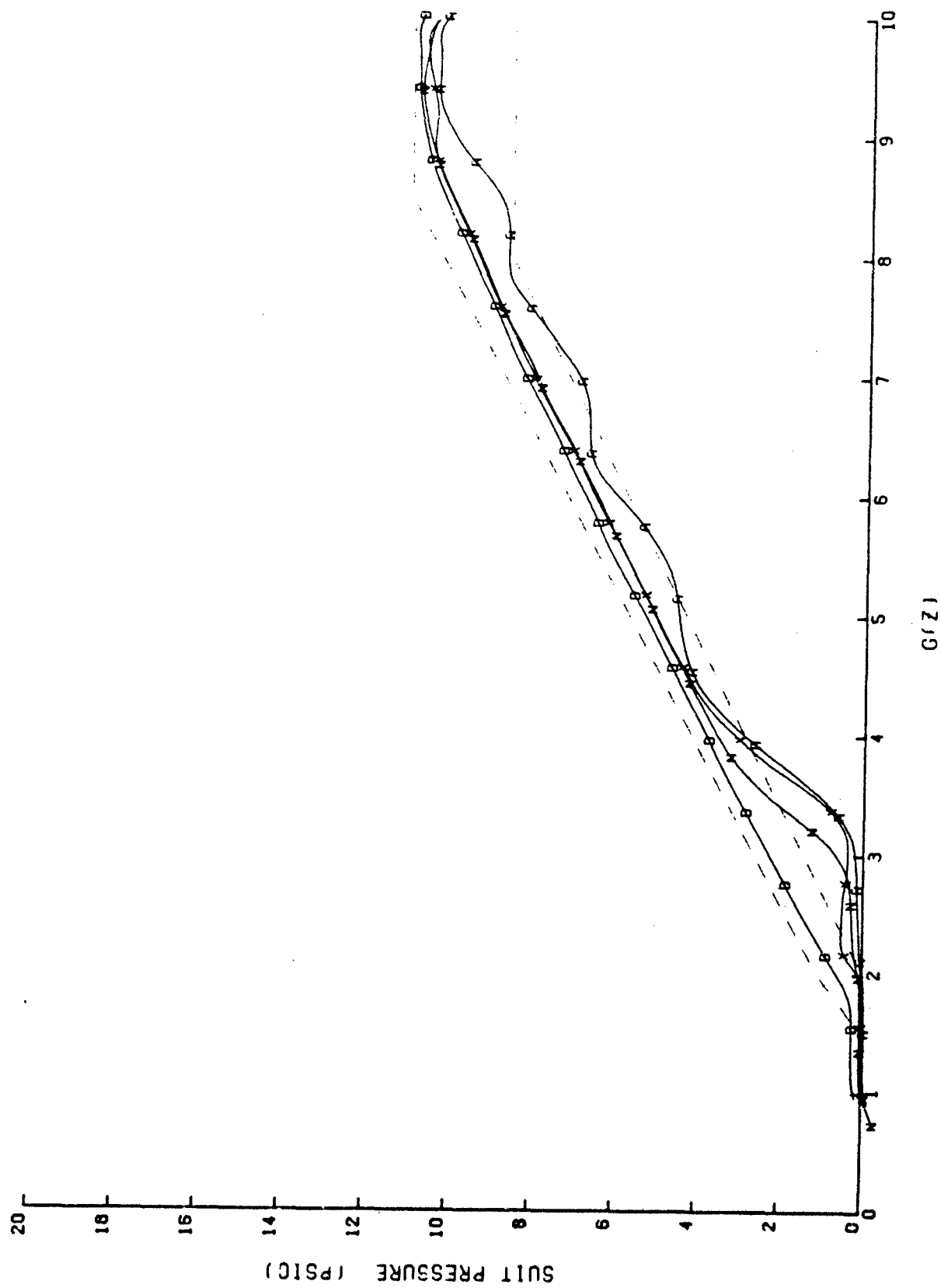


Figure 56. Electronic ACV 1.5 G/sec pressure profile as a function of source pressure.

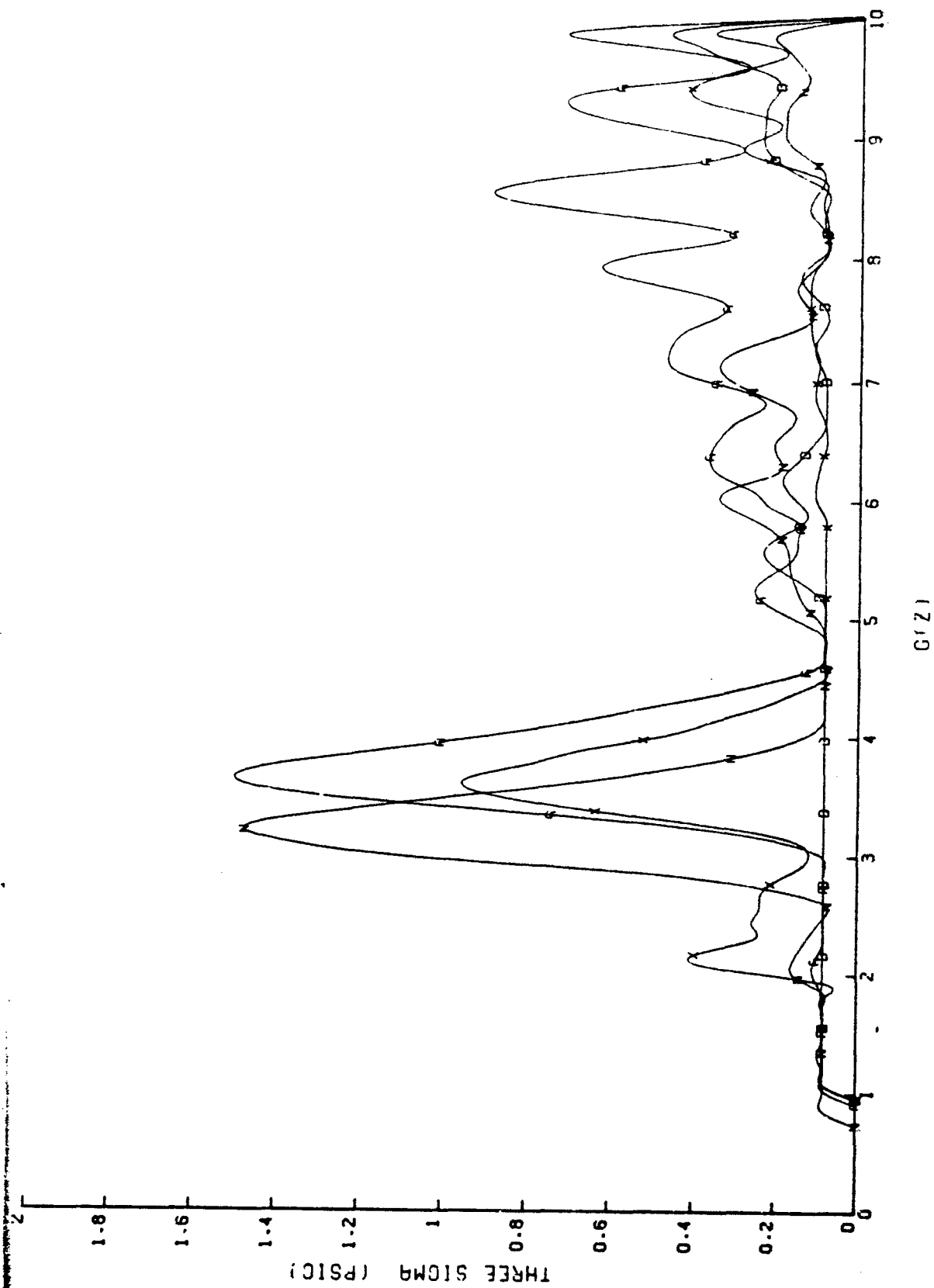


Figure 57. Electronic AGV 1.5 G/sec pressure variation as a function of source pressure.  
[Curves are: A, D, N, and X.]



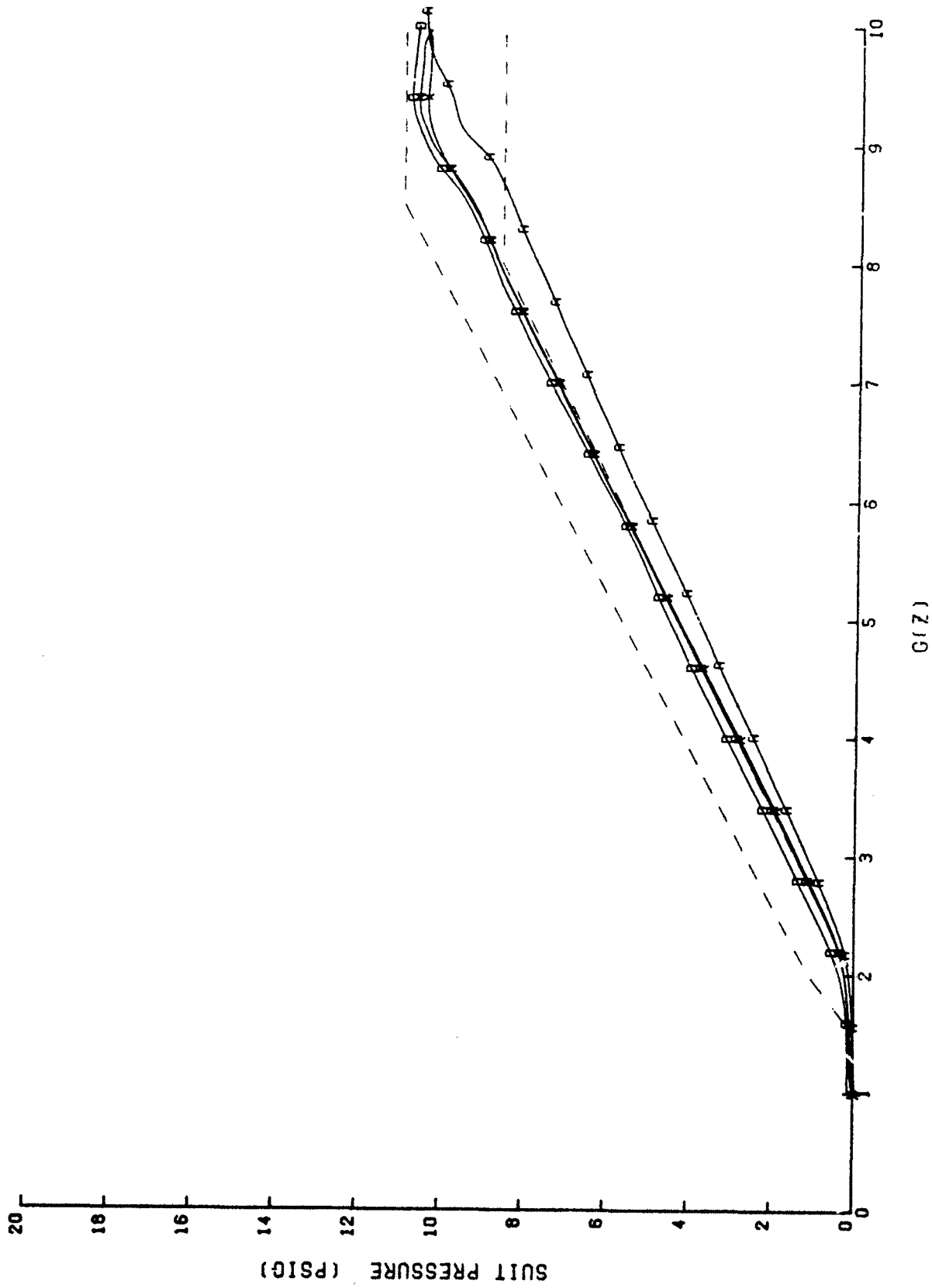
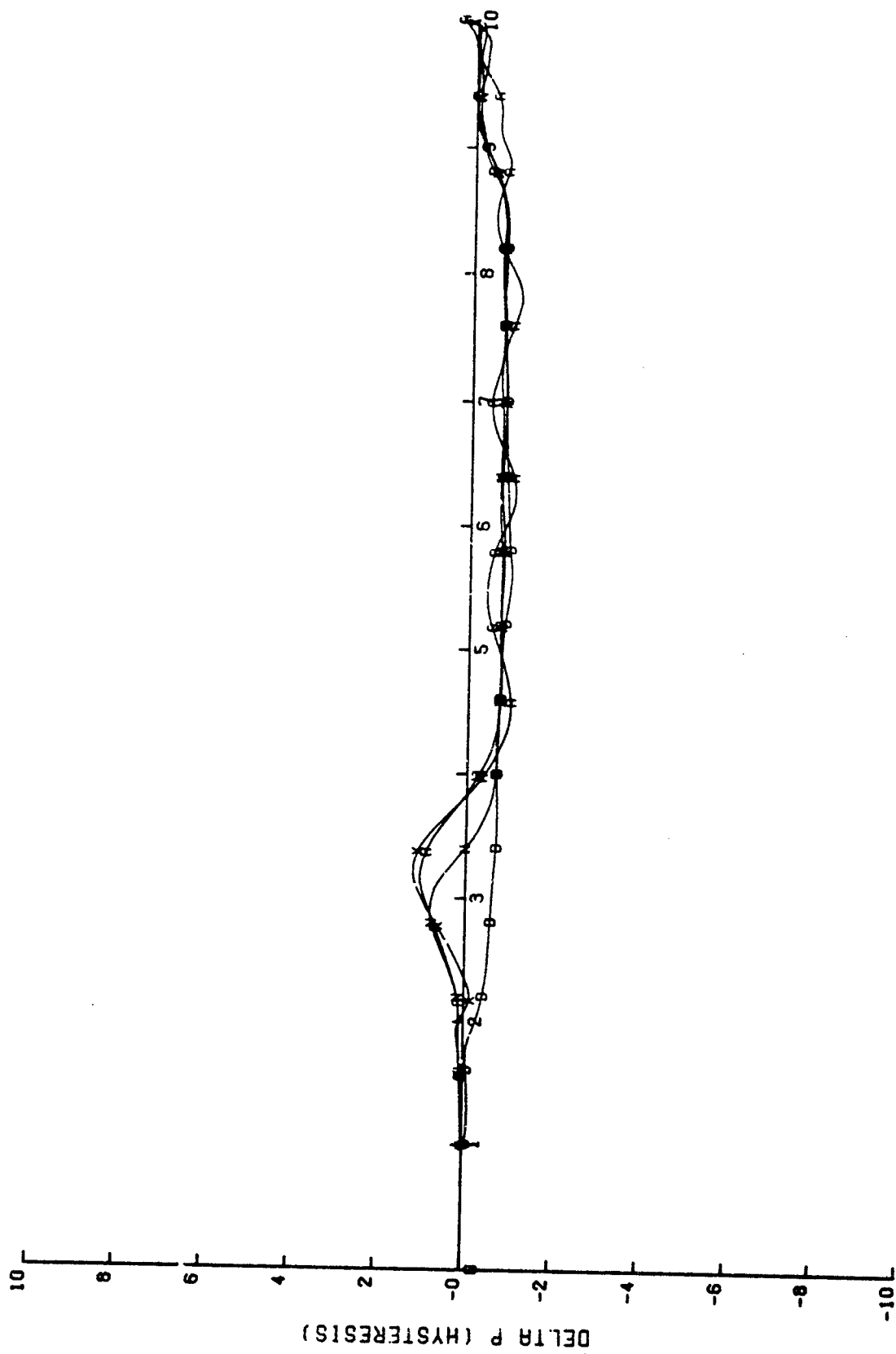


Figure 58. Electronic AGV 1.5 G/sec decreasing pressure profile as a function of source pressure.  
 [Curves are: A, D, N, and X.]



$G(Z)$

Figure 59. Electronic AGV 1.5 G/sec pressure hysteresis as a function of source pressure.  
[Curves are: A, D, N, and X.]

The pressure profiles in Figure 60 represent the actual and ideal pressures that should result from the G stimuli resulting from an SACM test when a minimum source pressure is applied to the AGV and a maximum "suit" volume is attached. The ideal pressure for all SACM tests was derived from the mid-source pressure profile shown in Figure 49, and from the actual instantaneous G-value applied. The differences between the real and ideal pressures, along with corresponding onset rates, are shown in Figure 61. The abscissa of this graph represents the integral of G with respect to time. This device allows a real (unweighted) indication of magnitudes, while the size of the excursion (actually the area under the curve) is weighted by the G level. In this manner, a 0.5-psig excursion at 6 G will appear twice as large as a 0.5-psig excursion at 3 G, even though the amplitudes are the same. The area under these curves is used as an evaluation factor in the PET. The E valve's min-max curves (Figs. 61, 63, 65, and 67), indicate pressure excursions never exceed 0.5 psig positive or negative, except for the G vector misalignment case, while the maximum onset rates achieved during the tests were +1.1 G/sec and -1.5 G/sec.

The last two figures in this report section (Figs. 66 and 67) are unique only in that the valve was run with its centerline at an angle of 20° to the G vector. Since the ideal pressure here was derived in the same manner as in the previous three sets, the actual pressure is expected to be low (refer to section 5.3.3); and Figure 67 confirms this expectation. Otherwise the curves are comparable with Figures 64 and 65, except that perhaps a little more tendency to overshoot is exhibited.

The applicability of the E valve to realistic tactical environments is supported by its excellent performance in these SACM tests. These tests (Figs. 60 - 67) suggest that a "militarized" version of the E valve, without the variable features necessary for research, may be very applicable to current and future tactical weapons systems developed by the Air Force.

#### 5.3.6 Conclusions on the E-Valve's Performance

The E valve exhibits excellent control and stability under all conditions tested, and promises these same characteristics in much more stringent environments.

### 5.4 Ready Pressure Anti-G Valve (RPV) Test Results

#### 5.4.1 RPV and Test Description

The RPV was developed by the USAFSAM/VNB staff at Brooks AFB, Texas. The unique operational characteristic of this valve is that it pre-inflates the anti-G suit to  $10 \pm 2.5$  mm Hg. This pre-inflation fills the dead space in the G suit, before the onset of G, in an effort to improve the high G-onset response.

The basic pneumatic regulation mechanism is a modified ALAR 8400A AGV. The modification consists of increasing the spring tension on the first-stage regulator, to increase the controlled pressure of that stage to 17 psig, and of enlarging several ports in the flow path through the second-stage regulator. Both of these modifications resulted in increases in the valve's open-flow capacity.

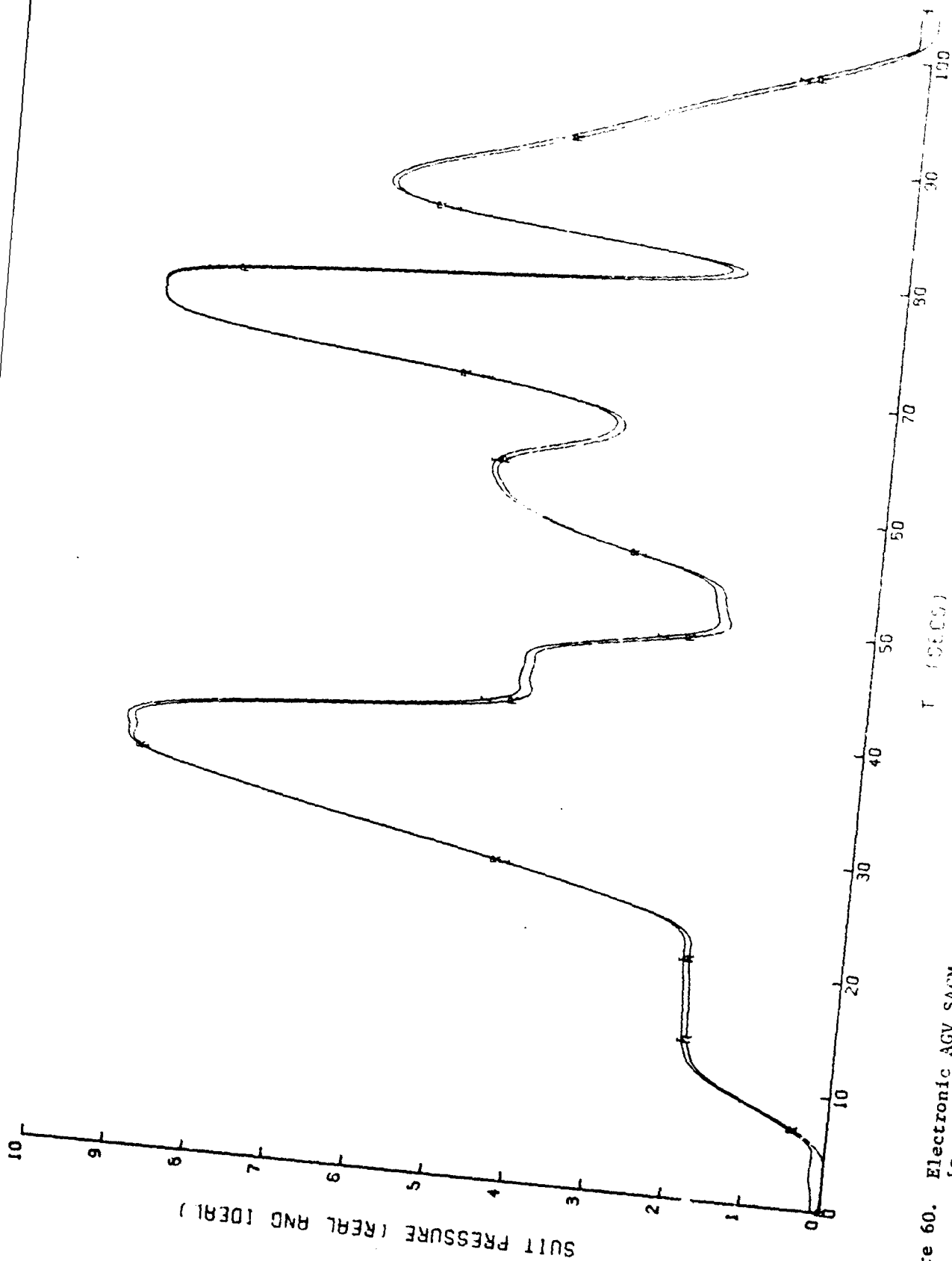


Figure 60. Electronic AGV SACM pressure-profile comparison with minimum source pressure and maximum suit pressure.  
[Curves are: I and R.]

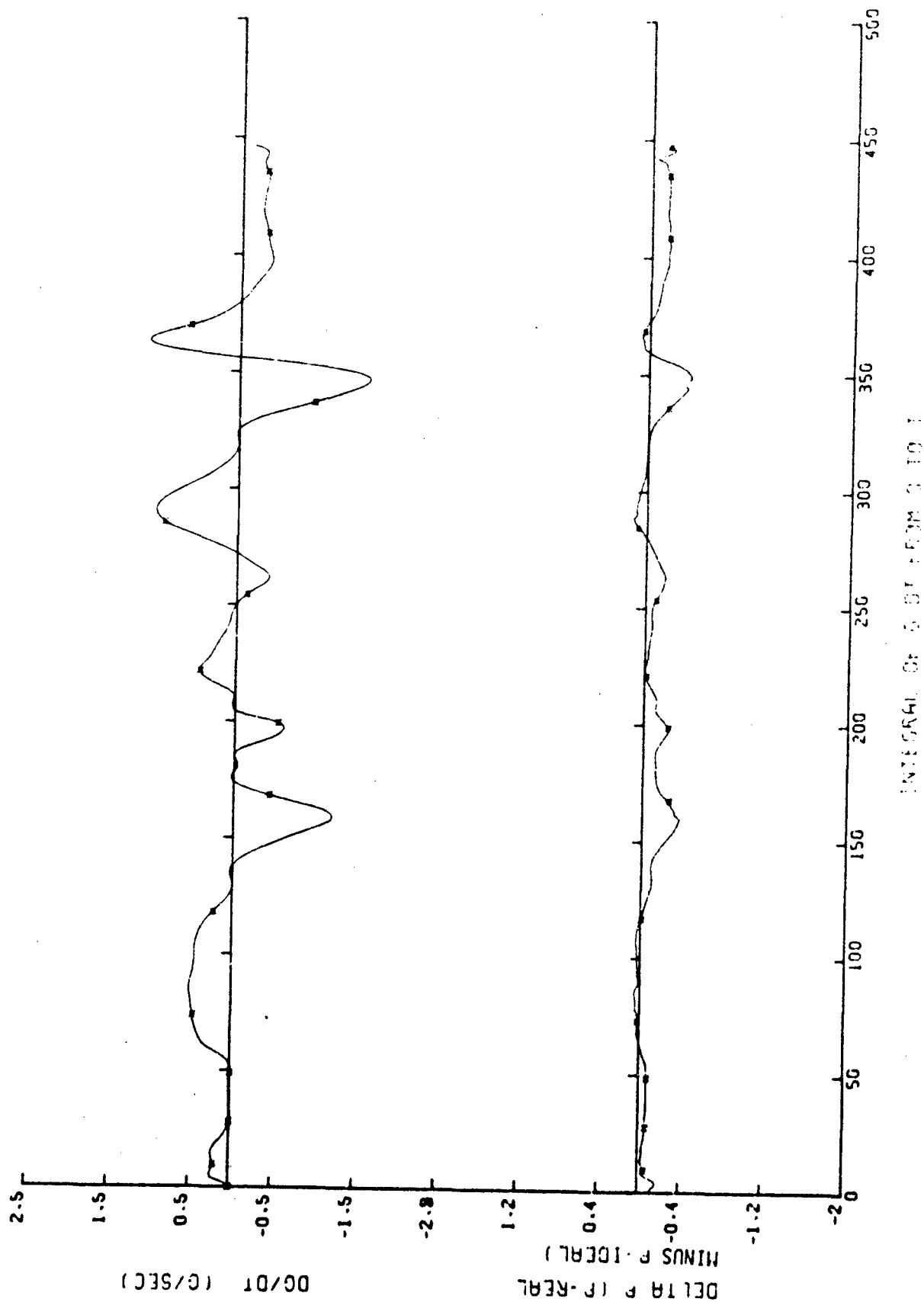


Figure 61. Electronic ACV pressure deviation and  $dG/dt$  for the minimum source pressure and maximum suit volume S100.  
[Curves are: \*.]

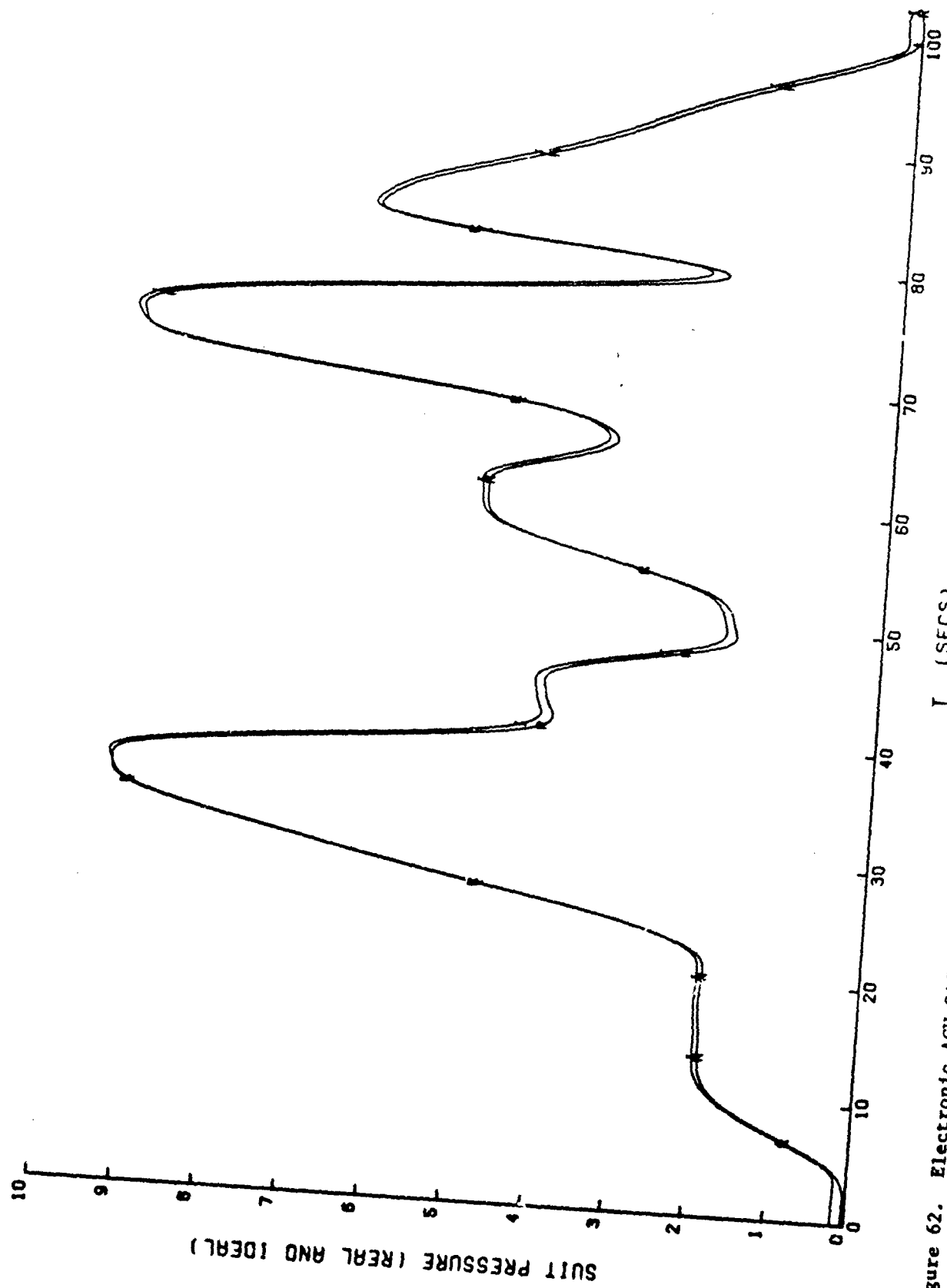
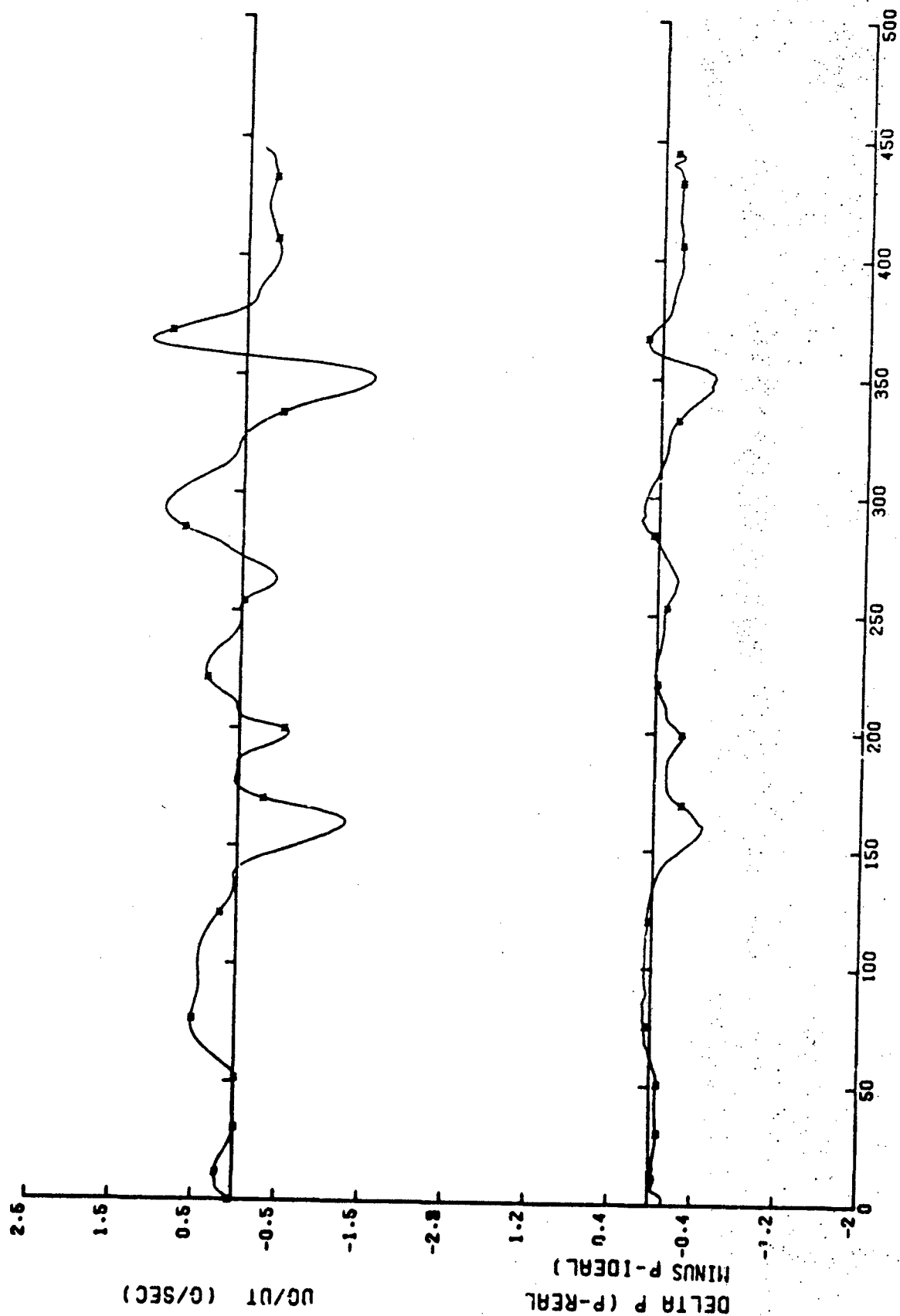


Figure 62. Electronic AGV SACM pressure profile comparison with maximum source pressure and minimum suit volume.  
 [Curves are: I and R.]



INTEGRAL OF  $\Delta P$  FROM 0 TO T

Figure 63. Electronic AGV pressure deviation and  $\Delta P$  for the maximum source pressure and minimum suit volume SACM. [Curves are: \*.]

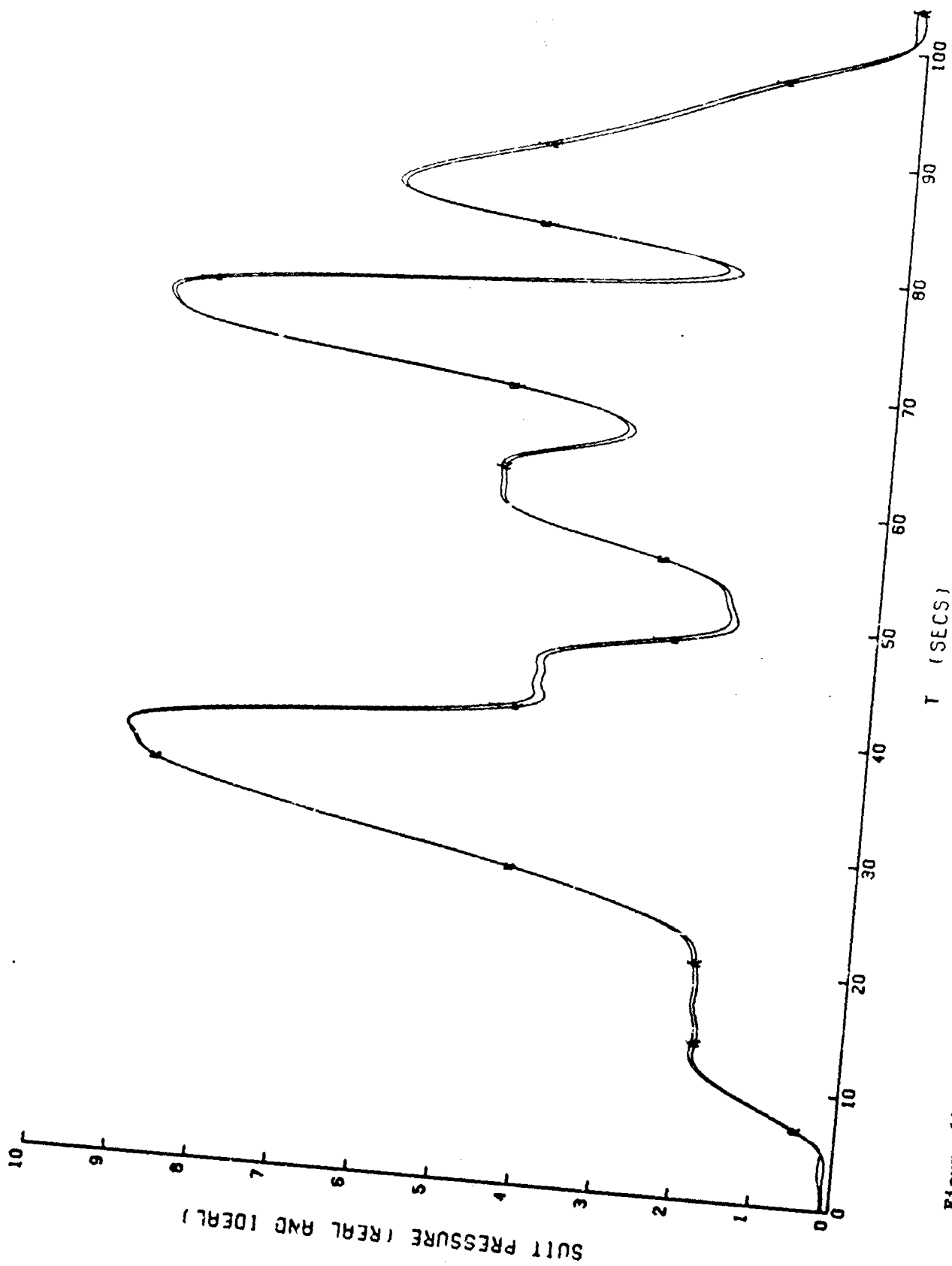


Figure 64. Electronic AGV SACM pressure profile comparison with median source pressure and suit volume.  
[Curves are: I and R.]



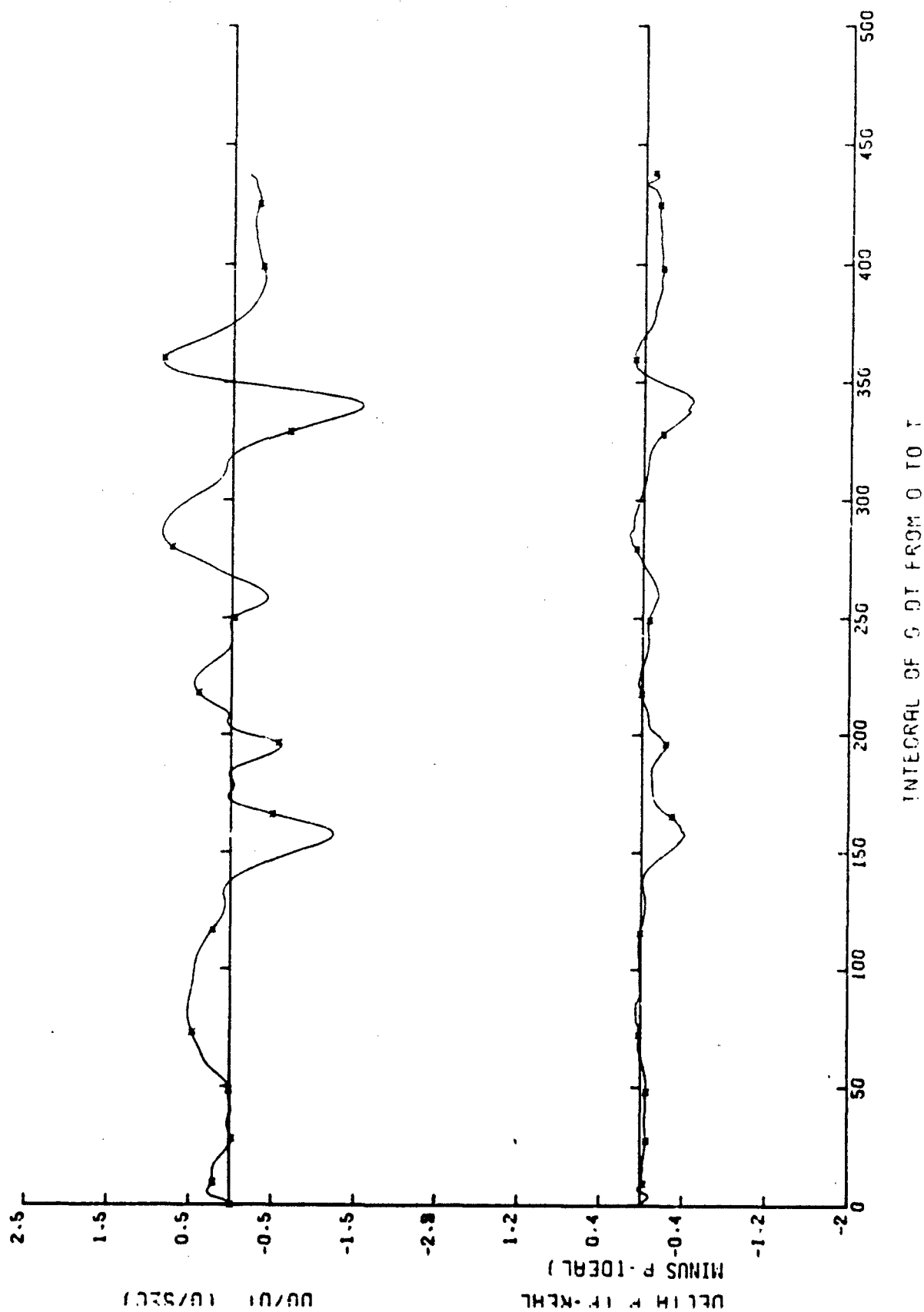


Figure 65. Electronic AGV pressure deviation and  $dG/dt$  for the median source pressure and suit volume SACM. [Curves are: \*,]

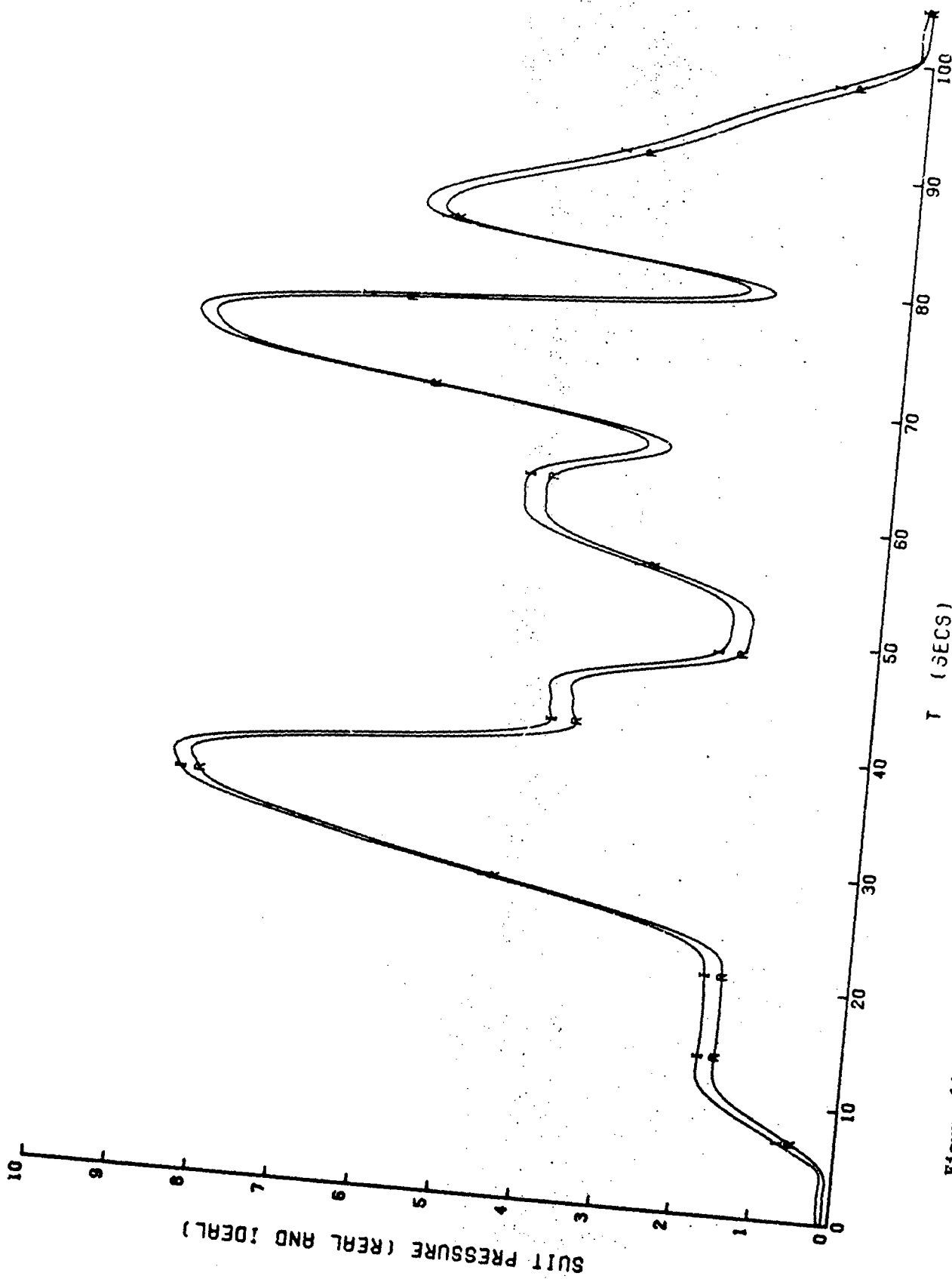


Figure 66. Electronic AGV SACM pressure profile comparison with the G vector misaligned.  
 [Curves are: I and R.]

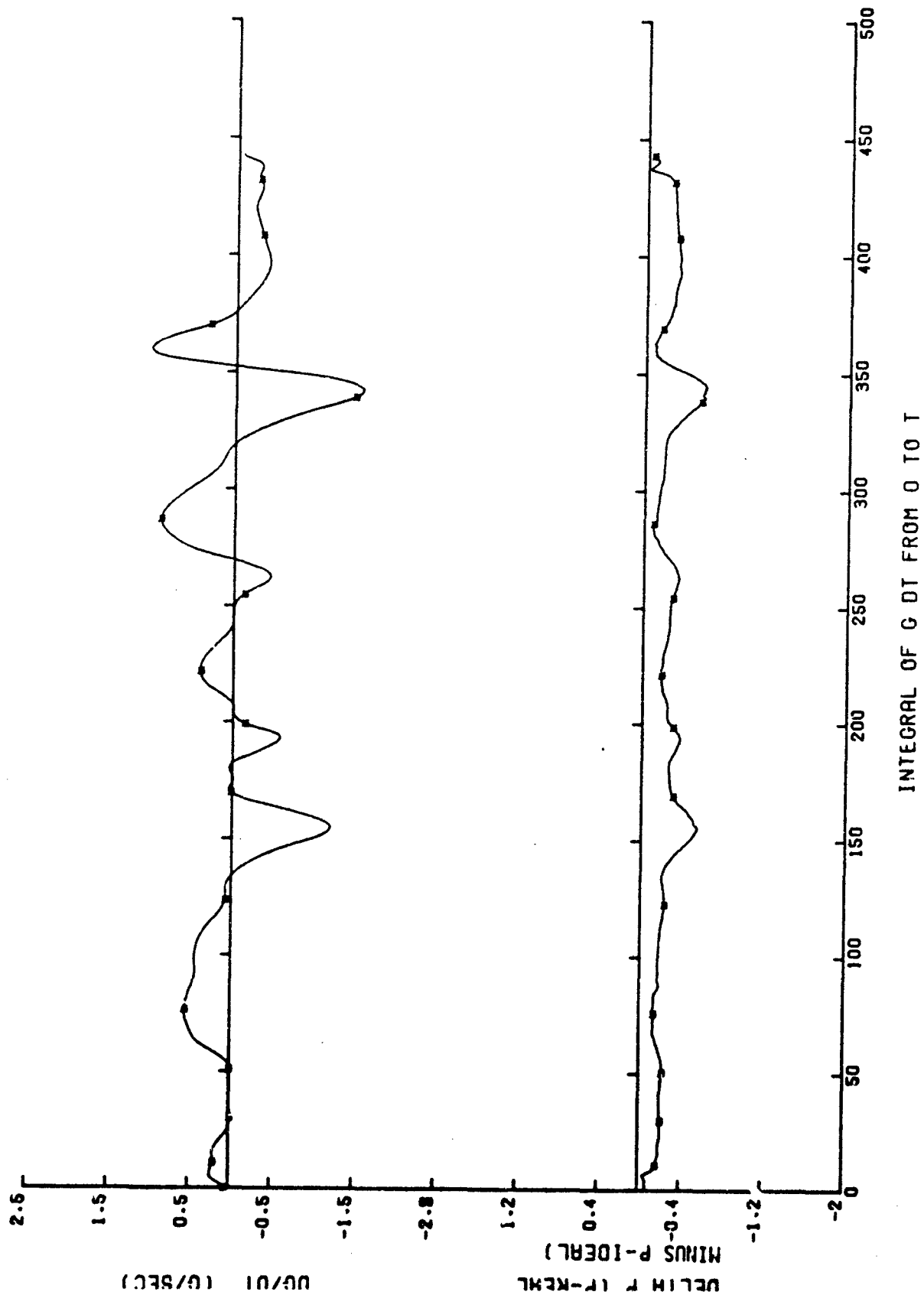


Figure 67. Electronic AGV pressure deviation and  $dG/dt$  for the G vector misaligned SACM.  
[Curves are: \*.]

Pre-inflation is accomplished through the attachment of a spring, lever, and pneumatic piston--so arranged that the lever depresses the "press-to-test" button on the 8400A with just enough force to initiate the 10 mm Hg "ready pressure." The pneumatic piston, driven by suit pressure, serves the further purpose of removing the spring-lever influence when G is applied since the higher suit pressure lifts the lever completely free of the 8400A press-to-test button. The normal mass-spring subassembly is thus left completely free (essentially unmodified) to operate in the normal manner.

For purposes of SVTP testing and GVALVPGM analysis, standard values assigned to the 8400A were assigned to the RPV, and are shown in the PET (lines 1 - 7, Table 5). In addition to being the design values for the valve, these values were selected as standards for the GVALVPGM analysis because they permitted direct application of the unit to a wide variety of weapons systems in the present USAF inventory. Since these values are the GVALVPGM standard, the RPV scored a perfect minimum of 3.0 on the PET design total.

#### 5.4.2 RPV Flow Tests

The flow test performance score of the RPV, 4.556 (line 16, Table 5), was the lowest (most desirable) score of the five valves tested under this contract. The total open-flow tests showed a group low of 1.438 (line 12, Table 5), with the Electronic AGV (E valve) the nearest challenger. The source pressure influence on the open-flow performance was essentially equal to the 8000A's (lines 13 - 14, Table 5), the median (Bendix) showing slightly more source pressure influence. Line 15 of Table 5 indicates the RPV open flow was slightly less stable at 0.186 than the median 8000A at 0.185 (Table 4).

The RPV open-flow profiles are shown in Figure 68. The increase in flow--with respect to applied G--reaching peak flow values at 6 G, is unusually slow. The distribution of flow, with respect to source pressure, is reasonably low. The fluctuations in the open-flow data are shown in Figure 69, as the  $3\sigma$  values, and appear to increase with source pressure in a relatively linear manner.

The principal importance of this test is to estimate the time required by this valve to fill an anti-G suit under very high onset conditions. This information is especially important in estimating performance at G-onset rates beyond the capability of the test facility. In the case of the RPV flow curves, the inexplicably low slope (increase in flow rate) between 2 G and 6 G, offset by the high total-flow values and the ready-pressure principle, represent good prospects for good performance under high G-onset rates. It would be desirable to reach maximum flow values at a lower G level.

#### 5.4.3 RPV Low G-Onset-Rate Tests

The low onset-rate test-performance score of 2.110 (Table 5, line 21) for the RPV was the lowest (most desirable) score of the five AGV's tested. The Bendix and Electronic AGV's produced considerably higher (less desirable) scores, while the 8000A and RPV valves produced only slightly higher scores. Line 17 of the PET (Table 5) shows the RPV scores moderately well in linearity (even though only the Bendix exhibited a less desirable performance),

while line 18 shows a low 0.634 on source-pressure influence. The RPV exhibits a reasonably low stability-repeatability score on line 19 (Table 5), while line 20 indicates an equally low hysteresis score.

In the low onset-rate pressure profile for the RPV (Fig. 70), the dotted lines indicate the band of acceptable pressure values according to MIL-V-9370D. The RPV started applying pressure to the AGS at approximately 2.3 G, but the prepressurization kept the pressure profile not only within the specifications limits but also well inside limits of acceptable pressure levels for all higher G levels. The variation in pressure profile with respect to source pressure is extremely small (Fig. 70), while the variation due to angular displacement of the valve (shown by the "A" trace) is only slightly larger than expected. When the valve is rotated with respect to the G vector, 20° in this case, the response is expected to respond proportionally to the cosine of the angle of rotation. The RPV response more closely represented 24° rotation, probably indicating some influence of frictional forces on the mass spring system. The variation in pressure (Fig. 71) was very low.

The low-onset decreasing G-pressure profiles are shown in Figure 72. The variation with respect to source pressure is very small and essentially random, as expected. The decreasing G-pressure profile of the angular displacement tests more closely represents theoretical values than the increasing G profile, especially at higher G levels.

The differences between the increasing and decreasing G-pressure profiles (hysteresis) are shown in Figure 73. In most cases, these values are acceptably low. The large peak at 2.7 G is primarily the result of the characteristic late start exhibited by the 8400A from which the RPV was constructed. The low-onset and high-onset pressure profiles (and hysteresis) are compared in Figure 74.

As indicated by the low total PET score, the RPV performed very well at low G-onset rates.

#### 5.4.4 RPV High G-Onset-Rate Tests

The RPV scored an exceptionally low total of 6.475 (Table 5, line 27) on the high onset-rate tests. This is the lowest total of the five valves tested, and well below the median (8000A at 21.061) valve performance. The RPV's linearity was the best of the AGV's tested, with the 0.087 shown on line 22 of the PET (Table 5). The source pressure influence is reflected by the score of 0.804 on high G-onset response (Table 5, line 23), and compared very favorably to the mean score (Table 5, line 23) of 6.597. The stability and repeatability score (line 24) is a low of 1.409, the mean of 4.591 resulting from a relatively poor performance by the Bendix AGV. A hysteresis score of 1.408 (line 25) is compared to a five-valve mean of 3.258 and a median of 3.030. The score on line 26 is related to the pressure profile lag resulting from increasing G-onset rates and, because of its importance, is weighted more heavily than the other high G-onset-rate scores. The RPV's 2.768 is the best of the scores from the valves tested, and is compared to the five-valve mean of 8.134.

TABLE 5. READY PRESSURE ANTI-G VALVE PERFORMANCE EVALUATION TABLE

TEST STANDARDS:

1. SPMIN = 30. PSIG
2. SPMID = 125. PSIG
3. SPMAX = 300. PSIG
4. THETA = 20. DEGREES
5. SVMIN = 6. LITERS
6. SVMID = 10. LITERS
7. SVMAX = 14. LITERS

CHARACTERISTIC NUMBERS:

8. XSPMX = 1.0000
9. XSPMN = 1.0000
10. XTHTA = 1.0000
11. DESIGN TOTAL: 3.000
12. XFLBR = 1.438
13. XDELF = 1.452
14. XDDLFL = 1.481
15. XSIGF = 0.186
16. FLOW TOTAL: 4.556
17. XCCP1 = 0.091
18. XDDP1 = 0.634
19. XSGP1 = 0.818
20. XDPP1 = 0.568
21. LOW-ONSET TOTAL: 2.110
22. XCCP2 = 0.087
23. XDDP2 = 0.804
24. XSGP2 = 1.409
25. XDPP2 = 1.408
26. XTDPP2 = 2.768
27. HIGH-ONSET TOTAL: 6.475
28. XIDPA = 2.006
29. XIDPB = 2.744
30. XIDPC = 1.937
31. XIDPD = 2.606
32. SACM TOTAL: 9.292
33. VALVE: READY PRESSURE TOTAL: 25.433

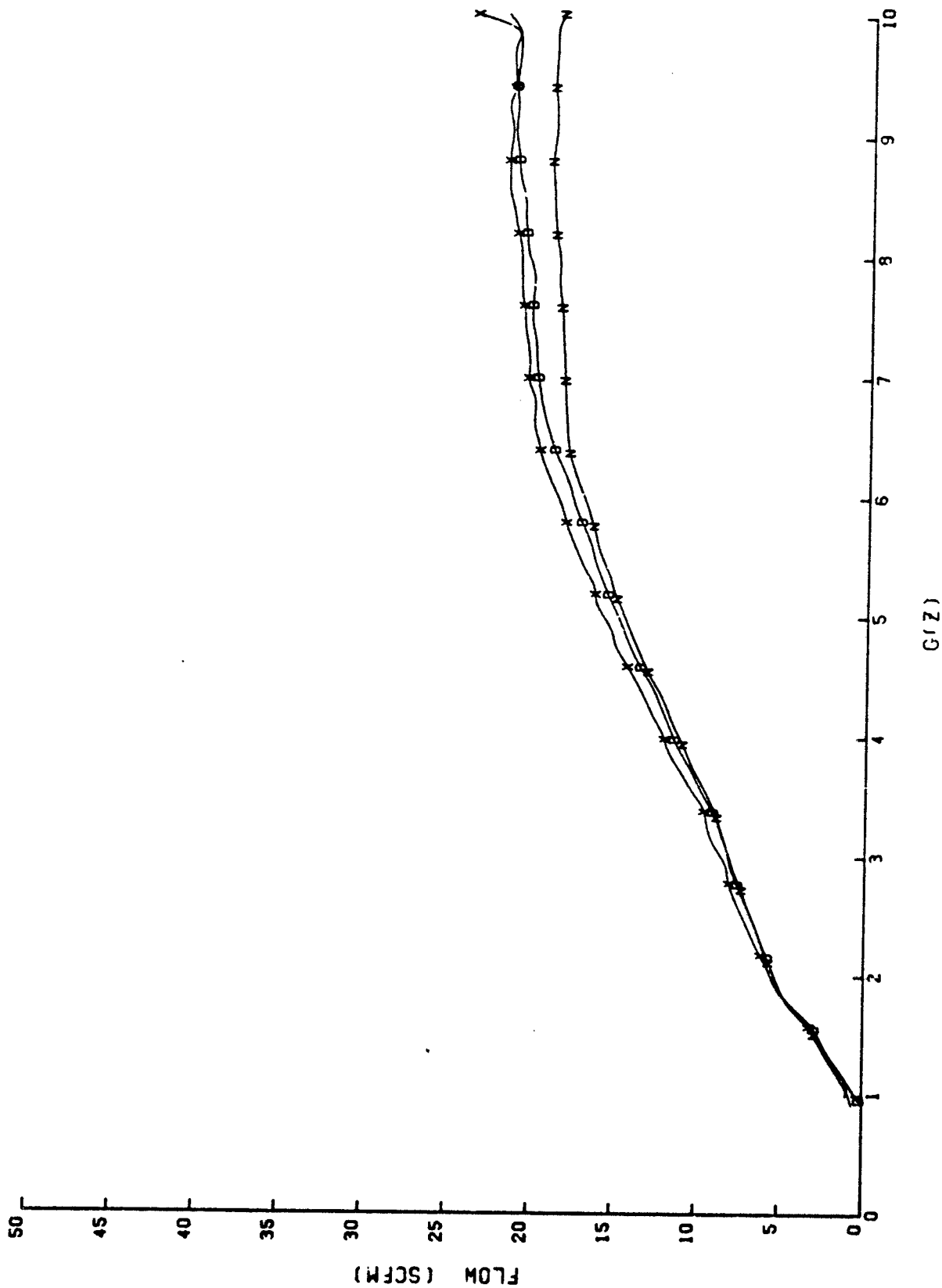


Figure 68. Ready Pressure AGV flow as a function of source pressure.  
 [Curves are: D, N, and X.]

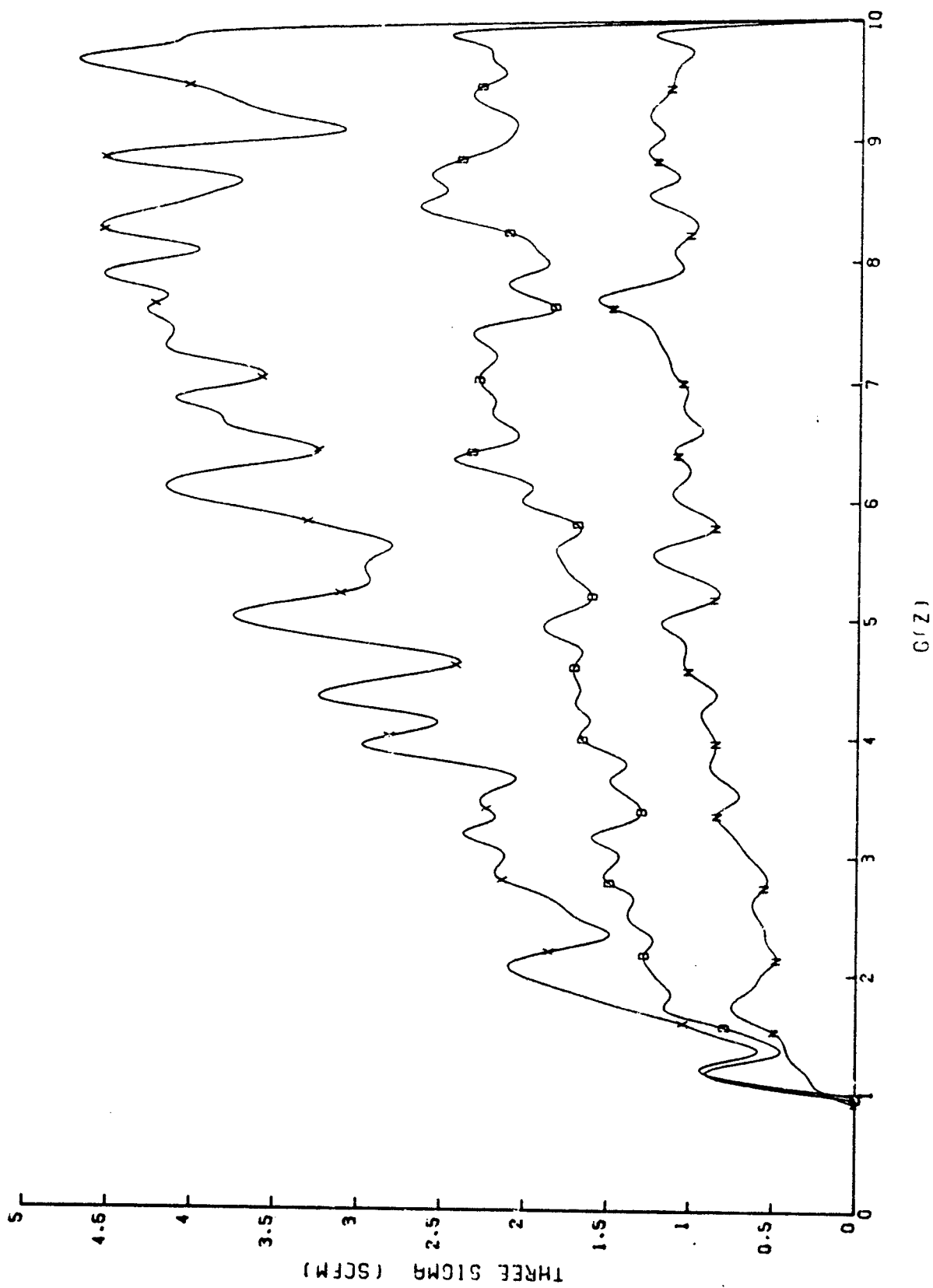


Figure 69. Ready Pressure AGV flow three sigma as a function of source pressure.  
 [Curves are: D, N, and X.]



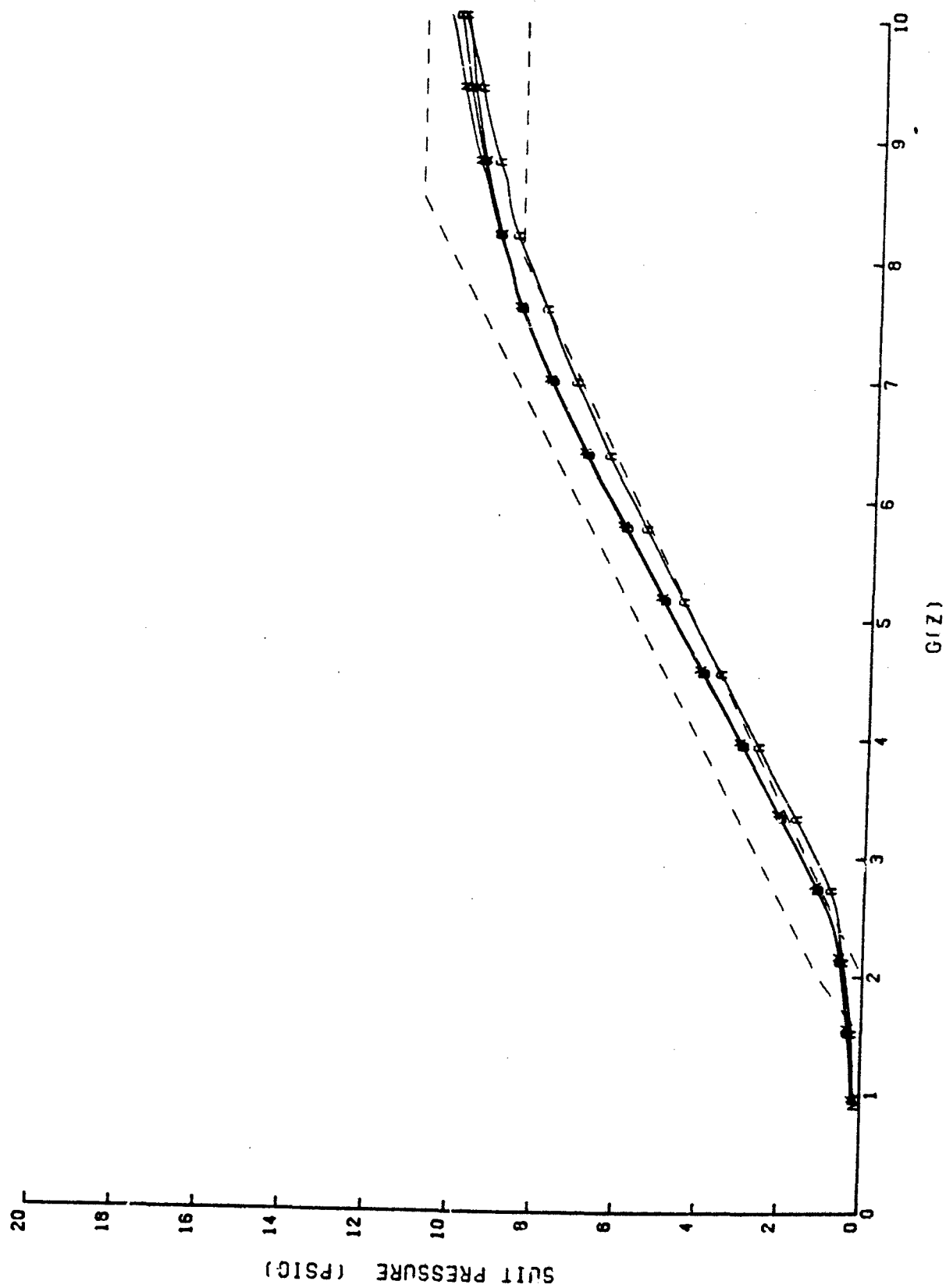


Figure 70. Ready Pressure AGV pressure profile as a function of source pressure.  
 [Curves are: A, D, N, and X.]

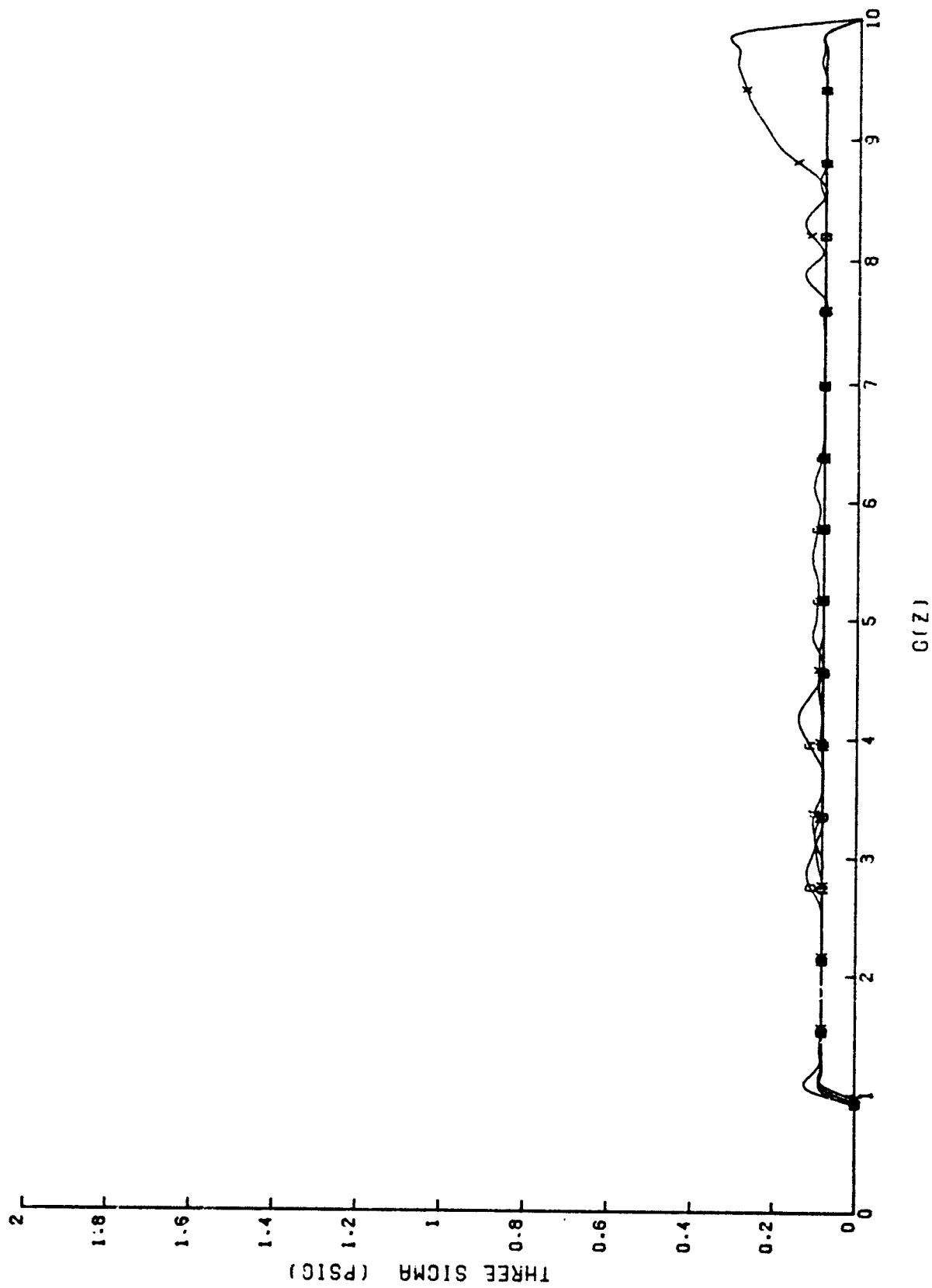


Figure 71. Ready Pressure AGV 0.1 G/sec pressure stability as a function of source pressure.  
[Curves are: A, D, N, and X.]

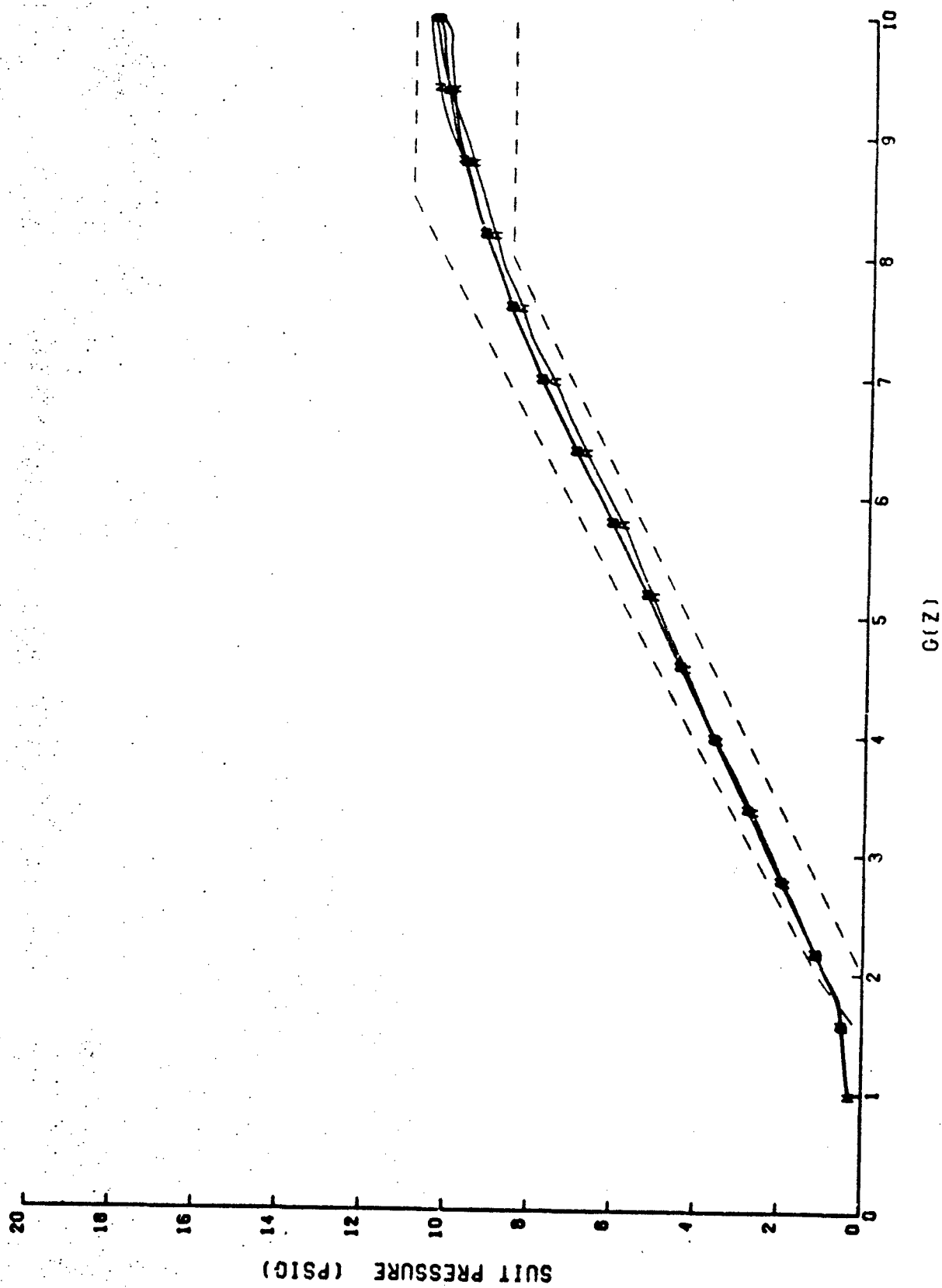
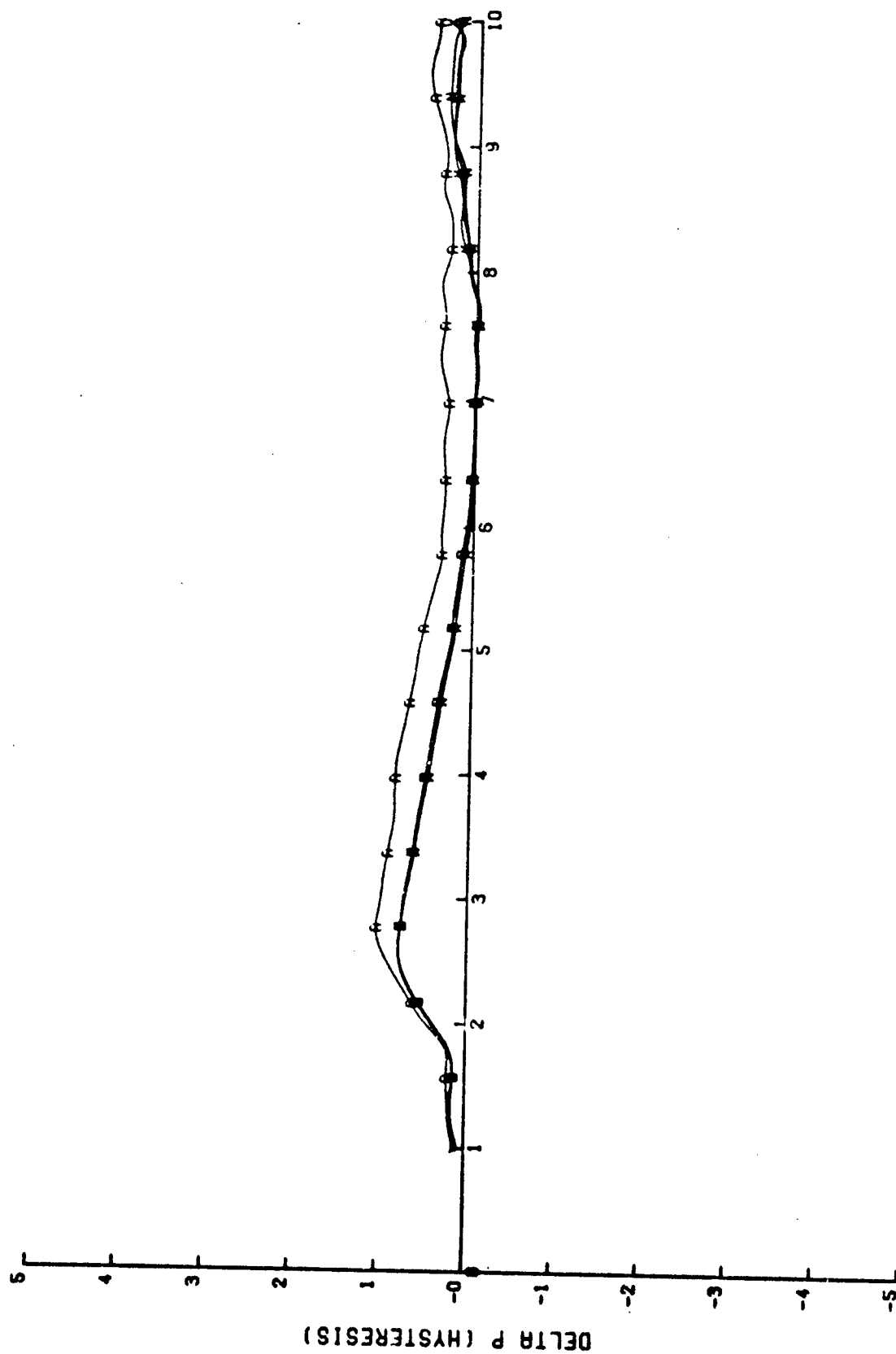


Figure 72. Ready Pressure ACV 0.1 G/sec decreasing pressure profile as a function of source pressure. [Curves are: A, D, N, and X.]



$G(Z)$

Figure 73. Ready Pressure AGV 0.1 G/sec pressure hysteresis as a function of source pressure.  
[Curves are: A, D, N, and X.]

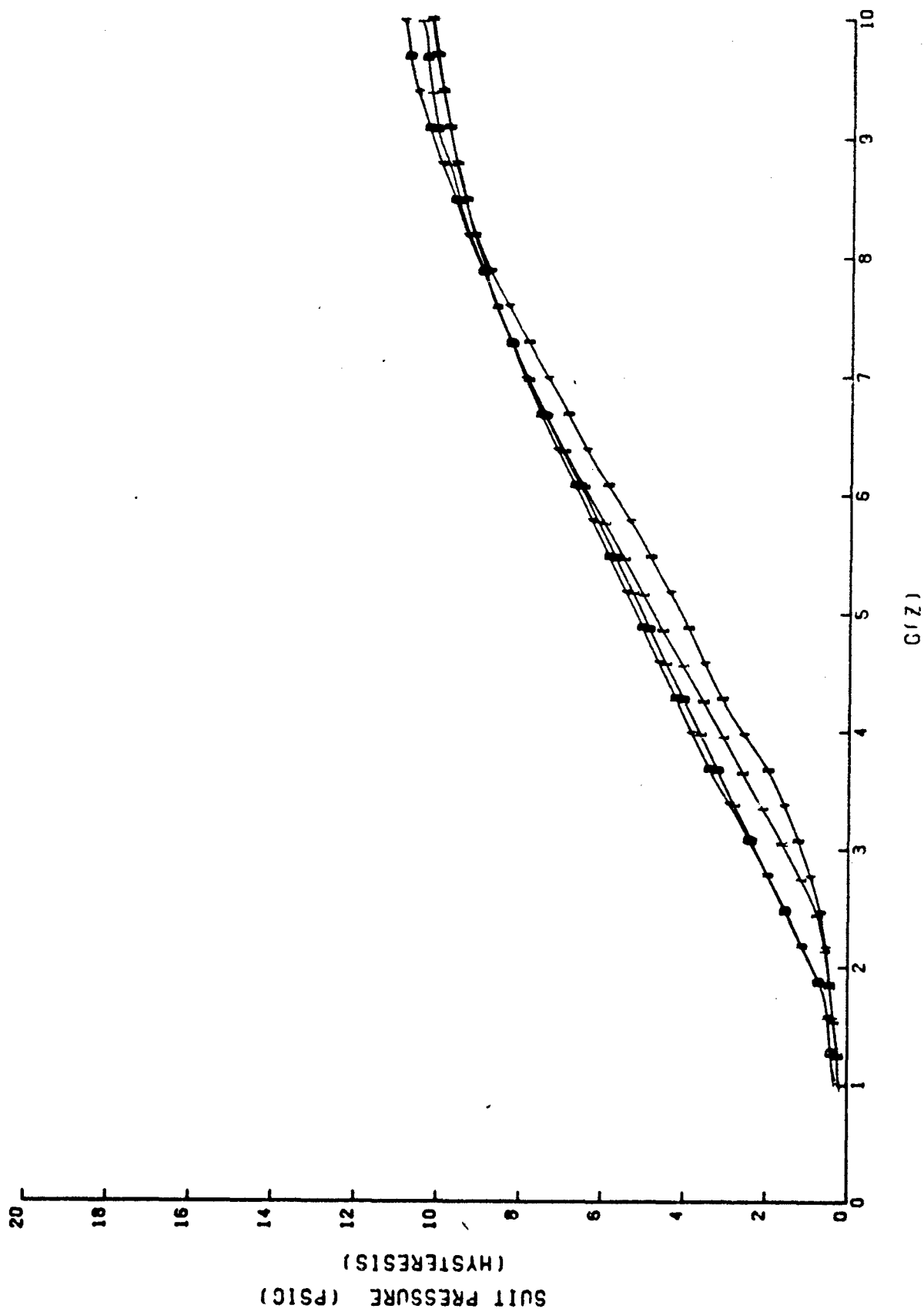


Figure 74. Ready Pressure AGV pressure-profile comparison as a function of onset rate.  
[Curves are: 1I, 4I, 1D, and 4D.]

The influence of G-onset rate on the RPV's pressure profile is shown in Figure 75. The minimum increase in lag in pressurization of the AGS is caused by pre-inflation of the "dead volume," which must be filled before pressure starts increasing. The essentially random rate of pressure increase for increasing G-onset rates (Fig. 76) indicates that the open-flow rates were adequate in all cases.

The near absence of source pressure influence on the high-onset performance of the RPV is shown in the profiles in Figure 77. These profiles, along with those of Figure 78, lend further credence to the observation that the RPV is entirely adequate for a 1.5 G/sec onset rate.

The 1.5 G/sec decreasing G profiles (Fig. 79) indicate that the RPV performs nearly as well at high "offset" rates as low "offset" rates. The similarity of the hysteresis profiles shown in Figure 73 (low onset) and Figure 80 (high onset) suggests that both represent true hysteresis in the valve's regulation system.

The RPV performs exceptionally well at all tested G-onset rates.

#### 5.4.5 SACM Tests

The RPV scored a very respectable 9.292, compared with a median 9.527, on the SACM tests (Table 5, line 32). The 8400A scored only slightly higher (less desirable), while the Electronic AGV scored considerably better. A review of the individual line scores (Table 4, lines 28-31) indicates the 8400A and RPV made essentially the same score, and together formed the median performance of the five valves tested. The 8400A scored better on lines 28-29 of the PET, while the RPV did better on lines 30-31. The 28-31 progression of scores has no known significance. In all cases, the Electronic valve performed considerably better; the 8000A, significantly worse; and the Bendix, very poorly.

The pressure profiles in Figure 81 represent the actual and ideal pressures that should result from the G stimuli resulting from a SACM test when a minimum source pressure is applied to the AGV and a maximum suit volume is attached. The ideal pressure for all SACM tests was derived from the mid-source pressure profile in Figure 70, and the actual instantaneous G value was applied. The differences between the real and ideal pressures, along with corresponding onset rates, are shown in Figure 82. The abscissa of this graph represents the integral of G with respect to time. This device allows a real (unweighted) indication magnitude, while the size of the excursion (actually the area under the curve) is weighted by the G level. In this manner, a 0.5-psig excursion at 6 G will appear twice as large as a 0.5-psig excursion at 3 G, even though the amplitudes are the same. The area under these curves is used as an evaluation factor in the PET. The RPV's min-max curves (Fig. 82) indicate a maximum pressure excursion of -0.8 psig, while the maximum onset rates achieved during the tests were +1.1 G/sec and -1.5 G/sec.

The SACM pressure profiles for the maximum source pressure and minimum suit volume are shown in Figure 83, while the associated difference curves are in Figure 84. In this case (Fig. 84), the pressure excursions never exceeded 0.4 psig, while the onset rates reached 1.1 G/sec and -1.4 G/sec. The median-source-pressure median-suit-volume case is shown in Figures 85 and 86. As might be expected, the pressure excursions reach only 0.5 psig. The onset rates attained in this SACM are comparable to those in the previous two tests.

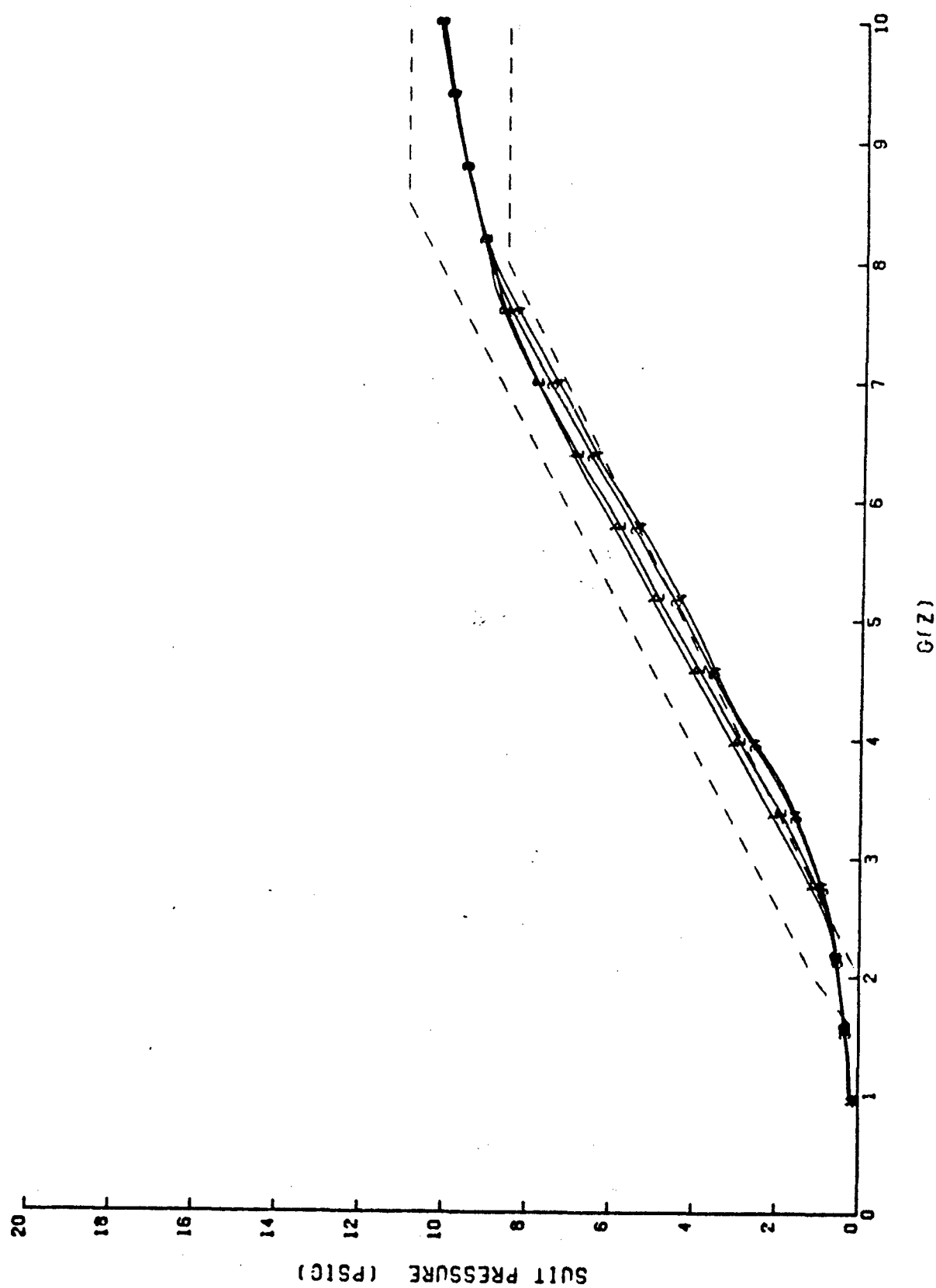


Figure 75. Ready Pressure AGV pressure profile as a function of G-onset rate.  
[Curves are: 1, 2, 3, and 4.]

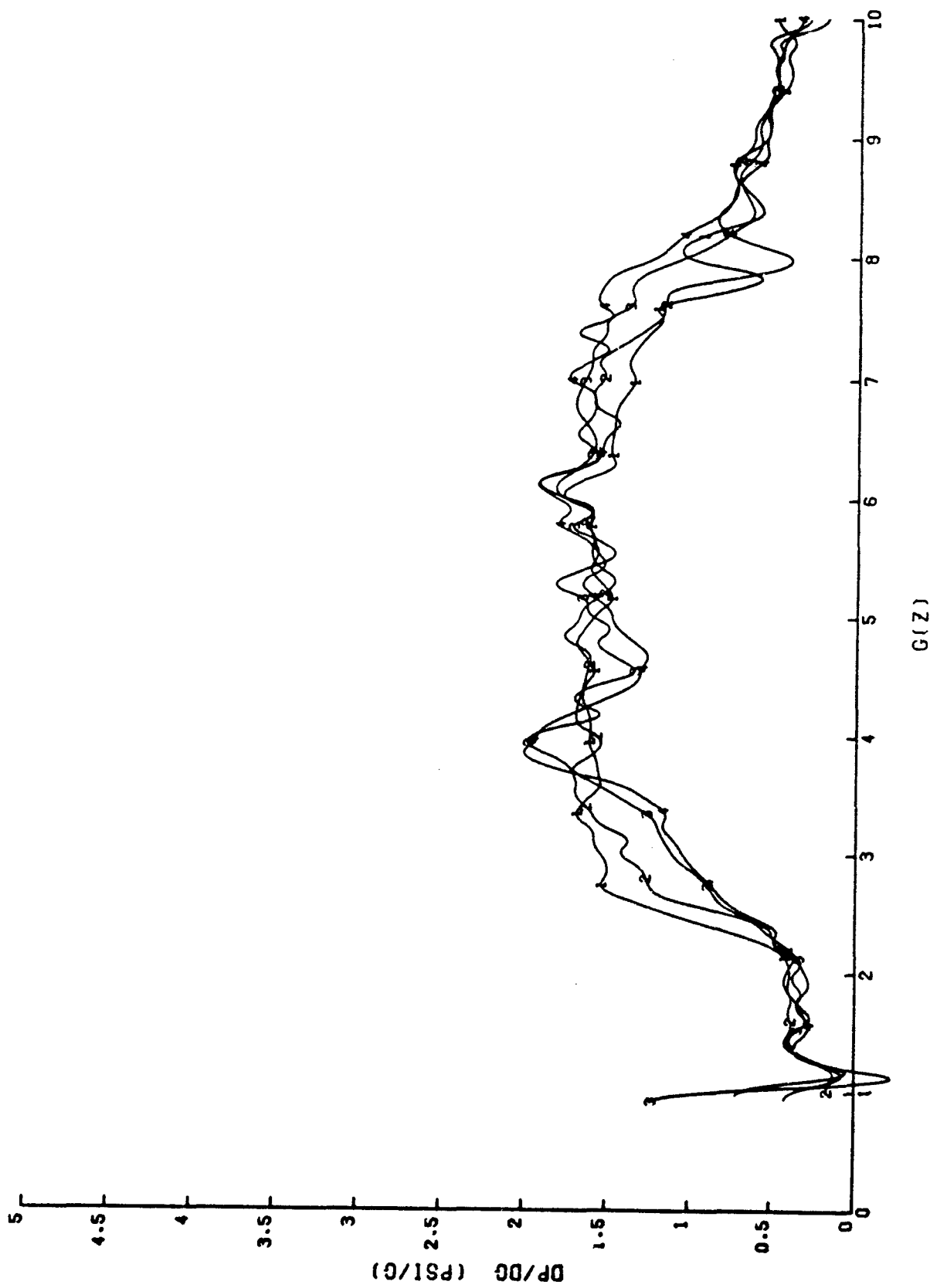


Figure 76. Ready Pressure AGV  $dP/dG$  as a function of G-onset rate.  
[Curves are: 1, 2, 3, and 4.]



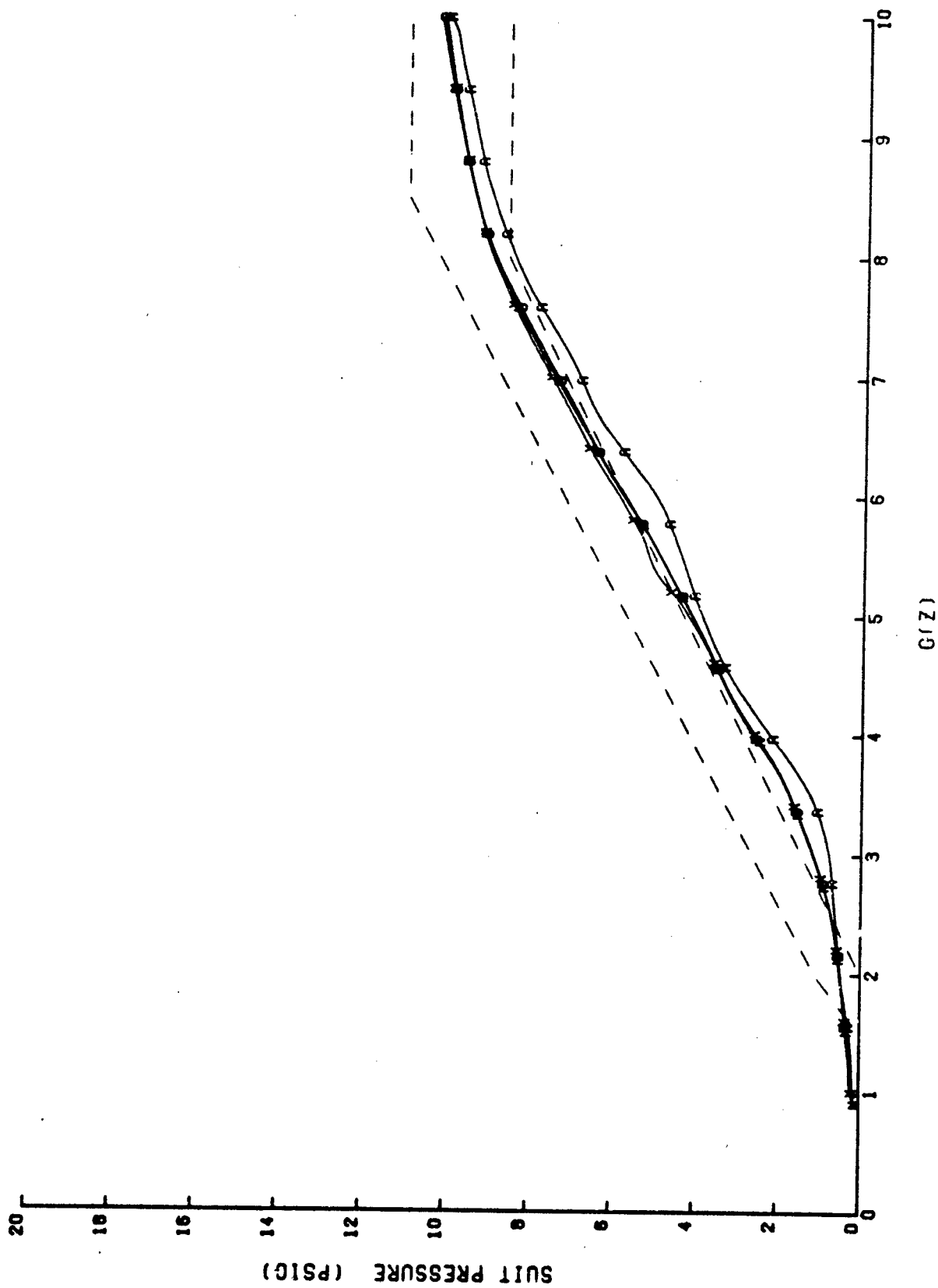


Figure 77. Ready Pressure AGV 1.5 G/sec pressure profile as a function of source pressure.  
[Curves are: A, D, N, and X.]

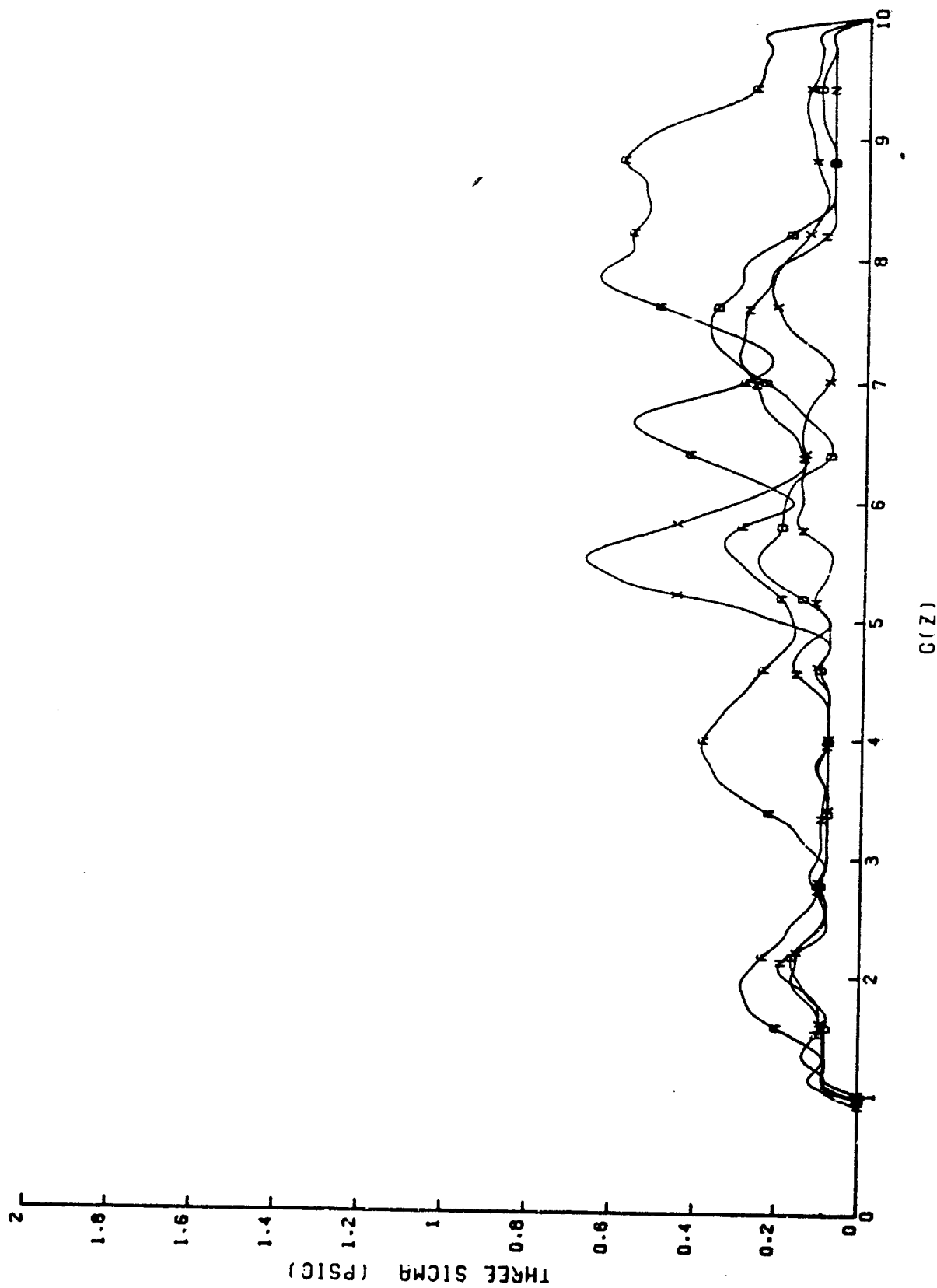


Figure 78. Ready Pressure AGV 1.5 G/sec pressure variation as a function of source pressure.  
 [Curves are: A, D, N, and X.]

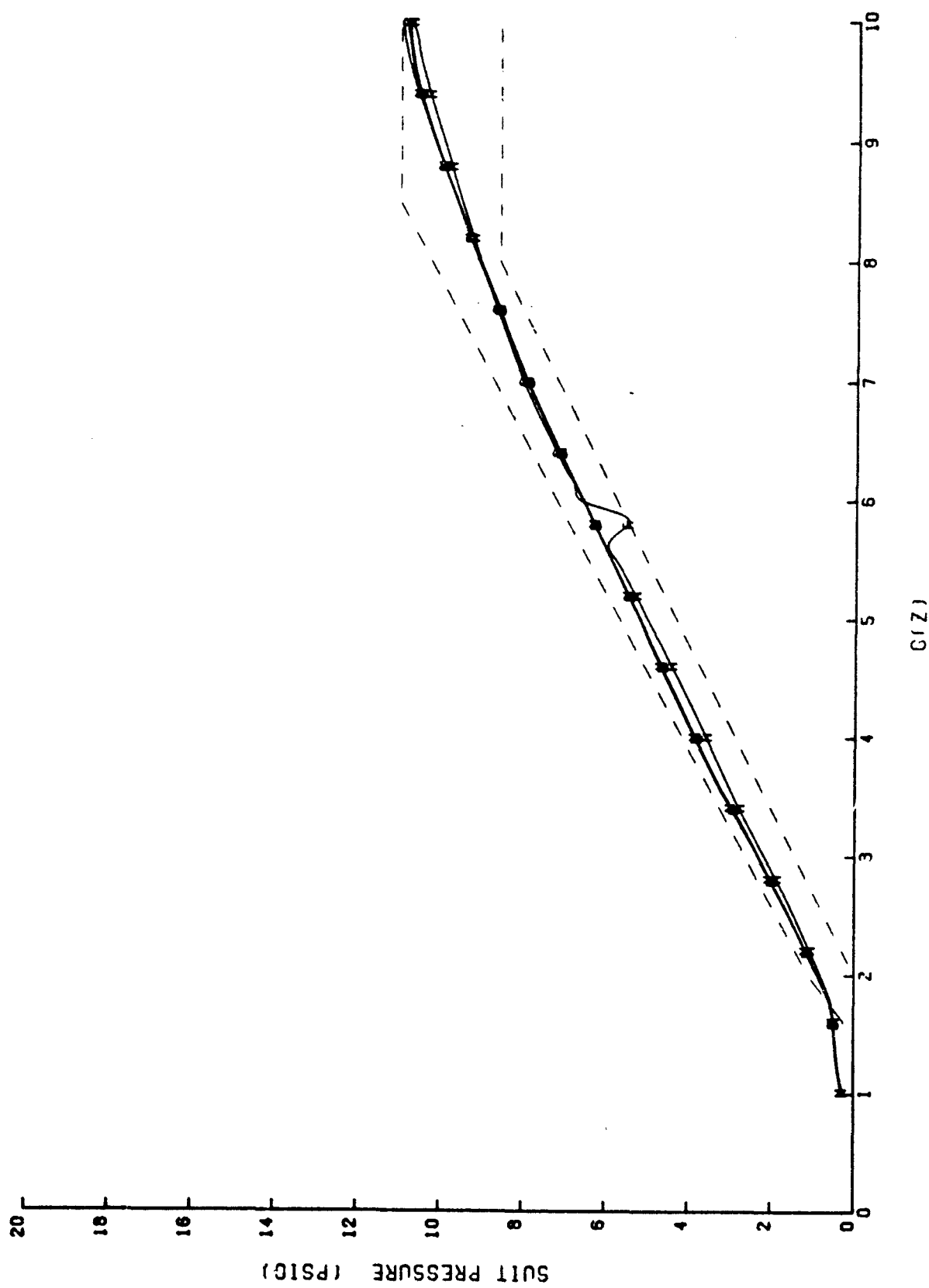
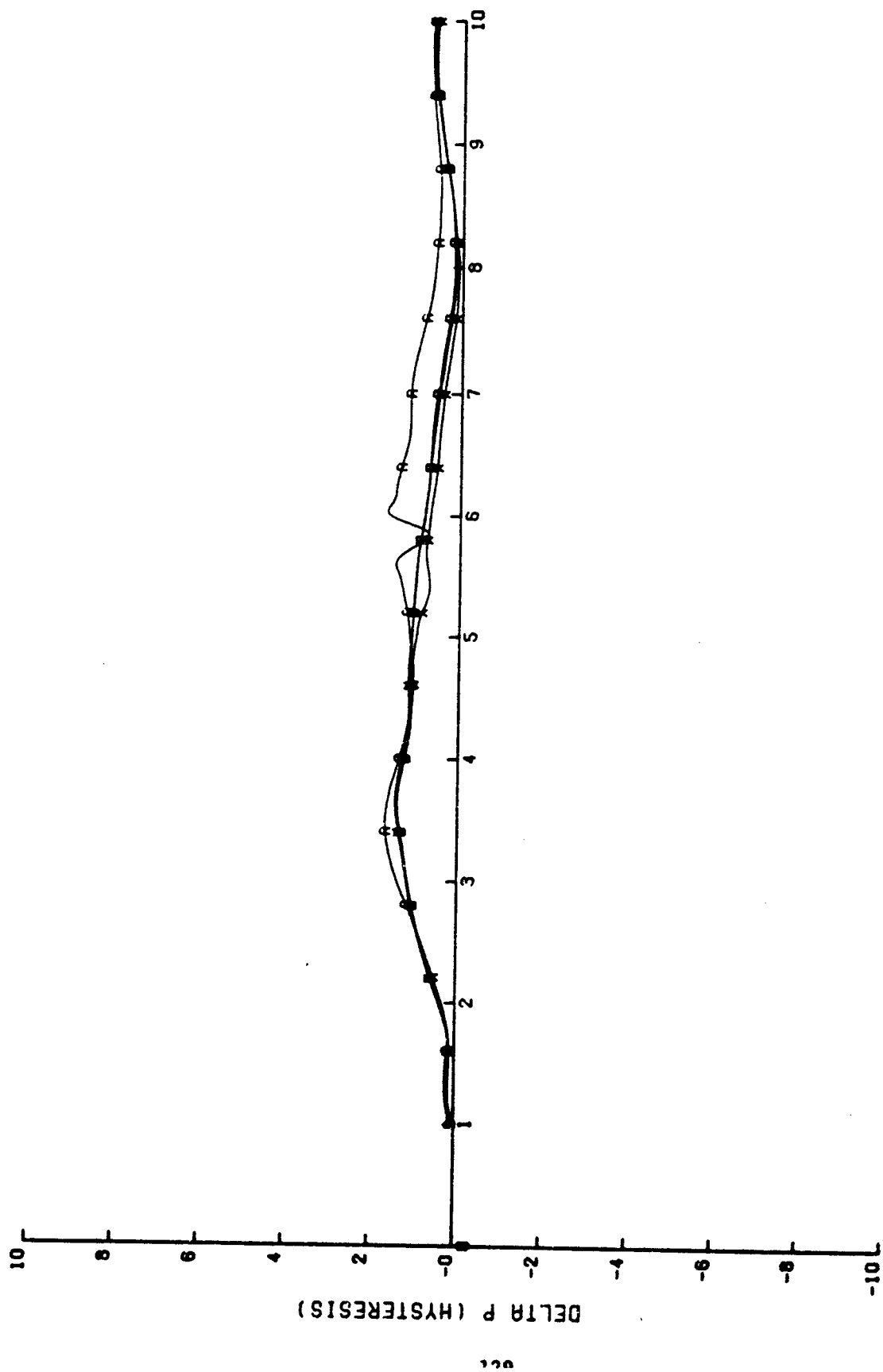


Figure 79. Ready Pressure AGV 1.5 G/sec decreasing pressure profile as a function of source pressure.  
[Curves are: A, D, N, and X.]



G(Z)

Figure 80. Ready Pressure AGV 1.5 G/sec pressure hysteresis as a function of source pressure.  
[Curves are: A, D, N, and X.]

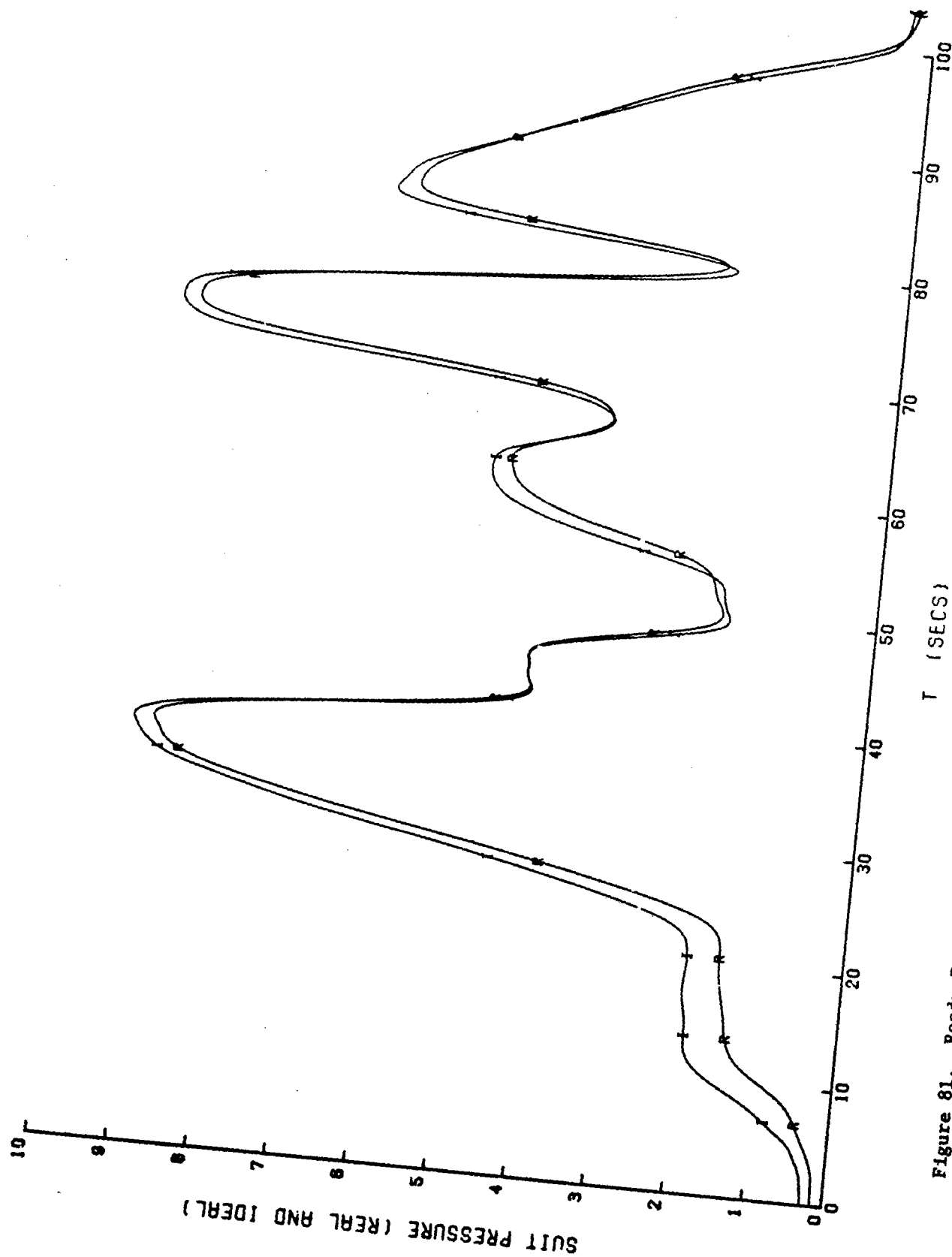
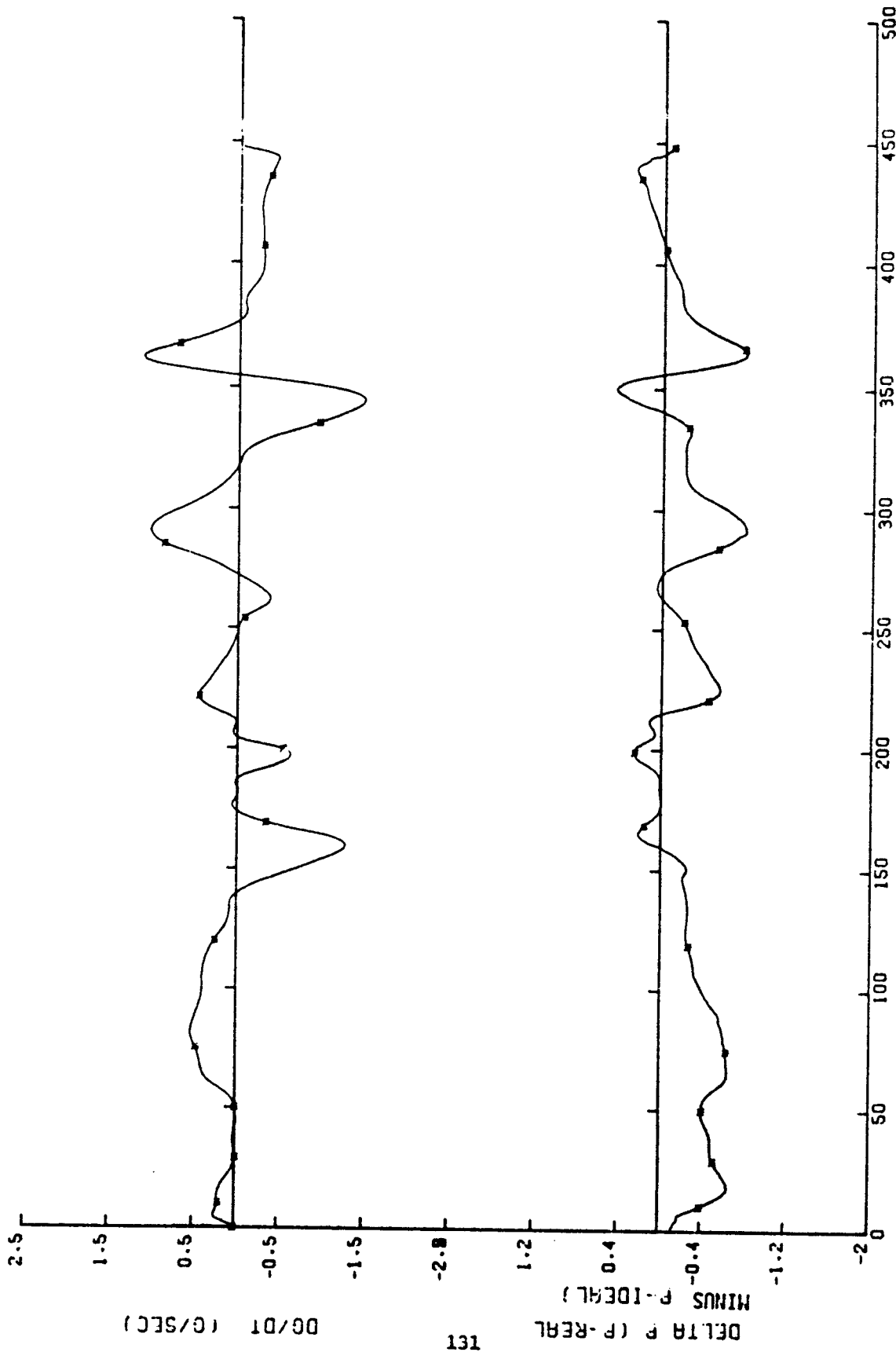


Figure 81. Ready Pressure AGV SACM pressure-profile comparison with minimum source pressure and maximum suit volume. [Curves are: I and R.]



INTEGRAL OF  $G/dt$  FROM 0 TO  $T$

Figure 82. Ready Pressure AGV pressure deviation and  $dg/dt$  for the minimum source pressure and maximum suit volume SACM. [Curves are: \*.]

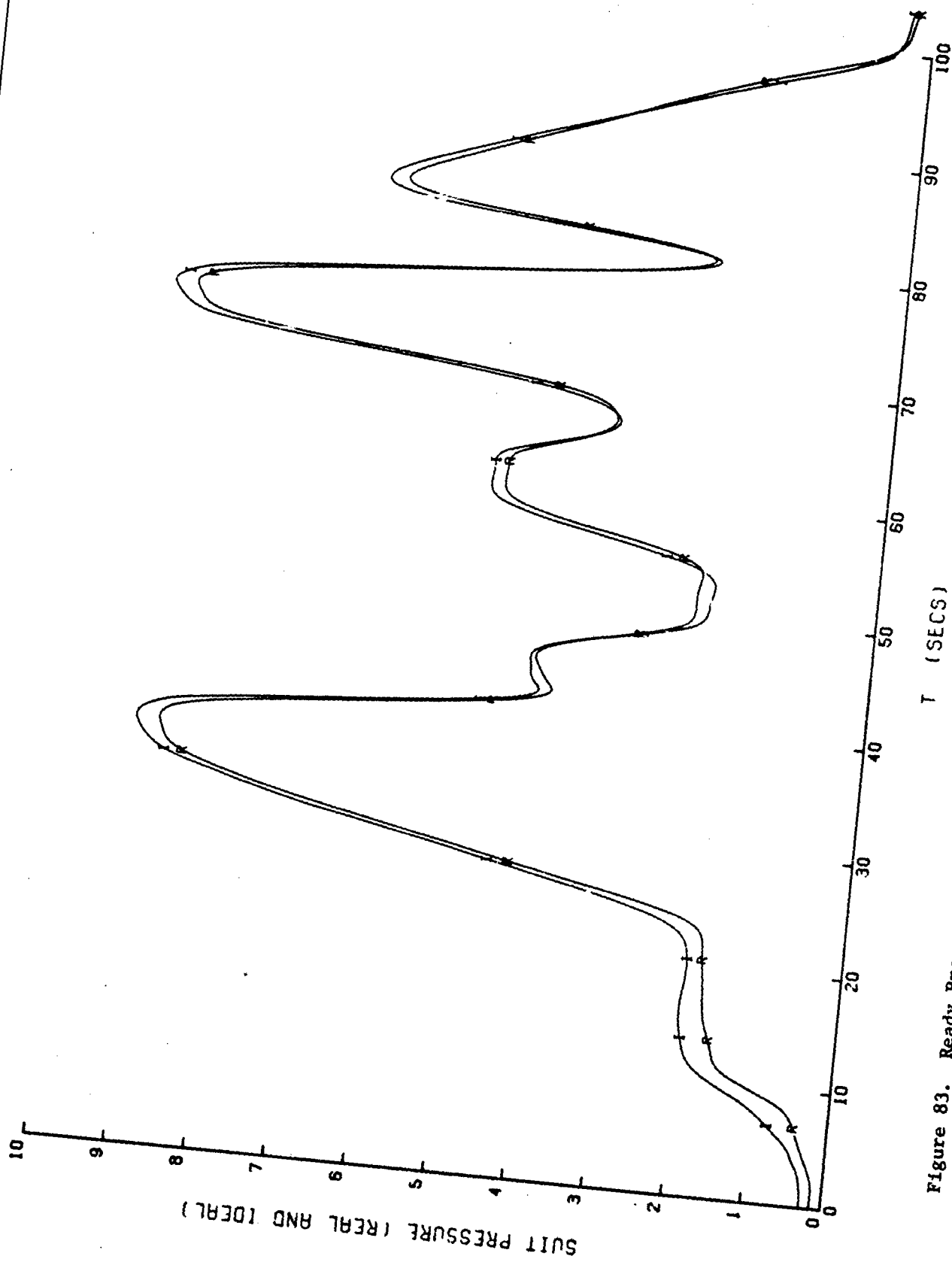


Figure 83. Ready Pressure AGV SACM pressure-profile comparison with maximum source pressure and minimum suit volume. [Curves are: I and R.]

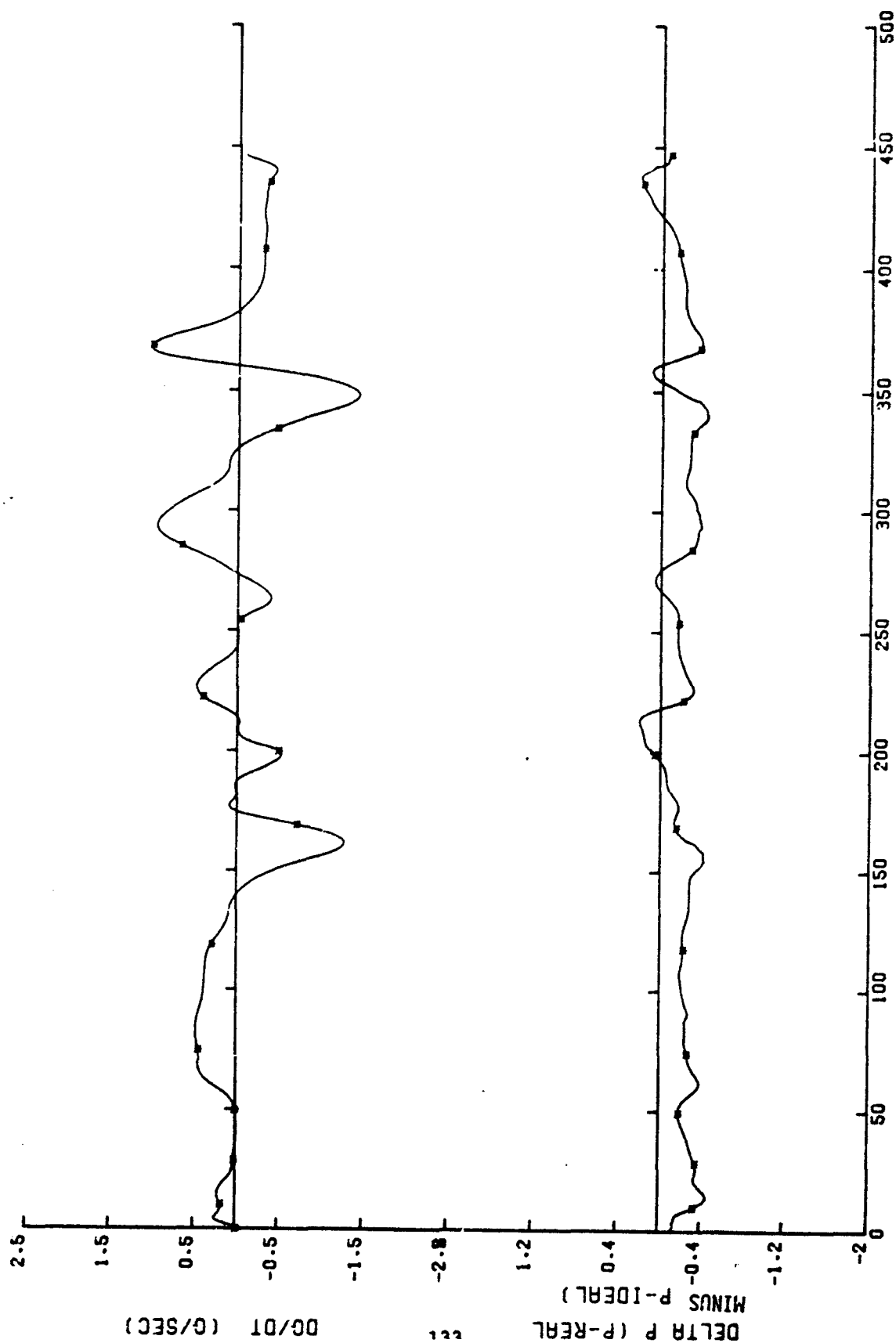


Figure 84. Ready Pressure ACV pressure deviation and  $dC/dt$  for the maximum source pressure and minimum suit volume SACM. [Curves are: \*.]



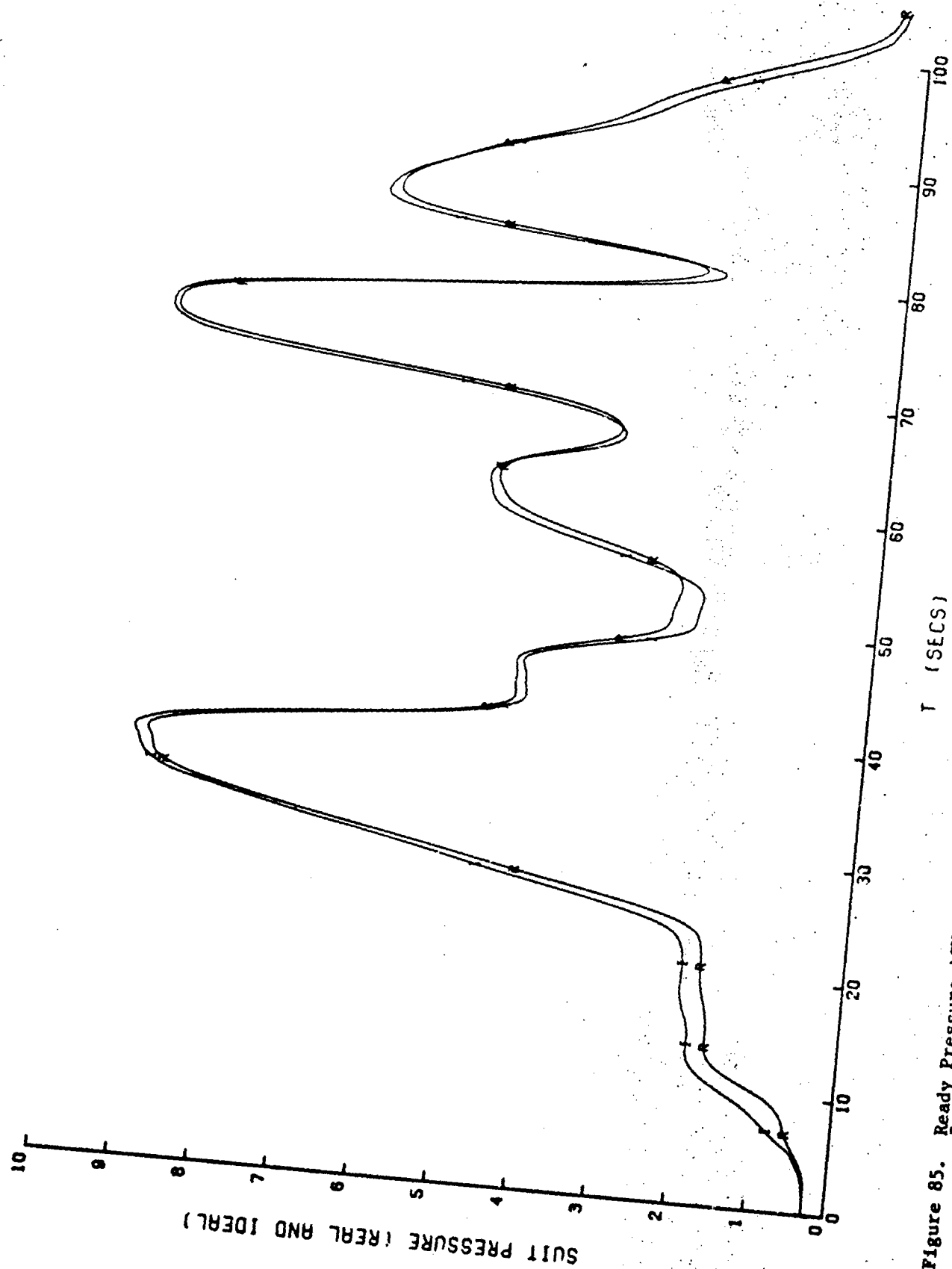


Figure 85. Ready Pressure AGV SACH pressure-profile comparison with median source pressure and suit volume.  
[Curves are: I and R.]

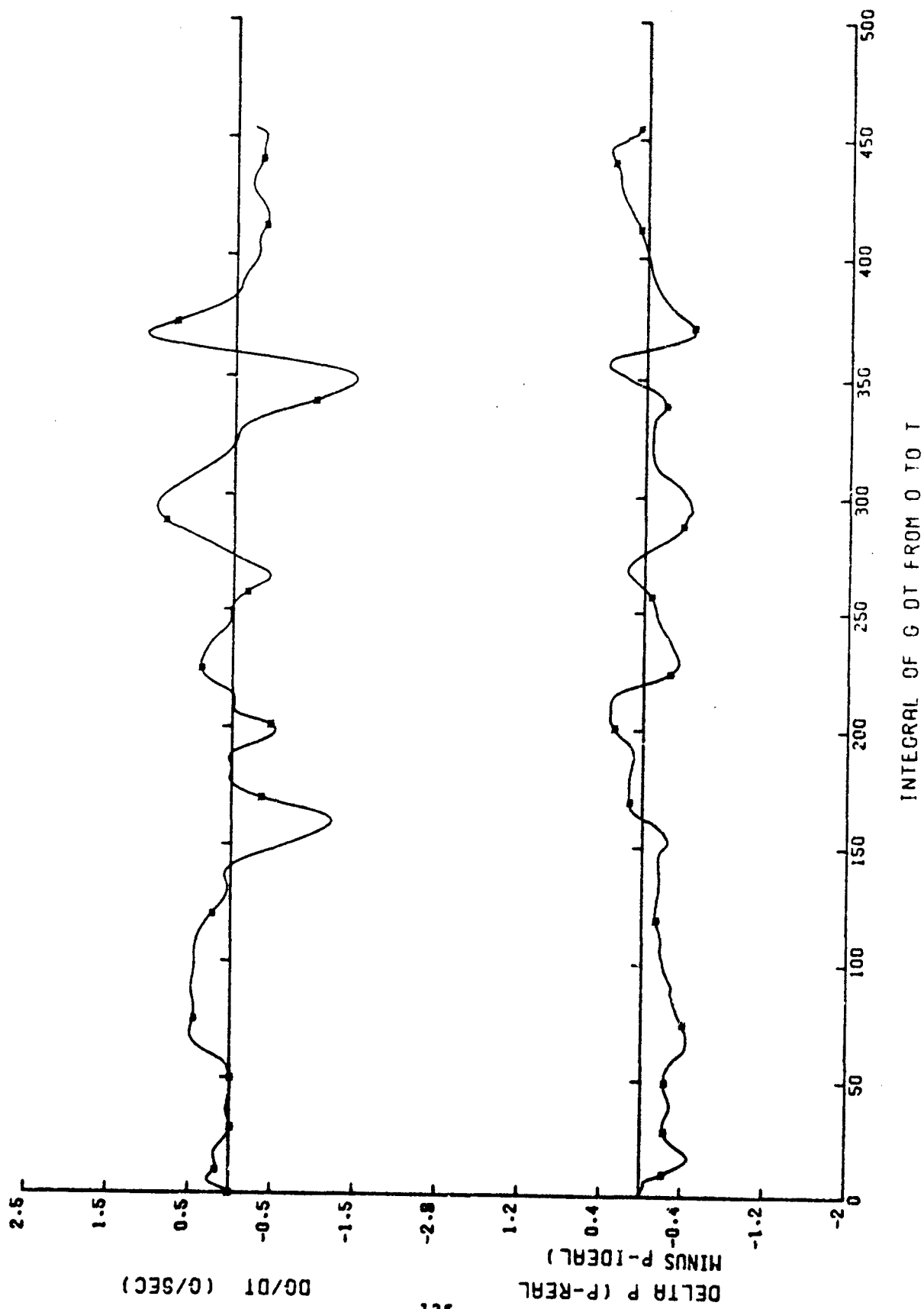


Figure 86. Ready Pressure ACV pressure deviation and  $dg/dt$  for the median source pressure and suit volume SACM.  
[Curves are: \*.]

Figures 87 and 88 are unique only in that the valve was run with its centerline at an angle of 20° to the G vector. Since the ideal pressure here was derived in the same manner as in the previous three sets, the actual pressure is expected to be low (refer to section 5.1.3); and Figure 88 confirms this expectation. Otherwise, the curves are comparable with those in Figures 85 and 86, except that perhaps a little more tendency to overshoot is exhibited.

The relative performance results, of the RPV's high G-onset-rate tests and of the SACM tests, suggest a dichotomy. The results of the SACM tests suggest acceptable performance under simulated combat conditions, while those of the high G-onset tests suggest excellent performance. Since the SACM profile starts with a gentle 0.2 G/sec onset, the 8400A is allowed to fill the dead space in the AGS, thus eliminating the lag in onset pressurization. Furthermore, since the RPV is an 8400A, modified to pre-inflate the suit, it is not surprising that the SACM scores are nearly identical for these two valves. A revised SACM profile may be necessary for future testing.

#### 5.4.6 Conclusions on the RPV's Performance

The RPV anti-G valve performs very well under widely varying conditions, and excellently at 1.5 G/sec. It is probably the most promising valve tested for weapons-system-mission combinations which require response to high G-onset rates.

### 5.5 ALAR 8000A Anti-G Valve Test Results

#### 5.5.1 ALAR 8000A Valve and Test Description

The PTAP contract did not require the SVTP testing and GVALVPGM analysis of the 8000A. However, a complete set of tests were run in order to test the multiple valve capability of GVALVPGM. Rather than discard the data, a single valve analysis was run and included here for the reader's interest. The design differences between the 8000A and the 8400A are too subtle to warrant description here. [For details already presented in this volume, review section 5.1.1.]

For purposes of SVTP testing and GVALVPGM analysis, standard values were assigned for the 8000A and are shown in the PET (Table 6, lines 1 - 7). In addition to being the design values for the valve, these values are identical to those of the ALAR 8400A, and were selected as standards for the GVALVPGM analysis because they permitted direct application of the unit to a wide variety of weapons systems in the present USAF inventory. Since the values are the GVALVPGM standard, the 8000A scored a perfect minimum of 3.0 on the PET design total.

#### 5.5.2 ALAR 8000A Flow Tests

The flow-test performance score of the ALAR 8000A AGV (represented by line 16 of Table 6) was 5.767, and below the median score of the five valves tested under this contract. The total open-flow test showed

TABLE 6. ALAR 8000A ANTI-G VALVE PERFORMANCE  
EVALUATION TABLE

TEST STANDARDS:

1. SPMIN = 30. PSIG
2. SPMID = 125. PSIG
3. SPMAX = 300. PSIG
4. THETA = 20. DEGREES
5. SVMIN = 6. LITERS
6. SVMID = 10. LITERS
7. SVMAX = 14. LITERS

CHARACTERISTIC NUMBERS:

8. XSPMX = 1.0000
9. XSPMN = 1.0000
10. XTHTA = 1.0000
11. DESIGN TOTAL: 3.000
12. XFLBR = 2.871
13. XDELF = 1.325
14. XDDL F = 1.387
15. XSIGF = 0.185
16. FLOW TOTAL: 5.767
17. XCCP1 = 0.073
18. XDDP1 = 0.910
19. XSGP1 = 0.794
20. XDPP1 = 1.075
21. LOW-ONSET TOTAL: 2.852
22. XCCP2 = 2.026
23. XDDP2 = 3.798
24. XSGP2 = 4.062
25. XDPP2 = 3.030
26. XTDP2 = 8.144
27. HIGH-ONSET TOTAL: 21.061
28. XIDPA = 2.348
29. XIDPB = 3.553
30. XIDPC = 3.318
31. XIDPD = 4.155
32. SACM TOTAL: 13.381
33. VALVE: ALAR 8000A TOTAL: 46.061

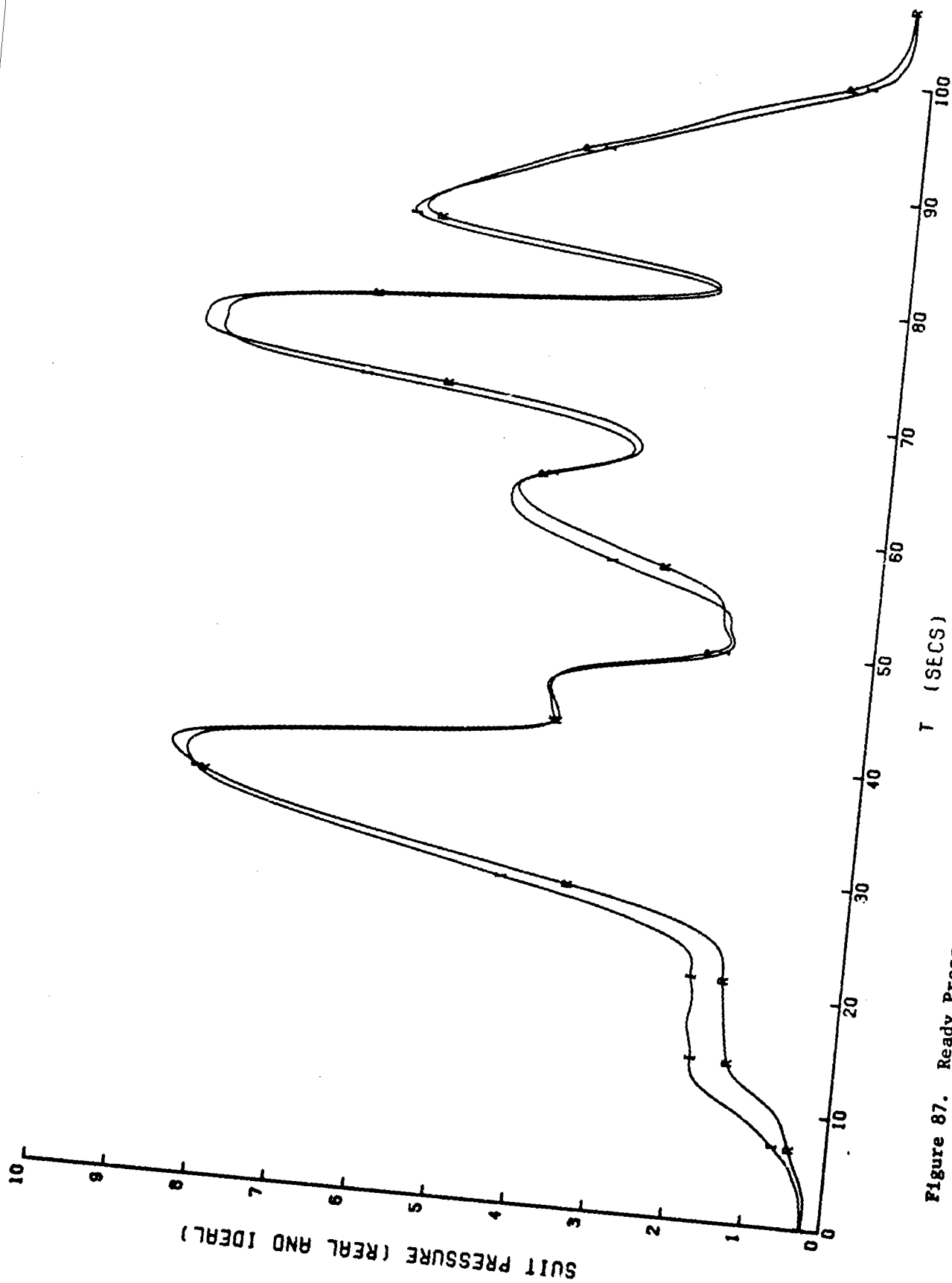
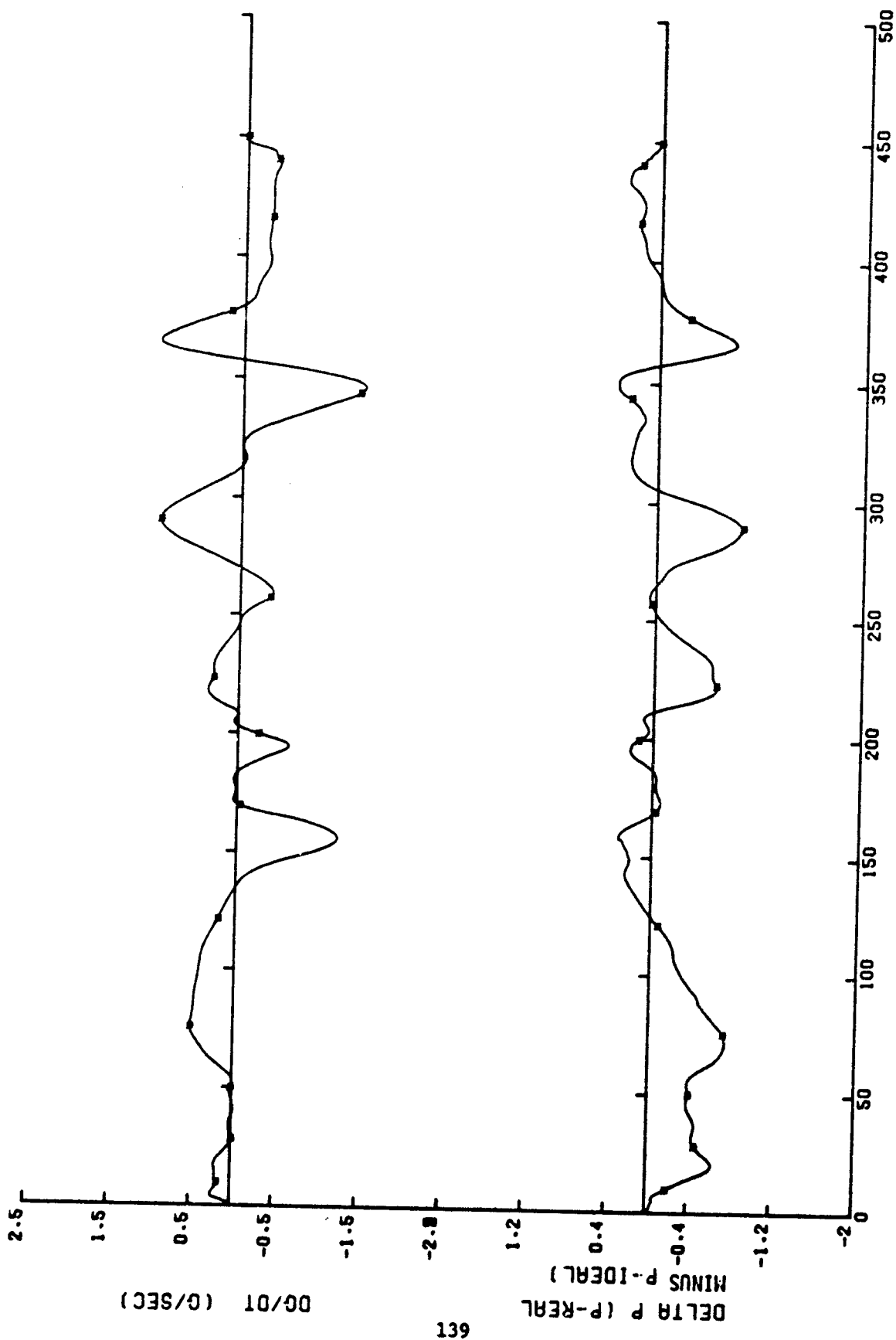


Figure 87. Ready Pressure AGV SACM pressure-profile comparison with the G vector misaligned.  
 [Curves are: I and R.]



INTEGRAL OF  $\Delta P$  FROM 0 TO T

Figure 88. Ready Pressure AGV pressure deviation and  $dG/dt$  for the G vector misalignment SACM.  
[Curves are: \*.]

a slightly above median performance of 2.871 (Table 6, line 12), with the E valve and the RPV having significantly higher flows. The source pressure influence on the open-flow performance was the lowest of the five valves tested (as shown on lines 13 and 14 of Table 6), and is the major reason for the 8000A's good showing on the total flow score. Line 15 of Table 6 represents the stability and repeatability of the 8000A's open flow and is the median score of the five valves tested, although the fluctuations in flow were essentially equal for all valves.

The 8000A flow curves (Fig. 89) are very representative of a standard anti-G valve. The increase in flow--at a decreasing rate, with respect to applied G--and attainment of peak flow values at 6 G are reasonably typical of an anti-G valve with adequate performance characteristics. The distribution of peak flow rates with respect to source pressure shows some "starving" at minimum source pressure. In this valve, this distribution primarily reflects the flow impedance into the first stage regulator. The fluctuations in the open-flow data are shown in Figure 90, as the  $3\sigma$  values, and appear to increase with source pressure in a relatively linear manner.

The principal importance of this test is to estimate the time required by this valve to fill an anti-G suit under very high onset conditions. This consideration is especially important to estimate performance at G-onset rates beyond the capability of the test facility. In the case of the 8000A flow curves, the high slope (i.e., increase in flow rate) between 2 G and 3 G, and the moderately high total-flow values represent good prospects for good performance under high G-onset rates. On the other hand, it would be desirable to reach maximum flow values at a lower G level, and probably should not be forced to operate at the minimum source pressure.

#### 5.5.3 ALAR 8000A Low G-Onset-Rate Tests

The low G-onset-rate test-performance score, 2.852 (Table 6, line 21), for the 8000A was essentially equal to the 8400A's 2.857--the median score of the five AGVs tested. The Bendix and Electronic AGV's produced considerably higher (less desirable) scores, while the RPV valve produced somewhat better scores. Line 17 of the PET shows the 8000A scores moderately well in linearity, while line 18 shows a slightly below median score on source pressure influence. The 8400A exhibits the lowest stability-repeatability score of 0.794 on line 19, while line 20 indicates a high hysteresis score.

The low-onset-rate pressure profile for the 8000A is shown in Figure 91. Although only one test item was subjected to this protocol, previous experience indicates this profile is typical of 8400A performance, and is probably typical of the family of valves. The dotted lines in Figure 96 indicate the band of acceptable pressure values according to MIL-V-9370D. The 8000A started applying pressure to the AGS at approximately 2.6 G (approximately 0.6 G late), reached acceptable pressure levels at approximately 3.1 G, and remained near the lower limit of acceptable pressure levels for all higher G levels. The variation in pressure profile with respect to source pressure is extremely small (Figure 91), while the variation due to angular displacement of the valve (shown by the "A" trace) is slightly larger than expected. When the valve is rotated with respect to the G vector,  $20^\circ$  in this case, the response is expected to respond proportionally to the cosine of the angle of rotation. The 8000A response more closely represented  $24.8^\circ$  rotation, probably indicating the influence of frictional forces on the mass spring system. The variation in pressure (Fig. 92) is especially low.

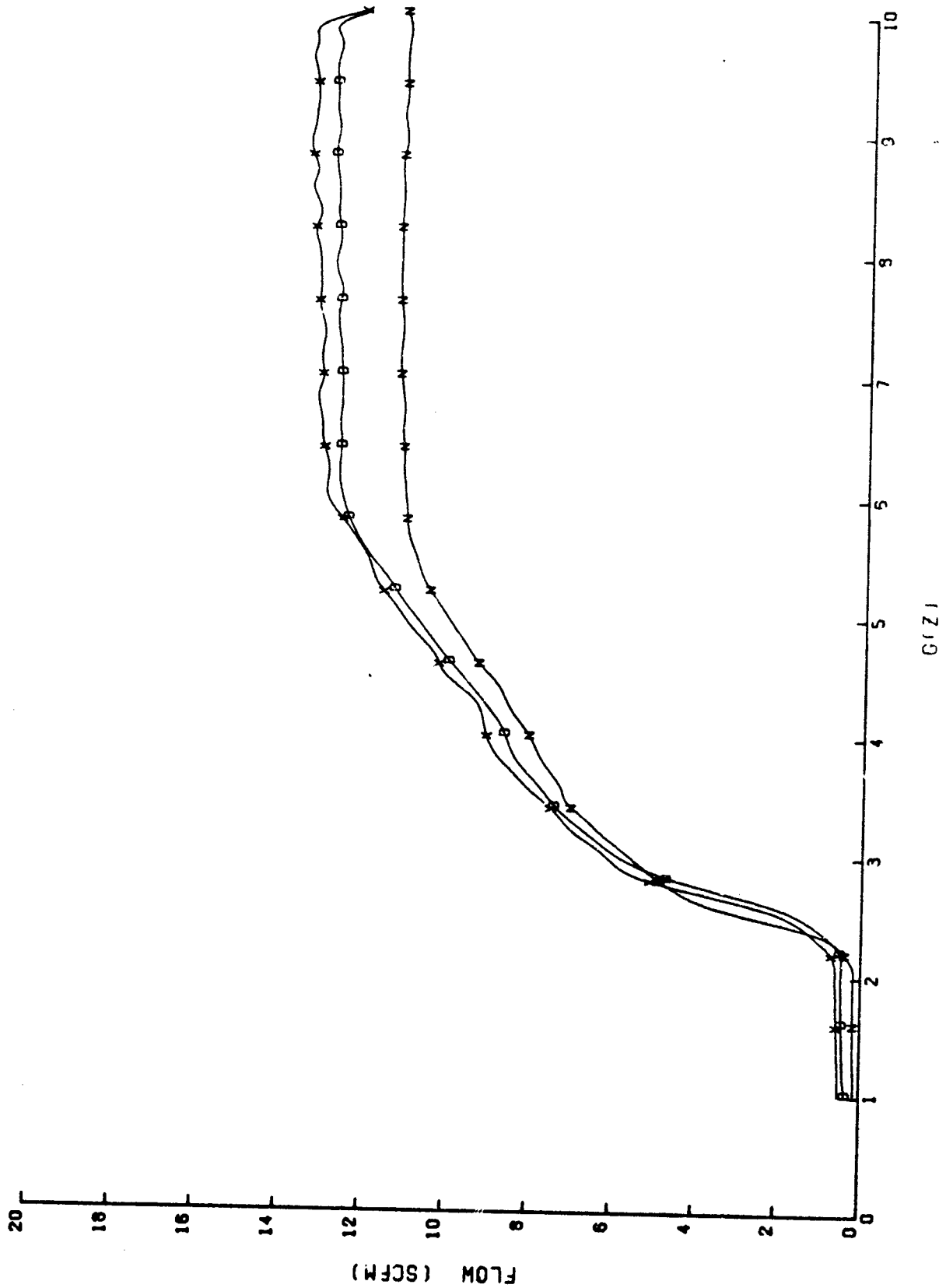


Figure 89. ALAR 8000A flow as a function of source pressure.  
[Curves are: D, N, and X.]



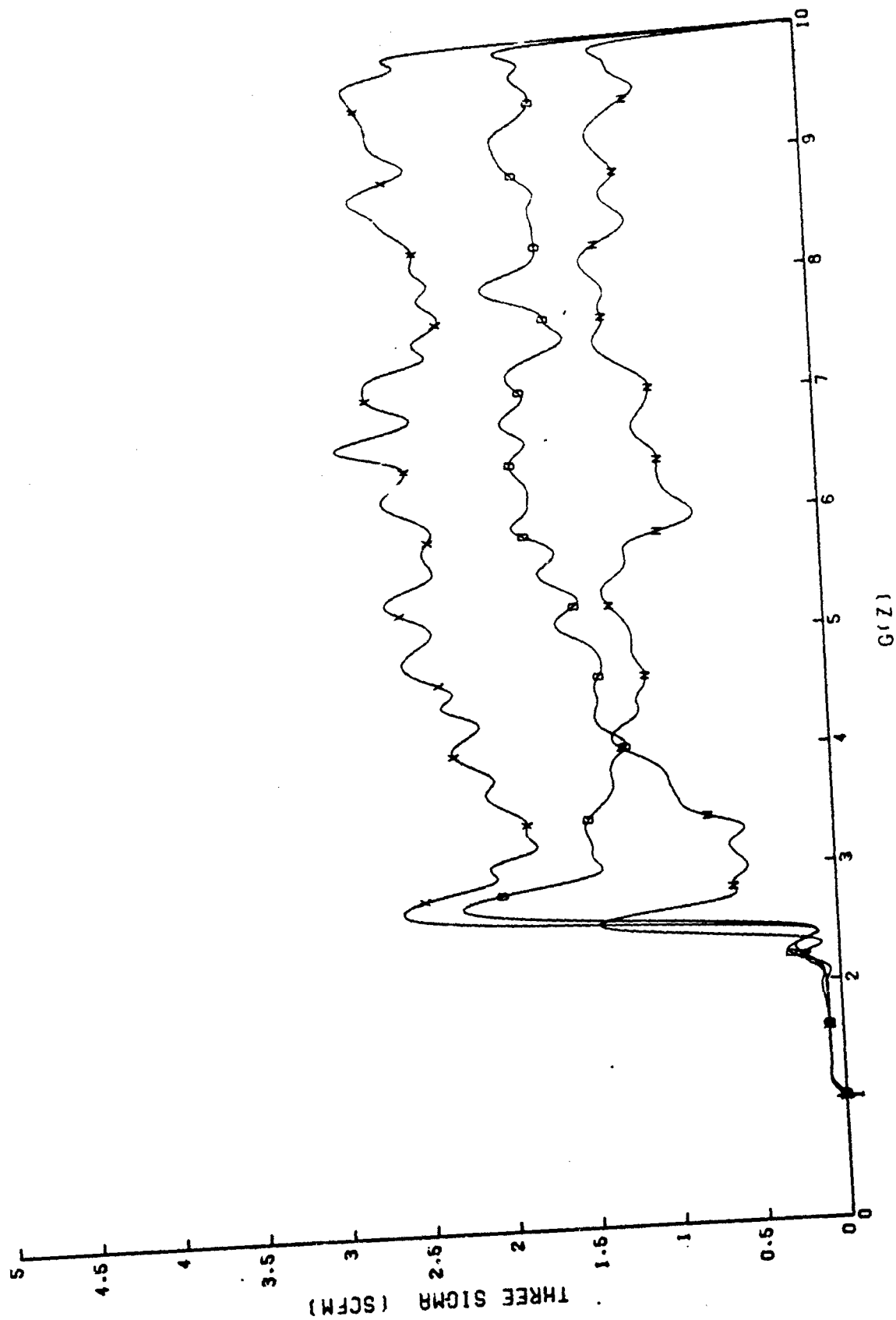


Figure 90. ALAR 8000A flow three sigma as a function of source pressure.  
[Curves are: D, N, and X.]

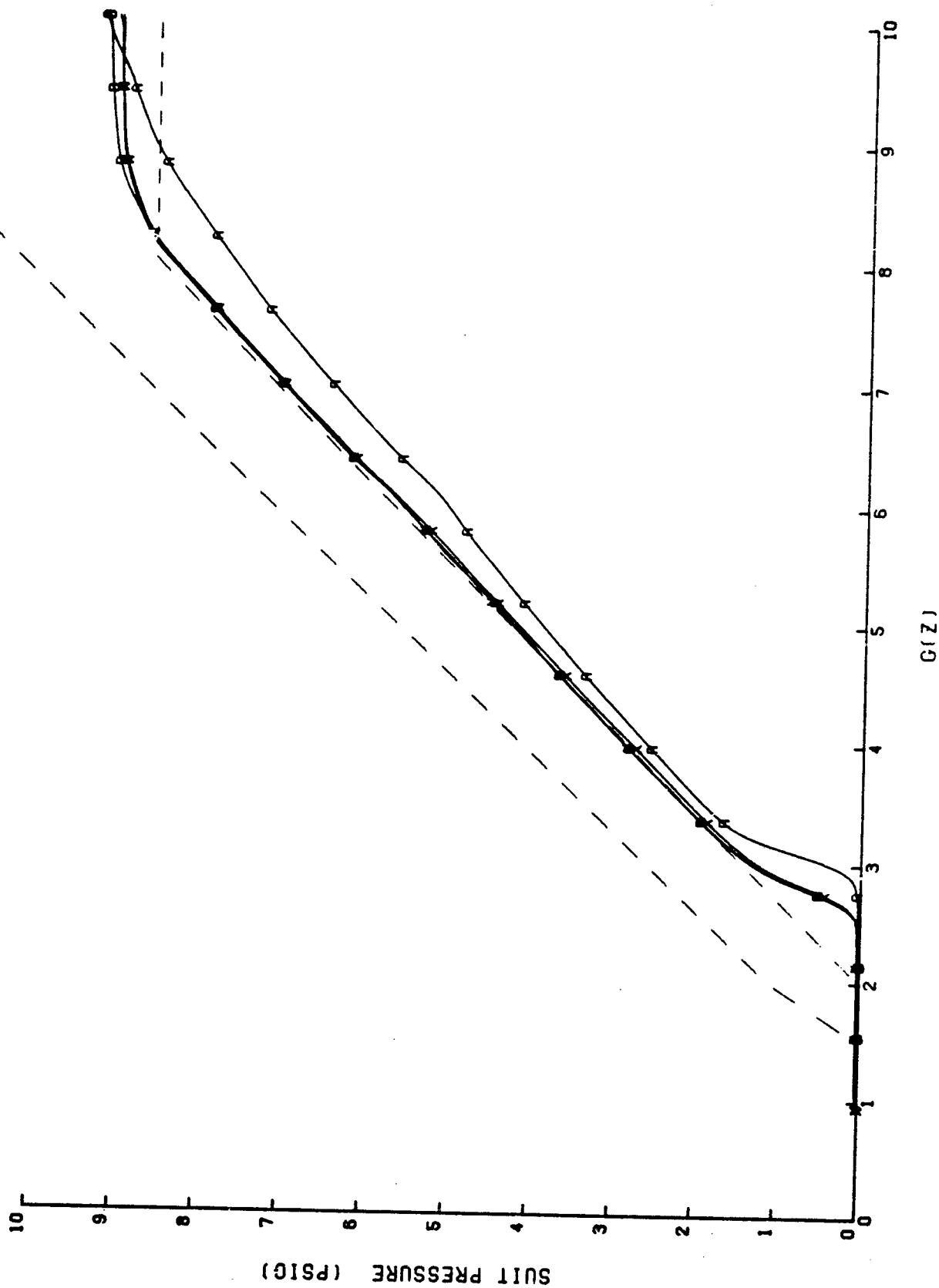


Figure 91. ALAR 8000A 0.1 G/sec pressure profile as a function of source pressure.  
[Curves are: A, D, N, and X.]

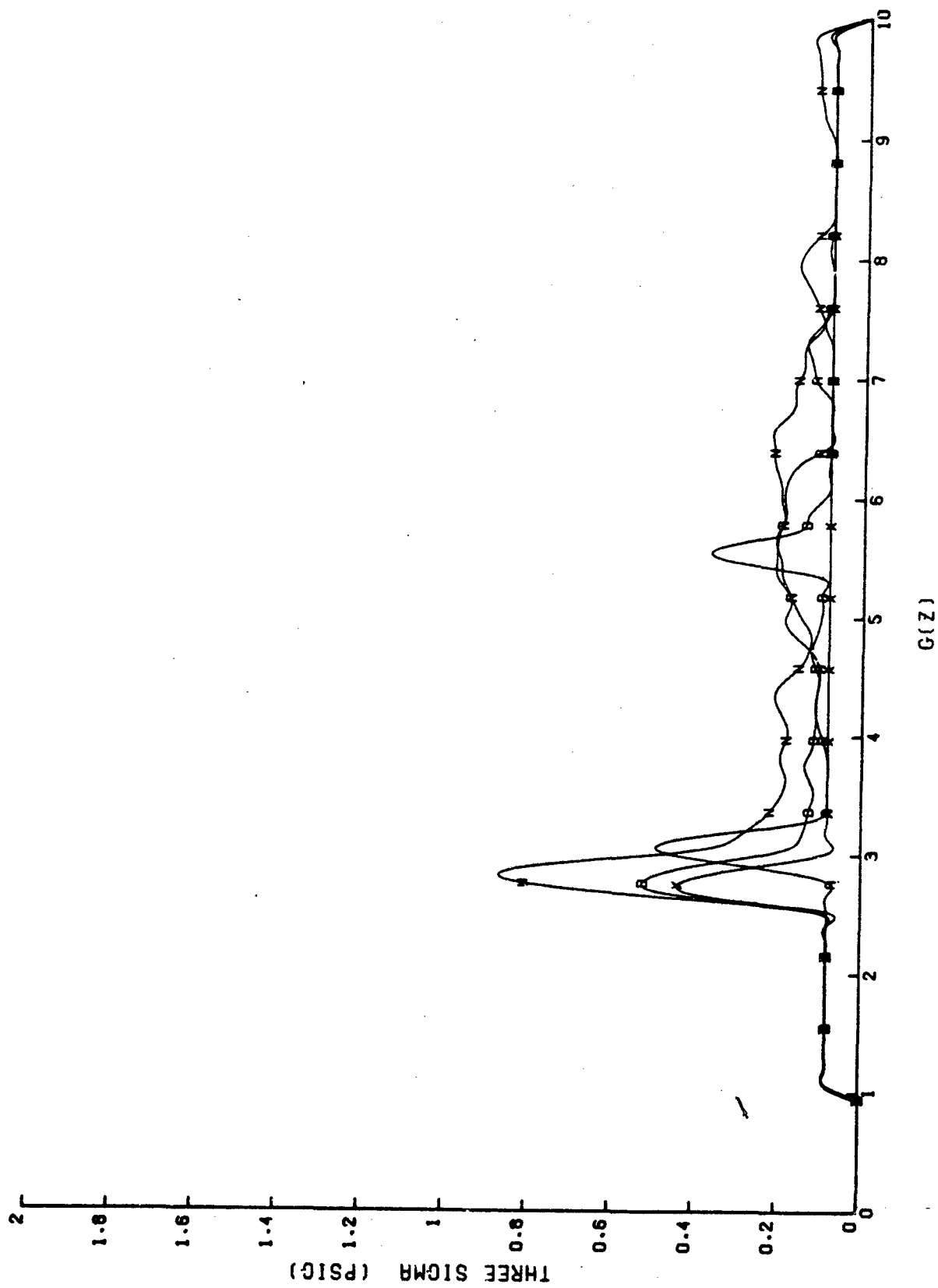


Figure 92. ALAR 8000A 0.1 G/sec pressure stability as a function of source pressure.  
[Curves are: A, D, N, and X.]

The low-onset decreasing G pressure profiles are shown in Figure 93. The variation with respect to source pressure is very small and essentially random, as expected. The decreasing G pressure profile of the angular displacement tests are higher than expected.

The differences between the increasing and decreasing G pressure profiles (hysteresis) are shown in Figure 94. In most cases, these values are acceptably low. The large peak at 2.7 G is primarily the result of the characteristic late start exhibited by the 8000A. A comparison of the low-onset and high-onset pressure profiles (and hysteresis) is shown in Figure 95.

Although the pressure profile starts late and tends to remain near the lower limits of acceptable pressure, the ALAR 8000A performs in a reasonably acceptable manner at low G-onset rates.

#### 5.5.4 ALAR 8000A High G-Onset-Rate Tests

The ALAR 8000A scores 21.061 (line 27 of Table 6) on the high onset-rate tests. This is the median score of the five valves tested. The 8000A's linearity, shown on line 22 of the PET (Table 6), was also the median of the five valves tested--the 8400A and the Bendix doing considerably worse, and the E valve and RPV doing considerably better. The source pressure influence on high G-onset response (Table 6, line 23) was well below the median (the 8400A at 6.642) of the five valves tested. The stability and repeatability score (line 24) was slightly higher than the median of 3.809, the mean of 4.591 resulting from a relatively poor performance by the Bendix AGV. Line 25 of Table 6 shows a median hysteresis score of 3.030, matching a five-valve mean of 3.258. The score on line 26 is related to the pressure-profile lag resulting from increasing G-onset rates and, because of its importance, is weighted more heavily than the other high G-onset-rate scores. The 8000A's median, 8.144, is relatively poor compared to the RPV's 2.768, but shows well against a five-valve mean of 8.134.

The influence of G-onset rate on the 8000A's pressure profile is shown in Figure 96. The increasing lag in pressurization of the AGS is caused by a "dead volume," characteristic of deflated bladders, which must be filled before pressure starts increasing. This delay is also shown in Figure 97. The reasonably stable nature and decreased amplitude of the 1.5 G/sec profile in Figure 97 indicates the valve capacity may not have been outrun by the G-onset rate, as was the case in the 8400A tests.

The influence of source pressure on the high-onset performance of the 8000A is shown in Figure 98. These profiles, along with those of Figure 99, lend further credence to the observation that the 8000A was not outrun by the 1.5 G/sec onset rate, as the 8400A test shows. The curves indicate the median source pressure resulted in the least pressure lag, while the maximum source pressure resulted in the greatest pressure lag. The extremely high run-to-run variation, indicated by Figure 99, suggests the relative position of these curves is nearly random and has no particular significance.

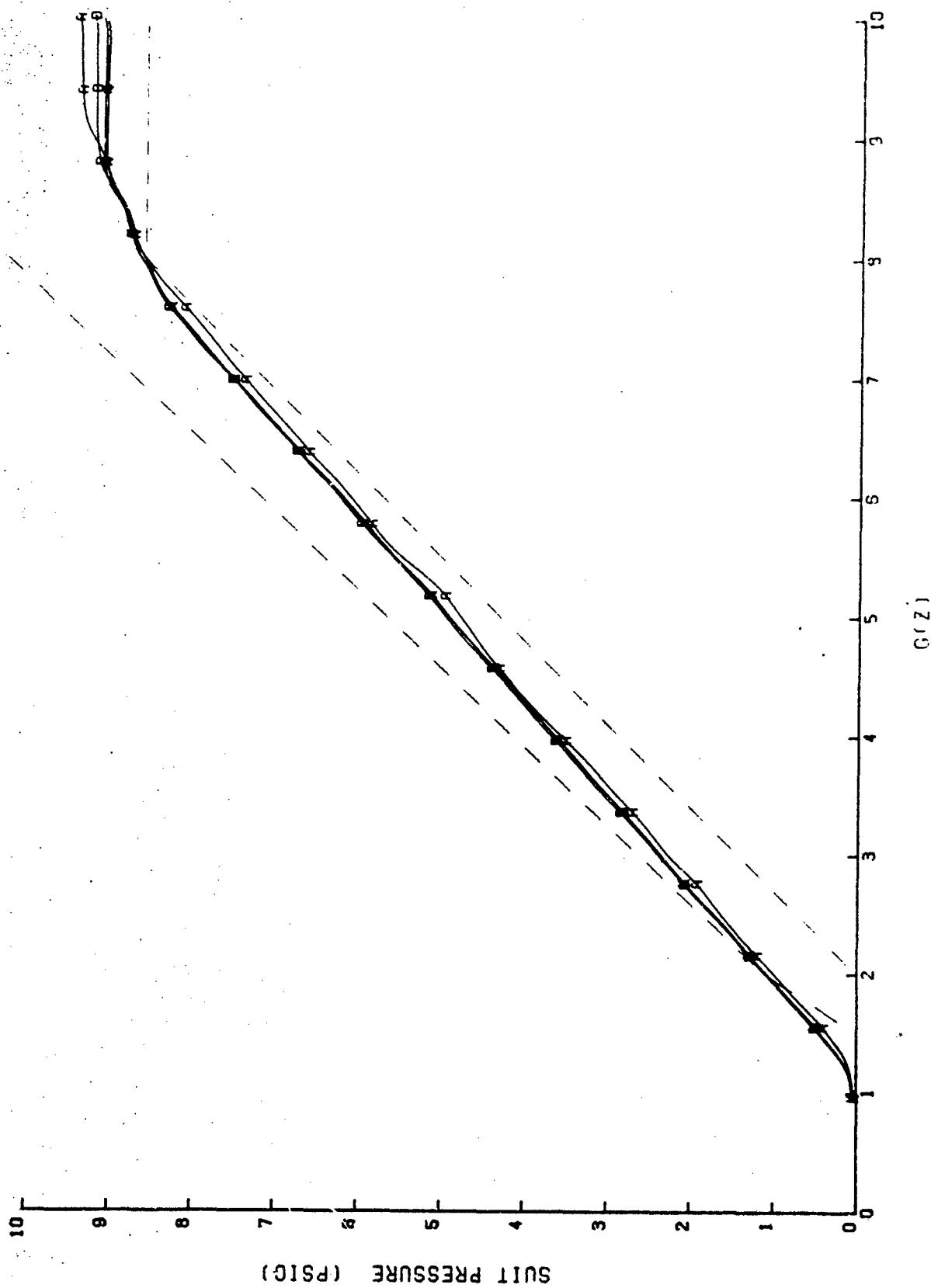
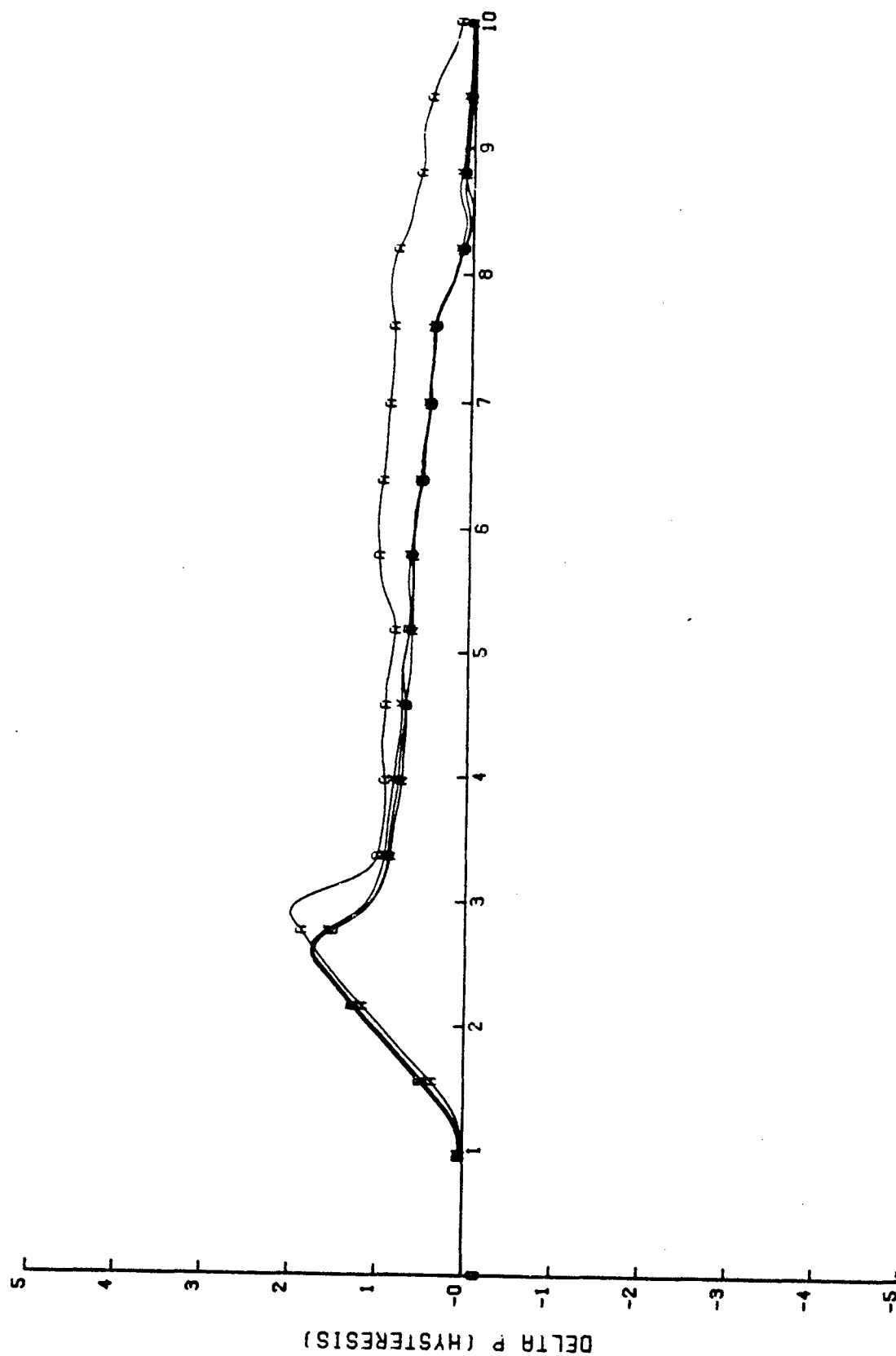


Figure 93. ALAR 8000A 0.1 G/sec decreasing pressure profile as a function of source pressure.  
[Curves are: A, D, N, and X.]



G(Z)

Figure 94. ALAR 8000A 0.1 G/sec pressure hysteresis as a function of source pressure.  
[Curves are A, D, N, and X.]

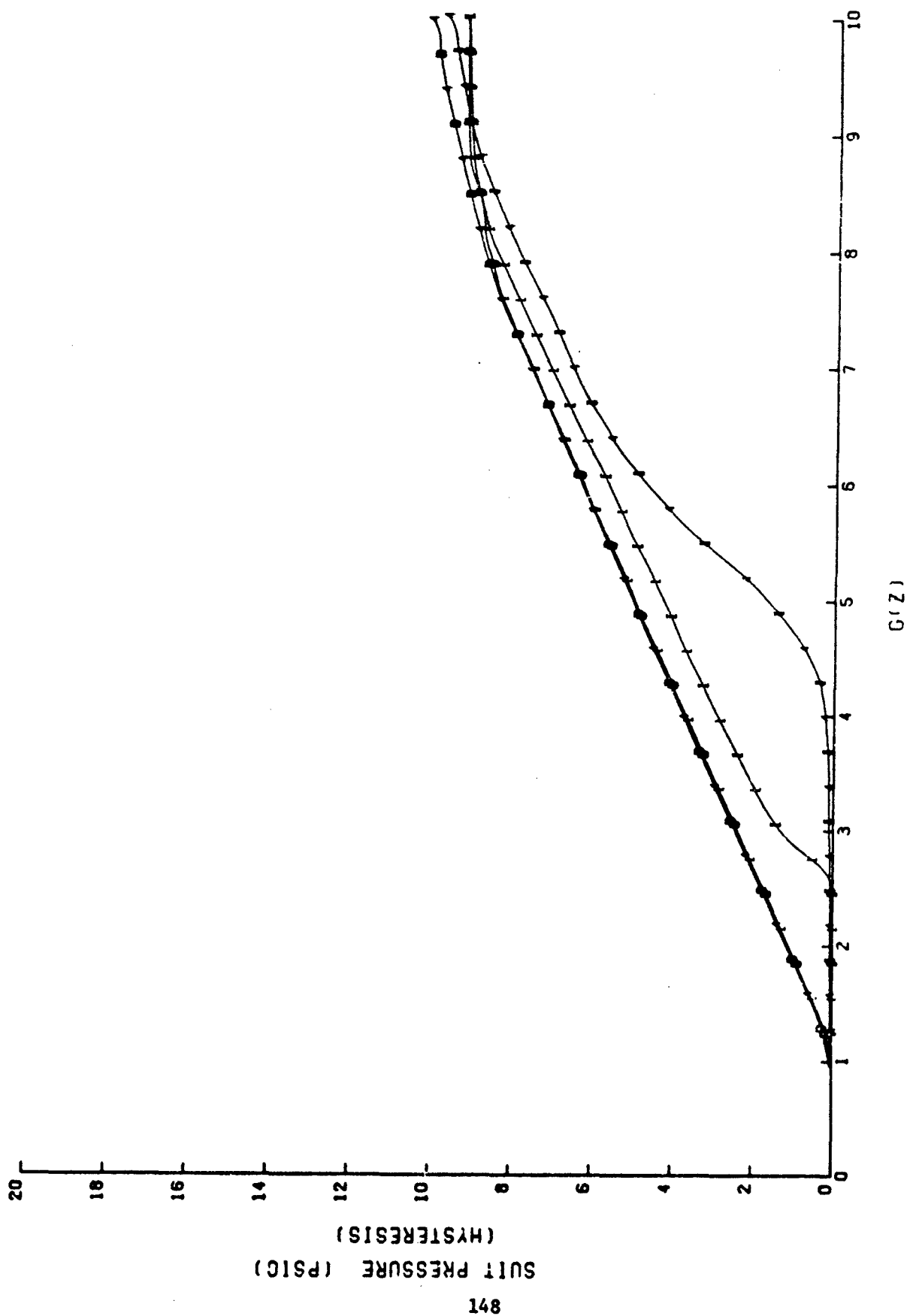


Figure 95. ALAR 8000A pressure-profile comparison as a function of onset rate.  
[Curves are 1I, 4I, 1D, and 4D.]

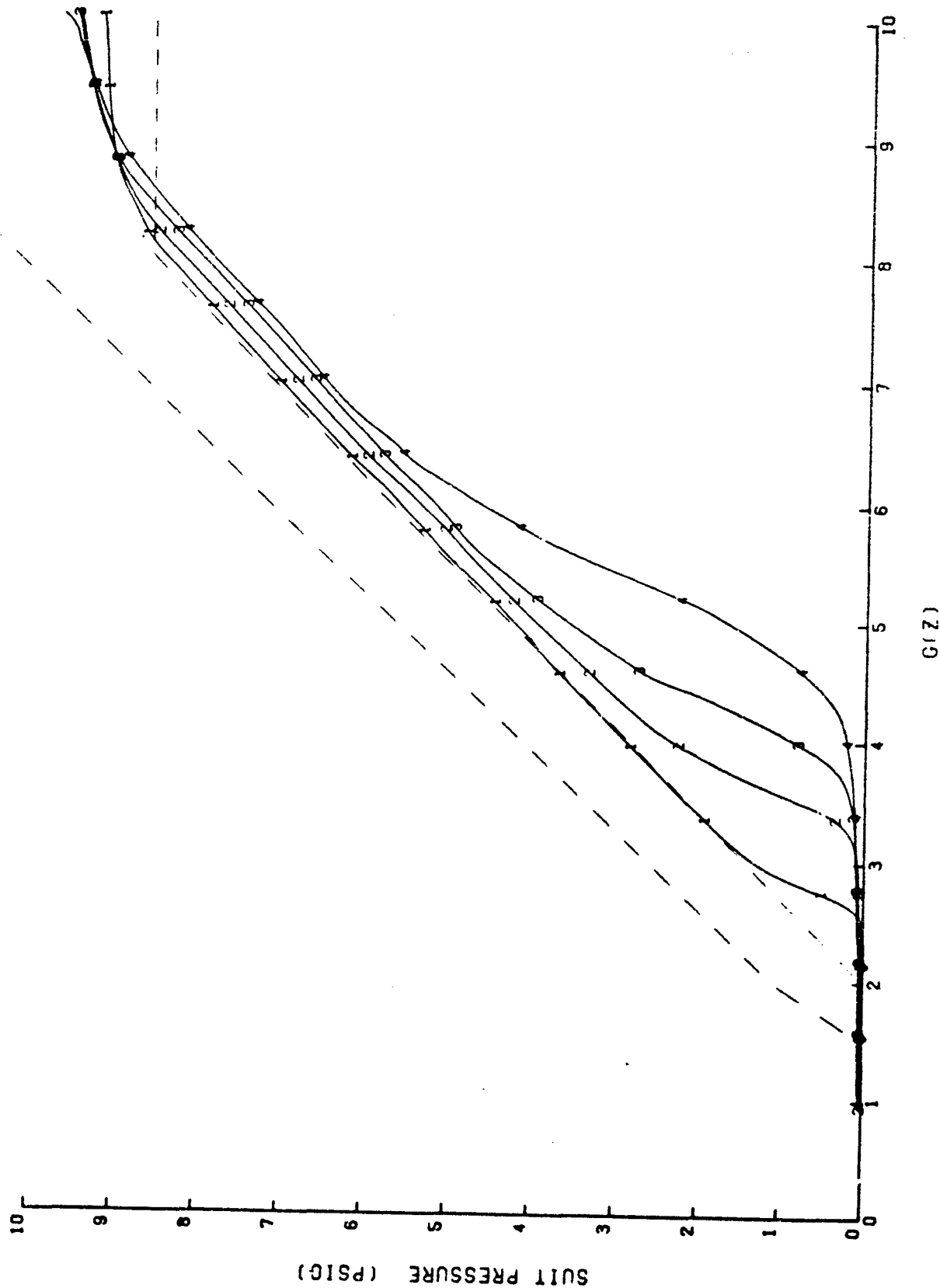


Figure 96. ALAR 8000A pressure profile as a function of G-onset rate.  
[Curves are: 1, 2, 3, and 4.]



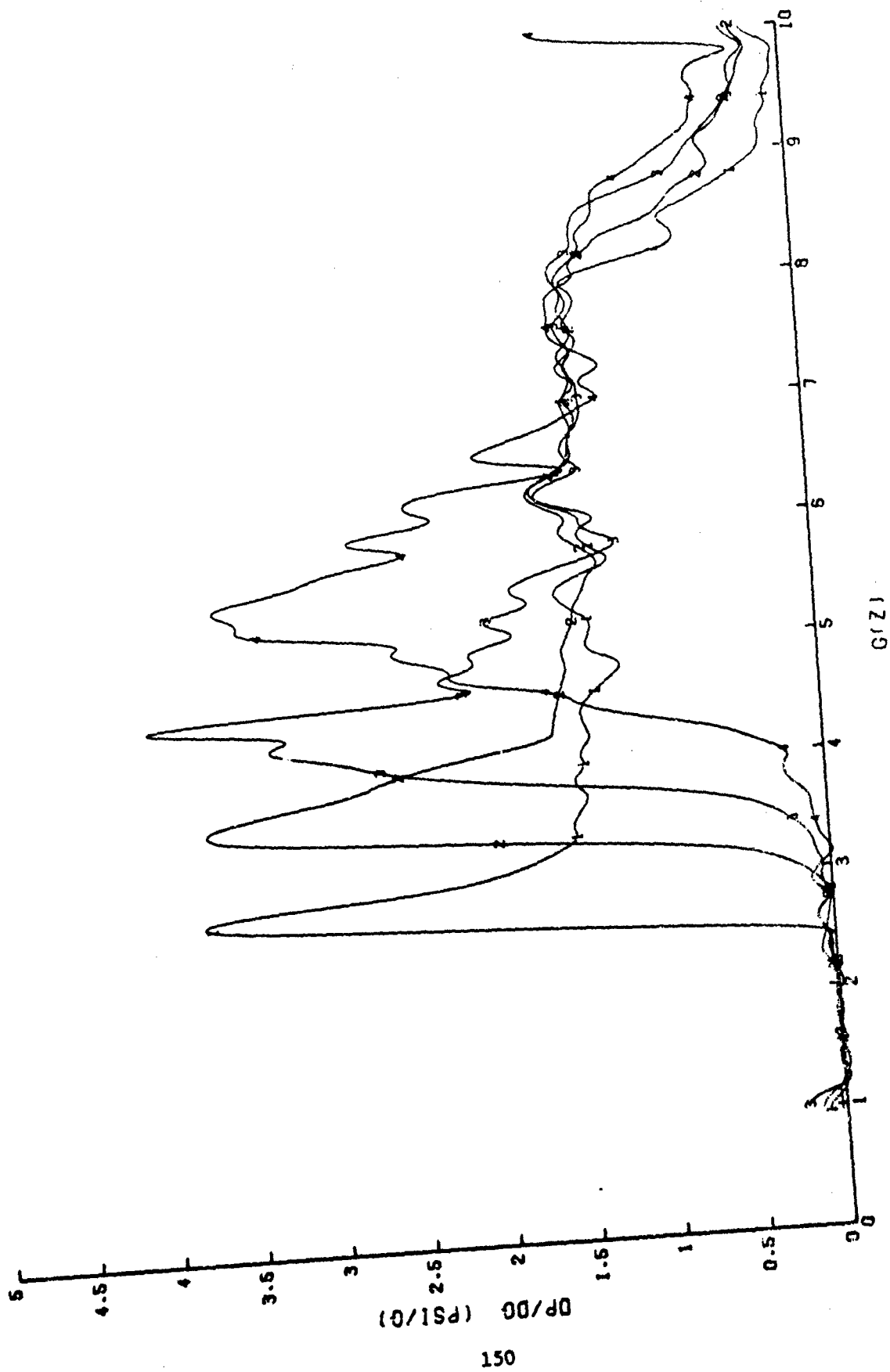


Figure 97. ALAR 8000A  $dp/dG$  as a function of G-onset rate.  
[Curves are: 1, 2, 3, and 4.]

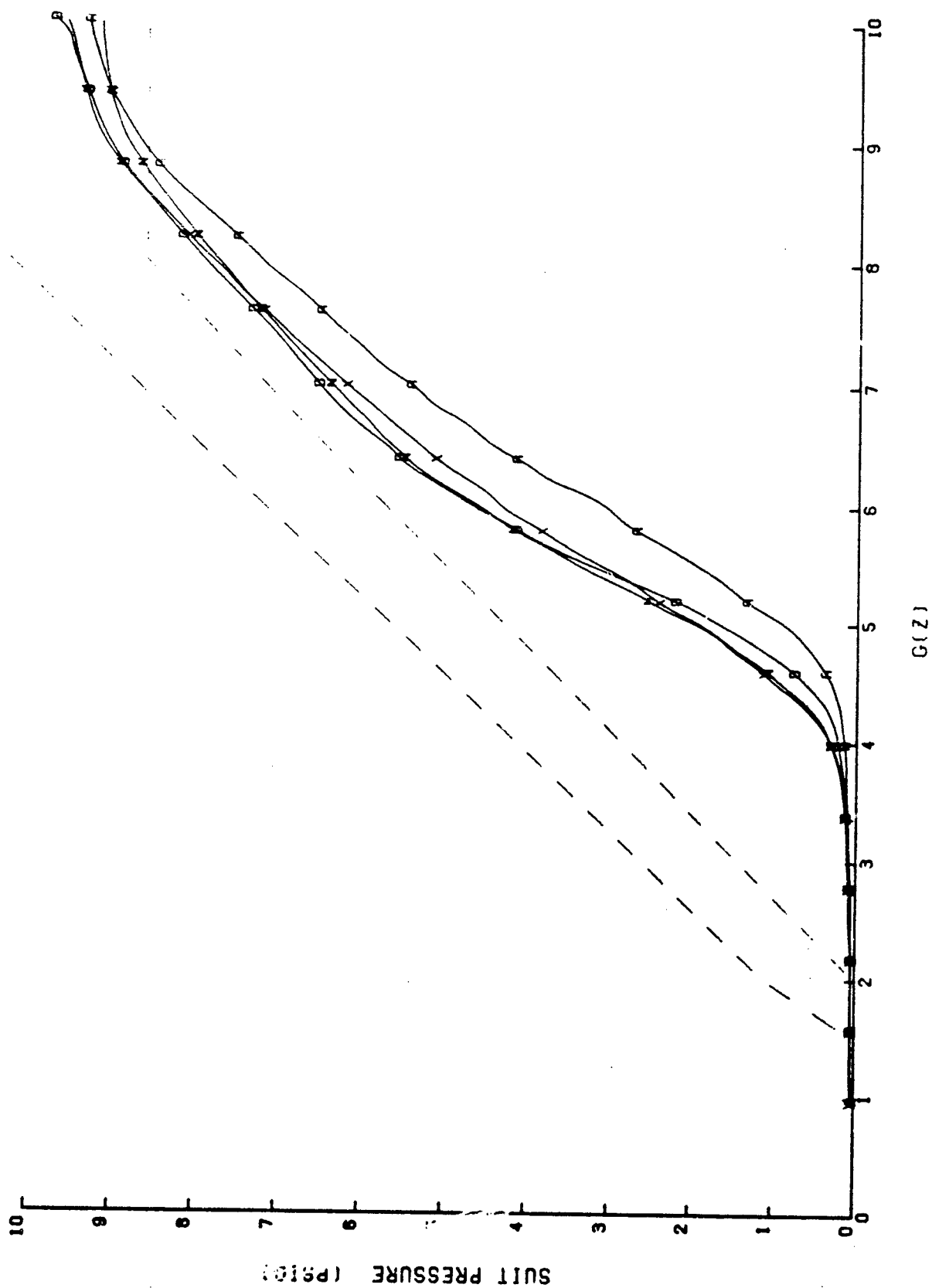


Figure 98. ALAR 8000A 1.5 G/sec pressure profile as a function of source pressure.  
[Curves are: A, D, N, and X.]

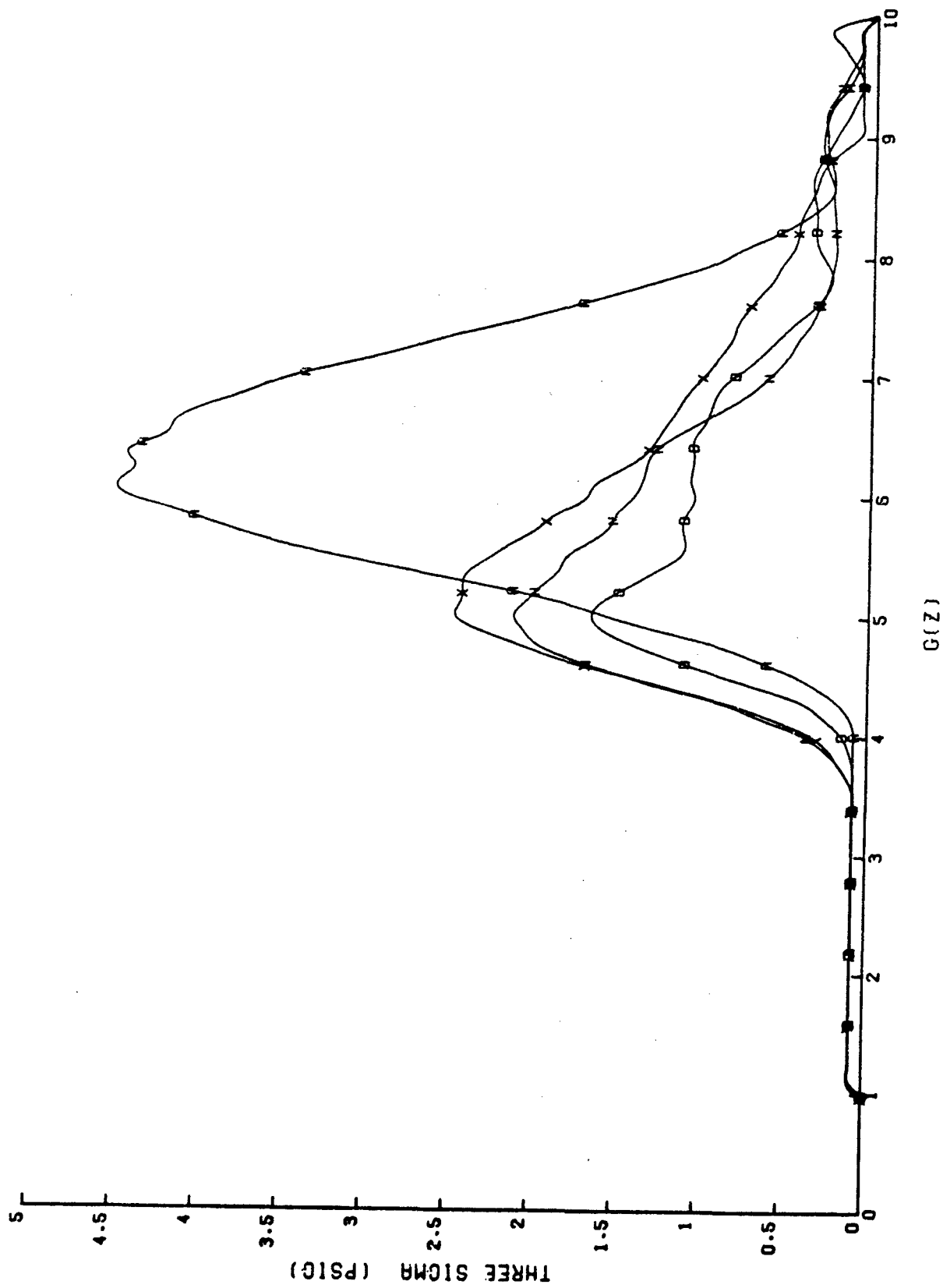


Figure 99. ALAR 8000A 1.5 G/sec pressure variation as a function of source pressure.  
[Curves are: A, D, N, and X.]

The 1.5 G/sec decreasing-G profiles (Fig. 100) indicate the 8000A performs nearly as well at high "offset" rates as low "offset" rates. The large hysteresis peaks (Fig. 101) result entirely from the pressurization lag.

The ALAR 8000A performs acceptably at low G-onset rates. The performance may be rated marginal at 0.5 G/sec, and probably unacceptable at 1.0 G/sec. Although the pressurization of the AGS was well under control, the time lag while the suit dead volume was being filled makes the 8000A performance unacceptable at 1.5 G/sec and higher onset rates.

#### 5.5.5 SACM Tests

The ALAR 8000A produced an inexplicably high total SACM score of 13.381 on line 32 of the PET (Table 6). Since the 8400A and the RPV use essentially the same regulation mechanism, and since the 8000A and 8400A performed about the same on the high G-onset tests, the 8000A was expected to produce approximately 9.5 on the SACM tests. However, the total and individual line scores are still half, or less, of the scores produced by the Bendix AGV.

The pressure profiles shown in Figure 102 represent the actual and ideal pressures that should result from the G stimuli from a SACM test when a minimum source pressure is applied to the AGV and a maximum "suit" volume is attached. The ideal pressure for all SACM tests was derived from the mid-source pressure profile shown in Figure 91, and the actual, instantaneous G value applied. The differences between the real and ideal pressures, along with corresponding onset rates, are shown in Figure 103. The abscissa of this graph represents the integral of G with respect to time. This device allows a real (unweighted) indication magnitude while the size of the excursion (actually the area under the curve) is weighted by the G level. In this manner, a 0.5-psig excursion at 6 G will appear twice as large as a 0.5-psig excursion at 3 G, even though the amplitudes are the same. The area under these curves is used as an evaluation factor in the PET (Table 6). The 8000A's min-max curves (Fig. 103) indicate frequent pressure excursions of -1.35 psig and +0.75 psig, while the maximum onset rates achieved during the tests were +1.25 G/sec and -1.45 G/sec.

The SACM pressure profiles for the maximum source pressure and minimum suit volume are shown in Figure 104, while the associated difference curves are in Figure 105. In this case (Fig. 105), the pressure excursions were -0.9 psig and +0.65 psig, while the onset rates reached 1.0 G/sec and -1.45 G/sec. The median-source-pressure median-suit-volume case is shown in Figures 106 and 107. As might be expected, the pressure excursions reach -1.1 psig and +0.7 psig, larger than the min-max case. The onset rates attained in this SACM are comparable to those in the previous two tests.

The last two figures (Figs. 108 and 109) are unique only in that the valve was run with its centerline at an angle of 20° to the G vector. Since the ideal pressure here was derived in the same manner as in the previous three sets, the actual pressure is expected to be low (refer to section 5.1.3); and Figure 109 confirms this expectation. Otherwise the curves are comparable to those in Figures 106 and 107, except that perhaps a little more tendency to overshoot is exhibited.

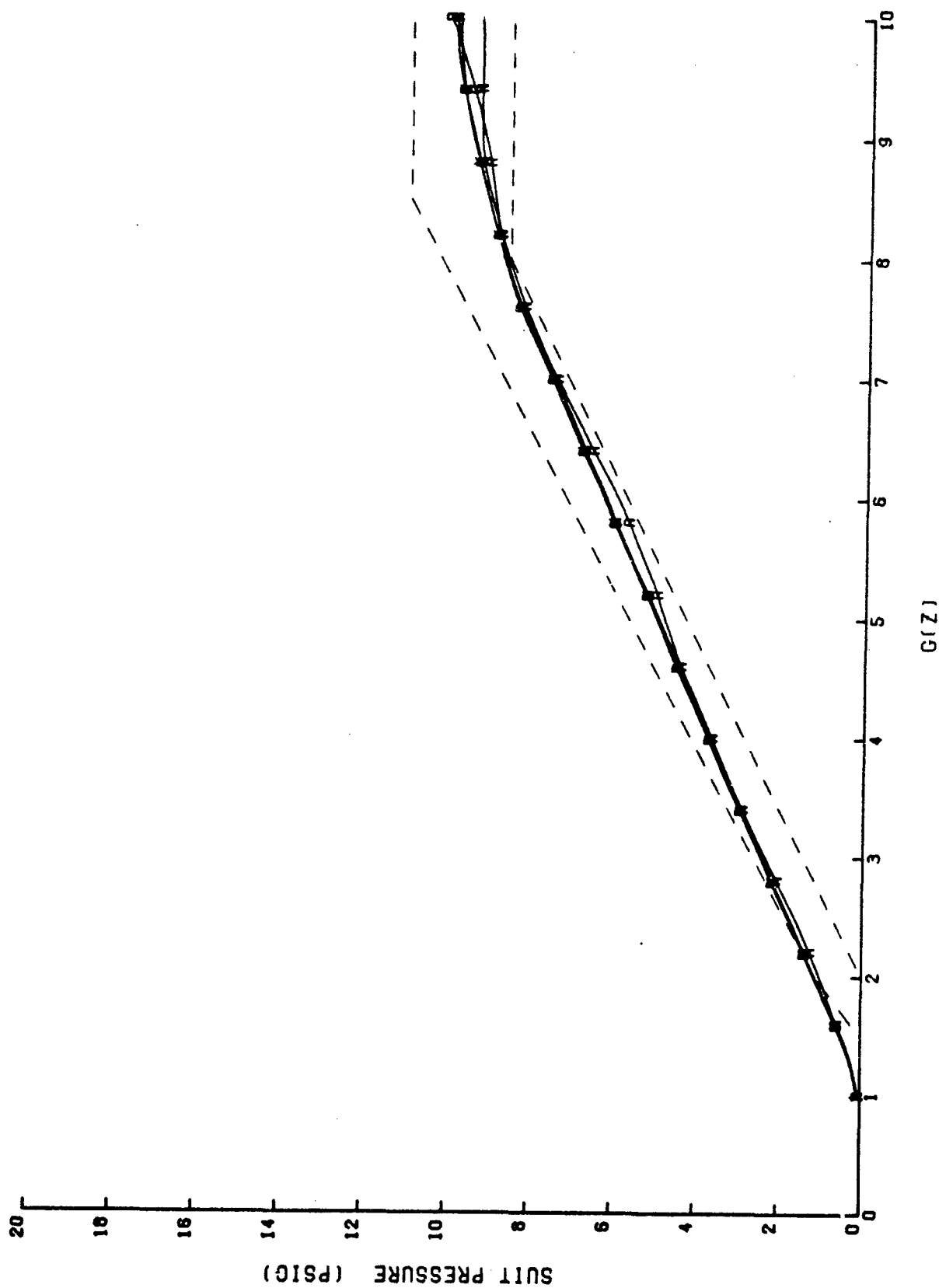
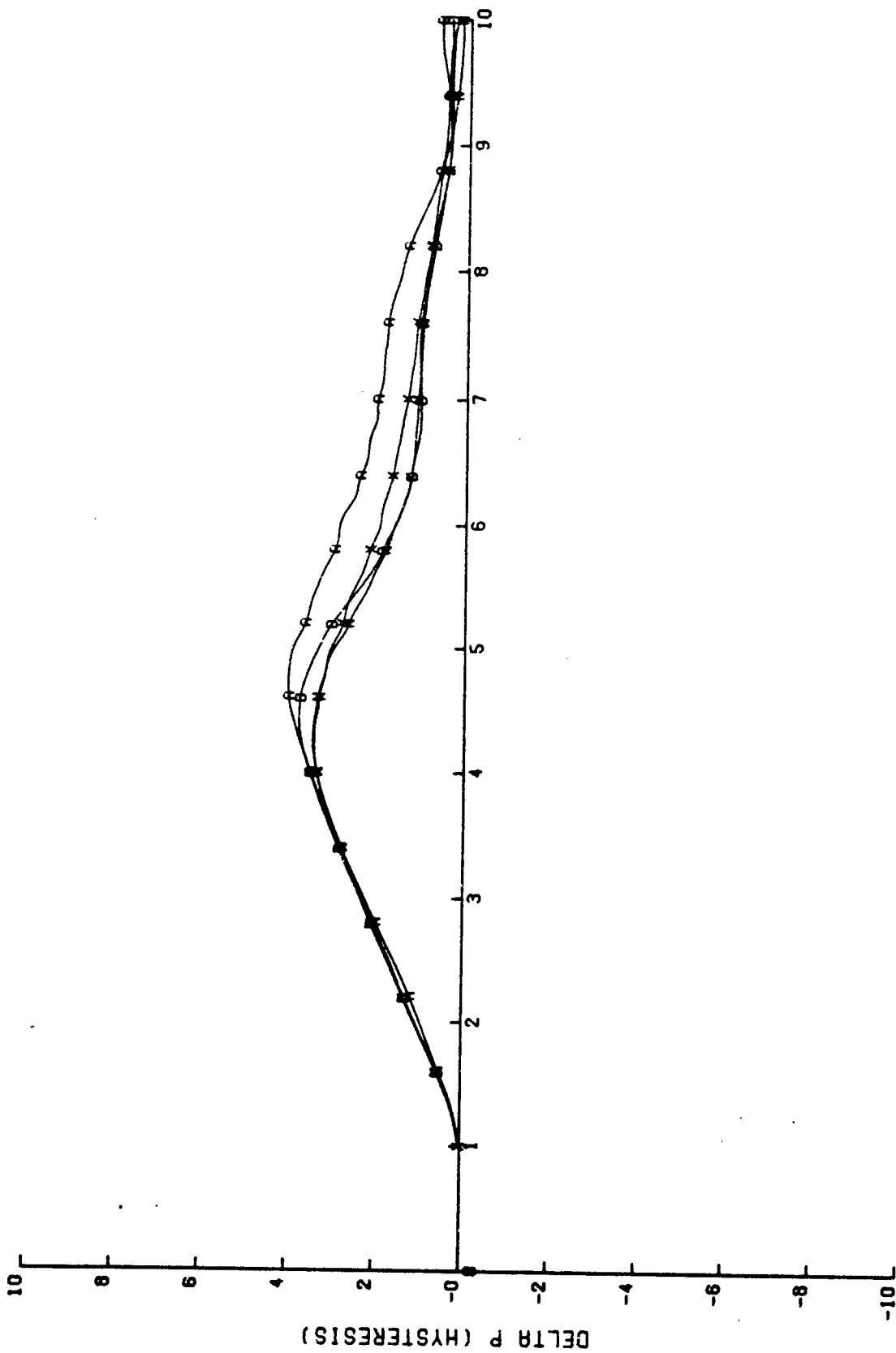


Figure 100. ALAR 8000A 1.5 G/sec decreasing pressure profile as a function of source pressure.  
 [Curves are: A, D, N, and X.]



G(Z)

Figure 101. ALAR 8000A 1.5 G/sec pressure hysteresis as a function of source pressure.  
[Curves are: A, D, N, and X.]

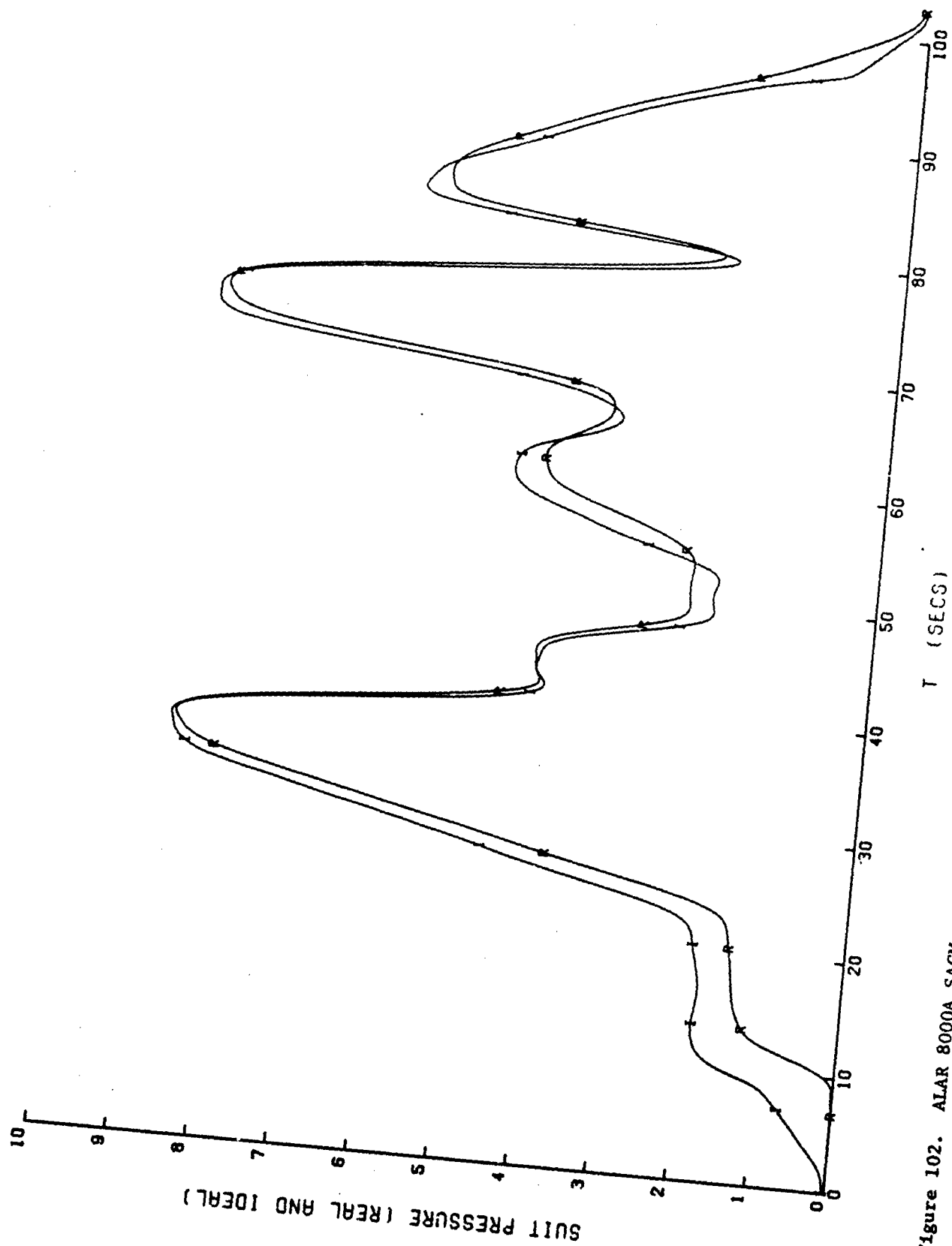
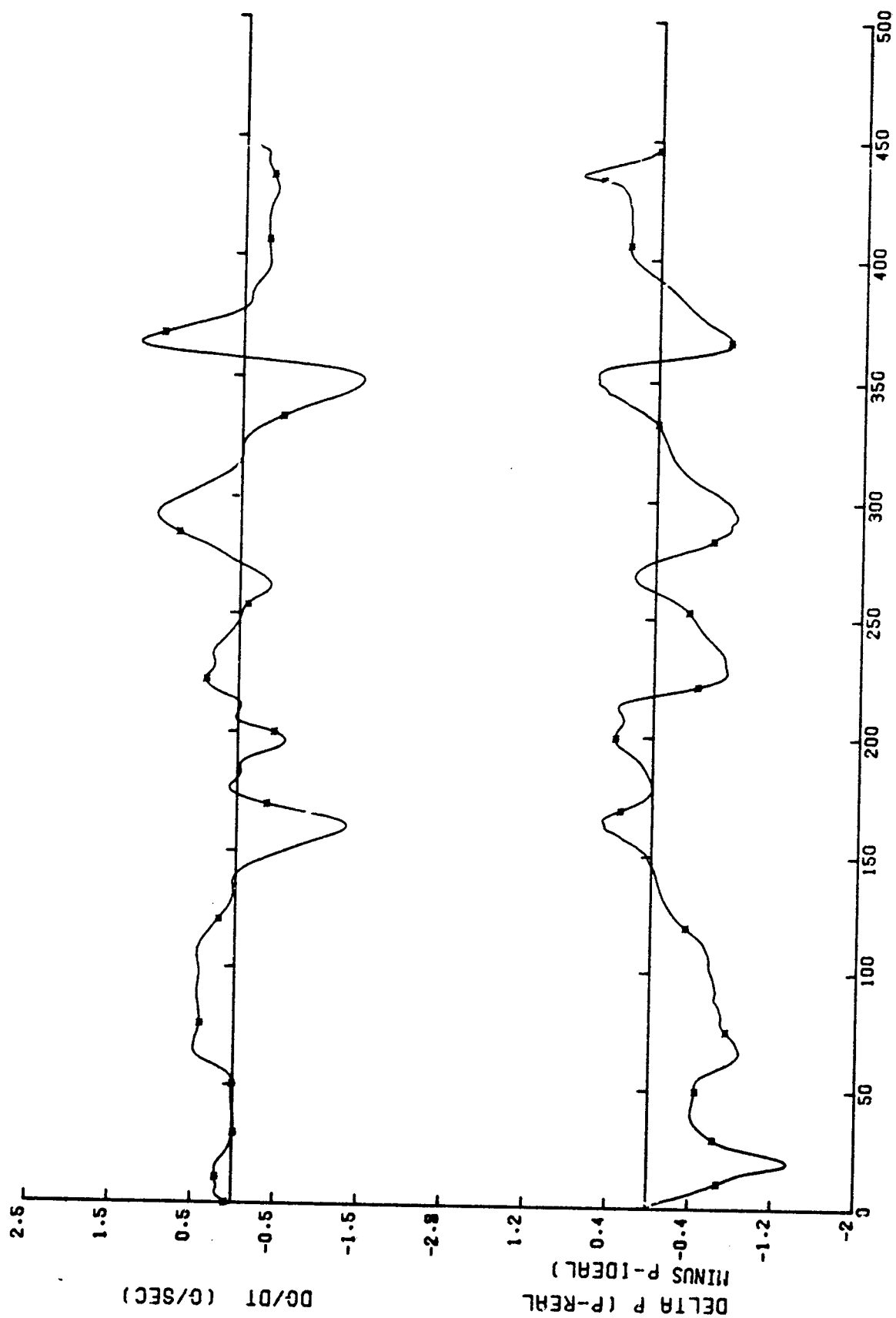


Figure 102. ALAR 8000A SACM pressure-profile comparison with minimum surface resistance



INTEGRAL OF  $G \, dt$  FROM 0 TO  $T$

Figure 103. ALAR 8000A pressure deviation and  $dG/dt$  for the minimum source pressure and maximum suit volume SACM.  
[Curves are: \*.]



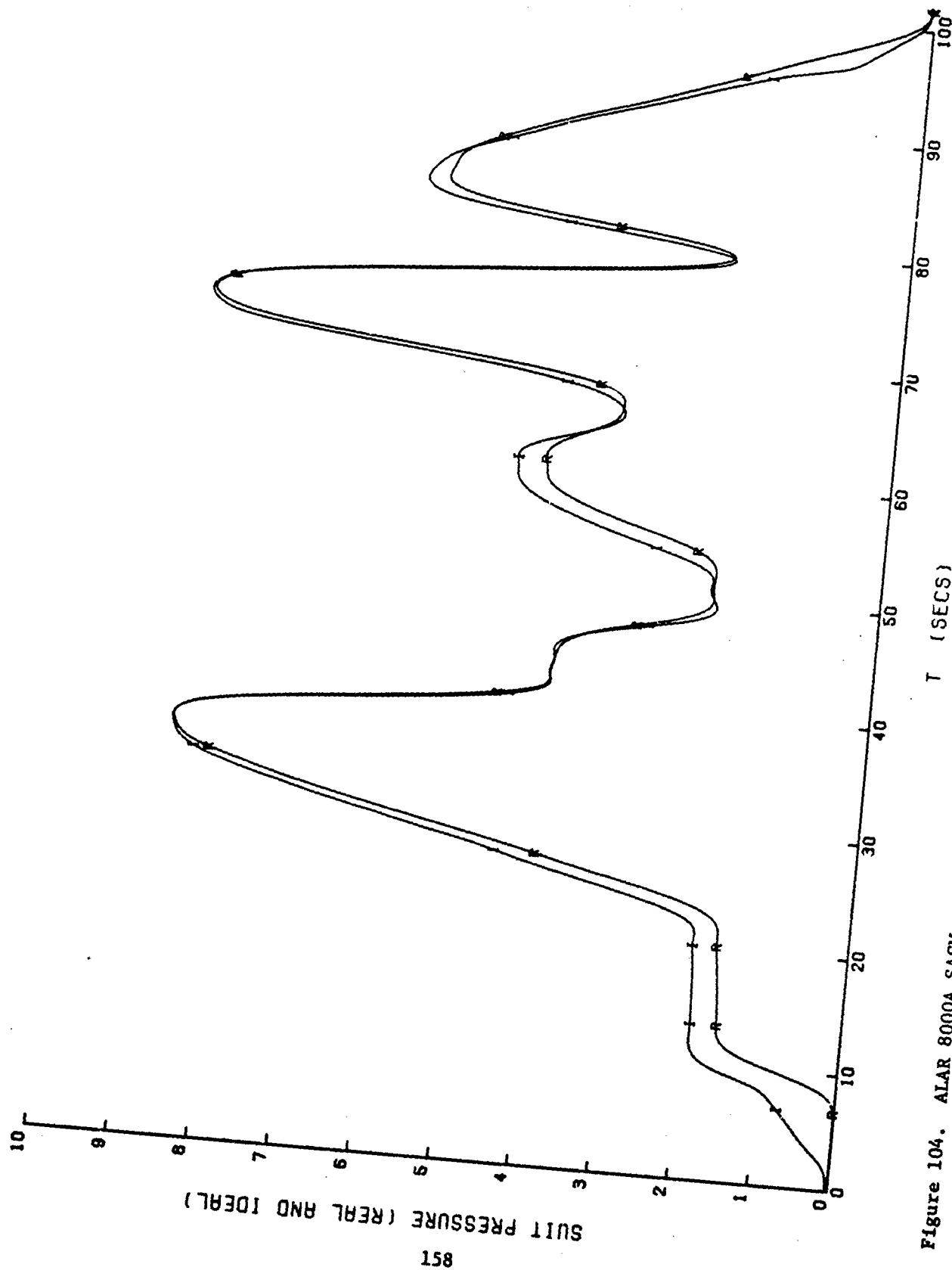


Figure 104. ALAR 8000A SACM pressure-profile comparison with maximum source pressure and minimum suit volume.  
[Curves are: I and R.]

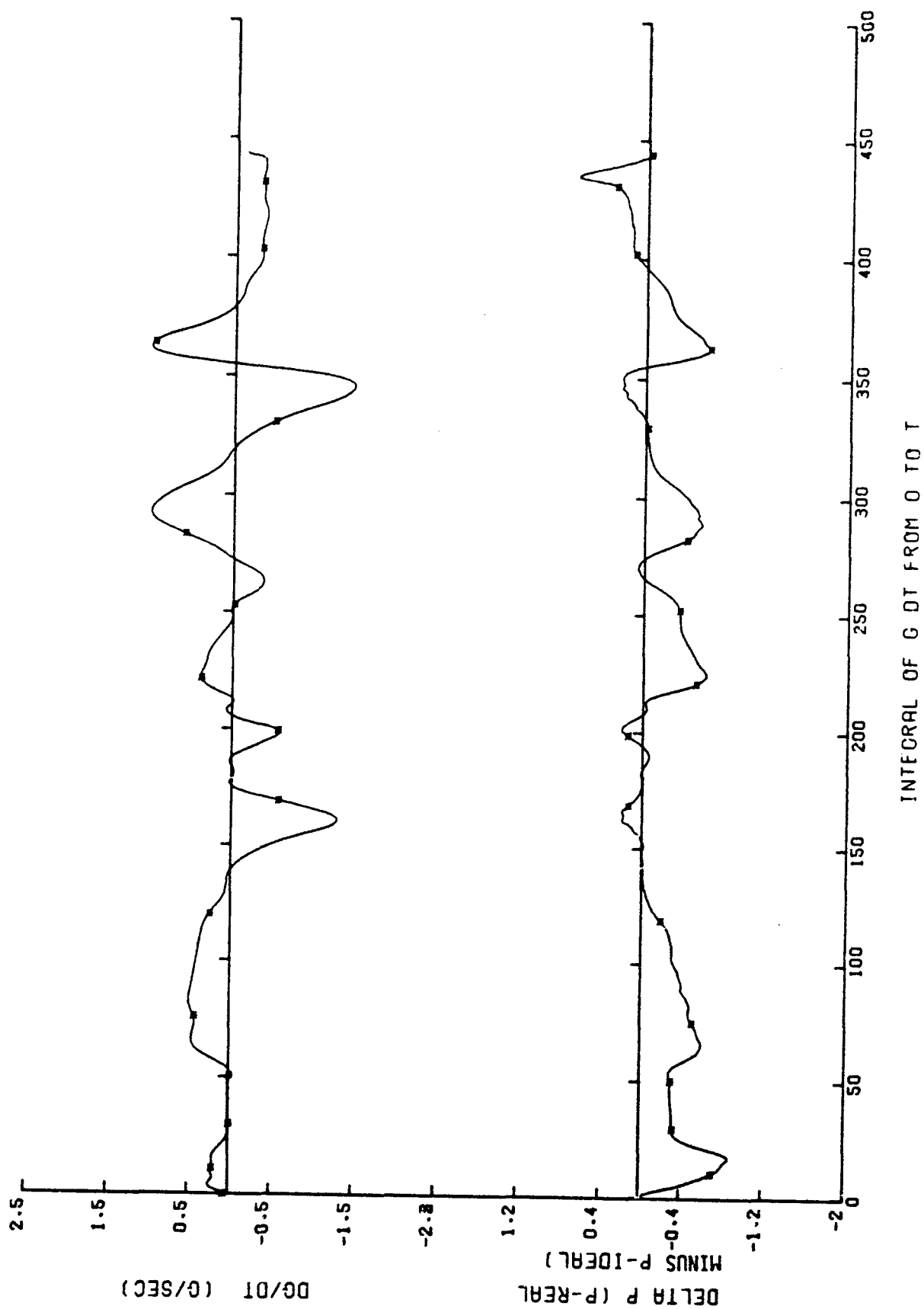


Figure 105. ALAR 8000A pressure deviation and  $dG/dt$  for the maximum source pressure and minimum suit volume SACM.  
[Curves are: \*.]

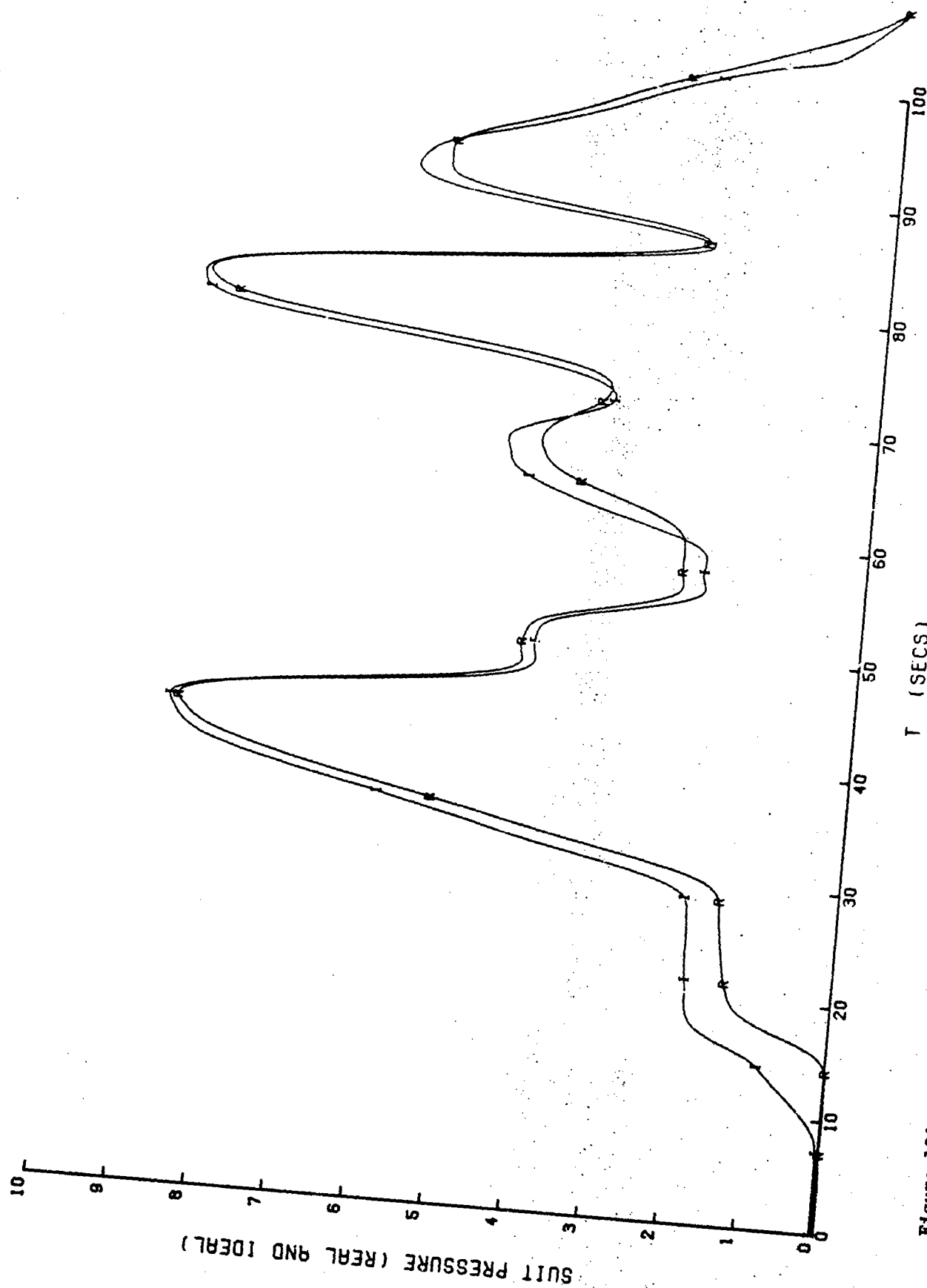


Figure 106. ALAR 8000A SACM pressure-profile comparison with median source pressure and suit volume.  
[Curves are: I and R.]

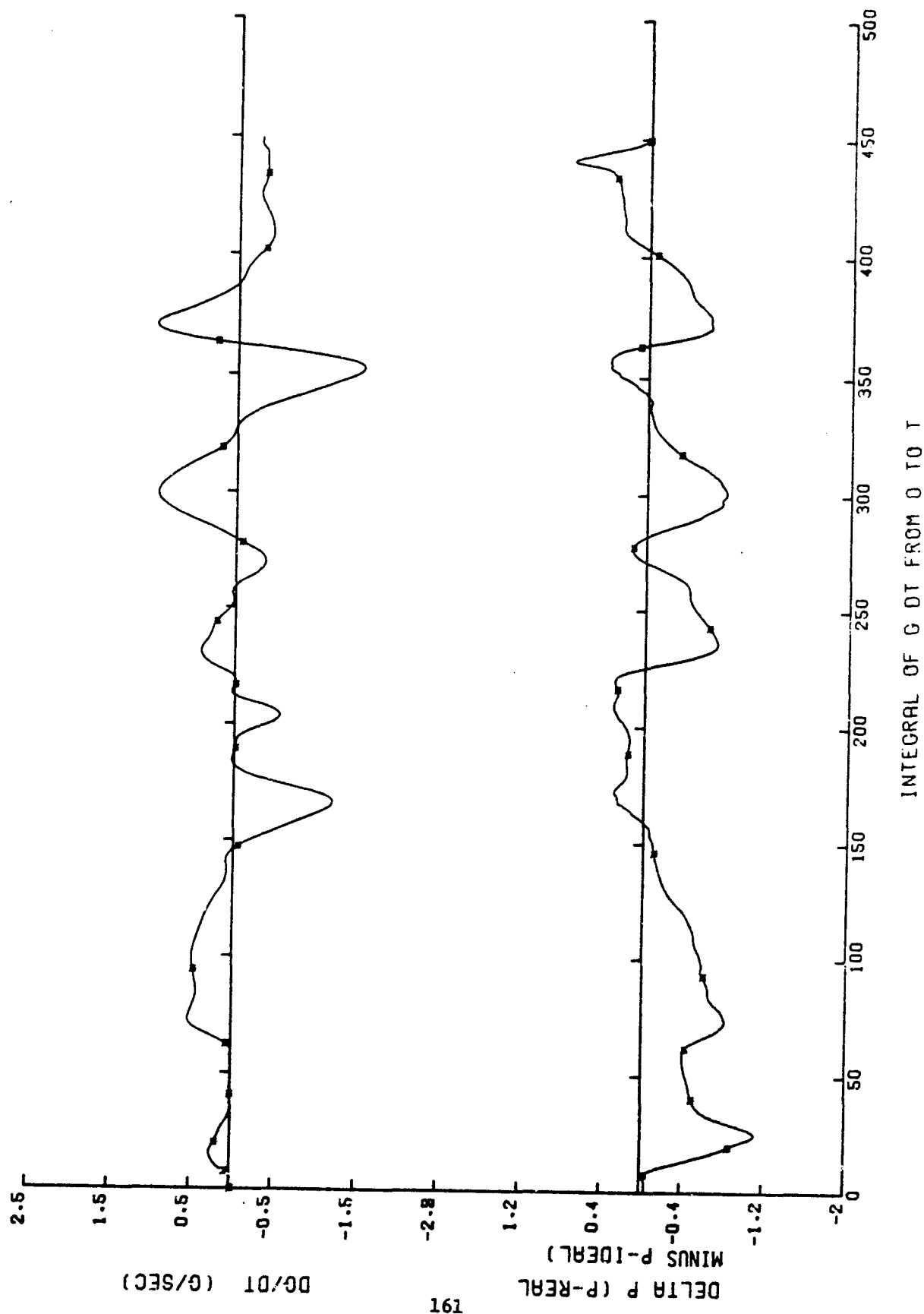
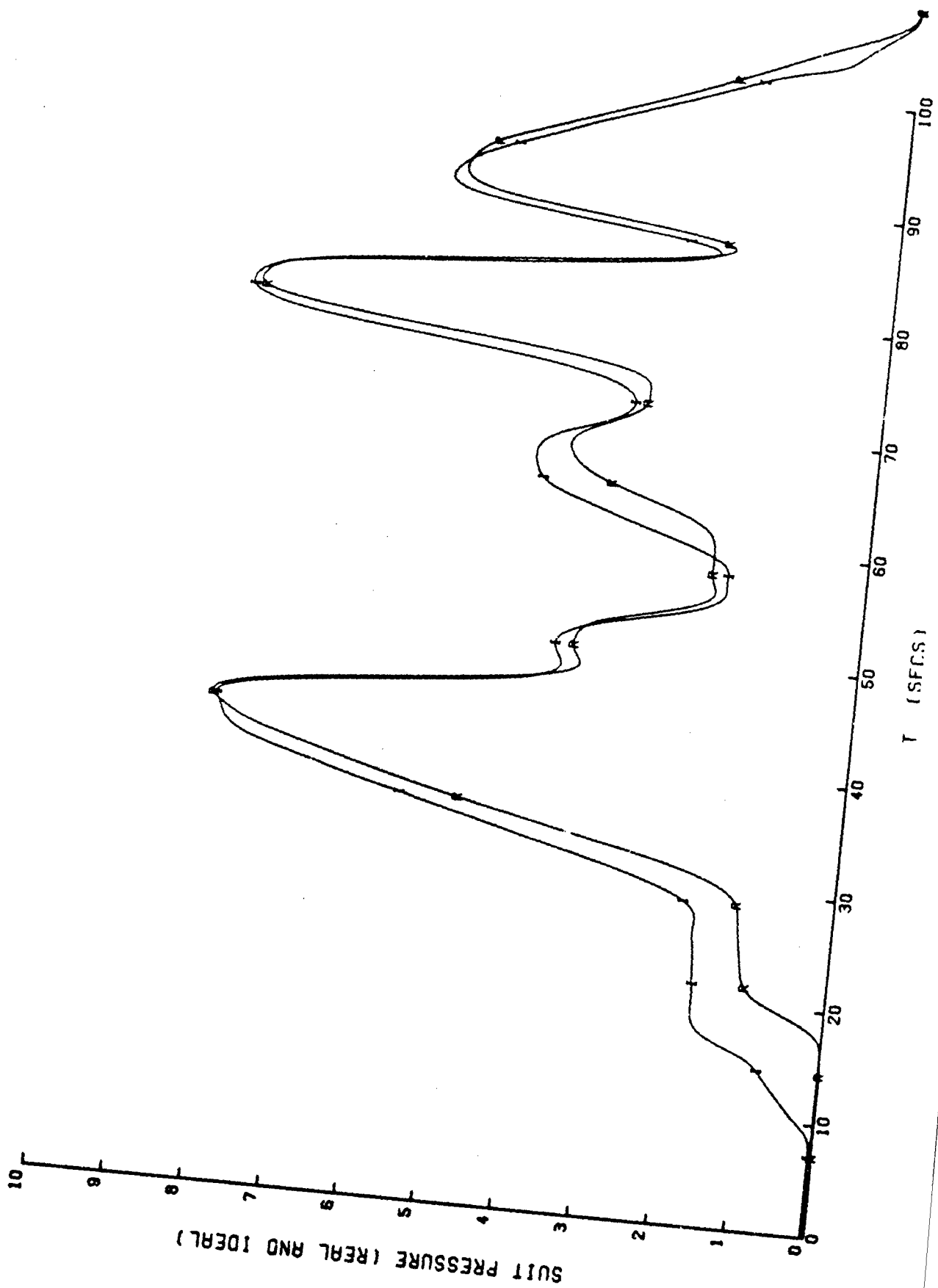


Figure 107. ALAR 8000A pressure deviation and  $dG/dt$  for the median source pressure and sult volume SACM. [Curves are: \*.]



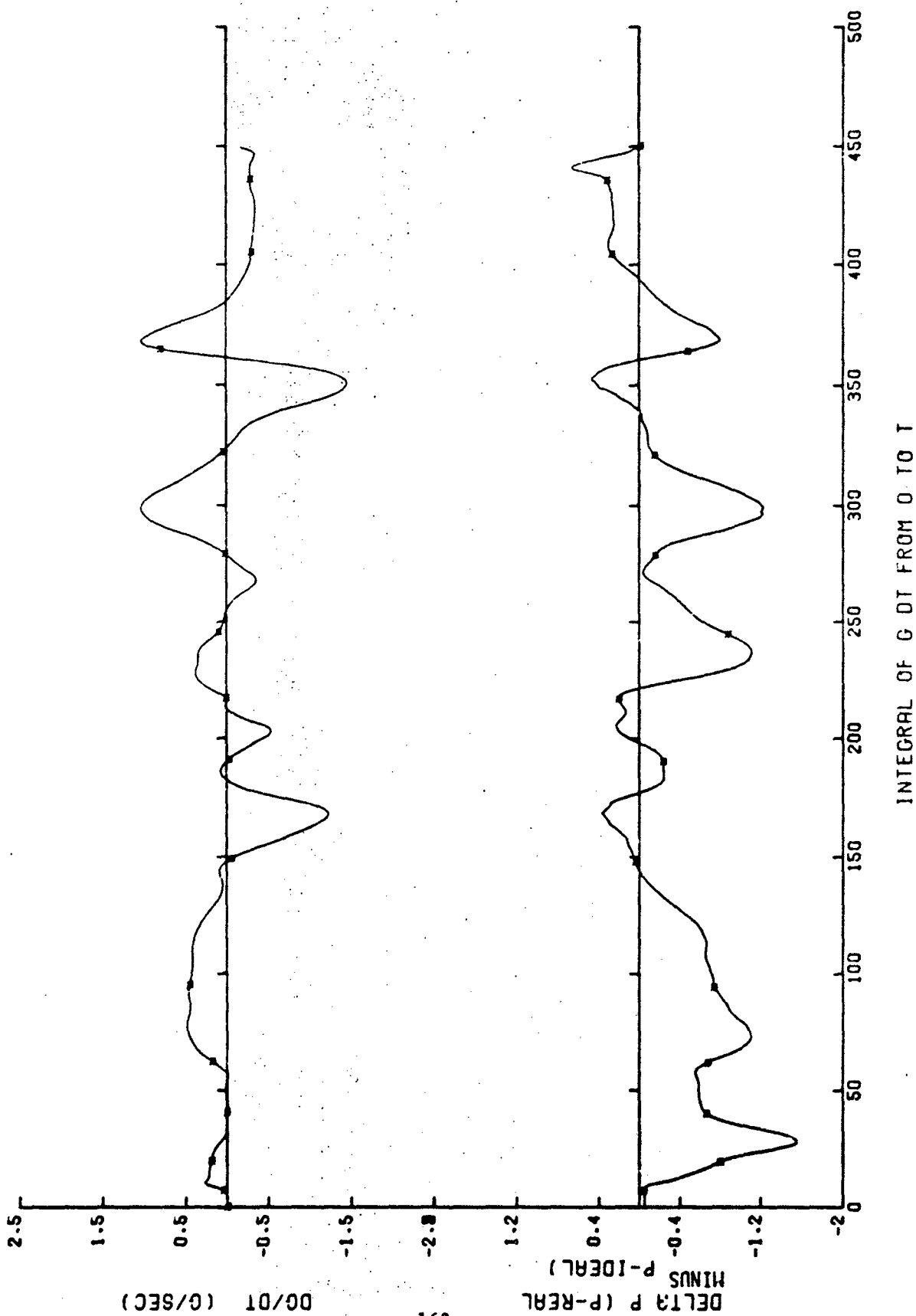


Figure 109. ALAR 8000A pressure deviation and  $dG/dt$  for the G vector misalignment SACM. [Curves are: \*.]

#### 5.5.6 Conclusions on the ALAR 8000A's Performance

The ALAR 8000A performs very well under a wide variety of conditions. In spite of the relatively poor showing on the SACM test, the performances of the 8000A and the 8400A are essentially equal, as might be expected, since they are essentially the same valve. Along this same line of reasoning, the failure tests on the 8400A (SAM-TR-79-31, Vol. II, section 1.3.2) suggest that it (and, by inference, the 8000A) is, in addition, an extremely reliable piece of equipment. The ALAR 8400A probably should be limited to weapons-system-mission combinations which do not require response to G-onset rates greater than 1 G/sec.

[How to order Appendix A]

RE: The USAF School of Aerospace Medicine's Technical Report Series  
on Procedural Tests for Anti-G Protective Devices--  
Volume I (SAM-TR-79-30), and Volume II (SAM-TR-79-31).

APPENDIX A:

In order for comprehensive information on this research  
to be readily accessible, microfiche have been made of  
this Appendix. The microfiche are available through:

The Strughold Aeromedical Library  
Documentation Section (USAFSAM/TSK)  
USAF School of Aerospace Medicine  
Brooks AFB, Texas 78235



ABBREVIATIONS, ACRONYMS, AND SYMBOLS

ACM	Aerial Combat Maneuver
AGS	anti-G suit
AGV	anti-G valve
dc	direct current
dG/dt	rate of change of acceleration with respect to time [In some figures: DG/DT]
dP/dG	rate of change of pressure with respect to acceleration [In some figures: DP/DG]
F <sub>v</sub>	air flow
GVALVPGM	A specialized computer program for the analysis of anti-G valve data recorded in accordance with the SVTP
G <sub>z</sub>	acceleration along the Z axis (head-to-foot) [In some figures: G(Z)]
Hz	Hertz (cycles per second)
kHz	kilohertz (1000 cycles per second) source pressure
min-max	Minimum source pressure - maximum suit volume
mid-mid	Median source pressure - median suit volume
max-min	Maximum source pressure - minimum suit volume
NC	normally closed
NO	normally open
PET	Performance Evaluation Table
P <sub>s</sub>	source pressure
PTAP	Procedural Tests for Anti-G Protective Devices
P <sub>v</sub>	suit pressure
rms	root mean square
RPV	Ready Pressure Valve
SACM	Simulated Aerial Combat Maneuver
SVTP	Standardized Anti-G Valve Test Protocol
TEHG	Engineering Test and Evaluation During High G (Program)
VAC	volts (alternating current)
VDC	volts (direct current)
VNB	Biodynamics Branch, Crew Technology Division, USAFSAM
WRT	with respect to
XDCR	transducer